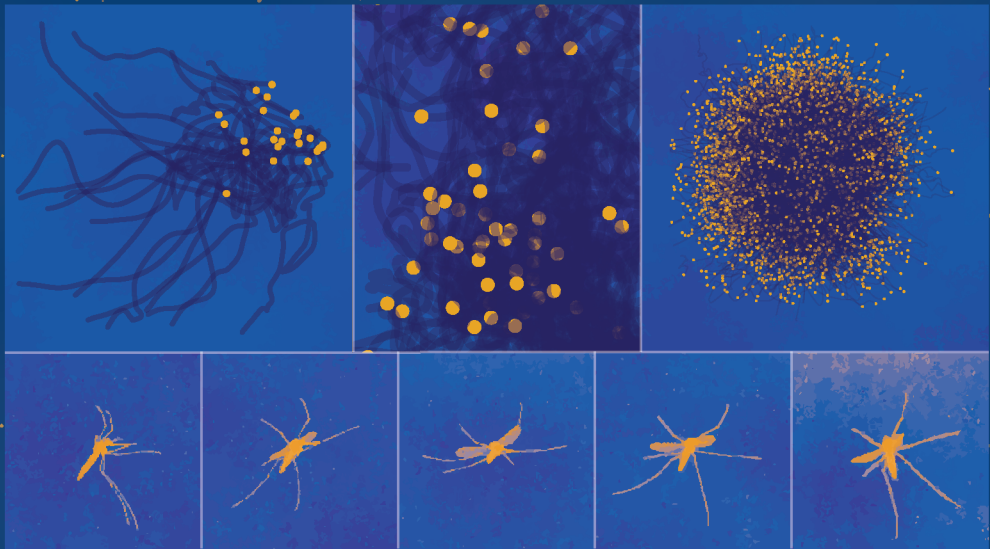# BIOMECHANICS
of FLYING MOSQUITOES
during CAPTURE and ESCAPE

Antoine Cribellier

Propositions

1. A detailed understanding of mosquito flight dynamics around traps accelerates the improvement of mosquito trapping solutions.
   (this thesis)

2. To avoid being swatted, mosquitoes actively surf the bow wave induced by the attacker.
   (this thesis)

3. To find thriving extra-terrestrial life, the moons of Jupiter are a much more promising destination than Mars.

4. Austerity in an economic crisis is like treating a patient with bloodletting.

5. Not knowing how scientific knowledge is gained is a worse deficiency than not knowing that the earth is round.

6. The biggest problem with privately funded research is the doubts it can create which can lead to major delays in reaching consensus and in passing of protecting policies.

7. Art has a bigger role to play than science in achieving the cultural shift necessary to resolve the current environmental crisis.

8. Panels of randomly selected citizens are a better reflection of society and can be better policy-makers than elected politicians.

Propositions belonging to the thesis, entitled

Biomechanics of flying mosquitoes during capture and escape

Antoine Cribellier
Wageningen, 11 October 2021

Biomechanics of flying mosquitoes during capture and escape

Antoine Cribellier

Biomechanics of flying mosquitoes during capture and escape

Antoine Cribellier

Table of contents

Chapter 1

General introduction

Through their lives, flying insects often must interact with vertebrates many times their own size. Some insectivorous bats or birds such as swifts, swallows and whispering bats feed almost exclusively on flying insects (Hespenheide, 1975; Kunz, 1982). Many other non-flying animals, such as chickens or frogs (Card, 2012; Darbro and Harrington, 2007; Raghavendra et al., 2008), are also capable of predating on flying insects. In addition, numerous flying insects, dipterans such as horse flies or tsetse flies, blood feed on large vertebrates (Allan et al., 1987; Clements, 1999). Among those insects, mosquitoes are certainly the best known, both because of their prevalence (they can be found on most continents) and because they can be vectors of many deadly human diseases such as malaria, dengue or Zika. Although some aspects of the interactions between insects and vertebrates have been well studied already – such as how insects detect and approach their blood hosts (Allan et al., 1987; Cardé, 2015; Clements, 1999) – many aspects of such interactions are still poorly understood. One important example of these aspects is: "How do flying insects behave around vertebrates that try to kill or chase them?". And another is: "How do environmental conditions and the available cues, such as heat or airflow, influence flying insects' success in such interactions?"

In this thesis, I aim to contribute to answering these two questions by investigating: **How flying mosquitoes interact with odour-baited traps or a mechanical swatter** and **how factors such as the presence of host cues, airflow or light intensity influence these interactions.** I will study this by using a biomechanics approach where engineering techniques, such as high-speed videography and airflow simulations, are used to answer biologically relevant questions about insect movements. This is a multidisciplinary approach involving biomechanists, medical entomologists and industrial designers. I tackle the previously mentioned research questions by simulating human presence near flying mosquitoes using odour-baited traps and a mechanical swatter in both applied and fundamental studies. For these studies, I developed several new tools that I used to analyse large datasets of three-dimensional mosquito flight tracks as well as their body and wings kinematics. Thus, a new understanding of mosquito flight behaviour around traps was reached that led to the development of a mosquito trap with improved capture performances. Finally, my work on how mosquitoes performed successful escapes when attacked led to the discovery of previously unknown escaping mechanisms as well as the exploration of evolutionary trade-offs of insect flight in darkness.

Here, I will first introduce how insects evolved the ability to fly and why this had an important impact on their success. I will also explain how insects generate the aerodynamic forces necessary to power their flight and what the role of the neuro-sensory system of insects is in stabilizing and controlling flight. In particular, I will describe why studying escape manoeuvres of insects is a good way to learn about flight mechanics and consequently about flight physiology. Then, I will introduce how mosquitoes interact with vertebrates, especially for blood feeding. I will describe mosquito host-seeking behaviour and how hosts can defend themselves against mosquito nuisance. Finally, I will list the aims of this thesis and describe its content.

1.1 Evolution, physiology and biomechanics of insect flight

In the history of life on Earth, powered flight appears to have evolved independently at least four times among very different animal groups: insects, pterosaurs, birds and bats. All these flying animals achieved flying using wings, made of cuticles, skin membrane or feathers, which they flapped using powerful flight muscles (Dudley, 2000; Templin, 2000). This ability to fly gave these animals several evolutionary advantages over other species and allowed them to occupy a previously unoccupied aerial ecological niche. By achieving powered flight, these animals could escape from terrestrial predators and had access to a new set of aerial preys. They could also hunt down both terrestrial and aquatic animals with a certain advantage. However, perhaps more importantly, flying could be used to travel long distances very quickly and efficiently (Schmidt-Nielsen, 1972). Thus, flying animals could then disperse fast if living conditions in a region were not favourable anymore, or conversely, gather for seasonal grazing and migrate over long distances to adapt to local food availability (Rainey, 1978). These advantages probably contributed greatly to the fact that powered flyers are today a very successful group of animals, which is supported by the large number of species that evolved among powered flyers (Kuhl et al., 2021; Solari and Baker, 2007; Stork, 2018). Of course, from the pterosaurs that were larger than giraffes to insects with the size of a pinhead, the advantages (and costs) that came with flying varied greatly.

1.1.1 The specificity of insect flight

Insects were the first class in the animal kingdom that evolved the ability to fly. However, there is still little known about how they did so. This is mainly because of an existing gap in our fossil record between what is the first known winged insect (325 million years ago) and its earliest discovered ancestors (around 400 million years ago) (Alexander, 2018; Dudley and Yanoviak, 2011; Engel and Grimaldi, 2004). There are currently several competing theories about the origin of insect wings. The tergal origin hypothesis states that wings expanded from the dorsal body wall (tergum), and the pleural origin hypothesis proposes that wings originated from pleural (lateral body wall) tissues and the branches (exites) connected to them (Hamilton, 1971; Kukalová-Peck, 1983; Linz and Tomoyasu, 2018). A third theory, the dual-origin hypothesis, tries to unify these two competing theories by proposing that both tergal and pleural components may have played a role in the evolution of insect wings (Crampton, 1916; Linz and Tomoyasu, 2018). Even more is unknown about how insects might have evolved all other flight-related morphological traits (Alexander, 2018; Linz and Tomoyasu, 2018). As for vertebrates, it is possible that insects acquired powered and controlled flight via gliding ("trees down" origin) or via jumping ("ground up" origin) (Dudley and Yanoviak, 2011). However, also, it might be that insects' small mass allowed them to use wind and air gusts to take off passively (Dudley and Yanoviak, 2011). In this

way, primitive insects might have benefited from such initially passive excursions in the air to evolve the neuromuscular traits and wing morphology necessary for the control of powered flight.

Achieving powered flight was certainly a tremendous success for insects. There are more species among insects than among all other animal classes, and most insects need to fly at some point in their life cycle. They use flight for many different behaviours such as feeding, mating, egg laying and migrating (see Fig. 1.1). For this, flying insects have two or four wings of diverse shapes and sizes (Wootton, 1992). Contrary to the majority of birds or bats, most flying insects are capable of hovering, and therefore can manoeuvre with ease in confined spaces. However, achieving flight is very energetically demanding for insects, as they are constrained by their capacities to move their wings at high speeds (Dickinson, 2006). Generating aerodynamic forces with decreasing size relies more and more on viscous effects and less on inertial effects. As a consequence, a small flyer cannot achieve an energetically efficient means of flight such as gliding. One possible solution to this problem is to grow in size, and thus it is not a surprise that the only insects capable of gliding (e.g. dragonflies and butterflies) are among the largest. Nevertheless, diffusional limits on oxygen supply for insect tracheal systems likely constrain their maximum body size (Dudley, 2000). And consequently, insects never reached the size of an average bird since the extinction of giant dragonflies (*Meganeura)*, which could only survive in the oxygen-rich atmosphere of the Palaeozoic era (Dudley, 2000).

To achieve hovering flight, insects flap their wings back and forth (and not up and down) at wingbeat frequencies that can be much higher than the ones of all other fliers (Ha et al., 2013). To move their wings at these high frequencies, many insects such as dipterans (i.e. two winged insects) rely on very fast stretch-activated and indirect flight muscles (Dickinson, 2006; Pringle, 1978). Additionally, some of these insects use asynchronous flight muscles which allow them to beat their wings at higher frequencies than their neuronal activation impulses. In this way, insects rotate each of their wings around their hinges in order to follow a "u-shaped" pattern and achieve high angles of attacks of their wings during almost the entire forward and backward strokes (Fig. 1.2).

Thanks to the regular and fast rotation of their wings, insects are able to the generate aerodynamic forces necessary to achieve and control flight. Certainly, the most important aerodynamic mechanisms that have been identified among insects are the leading-edge vortex. Most insects were shown to create such leading-edge vortex attached to each of their wings and which contributes greatly in the production of aerodynamic lift (Ellington et al., 1996). Other important aerodynamic mechanisms have also been identified and shown to contribute to the generation of the lift (Birch and Dickinson, 2003; Wagner, 1986). Among them, wake capture describes how a flapping wing of insects will encounter higher airspeeds after reversing its course, thus resulting in higher aerodynamic forces (Sane, 2003). The rotational lift is the mechanism by which insect generates aerodynamic lift when reversing from one stroke to another, and the added-mass effect describe how airflow acceleration contribute to the production of forces (Sane, 2003).

Figure 1.1: Diversity of flying insects. Examples of insects using flight for various ecological purposes. (*a*) Bee fly (*Bombyliidae*) pollinating flowers. (*b*) Monarch butterflies (*Danaus plexippus*) wintering at Michoacan, Mexico, after their parents migrated from Canada. (*c*) Two European bee-eater (*Merops apiaster*) that just caught a hawkmoth each. (*d*) Flying wild bee, probably commuting between flowers to forage. (*e*) Female dragonfly (*Libellula depressa*) laying eggs while flying. (*f*) Mating swarm of mayflies (*Rhithrogena*) on Tisza river in Serbia. Images from AdobeStock.
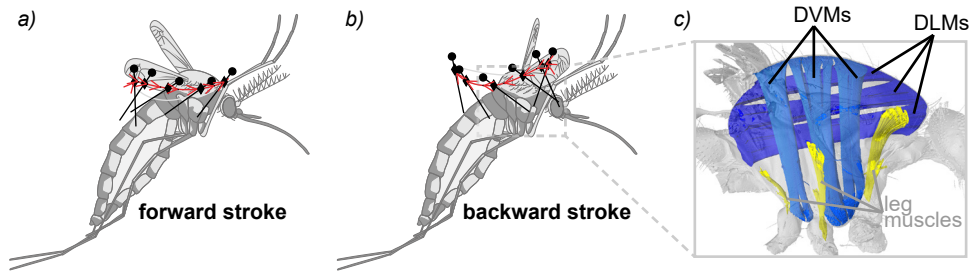
Figure 1.2: How mosquitoes fly. Mosquitoes generate aerodynamic forces required for flight by moving back and forth their wings at high flapping frequencies. (*a,b*) Schematics showing the wing kinematics of a hovering female mosquito (*Anopheles coluzzii*). (*c*) micro-CT reconstruction of the dorso-longitudinal (DLMs) and dorso-ventral (DVMs) flight power muscles used to move the wings back and forth. Figures adapted from (Muijres et al., 2017; Veen and van Veen, 2020)

1.1.2 Insect flight control system

To achieve powered flight that is both stable and manoeuvrable, insects use a closed loop neurosensory system. In such system, sensory information will be collected and used to control wings kinematics, for example to correct a perturbation. These changes in wing kinematics will alter the aerodynamic forces and torque generated and thus indirectly influence body motion. This will therefore change the sensory information available and close the feedback loop. To control their wing kinematics, flying insects rely on around 12 steering muscles, each controlled by a single motor neuron (Dickinson, 2006; Walker et al., 2014). And, to control wing motions, these muscles adjust the gearing of the wing hinges by acting as variable-stiffness springs (Dickinson, 2006). Because small changes in the wing kinematics will have important consequences on the aerodynamic forces generated, it is crucial for insects to be able to control these kinematics accurately and fast. Consequently flying insects need to be able to rely on an accurate and fast neurosensory system to inform their neuromotor system.

1.1.3 To avoid crashing, nothing beats a good neurosensory system

Managing to control flight requires the ability to measure, directly or not, the animals' own body motions and to detect perturbations and approaching objects like a looming threat. To do that, flying insects have an elaborate sensory system. Important receptors for flight are:

- Visual sensors, namely compound eyes and ocelli (simple photo-receptors), that allow insects to receive rich information instantaneously from far away. The perceived light can inform insects in detail about the characteristics (e.g. size or orientation) of surroundings objects. Additionally, insects can detect self-motion in reference to the surrounding environment using the apparent motion of neighbouring objects in their own visual field (i.e. optic flow) (Taylor and Krapp, 2007).

- Mechanosensory receptors, such as sensible hairs or antennae. These receptors can inform an insect about sound, or about local air movement. Insects ears are sensitive to minute air particle speed or air pressure changes (Göpfert and Hennig, 2016), whereas more classical airflow sensors are used to measure wind speed or direction (Fuller et al., 2014; Taylor and Krapp, 2007). One of these airflow sensors is the Johnson's organ, that measures motion at the base of antennae. These sensors are crucial for insect flight because they reveal information about the motion of an insect with respect to the surrounding air mass. Such motion can be different from the motion of an insect with respect to a visual frame of reference. For example, a hovering insect in windy condition will not see itself moving, but might be able to feel the wind direction and speed using its airflow sensors. Consequently, these sensors are providing information that is directly relevant for aerodynamic forces and torque production. Some mechanosensory receptors are particularly important for flight because they can measure the linear or angular acceleration of the insect body (i.e. Coriolis forces). For this, some insects such as moths use sensors on their antennae or probably also their wings (Eberle et al., 2015; Hinson and Morgansen, 2015; Pratt et al., 2017; Sane et al., 2007; Taylor and Krapp, 2007), and Dipterans have halteres, club-shaped organs evolved from hindwings. They play the role of vibratory gyroscopes, that oscillate in antiphase to the forewings (Fraenkel and Pringle, 1938; Taylor and Krapp, 2007). In this way, they are used for body stabilization thanks to a simple feedback loop with the wings via the steering muscles (Dickinson, 2006).

- Olfactory sensors, such as receptor neurons on the antennae and specialized mouth parts called the maxillary palps. These sensors can differentiate between many volatile compounds, sometimes at very low concentrations (Sato and Touhara, 2009). Although these sensors are not used for flight control, they can be crucial for navigation during flight. Insects use their olfactory sensors to detect cues indicating the presence of a food source (e.g. CO_2 or ethanol), prey or potential mates (e.g. pheromones).

- Thermo- and hygroreceptors, which can be used to inform insects about environmental conditions, as well as to orient themselves along heat or humidity gradients (Steinbrecht, 1984). Like olfactory sensors, these sensilla are not used for flight control, but can help a flying insect in identifying vertebrates (increased heat and humidity) and navigate close to them (van Breugel et al., 2015; Spitzen et al., 2013).

1.1.4 Studying escape manoeuvres to understand flight mechanics

Much of our understanding on insects sensory and control systems has been gained thanks to experiments with tethered animals (Taylor et al., 2008; Taylor and Krapp, 2007). This is because such experiments allow the direct measurement of insect neurosensory performances as well as the forces and torques generated by the tethered insect; and this while controlling precisely the environment and experimental condition. However, there is a fun-

damental problem with tethered-insect experiments since it breaks the feedback loop that naturally operates in free flight (Taylor et al., 2008). Although one can aim to simulate free-flight conditions to fix such broken loop, these simulated conditions will remain abnormal, and often that will result in exaggerated responses of tethered flying insects (Dawson et al., 2004; Fry et al., 2005). Additionally, to fully understand the adaptive significance of flight physiology (i.e. sensory and control system), one has to understand flight mechanics (Taylor and Krapp, 2007). This is because insect sensors seem to be sensitive to the insect's modes of motion rather than to kinematic quantities such as airspeed. Consequently, to understand how insects control their flights, it is necessary to study the flight mechanics of free-flying insects, and this despite the difficulty of indirect measurements associated with such experiments.

Biomechanical studies on the free-flight manoeuvres of insects (e.g. the motion of body and wings) are still relatively scarce, and these studies focused a few insects such as moths and dragonflies (Greeter and Hedrick, 2016; Li and Dong, 2017; Wang et al., 2008, 2003). *Drosophila* or fruit flies, which are dipterans like mosquitoes, have received the most detailed attention (Dickinson and Muijres, 2016; Fry et al., 2003; Muijres et al., 2014). Therefore, I will mostly discuss manoeuvres of fruit flies, starting with their body saccades, which are performed to change heading between straight flight segments, as well as their escape manoeuvres. The so-called "helicopter model" was shown to describe well the dynamic of fruit flies when manoeuvring (Muijres et al., 2015; Ros et al., 2011). This model describes how some flying animals such as pigeons, cicada, moths and fruit flies (Greeter and Hedrick, 2016; Muijres et al., 2014; Ros et al., 2011; Zeyghami et al., 2016), manoeuvre in an analogous way as helicopters, namely by rotating their bodies to change the direction of the aerodynamic force that they generate. For example, to generate thrust, a helicopter would pitch its nose down (see Fig. 1.3 for the definition of wing angles), and thus direct its aerodynamic force vector forward (David, 1978). Similarly, it was shown that fruit flies are performing body saccades by executing a banked turn, through pitching up and rolling on their side, in a stereotypical way (Muijres et al., 2015). This helicopter model assumes that the change of orientation of the aerodynamic force vector with respect to the animal body will remain small. During a manoeuvre, a flying animal needs to generate changes in its wings kinematics in order to generate the torques required to rotate its body. This will result in variation of the orientation of the aerodynamic force vector in the animal body reference frame, and therefore in the violation of the assumption. However, it appears that in the case of fruit flies, kinematic changes are very subtle and therefore can be mostly ignored when considering if the model apply to them (Cheng et al., 2016; Dickinson and Muijres, 2016). In addition, some large wing kinematic alterations do not contradict the helicopter model, for example, insects can change the magnitude (and not the orientation) of the aerodynamic force that they generate by modulating their wingbeat amplitude and frequency.

Among all manoeuvres done by flying animals, escape manoeuvres are particularly in-
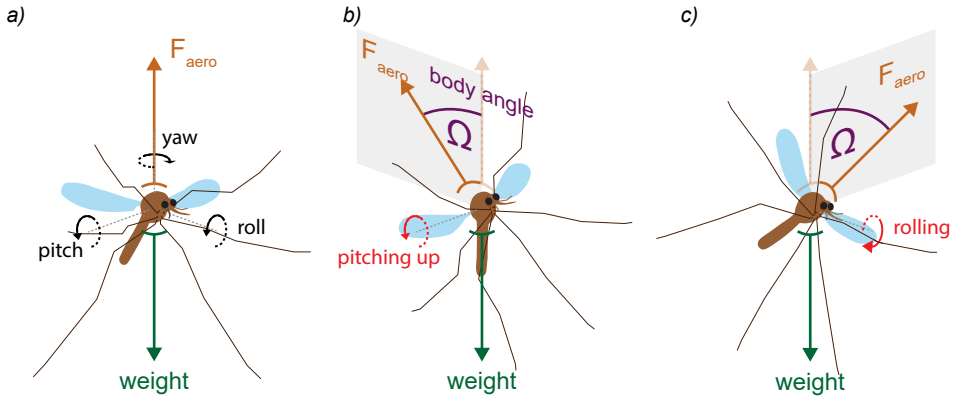
Figure 1.3: How would the helicopter model function for mosquitoes? Although mosquitoes were shown to follow the helicopter model when taking-off (VanVeen et al. 2020), it is still unknown whether they also do so while manoeuvring. (*a*) Schematic of mosquito body angles (yaw, pitch and roll, Tait–Bryan convention), and the forces applied to its body. When hovering, a mosquito generates an upward aerodynamic force equal to its own weight. If the mosquito follows the helicopter model, then it will reorient its aerodynamic force vector by rotating its body during a manoeuvre. (*b*) When pitching up, the mosquito accelerate backward by redirecting its aerodynamic force vector. (*c*) When rolling on its side, the mosquito will make a banked turn.

teresting because they are ecologically and evolutionary relevant behaviours, and this despite being exhibited in relatively rare occasions. When escaping, an animal must exhibit a high flight-mechanical performance as its survival will depend on its success. Such success can result from a short response time, a high locomotor performance and a good escape strategy (Corcoran and Conner, 2016; Domenici et al., 2011; Muijres et al., 2014). Achieving these objectives rely on specific characteristics like having rapidly conducting giant neurons that mediate responses (Bullock, 1984). Therefore, studying escape manoeuvres can teach us about the performances of both the sensory system and the control system of the animal (Card, 2012). And as a consequence, it can help us understand potentially important drivers of evolution.

Escape manoeuvres are usually directed away from the threat or towards a safe area to the side of the attacker (Cheng et al., 2016; Corcoran and Conner, 2016; Muijres et al., 2014). Most insects probably rely on visual cues to detect the attack, but in the dark auditory cues or air gust are also used (Dangles et al., 2006; Ganihar et al., 1994; Ter Hofstede and Ratcliffe, 2016; Hoy et al., 1989; Ritzmann, 1984; Tauber and Camhi, 1995; Triblehorn and Yager, 2006). In particular, the arms race between moths and bat have been the subject of numerous studies (Corcoran and Conner, 2016; Dawson et al., 2004; Ter Hofstede and Ratcliffe, 2016; Kawahara and Barber, 2015; Roeder, 1962), and thus, moths have been shown to use various strategies to detect the attacks and to escape from it, or even to jam bat echolocation (Barber and Kawahara, 2013; Ter Hofstede and Ratcliffe, 2016; Kawahara and Barber, 2015). The reaction to (ultra)sounds of other flying insects such as locusts and praying mantis have also been studied (Roeder, 1962; Yager et al., 1990). And the wind-

evoked escape behaviour of insects such as crickets, cockroaches or praying mantis have also received some attention (Dangles et al., 2006; Ganihar et al., 1994; Ritzmann, 1984; Tauber and Camhi, 1995; Triblehorn et al., 2008; Triblehorn and Yager, 2006). Despite all these behavioural studies, there is much that is still unknown about the escape strategies of many insects and the role of non-visual cues on escape performance of small insects is still poorly understood.

Additionally, there is relatively little research done on the biomechanics of escape manoeuvres and even less on free-flying insects. Here again, *Drosophila* is the insect genus for which flying escape manoeuvres have been studied the most in detail. It was shown that, when "attacked" by a looming object, fruit flies performed evasive manoeuvres by executing visually direct banked turns (Muijres et al., 2014). These manoeuvres consisted of a body rotation -like saccades but much faster – followed immediately by an active counter-rotation. The visual motor delay during the escape was found to be low (around 60 ms), thus indicating the importance of a quick response. Additionally, the delay between the initial bank and counter-bank was found to be even shorter (around 25 ms), which suggest that halteres (the most likely source of very fast feedback) might play a role in the stabilization of such manoeuvres (Bender and Dickinson, 2006; Ristroph et al., 2010). More research is needed to verify if other insects like mosquitoes exhibit similar escape biomechanics.

1.2 Mosquito interaction with vertebrates

1.2.1 Why study the most annoying animal in the world?

Amongst flying insects, mosquitoes (*Culicidae*) are a particularly fascinating family. They are part of the order *Diptera*, which contains more species than all vertebrates together. In this order of insects, most of the research on flight has been done on fruit flies (*Drosophila*) (Dickinson and Muijres, 2016; Fuller et al., 2014; Tammero and Dickinson, 2002). But mosquitoes are an interesting alternative to fruit flies. For example, mosquitoes use a strikingly different wingbeat kinematics than fruit flies do. Fruit flies beat their wings at wingbeat amplitudes around 140°, and at frequencies around 220 Hz (Fry et al., 2005), where mosquito's wingbeat amplitudes and frequencies are respectively much lower (around 40° degrees) and much larger (350–750 Hz) (Bomphrey et al., 2017; Kim et al., 2021). It has been suggested that if mosquitoes exhibit such peculiar wing beat kinematics, it is because that enables efficient generation of high-intensity wing tones for acoustic communications between the males and the females (Seo et al., 2020). Additionally, this way of flying relies on specific aerodynamic mechanisms such as acceleration based lift generation or trailing-edge vortices which have not been observed in any other flying animal (Bomphrey et al., 2017; Veen and van Veen, 2020).

As an insect family, mosquitoes are also interesting from an ecological point of view. Mosquitoes can be found on all continents except Antarctica. They live in various envir-

onments such as tropical forest, plains or cities, and there are both nocturnal and diurnal species of mosquitoes. All of this diversity yield interesting comparisons between closely related species but that might differ on a specific point. For example, day- and night-active mosquitoes might rely very differently on visual information despite being very similar otherwise. Both larvae and adult mosquitoes are a primary source of nutriments for many other species such as dragonflies (both larvae and adults), spiders, fish, amphibians, birds and bats (Card, 2012; Darbro and Harrington, 2007; DuRant and Hopkins, 2008; Hespenheide, 1975; Kunz, 1982; Medlock and Snow, 2008; Raghavendra et al., 2008; Roitberg et al., 2003; Yuval and Bouskila, 1993). As adults, mosquitoes are (important) pollinators (Clements, 1999), and like many dipterans such as tsetse flies and tabanids, the females of most mosquito species need a blood meal to get the necessary proteins to start egg development. Consequently, mosquitoes have to interact with blood hosts. This interaction made them vectors of many deadly pathogens for their hosts and, thus have an effect on the population dynamics of vertebrate populations (Lapointe et al., 2012; Pedersen et al., 2007).

Through their biting habit, anthropophilic mosquitoes had an important impact on the human population and this through the entire course of human history. This is because they are vectors of various dangerous human diseases such as malaria, yellow fever, dengue or Zika. Malaria alone still infected around 229 million people in 2019, and killed an estimated 409,000 people of mostly young children (Who, 2020). This mosquito-borne infectious disease is caused by unicellular parasites from the *Plasmodium* group and is spread by infected female *Anopheles* mosquitoes. The *Aedes* genus is also an important vector of dangerous human pathogens such as the Zika virus, chikungunya virus, yellow fever virus and dengue virus. In addition to their high costs of human lives, mosquito-borne diseases are a great source of discomfort for hundreds of millions of people across the world. And they have a major economic impact on the most severely affected countries (Gallup and Sachs, 2001; Sarma et al., 2019).

Except for the yellow fewer and Japanese encephalitis (Frierson, 2010; Hoke et al., 1988), there is no highly effective and durable vaccine protecting against mosquito-borne disease (Aggarwal and Garg, 2018). In particular, no malaria vaccine is yet available despite promising progress during the past decade (Duffy and Patrick Gorres, 2020). Nevertheless, mostly due to vector control, there has been considerable progress in the fight against malaria over the last century. By focusing on reducing mosquito breeding sites, malaria has been eradicated from North America and Europe in the 1970s, thanks notably to the wide use of DDT (Enayati and Hemingway, 2010). Globally, the population at risk of getting malaria has been reduced from 77% in 1900, to around 40% now. During this period there has been a shift in the population that is most susceptible to die from malaria. Around 90% of malaria deaths occurred outside sub-Saharan Africa in the beginning of the 20th century, while now it is estimated that around 95% of malaria deaths occurs in sub-Saharan African countries (Enayati and Hemingway, 2010; Who, 2020). This shift being partly explained by existing inequalities of access to antimalarial drugs such as chloroquine and malaria vector control tools (Enayati and Hemingway, 2010).

Currently, the most widely used methods of malaria vector control are insecticide-treated mosquito nets (ITNs) and indoor residual spraying (IRS). By preventing biting during the night (when malaria mosquitoes are active) and killing mosquitoes that land on bet nets and walls, these methods have been mostly responsible for the steady decrease of the number of malaria deaths per population at risk over the last 20 years (Pluess et al., 2010; Pryce et al., 2018; Who, 2020). In 2020, almost 70% of households had bed nets in sub-Saharan Africa (Who, 2020). However, this wide use of bed nets resulted in a shift in malaria mosquitoes biting habits towards hours of the evening before people are safe inside their bed nets (Braimah et al., 2005; Carnevale and Manguin, 2021; Mbogo et al., 1996). Also, the insecticides used against mosquitoes can be highly toxic for wild animal species such as insects and aquatic organisms (Rehman et al., 2014). And, maybe most importantly for the fight against malaria, many mosquito species have been found to build resistance against those insecticides (Who, 2020). As a consequence, further decrease in malaria has halted over the last five years. And there is an increasing need for alternative, insecticide-free and novel vector control strategies such as house modification or traps that use mosquito host-seeking behaviour against them (Koenraadt et al., 2021).

1.2.2   Even if you hide, mosquitoes will find you

Mosquitoes have been studied more than any other haematophagous insect family, and their host seeking behaviour has been the subject of a particularly high attention. Thus, we know that, to detect their blood hosts, mosquitoes rely on a variety of host cues that they encounter at a range of distances from the source (i.e. the host) (see Fig. 1.4). At long range (more than 10 metres), mosquitoes are likely to be informed of the presence of a host by detecting the carbon dioxide (CO_2) that it emits (Cardé, 2015). After such detection, mosquitoes will be more sensible to host odours, that will confirm the host presence if also detected (Dekker et al., 2005; McMeniman et al., 2014). At this point, a mosquito still needs to find the source of the CO_2 and odour, for this, mosquitoes use a so-called "cast and surge" behaviour (Dekker and Cardé, 2011; Spitzen et al., 2013). This common insect flight behaviour consists of two different typical flight patterns: if an insect detects an odour plume, it will "surge" upwind in the direction of the odour source (van Breugel and Dickinson, 2014; Cardé and Willis, 2008). Then, when it loses the plume, the insect will "cast" crosswind to detect again the odour plume. When a mosquito reaches one or two metres from its host, it will start to inspect visually interesting and contrasting objects (van Breugel et al., 2015; Hawkes and Gibson, 2016). Finally, when very close to the host, a mosquito will use short-range cues such as heat and local humidity to select a landing spot (Cardé, 2015; McMeniman et al., 2014; Olanga et al., 2010).

There is, however, a notable difference in the host seeking behaviour of the various mosquito species. First, mosquitoes have distinct host preferences, with for instance *Anopheles gambia* and *Aedes aegypti* being highly anthropophilic, whereas species such as *Culex quinquefasciatus* and *Aedes canadensis* are respectively more attracted by birds and

amphibian (Wolff and Riffell, 2018). But already amongst anthropophilic mosquitoes, important differences of host-seeking behaviours have been observed. For instance, *Aedes aegypti* being day-active has been shown to rely greatly on visual cues to detect humans, and also to bite them when active (van Breugel et al., 2015; Cardé et al., 2010; Vinauger et al., 2019). Whereas *An. gambiae* is night-active and consequently often bites humans during their sleep, rely less on vision and only in the presence of host odours (Cardé et al., 2010; Hawkes and Gibson, 2016).
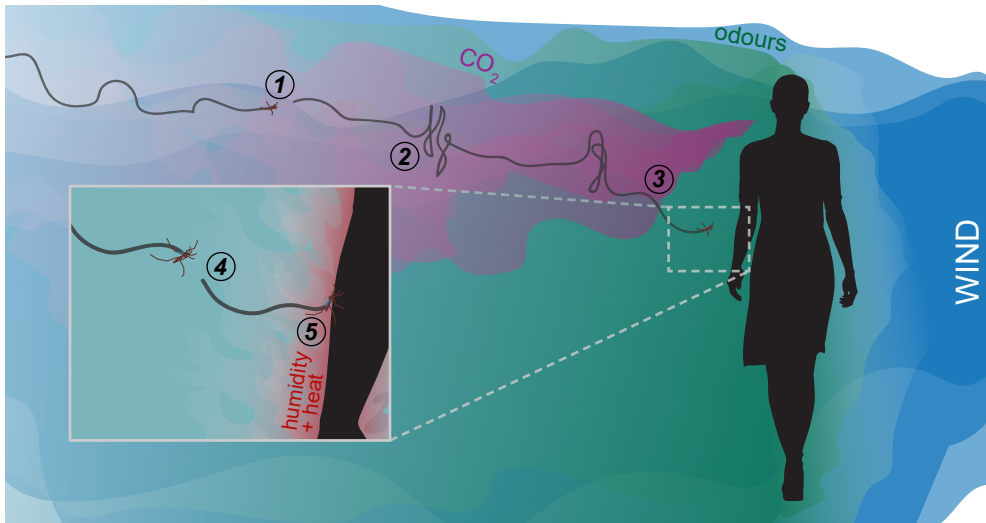

Figure 1.4: Infographic on how mosquitoes detect and fly towards a blood host. (**1**) A flying female mosquito encounters CO_2 and odour plumes. (**2**) The mosquito will surge upwind and cast crosswind to find the source. (**3**) The mosquito will inspect visually interesting objects, and then (**4**) will use short-range host cues such as heat and humidity to select a spot to land (**5**).

Despite all the research done on host-seeking behaviours of mosquitoes, we still have a relatively poor understanding of some of mosquitoes' key flight behaviours when approaching hosts. Indeed, the direct interaction between mosquitoes and their blood hosts have been little studied. And this, despite the fact that such interaction can be very dangerous for the hosts but, of course, also for mosquitoes because a host can exhibit various defensive behaviours (Darbro and Harrington, 2007; Edman et al., 1984; Edman and Scott, 1987; Matherne et al., 2018; Reid et al., 2014; Walker and Edman, 1985). Probably to protect themselves from discomfort, mosquitoes' blood hosts have developed many defensive behaviours such as tail swishing, pecking or swatting (Darbro and Harrington, 2007; Edman et al., 1984; Edman and Scott, 1987; Matherne et al., 2018; Reid et al., 2014; Walker and Edman, 1985). This means that to successfully get a blood meal, mosquitoes must approach, land, bite and take off quickly and undetected. If a mosquito is detected, it needs to be able to escape successfully to avoid being swatted. Except take-off behaviour

(Muijres et al., 2017), all these aspects of mosquito host seeking have not been the subject of detailed studies. Studying flight dynamics close to hosts could then inform us whether mosquitoes developed specific strategies to successfully interact with vertebrates and how they might detect host defensive behaviours. But also, gaining fundamental knowledge on these aspects of mosquito behaviour is likely to yield promising ideas for the development or improvement of vector control strategies such as bed nets, house design or traps.

1.2.3 Mimicking humans or how to fool mosquitoes?

To capture mosquitoes, many different mosquito traps have been developed over the years (Hiscox et al., 2014; Jawara et al., 2009; Kline, 2002; Kröckel et al., 2006). Amongst all these traps, a majority is aimed at capturing host-seeking female mosquitoes by mimicking human host cues (Bhalala and Arias, 2009; Kawada et al., 2007; Kline, 2002). Such traps are called odour-baited traps because they use CO_2 and odour blends to attract mosquitoes in their vicinity. These blends were developed based on the accumulated knowledge from many studies on mosquitoes attraction to CO_2 and chemical compounds such as ammonia and lactic acid (Cardé, 2015; Dekker et al., 2005; van Loon et al., 2015; Verhulst et al., 2009). Odour-baited traps often use counter-flows generated by a fan to, first, diffuse the odour and CO_2 and imitate the convection currents of a host, thus attracting host seeking mosquitoes in their vicinity; and second, capture mosquitoes that would have approached it by sucking them inside the trap (Hiscox et al., 2014; Kröckel et al., 2006). Until recently, odour-baited traps were exclusively used as tools for monitoring mosquito populations. However, they are now being considered as insecticide-free vector control tools that could effectively reduce mosquito populations when combined with bed nets (Hiscox et al., 2014; Homan et al., 2016).

Doing experiments with humans is notoriously difficult to organize because it requires to conform to strict regulations on human experimentation and the participation of volunteers who can be difficult to find. Also, such experiments are by nature limited in reproducibility and will constrain the amount of data that can be acquired. As a consequence, it is often better if we can simulate a human. Odour-baited traps have been designed to simulate human presence, and therefore they could be used to study mosquitoes flight behaviour close to a host. Using these traps, one can test the influence on mosquito behaviours of adding or removing host cues in reproducible experiments. But also, by facilitating the acquisition of large datasets, it opens many possibilities in the type of analysis that can be conducted (e.g. visualization of the average flight behaviour of mosquitoes). Although odour-baited traps will never be able to perfectly mimic humans, they may become valuable tools to study the three-dimensional flight behaviours of mosquitoes, in addition to the previously used wind tunnels and olfactometers (van Breugel et al., 2015; Dekker et al., 2005; Hawkes and Gibson, 2016; Spitzen et al., 2013).

To study escape behaviour of insects, we can probably learn more by simulating an attack than by recreating the conditions of a real one. For example, by systematically testing

how insects react to a simulated attack, we can unravel their escape strategies by computing their average dynamics during the escape. Moreover, we can learn how much a flying insect relies on some cues induced by a real attack by simulating only one or two of these cues. To simulate an attack, most studies tried to reproduce the visual looming target associated with it (Cheng et al., 2016; Muijres et al., 2014; Santer et al., 2012). This is usually done using LED panels, projectors or computer screens surrounding a tethered or freely flying animal. However, by doing so the other cues induced by an attack, especially the air gust, have been mostly ignored. To my knowledge, there is only one study that simulated the airflow conditions of an attack on ground-dwelling insects (i.e. a cricket being attacked by a simulated spider (Dangles et al., 2006), and none have been done on free-flying insects.

Finally, despite the fact that the escape manoeuvres of mosquitoes are probably important in mosquito interaction with humans, there is very little known about them. There have been only a couple of studies on the escape behaviour of mosquitoes during take-off (Muijres et al., 2017; Veen and van Veen, 2020), and none on their escape manoeuvres while flying. Therefore, it is still unknown whether mosquitoes exhibit any particular strategies to escape successfully, for example by using the airflow induced by a swatting hand; or whether nocturnal- and diurnal mosquitoes rely on different cues to detect an attack. Reaching a better understanding on these questions could help in improving current vector control strategies.

1.3 Aims and content of this thesis

With this thesis, I attempt to achieve two goals. My first goal is to contribute to the fundamental understanding of two distinct but related research topics:

1. The escape dynamics of flying insects and how escape strategies might be influenced by environmental conditions such as light intensity or by the airflow generated by an attack.

2. The flight behaviour of host-seeking mosquitoes around odour-baited traps (mimicking humans), and the role of close-range cues in mosquito attractiveness towards or repulsiveness from these traps.

Secondly, I aim to apply previous and new findings for the development of new or improved vector control strategies against mosquitoes. Also, I aim to develop analysis tools and methods that, if used in similar studies, could lead to discoveries on insect flight, especially among dipterans with high ecological or societal importance such as fruit flies, tsetse flies or midges (Sarwar, 2020).

In **chapter 2**, I present a study on mosquito host-seeking behaviour near odour-baited traps (Fig. 1.5). The aim of this study was two-fold. Firstly, to gain a better understanding of mosquito flight behaviours around odour-baited traps. And secondly, to learn about how

flight behaviour of host-seeking mosquitoes was influenced by airflow conditions. For this, we tracked in three-dimensions freely flying female malaria mosquitoes (*Anopheles coluzzii*) around a widely used odour-baited trap, the Suna trap. I used more than 2500 three-dimensional tracks to analyse in detail the flight behaviours of mosquitoes. This was done by visualizing the average flight behaviour of mosquitoes with two-dimensional heat maps of key flight metrics such as mosquito flight speeds or performance metrics such as their probability of capture. Then, by comparing the flight behaviour of mosquitoes around the trap in the hanging or standing orientation (thus changing the airflow conditions), I identified two stereotypical flight behaviours that let to strikingly different performances of the trap in those two orientations. These detailed findings on flight dynamics of mosquitoes informed us on the short-range attractiveness of odour-baited traps, and on whether mosquitoes exhibit escape-like behaviour when close enough to the trap to be captured.

Our findings from chapter 2 led to a collaborative project for the design of a new odour-baited trap. For this purpose, I brought together biomechanicists and entomologists from Wageningen University, and industrial designers from Delft University (The Netherlands). By iteratively testing various trap prototypes, we developed a novel trap, the M-Tego. In **chapter 3**, we systematically tested how the M-Tego performed in capturing malaria mosquitoes when compared with the Suna trap, and how the capture performance of the M-Tego varied if the trap generated additional short-range host cues such as humidity and heat (Fig. 1.5). These tests were conducted in both laboratory and semi-field conditions (Ifakara, Tanzania) to confirm the validity of our laboratory results but in more natural conditions. Then, using a similar but larger experimental setup than in chapter 2, we studied in detail how mosquitoes behaved when flying near the M-Tego with or without additional short-range cues. By visualizing the flight behaviours of mosquitoes on various two-dimensional heat maps, I aim to explain how the addition of short-range cues influences mosquito behaviour in very close vicinity of the trap and to quantify the impact of such addition on its overall capture performance.

With **chapter 4**, I start my focus on escape dynamics by studying the escape performance of diurnal and nocturnal mosquitoes (*Aedes aegypti* and *Anopheles coluzzii*, respectively) under various light conditions (Fig. 1.5). First, the aim of this study is to investigate how well mosquitoes perform when attacked by a looming threat that generates both visual cues and airflow. And secondly, to test whether day- and night-active mosquitoes exhibit different strategies to escape successfully in different light conditions. For this, I tracked free-flying mosquitoes in three dimensions and in real time. Based on this, I automatically triggered a mechanical swatter to simulate attacks. Then, I systematically tested how the flight dynamics of mosquitoes varied when attacked in various light conditions ranging from darkness to overcast daylight. Thus, by using thousands of tracks, I investigate whether the two species relied on different strategies to avoid collision. Finally, I examined how differences in the strategies of these diurnal and nocturnal species correlated with light condition and what this might mean concerning the evolution of these species.

In the last research chapter, **chapter 5**, I study the role of the airflow induced by an
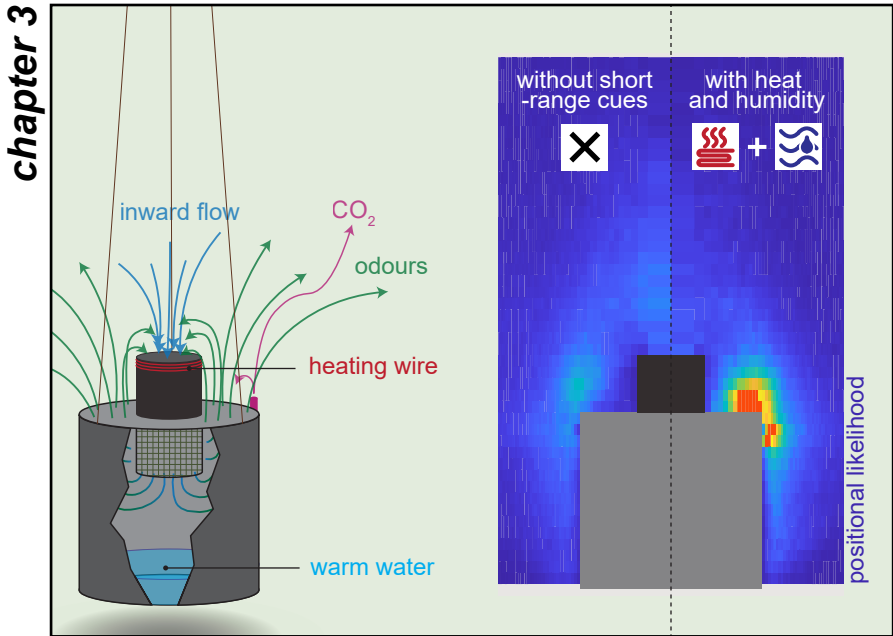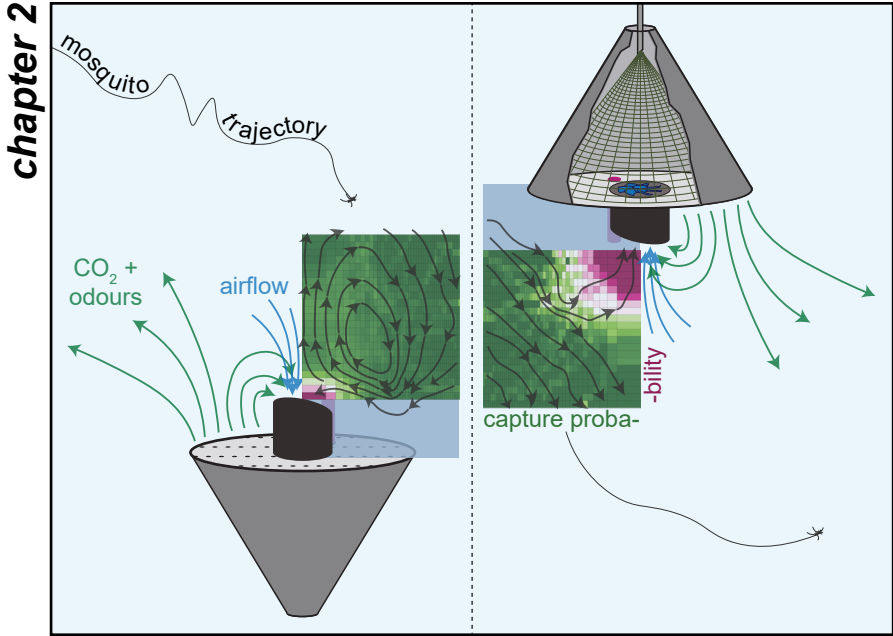
Figure 1.5: Graphical summary of the research chapters. In chapter 2, I studied how flying mosquitoes behaved around an odour-baited trap either standing or hanging. In chapter 3, I tested whether adding heat and humidity to an odour-baited trap resulted in improved trapping performance, and how this impacted mosquito flight behaviour.
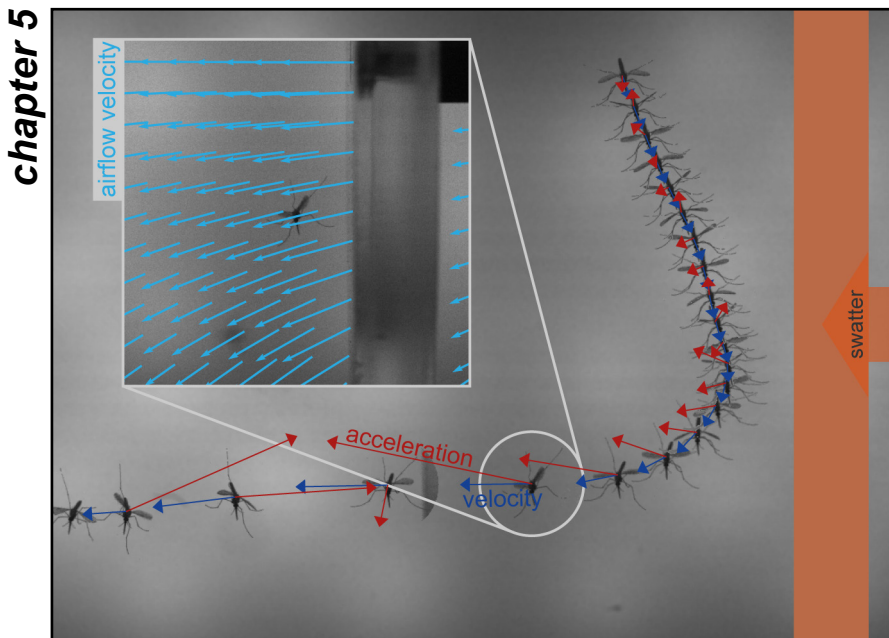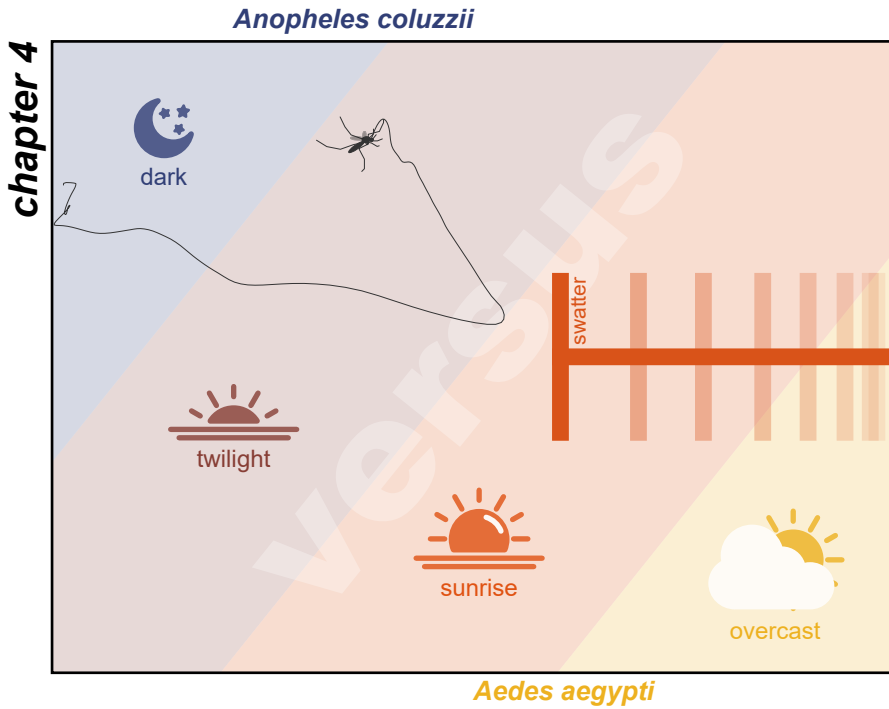
Figure 1.5: Graphical summary of the research chapters. In chapter 4, I investigated how the escape performance of diurnal (*Aedes*) and nocturnal (*Anopheles*) mosquitoes varied with light conditions, as well as what were their respective escaping strategies. Finally, in chapter 5, I examined how mosquitoes performed escape manoeuvres and what was the role of the airflow induced by the attacker in their escape success.

attack in the escape dynamics of the nocturnal mosquito *Anopheles coluzzii* (Fig. 1.5). The aim of this chapter is to understand how nocturnal mosquitoes are able to perform successful escapes in conditions where little to no visual information about the attack is available. Using the same experimental setup as in chapter 4,, I compared the escape performances of mosquitoes by varying the amount of air movement generated by a solid or a perforated swatter. Then, I tracked the body and wings kinematics of mosquitoes using high-speed videography (12500 fps) and a specially developed tracking tool based on a deep-learning network for pose estimation. This allows me to describe mosquito escape manoeuvres in detail and, combined with results from validated numerical simulations of the airflow, to estimate the aerodynamic forces generated during mosquito manoeuvres. Thus, I can evaluate how much mosquitoes themselves contributed to these manoeuvres, and consequently whether the airflow induced by the attack had any passive effect on mosquito escape dynamics or whether it triggered an active response.

In the **chapter 6**, I summarize our findings and integrate them with the existing knowledge on insect flight and on insect–vertebrate interactions. I address how our results inform us about mosquito interactions with humans and in particular about disruptive cues for mosquitoes. Then, I examine the strengths and limitations of my approach for studying the flight dynamics of insects, and how our studies on escape manoeuvres inform us on the physiology of insect flight. Moreover, I suggest directions for future research on key flight behaviours of mosquitoes. Finally, I describe how detailed knowledge on flight behaviour can be used for the development of vector control tools by resuming the development of the M-Tego trap, and by suggesting ideas for further improvements of such tools.

References

Aggarwal, A. and Garg, N. (2018). Newer vaccines against mosquito-borne diseases. *Indian J. Pediatr.* **85**, 406–407.

Alexander, D. E. (2018). A century and a half of research on the evolution of insect flight. *Arthropod Struct. Dev.* **47**, 322–327.

Allan, S. A., Day, J. F. and Edman, J. D. (1987). Visual ecology of biting flies. *Annu. Rev. Entomol.* **32**, 297–316.

Barber, J. R. and Kawahara, A. Y. (2013). Hawkmoths produce anti-bat ultrasound. *Biol. Lett.* **9**.

Bender, J. A. and Dickinson, M. H. (2006). A comparison of visual and haltere-mediated feedback in the control of body saccades in Drosophila melanogaster. *J. Exp. Biol.* **209**, 4597–4606.

Bhalala, H. and Arias, J. R. (2009). The Zumba mosquito trap and BG-Sentinel trap: Novel surveillance tools for host-seeking mosquitoes. *J. Am. Mosq. Control Assoc.* **25**, 134–139.

Birch, J. M. and Dickinson, M. H. (2003). The influence of wing-wake interactions on the production of aerodynamic forces in flapping flight. *J. Exp. Biol.* **206**, 2257–2272.

Bomphrey, R. J., Nakata, T., Phillips, N. and Walker, S. M. (2017). Smart wing rotation and trailing-edge vortices enable high frequency mosquito flight. *Nature* **544**, 92–95.

Braimah, N., Drakeley, C., Kweka, E., Mosha, F., Helinski, M., Pates, H., Maxwell, C., Massawe, T., Kenward, M. G. and Curtis, C. (2005). Tests of bednet traps (Mbita traps) for monitoring mosquito populations and time of biting in Tanzania and possible impact of prolonged insecticide treated net use. *Int. J. Trop. Insect Sci.* **25**, 208–213.

Bullock, T. H. (1984). Comparative Neuroethology of Startle, Rapid Escape, and Giant Fiber-Mediated Responses. In *Neural Mech. Startle Behav.*, pp. 1–13. Springer US.

Card, G. M. (2012). Escape behaviors in insects. *Curr. Opin. Neurobiol.* **22**, 180–186.

Cardé, R. T. (2015). Multi-cue integration: How female mosquitoes locate a human host. *Curr. Biol.* **25**, R793–r795.

Cardé, R. T., Gibson, G., Cardé, T. R. and Gibson, G. (2010). Host finding by female mosquitoes : mechanisms of orientation to host odours and other cues. In *Olfaction Vector-Host Interact.*, volume 2, pp. 115–136. Wageningen Academic Publishers.

Cardé, R. T. and Willis, M. A. (2008). Navigational strategies used by insects to find distant, wind-borne sources of odor. *J. Chem. Ecol.* **34**, 854–866.

Carnevale, P. and Manguin, S. (2021). Review of issues on residual malaria transmission. *J. Infect. Dis.* **223**, S61–s80.

Cheng, B., Tobalske, B. W., Powers, D. R., Hedrick, T. L., Wethington, S. M., Chiu, G. T. C. and Deng, X. (2016). Flight mechanics and control of escape manoeuvres in

hummingbirds. I. Flight kinematics. *J. Exp. Biol.* **219**, 3518–3531.

Clements, A. N. (1999). *The biology of mosquitoes. Volume 2: sensory reception and behaviour*, volume 2. CABI Publishing, 752 pp.

Corcoran, A. J. and Conner, W. E. (2016). How moths escape bats: predicting outcomes of predator-prey interactions. *J. Exp. Biol.* **219**, 2704–2715.

Crampton, G. (1916). The phylogenetic origin and the nature of the wings of insects according to the paranotal theory. *New York Entomol. Soc.* **24**, 1–39.

Dangles, O., Ory, N., Steinmann, T., Christides, J. P. and Casas, J. (2006). Spider's attack versus cricket's escape: velocity modes determine success. *Anim. Behav.* **72**, 603–610.

Darbro, J. M. and Harrington, L. C. (2007). Avian defensive behavior and blood-feeding success of the West Nile vector mosquito, Culex pipiens. *Behav. Ecol.* **18**, 750–757.

David, C. (1978). The relationship between body angle and flight speed in free-flying Drosophila. *Physiol. Entomol.* **3**, 191–195.

Dawson, J. W., Kutsch, W. and Robertson, R. M. (2004). Auditory-evoked evasive manoeuvres in free-flying locusts and moths. *J. Comp. Physiol. A Neuroethol. Sensory, Neural, Behav. Physiol.* **190**, 69–84.

Dekker, T. and Cardé, R. T. (2011). Moment-to-moment flight manoeuvres of the female yellow fever mosquito (Aedes aegypti L.) in response to plumes of carbon dioxide and human skin odour. *J. Exp. Biol.* **214**, 3480–3494.

Dekker, T., Geier, M. and Cardé, R. T. (2005). Carbon dioxide instantly sensitizes female yellow fever mosquitoes to human skin odours. *J. Exp. Biol.* **208**, 2963–2972.

Dickinson, M. (2006). Insect flight. *Curr. Biol.* **16**.

Dickinson, M. H. and Muijres, F. T. (2016). The aerodynamics and control of free flight Manoeuvres in Drosophila. *Philos. Trans. R. Soc. B Biol. Sci.* **371**, 20150388.

Domenici, P., Blagburn, J. M. and Bacon, J. P. Animal escapology II: Escape trajectory case studies.

Dudley, R. (2000). The evolutionary physiology of animal flight: Paleobiological and present perspectives. *Annu. Rev. Physiol.* **62**, 135–155.

Dudley, R. and Yanoviak, S. P. (2011). Animal aloft: The origins of aerial behavior and flight. In *Integr. Comp. Biol.*, volume 51, pp. 926–936. Oxford Academic.

Duffy, P. E. and Patrick Gorres, J. (2020). Malaria vaccines since 2000: progress, priorities, products. *npj Vaccines* **5**, 1–9.

DuRant, S. E. and Hopkins, W. A. (2008). Amphibian predation on larval mosquitoes. *Can. J. Zool.* **86**, 1159–1164.

Eberle, A. L., Dickerson, B. H., Reinhall, P. G. and Daniel, T. L. (2015). A new twist on gyroscopic sensing: body rotations lead to torsion in flapping, flexing insect wings.

J. R. Soc. Interface **12**, 20141088.

Edman, J. D., Day, J. F. and Walker, E. D. (1984). Field confirmation of laboratory observations on the differential antimosquito behavior of herons. *Condor* **86**, 91.

Edman, J. D. and Scott, T. W. (1987). Host defensive behaviour and the feeding success of mosquitoes. *Int. J. Trop. Insect Sci.* **8**, 617–622.

Ellington, C. P., Van Berg, C. D., Willmott, A. P. and Thomas, A. L. (1996). Leading-edge vortices in insect flight. *Nature* **384**, 626–630.

Enayati, A. and Hemingway, J. (2010). Malaria management: Past, present, and future. *Annu. Rev. Entomol.* **55**, 569–591.

Engel, M. S. and Grimaldi, D. A. (2004). New light shed on the oldest insect. *Nature* **427**, 627–630.

Fraenkel, G. and Pringle, J. W. (1938). Halteres of flies as gyroscopic organs of equilibrium. *Nature* **141**, 919–920.

Frierson, J. G. (2010). The yellow fever vaccine: A history. *Yale J. Biol. Med.* **83**, 77–85.

Fry, S. N., Sayaman, R. and Dickinson, M. H. (2003). The aerodynamics of free-flight, maneuvers in Drosophila. *Science (80-.).* **300**, 495–498.

Fry, S. N., Sayaman, R. and Dickinson, M. H. (2005). The aerodynamics of hovering flight in Drosophila. *J. Exp. Biol.* **208**, 2303–2318.

Fuller, S. B., Straw, A. D., Peek, M. Y., Murray, R. M. and Dickinson, M. H. (2014). Flying Drosophila stabilize their vision-based velocity controller by sensing wind with their antennae. *Proc. Natl. Acad. Sci. U. S. A.* **111**, E1182–e1191.

Gallup, J. L. and Sachs, J. D. (2001). The economic burden of malaria: Cross-country evidence. *Am. J. Trop. Med. Hyg.* **64**, 85–96.

Ganihar, D., Libersat, F., Wendler, G. and Camhi, J. M. (1994). Wind-evoked evasive responses in flying cockroaches. *J. Comp. Physiol. A Neuroethol. Sensory, Neural, Behav. Physiol.* **175**, 49–65.

Göpfert, M. C. and Hennig, R. M. (2016). Hearing in Insects. *Annu. Rev. Entomol.* **61**, 257–276.

Greeter, J. S. and Hedrick, T. L. (2016). Direct lateral maneuvers in hawkmoths. *Biol. Open* **5**, 72–82.

Ha, N. S., Truong, Q. T., Goo, N. S. and Park, H. C. (2013). Relationship between wingbeat frequency and resonant frequency of the wing in insects. *Bioinspiration and Biomimetics* **8**, 046008.

Hamilton, K. (1971). The insect wing, Part I. Origin and development of wings from notal lobes. *J. Kansas Entomol. Soc.* **44**, 421–433.

Hawkes, F. and Gibson, G. (2016). Seeing is believing: the nocturnal malarial mosquito Anopheles coluzzii responds to visual host-cues when odour indicates a host is nearby.

Parasites and Vectors **9**, 320.

Hespenheide, H. A. (1975). Selective predation by two swifts and a swallow in Central America. *Ibis (Lond. 1859).* **117**, 82–99.

Hinson, B. T. and Morgansen, K. A. (2015). Gyroscopic sensing in the wings of the hawk-moth Manduca sexta: The role of sensor location and directional sensitivity. *Bioinspiration and Biomimetics* **10**, 056013.

Hiscox, A., Otieno, B., Kibet, A., Mweresa, C. K., Omusula, P., Geier, M., Rose, A., Mukabana, W. R. and Takken, W. (2014). Development and optimization of the Suna trap as a tool for mosquito monitoring and control. *Malar. J.* **13**, 257.

Hoke, C. H., Nisalak, A., Sangawhipa, N., Jatanasen, S., Laorakapongse, T., Innis, B. L., Kotchasenee, S.-o., Gingrich, J. B., Latendresse, J., Fukai, K. et al. (1988). Protection against Japanese Encephalitis by Inactivated Vaccines. *N. Engl. J. Med.* **319**, 608–614.

Homan, T., Hiscox, A., Mweresa, C. K., Masiga, D., Mukabana, W. R., Oria, P., Maire, N., Pasquale, A. D., Silkey, M., Alaii, J. et al. (2016). The effect of mass mosquito trapping on malaria transmission and disease burden (SolarMal): a stepped-wedge cluster-randomised trial. *Lancet* **388**, 1193–1201.

Hoy, R., Nolen, T. and Brodfuehrer, P. (1989). The neuroethology of acoustic startle and escape in flying insects. *J. Exp. Biol.* **146**, 287–306.

Jawara, M., Smallegange, R. C., Jeffries, D., Nwakanma, D. C., Awolola, T. S., Knols, B. G. J., Takken, W. and Conway, D. J. (2009). Optimizing odor-baited trap methods for collecting mosquitoes during the malaria season in the Gambia. *PLoS One* **4**.

Kawada, H., Honda, S. and Takagi, M. (2007). Comparative laboratory study on the reaction of Aedes aegypti and Aedes albopictus to different attractive cues in a mosquito trap. *J. Med. Entomol.* **44**, 427–432.

Kawahara, A. Y. and Barber, J. R. (2015). Tempo and mode of antibat ultrasound production and sonar jamming in the diverse hawkmoth radiation. *Proc. Natl. Acad. Sci. U. S. A.* **112**, 6407–6412.

Kim, D., DeBriere, T. J., Cherukumalli, S., White, G. S. and Burkett-Cadena, N. D. (2021). Infrared light sensors permit rapid recording of wingbeat frequency and bioacoustic species identification of mosquitoes. *Sci. Rep.* **11**, 10042.

Kline, D. L. (2002). Evaluation of various models of propane-powered mosquito traps. *J. Vector Ecol.* **27**, 1–7.

Koenraadt, C. J., Spitzen, J. and Takken, W. (2021). *Innovative strategies for vector control*, volume 6 of *Ecology and Control of Vector-borne Diseases*. The Netherlands: Wageningen Academic Publishers.

Kröckel, U., Rose, A., Eiras, Á. E. and Geier, M. (2006). New tools for surveillance of adult yellow fever mosquitoes: Comparison of trap catches with human landing rates

in an urban environment. *J. Am. Mosq. Control Assoc.* **22**, 229–238.

Kuhl, H., Frankl-Vilches, C., Bakker, A., Mayr, G., Nikolaus, G., Boerno, S. T., Klages, S., Timmermann, B. and Gahr, M. (2021). An unbiased molecular approach using 3'-UTRs resolves the avian family-level tree of life. *Mol. Biol. Evol.* **38**, 108–127.

Kukalová-Peck, J. (1983). Origin of the insect wing and wing articulation from the arthropodan leg. *Can. J. Zool.* **61**, 1618–1669.

Kunz, T. H. (1982). *Ecology of bats*. Springer.

Lapointe, D. A., Atkinson, C. T. and Samuel, M. D. (2012). Ecology and conservation biology of avian malaria. *Ann. N. Y. Acad. Sci.* **1249**, 211–226.

Li, C. and Dong, H. (2017). Wing kinematics measurement and aerodynamics of a dragonfly in turning flight. *Bioinspiration and Biomimetics* **12**, 026001.

Linz, D. M. and Tomoyasu, Y. (2018). Dual evolutionary origin of insect wings supported by an investigation of the abdominal wing serial homologs in Tribolium. *Proc. Natl. Acad. Sci. U. S. A.* **115**, E658–e667.

Matherne, M. E., Cockerill, K., Zhou, Y., Bellamkonda, M. and Hu, D. L. (2018). Mammals repel mosquitoes with their tails. *J. Exp. Biol.* **221**, jeb178905.

Mbogo, C. N., Baya, N. M., Ofulla, A. V., Githure, J. I. and Snow, R. W. (1996). The impact of permethrin-impregnated bednets on malaria vectors of the Kenyan coast. *Med. Vet. Entomol.* **10**, 251–259.

McMeniman, C. J., Corfas, R. A., Matthews, B. J., Ritchie, S. A. and Vosshall, L. B. (2014). Multimodal integration of carbon dioxide and other sensory cues drives mosquito attraction to humans. *Cell* **156**, 1060–1071.

Medlock, J. M. and Snow, K. (2008). Natural predators and parasites of British mosquitoes–a review. *Eur. Mosq. Bull.* **25**, 1–11.

Muijres, F. T., Chang, S. W., van Veen, W. G., Spitzen, J., Biemans, B. T. T., Koehl, M. A. R. and Dudley, R. (2017). Escaping blood-fed malaria mosquitoes minimize tactile detection without compromising on take-off speed. *J. Exp. Biol.* **220**, 3751–3762.

Muijres, F. T., Elzinga, M. J., Iwasaki, N. A. and Dickinson, M. H. (2015). Body saccades of Drosophila consist of stereotyped banked turns. *J. Exp. Biol.* **218**, 864–875.

Muijres, F. T., Elzinga, M. J., Melis, J. M., Dickinson, M. H., Florian T. Muijres, 1 Michael J. Elzinga, 1 Johan M. Melis, 1, . M. H. D. and Avoiding (2014). Flies evade looming targets by executing rapid visually directed banked turns. *Science (80-.).* **344**, 172–7.

Olanga, E. A., Okal, M. N., Mbadi, P. A., Kokwaro, E. D. and Mukabana, W. R. (2010). Attraction of Anopheles gambiae to odour baits augmented with heat and moisture. *Malar. J.* **9**, 6.

Pedersen, A. B., Jones, K. E., Nunn, C. L. and Altizer, S. (2007). Infectious diseases and extinction risk in wild mammals. *Conserv. Biol.* **21**, 1269–1279.

Pluess, B., Tanser, F. C., Lengeler, C. and Sharp, B. L. (2010). Indoor residual spraying for preventing malaria. *Cochrane Database Syst. Rev.* **2010**.

Pratt, B., Deora, T., Mohren, T. and Daniel, T. (2017). Neural evidence supports a dual sensory-motor role for insect wings. *Proc. R. Soc. B Biol. Sci.* **284**.

Pringle, J. W. (1978). Stretch activation of muscle: function and mechanism. *Proc. R. Soc. London - Biol. Sci.* **201**, 107–130.

Pryce, J., Richardson, M. and Lengeler, C. (2018). Insecticide-treated nets for preventing malaria. *Cochrane Database Syst. Rev.* **2018**.

Raghavendra, K., Sharma, P. and Dash, A. P. (2008). Biological control of mosquito populations through frogs: Opportunities & constrains. *Indian J. Med. Res.* **128**, 22–25.

Rainey, R. C. (1978). The evolution and ecology of flight: the "oceanographic" approach. In *Evol. Insect Migr. Diapause*, pp. 33–48. Springer, New York, NY.

Rehman, H., Aziz, A. T., Saggu, S., Abbas, Z. K., Mohan, A. and Ansari, A. A. (2014). Systematic review on pyrethroid toxicity with special reference to deltamethrin. *J. Entomol. Zool. Stud. JEZS* **2**, 60–70.

Reid, J. N., Hoffmeister, T. S., Hoi, A. G. and Roitberg, B. D. (2014). Bite or flight: The response of mosquitoes to disturbance while feeding on a defensive host. *Entomol. Exp. Appl.* **153**, 240–245.

Ristroph, L., Bergou, A. J., Ristroph, G., Coumes, K., Berman, G. J., Guckenheimer, J., Wang, Z. J. and Cohen, I. (2010). Discovering the flight autostabilizer of fruit flies by inducing aerial stumbles. *Proc. Natl. Acad. Sci. U. S. A.* **107**, 4820–4824.

Ritzmann, R. E. (1984). The Cockroach Escape Response. In *Neural Mech. Startle Behav.*, pp. 93–131. Springer US.

Roeder, K. D. (1962). The behaviour of free flying moths in the presence of artificial ultrasonic pulses. *Anim. Behav.* **10**, 300–304.

Roitberg, B. D., Mondor, E. B. and Tyerman, J. G. (2003). Pouncing spider, flying mosquito: Blood acquisition increases predation risk in mosquitoes. *Behav. Ecol.* **14**, 736–740.

Ros, I. G., Bassman, L. C., Badger, M. A., Pierson, A. N. and Biewener, A. A. (2011). Pigeons steer like helicopters and generate down-and upstroke lift during low speed turns. *Proc. Natl. Acad. Sci. U. S. A.* **108**, 19990–19995.

Sane, S. P. (2003). The aerodynamics of insect flight. *J. Exp. Biol.* **206**, 4191–4208.

Sane, S. P., Dieudonné, A., Willis, M. A. and Daniel, T. L. (2007). Antennal mechanosensors mediate flight control in moths. *Science (80-.).* **315**, 863–866.

Santer, R. D., Rind, F. C. and Simmons, P. J. (2012). Predator versus prey: locust looming-detector neuron and behavioural responses to stimuli representing attacking bird predators. *PLoS One* **7**, e50146.

Sarma, N., Patouillard, E., Cibulskis, R. E. and Arcand, J. L. (2019). The economic

burden of Malaria: Revisiting the evidence. *Am. J. Trop. Med. Hyg.* **101**, 1405–1415.

Sarwar, M. (2020). Typical flies: Natural history, lifestyle and diversity of Diptera. In *Life Cycle Dev. Diptera*. IntechOpen.

Sato, K. and Touhara, K. (2009). Insect olfaction: Receptors, signal transduction, and behavior. *Results Probl. Cell Differ.* **47**, 121–138.

Schmidt-Nielsen, K. (1972). Locomotion: Energy cost of swimming, flying, and running. *Science (80-.).* **177**, 222–228.

Seo, J. H., Hedrick, T. L. and Mittal, R. (2020). Mechanism and scaling of wing tone generation in mosquitoes. *Bioinspiration and Biomimetics* **15**, 0–12.

Solari, S. and Baker, R. J. (2007). Mammal species of the world: a taxonomic and geographic reference. *J. Mammal.* **88**, 824–830.

Spitzen, J., Spoor, C. W., Grieco, F., ter Braak, C., Beeuwkes, J., Van Brugge, S. P., Kranenbarg, S., Noldus, L. P. J. J., van Leeuwen, J. L. and Takken, W. (2013). A 3D analysis of flight behavior of Anopheles gambiae sensu stricto malaria mosquitoes in response to human odor and heat. *PLoS One* **8**, 1–12.

Steinbrecht, R. A. (1984). Chemo-, Hygro-, and Thermoreceptors. In *Biol. Integument*, pp. 523–553. Springer Berlin Heidelberg.

Stork, N. E. (2018). How many species of insects and other terrestrial arthropods are there on Earth? *Annu. Rev. Entomol.* **63**, 31–45.

Tammero, L. F. and Dickinson, M. H. (2002). Collision-avoidance and landing responses are mediated by separate pathways in the fruit fly, Drosophila melanogaster. *J. Exp. Biol.* **205**, 2785–2798.

Tauber, E. and Camhi, J. M. (1995). The wind-evoked escape behavior of the cricket Gryllus bimaculatus: Integration of behavioral elements. *J. Exp. Biol.* **198**, 1895–1907.

Taylor, G. K., Bacic, M., Bomphrey, R. J., Carruthers, A. C., Gillies, J., Walker, S. M. and Thomas, A. L. (2008). New experimental approaches to the biology of flight control systems. In *J. Exp. Biol.*, volume 211, pp. 258–266.

Taylor, G. K. and Krapp, H. G. (2007). Sensory systems and flight stability: what do insects measure and why? *Adv. In Insect Phys.* **34**, 231–316.

Templin, R. J. (2000). Spectrum of animal flight: Insects to pterosaurs. *Prog. Aerosp. Sci.* **36**, 393–436.

Ter Hofstede, H. M. and Ratcliffe, J. M. (2016). Evolutionary escalation: The bat-moth arms race. *J. Exp. Biol.* **219**, 1589–1602.

Triblehorn, J. D., Ghose, K., Bonn, K., Moss, C. F. and Yager, D. D. (2008). Free-flight encounters between praying mantids (Parasphendale agrionina) and bats (Eptesicus fuscus). *J. Exp. Biol.* **211**, 555–562.

Triblehorn, J. D. and Yager, D. D. (2006). Wind generated by an attacking bat: Anemometric measurements and detection by the praying mantis cercal system. *J. Exp. Biol.*

209, 1430–1440.

van Breugel, F. and Dickinson, M. H. (2014). Plume-tracking behavior of flying drosophila emerges from a set of distinct sensory-motor reflexes. *Curr. Biol.* **24**, 274–286.

van Breugel, F., Riffell, J., Fairhall, A. and Dickinson, M. H. (2015). Mosquitoes use vision to associate odor plumes with thermal targets. *Curr. Biol.* **25**, 2123–2129.

van Loon, J. J. J. A., Smallegange, R. C., Bukovinszkiné-Kiss, G., Jacobs, F., De Rijk, M., Mukabana, W. R., Verhulst, N. O., Menger, D. J. and Takken, W. (2015). Mosquito attraction: crucial role of carbon dioxide in formulation of a five-component blend of human-derived volatiles. *J. Chem. Ecol.* **41**, 567–73.

Veen, W. G. V. and van Veen, W. G. (2020). *Aerodynamics of insect flight.* Ph.D. thesis, University of Wageningen.

Verhulst, N. O., Beijleveld, H., Knols, B. G., Takken, W., Schraa, G., Bouwmeester, H. J. and Smallegange, R. C. (2009). Cultured skin microbiota attracts malaria mosquitoes. *Malar. J.* **8**, 1–12.

Vinauger, C., van Breugel, F., Locke, L. T., Tobin, K. K., Dickinson, M. H., Fairhall, A. L., Akbari, O. S. and Riffell, J. A. (2019). Visual-olfactory integration in the human disease vector mosquito Aedes aegypti. *Curr. Biol.* **29**, 2509–2516.e5.

Wagner, H. (1986). Flight performance and visual control of flight of the free-flying housefly (Musca domestica L.) I. Organization of the flight motor. *Philos. Trans. R. Soc. London. B, Biol. Sci.* **312**, 527–551.

Walker, E. D. and Edman, J. D. (1985). The influence of host defensive behavior on mosquito (diptera: culicidae) biting persistence. *J. Med. Entomol.* **22**, 370–372.

Walker, S. M., Schwyn, D. A., Mokso, R., Wicklein, M., Müller, T., Doube, M., Stampanoni, M., Krapp, H. G. and Taylor, G. K. (2014). In vivo time-resolved microtomography reveals the mechanics of the blowfly flight motor. *PLoS Biol.* **12**, 1001823.

Wang, H., Ando, N. and Kanzaki, R. (2008). Active control of free flight manoeuvres in a hawkmoth, Agrius convolvuli. *J. Exp. Biol.* **211**, 423–432.

Wang, H., Zeng, L., Liu, H. and Yin, C. (2003). Measuring wing kinematics, flight trajectory and body attitude during forward flight and turning maneuvers in dragonflies. *J. Exp. Biol.* **206**, 745–757.

Who (2020). *World Malaria Report 2020*, volume 73. WHO Press, Geneva, 1–4 pp.

Wolff, G. H. and Riffell, J. A. (2018). Olfaction, experience and neural mechanisms underlying mosquito host preference. *J. Exp. Biol.* **221**.

Wootton, R. J. (1992). Functional morphology of insect wings. *Annu. Rev. Entomol.* **37**, 113–140.

Yager, D. D., May, M. L. and Fenton, M. B. (1990). Ultrasound-triggered, flight-gated evasive maneuvers in the praying mantis Parasphendale agrionina. I. Free flight. *J. Exp. Biol.* **152**, 17–39.

Yuval, B. and Bouskila, A. (1993). Temporal dynamics of mating and predation in mosquito swarms. *Oecologia* **95**, 65–69.

Zeyghami, S., Babu, N. and Dong, H. (2016). Cicada (Tibicen linnei) steers by force vectoring. *Theor. Appl. Mech. Lett.* **6**, 107–111.

I
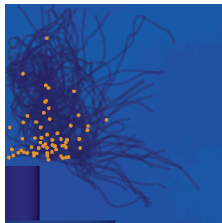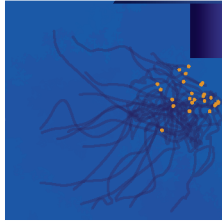
Chapter 2

Flight behaviour of malaria mosquitoes around odour-baited traps: capture and escape dynamics

Antoine Cribellier[1], Jens A. van Erp[1], Alexandra Hiscox[2], Martin J. Lankheet[1], Johan L. van Leeuwen[1], Jeroen Spitzen[2], Florian T. Muijres[1]

[1] Experimental Zoology Group, Wageningen University & Research, Wageningen, The Netherlands

[2] Laboratory of Entomology, Wageningen University & Research, Wageningen, The Netherlands

Abstract

Host-seeking mosquitoes rely on a range of sensory cues to find and approach blood hosts, as well as to avoid host detection. By using odour blends and visual cues that attract anthropophilic mosquitoes, odour-baited traps has been developed to monitor and control human pathogen-transmitting vectors. Although long-range attraction of such traps have already been studied thoroughly, close-range response of mosquitoes to these traps has been largely ignored. Here, we studied the flight behaviour of female malaria mosquitoes (*Anopheles coluzzii*) in the immediate vicinity of a commercially-available odour-baited trap, positioned in a hanging and standing orientation. By analysing more than 2500 three-dimensional flight tracks, we elucidated how mosquitoes reacted to the trap, and how this led to capture. The measured flight dynamics revealed two distinct stereotypical behaviours: 1) mosquitoes that approached a trap tended to simultaneously fly downward towards the ground; 2) mosquitoes that came close to a trap changed their flight direction by rapidly accelerating upward. The combination of these behaviours led to strikingly different flight patterns and capture dynamics, resulting in contrasting short-range attractiveness and capture mechanism of the oppositely-oriented traps. These new insights may help in improving odour-baited traps, and consequently their contribution in global vector control strategies.

2.1 Introduction

Haematophagous insects need blood meals for reproduction. As a result, they have to interact with vertebrate hosts that have various defence strategies and that are sometimes even their predators. Thus, mosquitoes need to minimize the risk induced by this interaction with their host by feeding quickly, stealthily and effectively (Lazzari, 2009; Muijres et al., 2017). Additionally, when approaching a host, mosquitoes must be aware of any cues announcing host defensive behaviours such as looming objects or air gusts. Surprisingly, the impact of such disruptive cues on the short-range attraction of anthropophagic mosquitoes towards human hosts has been studied very little (Edman and Scott, 1987; Vinauger et al., 2018). Actually, mosquito flight dynamics in reaction to humans or objects imitating hosts also received little attention (Cooperband and Cardé, 2006a).

By contrast, the odour-mediated host-seeking behaviour of mosquitoes has been studied extensively, because it is relevant for mosquito population management (vector control). Anthropophilic female mosquitoes are attracted to their hosts by a species-specific cocktail of human odours and CO_2 (Dekker and Cardé, 2011; McMeniman et al., 2014; Takken and Verhulst, 2013). When a host-seeking mosquito encounters these cues, it performs a stereotypical 'cast and surge' flight behaviour in order to locate the host (van Breugel et al., 2015; Dekker and Cardé, 2011; Spitzen et al., 2013). Similar flight behaviour is observed in many species of insects, such as moths, fruit flies and mosquitoes to find potential mates, food or hosts, respectively (Baker and Haynes, 1987; van Breugel and Dickinson, 2014; Cardé and Willis, 2008).

Detailed studies on host-seeking behaviour showed that flying *Aedes aegypti* mosquitoes (vectors of e.g. dengue and Zika fever) use a combination of cues to find and approach hosts (Dekker and Cardé, 2011; Dekker et al., 2005; Gillies and Wilkes, 1972). At long distances, they only use CO_2 and odours to find a potential host via 'cast and surge' flights. At intermediate distances (in the order of metres) they start to inspect visual cues (highly contrasting objects) near the ground. And at short ranges (less than one metre) they use heat and moisture cues to find a landing spot on the host (van Breugel et al., 2015; Cardé, 2015; McMeniman et al., 2014; Raji and DeGennaro, 2017). One could suppose that the relatively high importance of visual cues in *Aedes aegypti* arises from their diurnal behaviour, but recent studies on host-seeking *Anopheles* mosquitoes show that these nocturnal mosquitoes have a similar reaction to visual cues under moonlit or starlit conditions (Hawkes and Gibson, 2016; Hawkes et al., 2017).

Based on the developed knowledge of host-seeking behaviour in mosquitoes, a range of different mosquito traps has been developed (Bhalala and Arias, 2009; Jawara et al., 2009; Kline, 2002). One promising odour-baited trap type is the counter-flow trap that uses a single fan to generate both an inward airflow for capturing mosquitoes as well as an outward directed airflow carrying attractive odour away from the trap (Fig. 2.1*a*). The odour bait consists of a combination of chemicals mimicking human skin odour. Trap models usually combine the odour bait with CO_2 and/or visual cues in contrasting black and white, such as the BG-Sentinel trap and the BG-Suna trap (Biogents AG, Regensburg, Germany) (Farajollahi et al., 2009; Kawada et al., 2007). Although odour-baited traps were originally developed as research tools (Hiscox et al., 2014), a recent large-scale field study in Kenya showed that in combination with pre-existing bed nets, odour-baited traps reduced the number of human malaria cases by 30% (Homan et al., 2016). This study indicated that the use of such insecticide-free traps could now be considered as an effective supplement to conventional vector-control systems.

By combining multiple host cues such as odours, CO_2 and visual contrast, odour-baited traps aim to trigger the natural host seeking behaviour of mosquitoes. But surprisingly little attention has been given to the optimization of the capture mechanism of the trap. This might, at least partly, be due to a lack of detailed knowledge on the flight dynamics of mosquitoes in the vicinity of traps. In addition, until now, mosquito traps have been primarily optimized via an iterative design process, whereby the number of mosquitoes caught is compared between different trap designs (Hiscox et al., 2014; Kline et al., 2012; Schmied et al., 2008). Thus, obtaining detailed knowledge on mosquito flight dynamics around traps should open new paths for trap improvement and could be crucial in identifying the short-range approach and capture mechanisms involved (Ferguson et al., 2010).

To our knowledge, Cooperband and Carde (2006) are the only ones to have studied mosquitoes flight behaviours near traps (Cooperband and Cardé, 2006a). They analysed three-dimensional tracks of *Culex quinquefasciatus* and *Culex tarsalis* approaching four models of CO_2-baited traps in a large field wind tunnel, and showed that the traps had very

different capture efficiency (4% to 26% of upstream released mosquitoes were captured). In addition, they highlighted that, when approaching the trap, mosquitoes decelerated and adopted tortuous flights that varied in dynamics between the traps. These differences in dynamics, especially in the close vicinity of the traps, might help explain the differences in capture rate among the traps, but the spatial and temporal resolution of their flight tracking system did not allow for a detailed analysis of these dynamics (Cooperband and Cardé, 2006a).

Here, we will zoom in on these tortuous flight manoeuvres close to the trap to elucidate how the close-range response of the mosquitoes affects their capture dynamics. These close-range dynamics complement the long-distance approach dynamics as previously studied by Cooperband and Carde (Cooperband and Cardé, 2006a). We specifically address the tortuous flight paths close to the trap, and how these flight manoeuvres eventually lead to capture or escape from the trap.

For this study we used female malaria mosquitoes *Anopheles coluzzii*, and the odour-baited BG-Suna trap (Biogents AG, Regensburg, Germany), which was developed and is used for malaria vector control in Africa (Homan et al., 2016). We tested the trap in two orientations, the original hanging orientation and an upside-down standing orientation. The trap in its original hanging orientation has an upward-directed airflow for capturing mosquitoes (Fig. 2.2*a*), whereas the upside-down standing trap has a downward directed airflow for mosquito capture, and thus simulated the widely used and similar BG-Sentinel trap (Fig. 2.2*b*) (Farajollahi et al., 2009; Kawada et al., 2007). The use of these two trap orientations allowed us to investigate whether mosquitoes exhibit distinct behaviours in response to odour cues and opposite airflow orientations, and how this affects the capture dynamics.

We filmed a total of 530 mosquitoes flying around the trap using a stereoscopic high-speed videography system, from which we reconstructed more than 2500 three-dimensional flight paths. Based on these results, we found that the tortuous flight behaviour of mosquitoes near odour-baited traps were the result of two distinct and stereotypic behavioural responses of the mosquitoes to the trap: 1) when a mosquito flew towards the trap, it would tend to simultaneously fly downwards towards the floor, possibly in order to seek for hosts near the ground; 2) when a mosquito came close to the trap, it responded to the strong air currents induced by the trap or to a lack of short-range host cues, by performing an upward-directed manoeuvre, leading to high vertical accelerations in the flight path. Similar behaviours have been described previously in literature (van Breugel et al., 2015; Dekker et al., 1998; Hawkes and Gibson, 2016; Thorsteinson et al., 1965; Townes, 1962). Here we showed that the combination of these two stereotypical behaviours can lead to strikingly different flight dynamics depending only on trap orientation, which consequently led to similar differences in capture dynamics and capture efficiencies between the traps. These new insights into the close-range interaction between mosquito and traps may help in improving future trap designs.

2.2 Materials and methods

2.2.1 Experimental animals

For this study, we used a colony of *Anopheles coluzzii* (from the *Anopheles gambiae* complex (Coetzee et al., 2013)) that originated from Suakoko, Liberia in 1987. Since then, the colony has been reared at the Laboratory of Entomology (Wageningen University & Research, The Netherlands) at a temperature of 27°C, a relative humidity of 70%, and with a clock shifted 12-hour day/night cycle. Adults were kept in BugDorm cages (30x30x30 cm) in which they were fed on sugar-water with 6% glucose solution and offered daily blood meals from a blood bank (Sanquin, Nijmegen, The Netherlands) via a membrane feeding system (Hemotek, Discovery Workshop, UK). Thereafter, they were allowed to lay eggs on wet filter paper, which were then moved to a plastic tray filled with water. Liquifry No.1 fish food and TetraMin Baby were provided for larvae feeding. Finally, pupae were placed in new BugDorm cages to emerge. During our experiments, we used non-blood fed female malaria mosquitoes, which had most likely mated (5–10 days post-emergence with males and females housed together). They were collected between 12 and 16 hours before experiments and were not blood fed in order to increase host-seeking responses.

2.2.2 Experimental setup

Experiments were conducted in a 3.01 x 4.92 x 3.25 m (width x length x height) climate room at the Laboratory of Entomology (Wageningen University & Research, The Netherlands). The room was maintained at 27°C and 70% relative humidity and had a continuously running air filter system preventing accumulation of odours or CO_2 (see Spitzen et al. 2013 for more details (Spitzen et al., 2013)). The experimental setup consisted of a stereoscopic high-speed camera system that filmed the vicinity of a BG-Suna trap (Biogents AG, Regensburg, Germany) positioned in front of two perpendicular walls, with the trap centre at 35 cm from each wall (Fig. 2.1). A net covered a volume of approximately 8 m³ around the setup in order to prevent mosquitoes from escaping.

The BG-Suna trap is an odour-baited trap with a diameter of 52 cm and height of 39 cm, that was developed for malaria vector control in Africa (Homan et al., 2016). For each separate experimental trial, the trap was randomly positioned in its original hanging orientation (Fig. 2.2*a*), or in a standing orientation in which it resembled a BG-Sentinel trap (Fig. 2.2*b*) (Farajollahi et al., 2009; Kawada et al., 2007). In its original hanging orientation, the trap produced an upward-directed airflow for capture, whereas the upside-down standing trap produced a downward-directed airflow for mosquito capture. The capture entrance of the hanging and standing trap had a respective height of 81 cm and 54.5 cm above ground level (Fig. 2.2*a* and 2*b*, respectively). These heights were chosen to keep the camera heights equal to 62 cm in order to avoid repetitive realignment and recalibration of the camera system. Note that because of this reason, the hanging trap was positioned
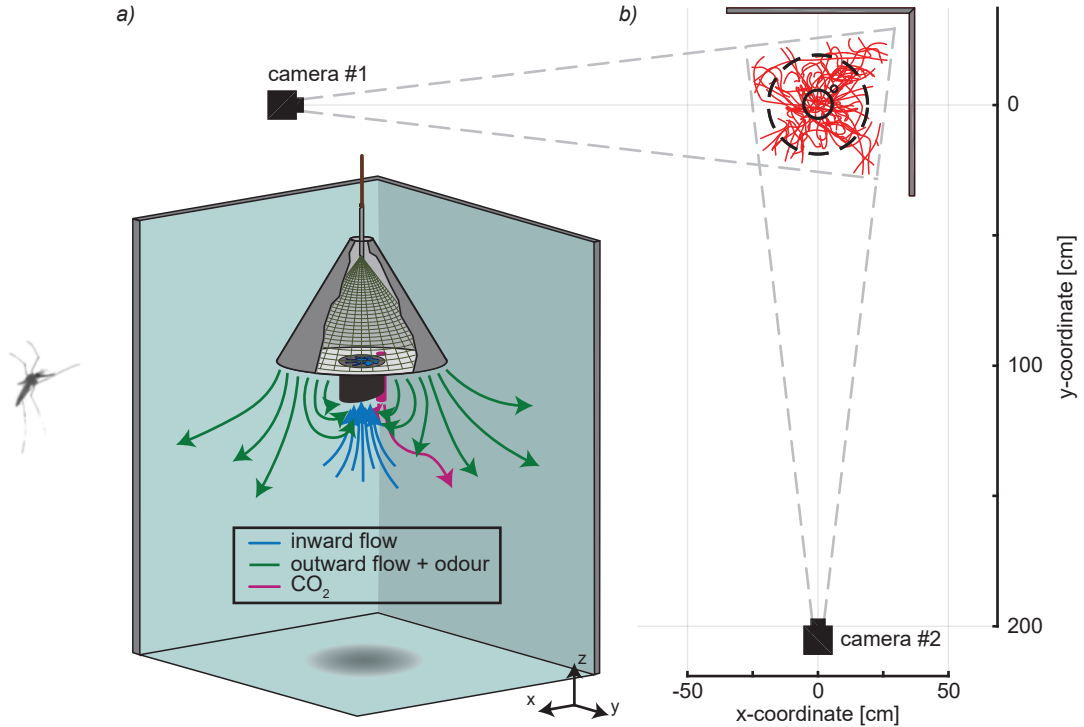
Figure 2.1: The Experimental setup. Mosquitoes generate aerodynamic forces required for flight by moving back and forth their wings at high flapping frequencies. (*a*) Experimental setup with floor, side-walls and a hanging Suna trap. A slice removed from the circular pyramid makes the inside of the trap visible. The fan of the trap (blue) creates a circulating airflow that attracts mosquitoes by pushing air mixed with the human-odour mimicking MB5 blend away from the trap (green arrows), and captures mosquitoes by sucking air (blue arrows) into the main entry tube (black). Mosquitoes are then confined inside by a net and by a trap door that closes when the fan is not working. A pipe (purple) releases CO_2 to simulate human breath. Arrows illustrate how the trap used airflow to attract and capture mosquitoes. (*b*) Top-down view of the experimental setup including the two high-speed video cameras, placed perpendicular to one another at 2 m from the trap centre. The filmed region, near the two background walls, is limited by the angle of view of each camera (grey dotted lines). The flight tracks recorded during a 15 minutes session (with a standing trap) are shown in red as an example. The outflow platform of the trap, its entrance and its CO_2 pipe are represented by the dashed circle and the large and small solid circles, respectively.

higher than the 30 cm height that has been found optimal for capturing mosquitoes (Hiscox et al., 2014).

We used the MB5 blend of five attractants (van Loon et al., 2015) inside each trap to simulate human odour. The CO_2 release pipe of the trap was connected to a pressurized gas canister containing a mixture of 5 % CO_2 + 95 % air and with a flow rate of 200 ml min^{-1}. To minimize blind spots in the camera views, this CO_2 pipe was shortened by 3.25 cm relative to the original length for the Suna trap. All handling of the materials and mosquitoes was done wearing nitrile gloves to minimize the risk of skin odour contamination of the traps.
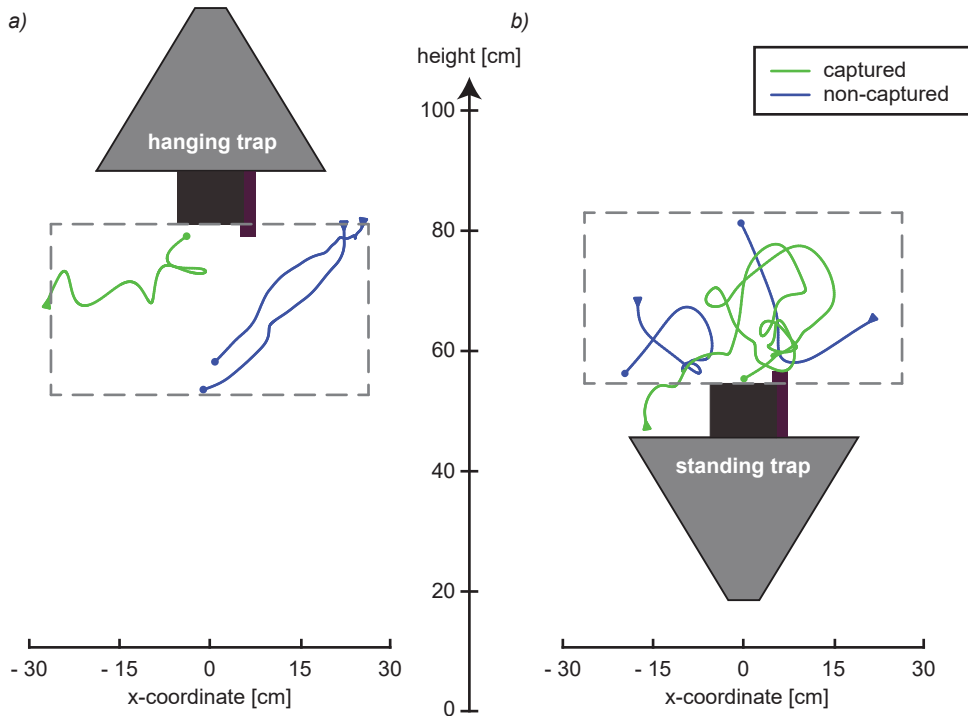
Figure 2.2: Examples of flight tracks around the two traps.(*a,b*) Examples of three flight tracks around the hanging trap (*a*) and standing trap (*b*), as viewed by camera #2. Tracks that lead to capture are in green and tracks from non-captured mosquitoes are in blue. The start and end of each track is represented by an arrowhead and a dot, respectively. Videos of these flight tracks can be found in the supplementary videos S1 and S2. The grey dashed line indicates the cylindrical volume for which we plotted the distribution of various flight parameters in the form of heat maps (Fig. 2.4, 2.6, and 2.8).

Because *Anopheles* mosquitoes are night active, we performed the experiments in dimmed light conditions, using a single spotlight (15 W incandescent bulb) directed towards the ceiling, and experiments were carried out during the period of the day which corresponded to the dark phase of the mosquito rearing; the period when the *An. coluzzii* were expected to exhibit the greatest degree of host-seeking behaviour.

Mosquito tracks around the trap were recorded using two synchronized high-speed cameras (PROMON 501 camera head with NIR sensors and 45 mm lenses), filming at 90 frames per second with a resolution of 1240 x 1080 pixels. Because mosquitoes cannot see infrared (IR) light (Gibson, 1995), we used two infrared light emitting lamps (Bosch Aegis SuperLed, 850 nm, 10° beam pattern (SLED10-8BD)) as illumination for the camera system. The camera system was calibrated at the start of each experimental day, with the use of a modified Direct Linear Transformation (DLT) algorithm (Hatze, 1988), by comparing known *x*, *y*, *z* coordinates of twenty-five suspended lead beads to their detected pixel coordinates in each camera. In addition, lens corrections were applied using pictures of a

chequerboard pattern and using a Matlab script (Bouguet, 2015).

For each trial, ten female mosquitoes were released from a holding container within the flight arena, after which the experimenter immediately left the room. From outside the room, the experimenter then started the 15-minute video recording, and thus all experiments were performed without a potentially disturbing human present in the room. Five minutes after each trial, captured and non-captured mosquitoes were collected and killed. Out of the 61 successfully performed trials, a total of 53 trials were analysed (32 for the hanging trap and 21 for the standing trap). Five trials were discarded because male mosquitoes were found in the arena or trap and three other trials were discarded due to illumination or calibration errors.

2.2.3 Simultaneous tracking of multiple flying mosquitoes

To compute the three-dimensional tracks (flight segments) from the stereoscopic recordings of flying mosquitoes, we first determined the two-dimensional positions of the mosquitoes within each image using the image processing toolbox of Matlab (MathWorks). Then, for each camera recording, the two-dimensional flight tracks were constructed using a 'Hungarian linker' algorithm (Kuhn, 1955). This algorithm reconstructs the tracks by finding the minimum distance between the detected positions of the mosquitoes in subsequent frames. Missed detections were taken into account by keeping tracks alive for 10 frames before deciding that they had ended. In the rare event that two tracks merged and then split up, two new tracks were started.

Next, the two-dimensional tracks within each camera view were combined into three-dimensional tracks using a DLT method (Hatze, 1988). A DLT error was calculated as the root mean square of the error (RMSE) between the original time-overlapping two-dimensional tracks and the two-dimensional back projections of the three-dimensional reconstructed tracks. To find the correct matches between two-dimensional tracks we used a RMSE threshold that separated RMSE distributions for matching and non-matching tracks.

Finally, pieces of three-dimensional tracks were stitched together whenever a single two-dimensional track matched multiple two-dimensional tracks in the other image. A Hampel filter was added to remove positional outliers on the three-dimensional tracks. In this way, the complete flight track of a mosquito could be reconstructed. Individuals were, however, not identified because mosquitoes could enter and exit the filmed volume multiple times during one experiment. Throughout each resulting three-dimensional flight track, we calculated the mosquito's linear and angular flight speeds, and its linear acceleration (supplementary materials, Fig. S2.1). The angular flight speed was calculated as $\omega = \frac{\Delta\theta}{\Delta t}$, whereby $\Delta t = t_n - t_{n+1}$ is the time elapsed between two consecutive video frames n and $n+1$, and $\Delta\theta$ is the turn angle defined as

$$\Delta\theta = \tan^{-1} \frac{|\overrightarrow{v_n} \times \overrightarrow{v_{n+1}}|}{\overrightarrow{v_n}.\overrightarrow{v_{n+1}}} \tag{2.1}$$

where $\overrightarrow{v_n}$ and $\overrightarrow{v_{n+1}}$ are the three-dimensional velocity vectors of the mosquito at video frames n and $n+1$.

2.2.4 Analyzing three-dimensional flight tracks

Owing to the high number of reconstructed tracks, a statistical approach was needed to visualise the flight dynamics of the mosquitoes around the two traps. For this purpose, we assumed the average flight behaviour of the mosquitoes around the trap to be axially symmetric, despite the presence of the trap's CO_2 pipe and the slope of the trap's entry tube (visible in Fig. 2.3a).We divided the filmed volume into multiple three-dimensional rings (Fig. 2.3a), which were centred around the trap's axis of symmetry. We computed statistical metrics from the mosquito's position over time in each of the rings. To allow metric comparisons across the rings, the volume of all rings was the same. We then projected each three-dimensional ring onto a two-dimensional parametric space with radial distance and vertical position as the key dimensions (Fig. 2.3b). Similarly, top-down view projections were reconstructed by dividing the flight volume into three-dimensional vertical rods projected onto a two-dimensional horizontal plane.
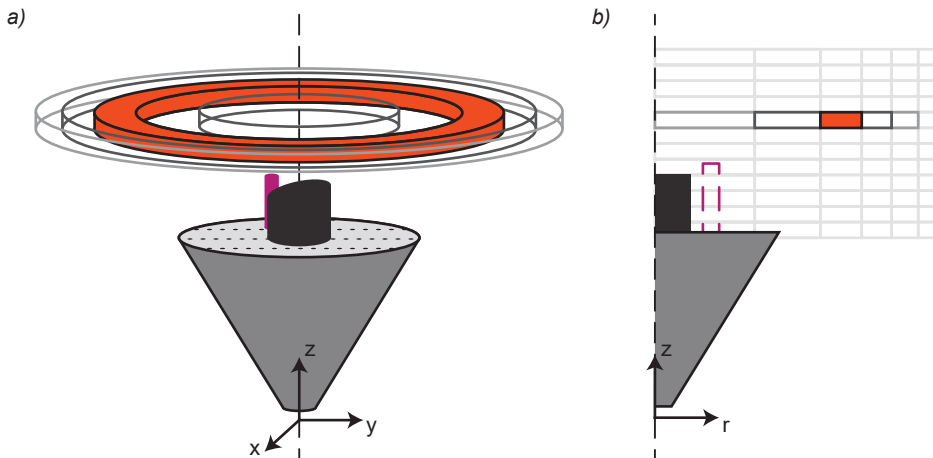
Figure 2.3: Visualization of three-dimensional flight dynamics in two-dimensional heat-maps.(a) The filmed volume above the trap was divided into 1012 three-dimensional rings of equal volume, centred around the symmetry axis of the trap. (b) Various flight dynamics metrics were computed based the measured mosquito track dynamics inside each ring, and projected onto a two-dimensional parametric space comprising the vertical position (z-axis) and the radial position (r-axis) of each ring.

Using this method, each flight dynamics metric was visualized as a set of two-dimensional heat-maps, one on the radial-vertical plane and one on the horizontal plane. In addition to the translational speed, angular speed and acceleration, we also visualized the distribution of positional likelihood and capture probability of mosquitoes around the trap. The estimated capture probability was expressed by the percentage of mosquito tracks in each sub-volume that ended in capture. We defined the positional likelihood as the normalized probability of a mosquito to fly within a certain sub-volume (e.g. a specific three-dimensional ring) of the field of view. It was calculated as

$$P_i = \frac{n_i}{N} \cdot I \tag{2.2}$$

where P_i is the likelihood that a mosquito is present in cell i, where the cell i represents a three-dimensional ring projected onto the previously described two-dimensional parametric space. n_i is the number of video frames that a mosquito was present in cell i throughout all sets of recordings, N is the total number of frames recorded, and I is the total number of cells within the recording volume. Thus, a random flight behaviour would result in a uniform probability throughout the region of interest, with P_i equal to one for all cells.

Furthermore, we visualized the mean flight dynamics as velocity vectors within the axi-symmetrical radial-vertical plane. Based on the resulting velocity fields, we visualized the average flight paths of mosquitoes by computing streamlines based on their velocity fields using the Linear Integral Convolution (LIC) algorithm (Cabral and Leedom, 1993).

For all calculated parameters, we performed sensitivity analyses to test the independence of our results to cell size, to the total number of analysed tracks and experimental duration (see supplementary materials, Fig. S2.2–S2.4). Additional data as well as 95% confidence intervals of the metrics presented on Fig. 2.1–2.1 are shown in the supplementary materials, Fig. S2.5–S2.10. For the statistical tests, we used a One-sample Kolmogorov-Smirnov test to determine whether data were normally distributed. Because all tested parameters were not normally distributed, we used the non-parametric Wilcoxon rank sum test to compare results between the hanging and standing trap (supplementary materials, Table S1). We report results as *median [first quartile – third quartile]*. We used several Matlab colormaps from ColorBrewer (Cynthia, 2013) and from a published guide by Kovesi (Kovesi, 2015) to assign a unique colormap for each visualized metric (Fig. 2.4–2.8).

2.2.5 Analysing the airflow dynamics around the mosquito trap

The path of a mosquito flying around a trap results from a combination of the mosquito's manoeuvre dynamics and the air movements induced by the trap. Thus, to determine the effect of air movements on mosquito flight dynamics, we measured the vertical speed component of the airflow using a one-dimensional hotwire anemometer (tetso 405i). This device had a 1 Hz sample rate, and thus did not allow us to quantify turbulence levels. For these measurements, we again assumed the axial symmetry of the airflow, and thus ignored

possible local differences in airflow around the CO_2 pipe or due to the asymmetric design of the Suna tube entrance (see positional likelihood around the CO_2 tube in supplementary materials, Fig. S2.11). Horizontal air velocities were not measured, as we expect that these were much lower than the vertical velocities induced by the vertically oriented fan.

With a custom-built setup, we used the hotwire anemometer to measure the vertical airspeed at 76 locations within a two-dimensional vertical plane oriented perpendicularly to the open trapdoor in the trap entry tube and at the opposite side of the CO_2 pipe. The standing trap was set at 59.2 cm above the floor, which was 3.7 cm higher than for the mosquito flight experiments. The hanging trap was kept at the same height as for the mosquito flight experiments (81 cm), because for this orientation, ground effects on the flow dynamics might be particularly important. Each velocity value was taken as an average over 45 s of measurements (at 1 Hz).

2.3 Results

2.3.1 Activity and capture rates of mosquitoes

We analyzed 8 hr of video recordings around the hanging trap, and 5 hr 15 min around the standing trap. Despite the longer recording duration for the hanging trap experiments, only 897 mosquito tracks (pseudo-replicates) were detected around the hanging trap against 1673 tracks around the standing trap (supplementary materials, Table S1). The number of flight tracks per trial (N_{tracks}/N_{trial}) for the standing trap was 2.7 times that for the hanging trap (hanging trap: $N_{tracks}/N_{trial} = 27.5$ [20–33], n=32 trials; standing trap: $N_{tracks}/N_{trial} = 75$ [61.25–87.25], n=21; $p < 0.001$). In addition, the duration of each track around the hanging trap was on average shorter compared to that around the standing trap (median track duration of 0.66 s and 0.99 s, respectively). Accordingly, the total flight duration per time recorded (($\sum T_{track})/T_{trial}$) for mosquitoes flying around the standing trap was 5.1 times that for mosquitoes around the hanging trap (hanging trap: ($\sum T_{track})/T_{trial} = 1.53$ [1.18–1.91]; standing trap: $\sum (T_{track})/T_{trial} = 7.84$ [6.43–9.05]; $p < 0.001$). All these metrics show that flight activity around the hanging trap is lower compared to the activity around the standing trap.

Of all the 2570 recorded flight tracks, only 87 tracks resulted in capture of the mosquito by the trap, divided into 25 captures by the hanging trap and 62 by the standing trap. Because of the low number of tracks that led to capture, we were unable to compare the flight dynamics of the captured and non-captured tracks using our two-dimensional parametric space. Instead, to determine what causes the differences in number of captures between the traps, we calculated three different capture ratios: 1) the percentage of released mosquitoes that were captured ($R_{mosquitoes} = N_{captures}/N_{released} \cdot 100\%$); 2) the percentage of recorded tracks that led to capture ($R_{tracks} = N_{captures}/N_{tracks} \cdot 100\%$); and 3) the number of captures per minute flight duration (capture frequency $f_{captures} = N_{captures}/T_{tracks}$).

On average, only 8% of the mosquitoes released were captured by the hanging trap,

whereas 30% of the mosquitoes were captured by the standing trap (supplementary materials, Table S1). Therefore, the standing trap captured almost four times the percentage of released mosquitoes captured by the hanging trap. However, because there were many more flight tracks around the standing trap, the average percentage of flight tracks that led to capture by the standing trap was only 1.4 times higher than that for the hanging trap (supplementary materials, Table S1). Because track duration was also longer for the standing trap, the number of captures per minute flight duration was not significantly different between the hanging and the standing trap (median of hanging trap: $f_{captures}$ = 0 [0–3] min^{-1}, standing trap: $f_{captures}$ = 1.18 [0.96–1.98] min^{-1}; p = 0.35). Thus, the hanging trap captured fewer mosquitoes than the standing trap. This difference can be explained by the higher activity of mosquitoes flying around the standing trap, which resulted in more and longer flight tracks around this trap.

2.3.2 Positional likelihood of mosquitoes

Heat-maps of the positional likelihood of mosquitoes flying around the traps allow the identification of regions with increased activity, which are quite different between the two trap orientations (Fig. 2.4). Above the standing trap, a cone-shaped region of increased activity is visible, in which mosquitoes were up to five times more likely to be present compared to the average. By contrast, around the hanging trap no such clearly defined region of increased activity was found, except for a smaller, cylindrical region directly underneath the entry tube edge within which mosquitoes are up to four times more likely to be found.

The top-down views (Fig. 2.4*b,d*) show that flight activity is approximately axially symmetric, except for a small reduction in activity near the CO_2 pipe (see also supplementary materials, Fig. S2.11), and for the hanging trap an interesting concentration of mosquitoes near the bottom corner of the back walls of our experimental setup was present (Fig. 2.1).

2.3.3 Airflow dynamic of the traps

We visualized the airflow dynamics around the standing and hanging trap as the two-dimensional distribution of vertical speeds (Fig. 2.5). The distribution of airspeed around the traps was consistent with previous findings (Hiscox et al., 2014), where vertical airflow speeds were

Figure 2.4: The spatial distribution of mosquito activity around the two traps, expressed by the positional likelihood. The positional likelihood, P_i, was defined as the normalized probability of a mosquito to fly within a certain three-dimensional ring of the field of view. Random flight behaviour would result in a uniform probability throughout the region of interest, with P_i equal to one for all cells. (*a,b*) The radial-vertical heat map (*a*) and the horizontal heat-map (*b*) of the positional likelihood of all mosquitoes flying around the hanging trap, as indicated by the colour bar on the top. (*c,d*) Equivalent data for mosquitoes flying around the standing trap. (*a,c*) The solid black rectangle represents the trap entry tube, and the dashed rectangle indicates the radial distance at which the CO_2 pipe was present. (*b,d*) The dashed circle, the large and small solid circles represent the circumference of the trap platform, the entry tube and the CO_2 pipe, respectively.

positional likelihood

a) **hanging trap**

c) **standing trap**

b)

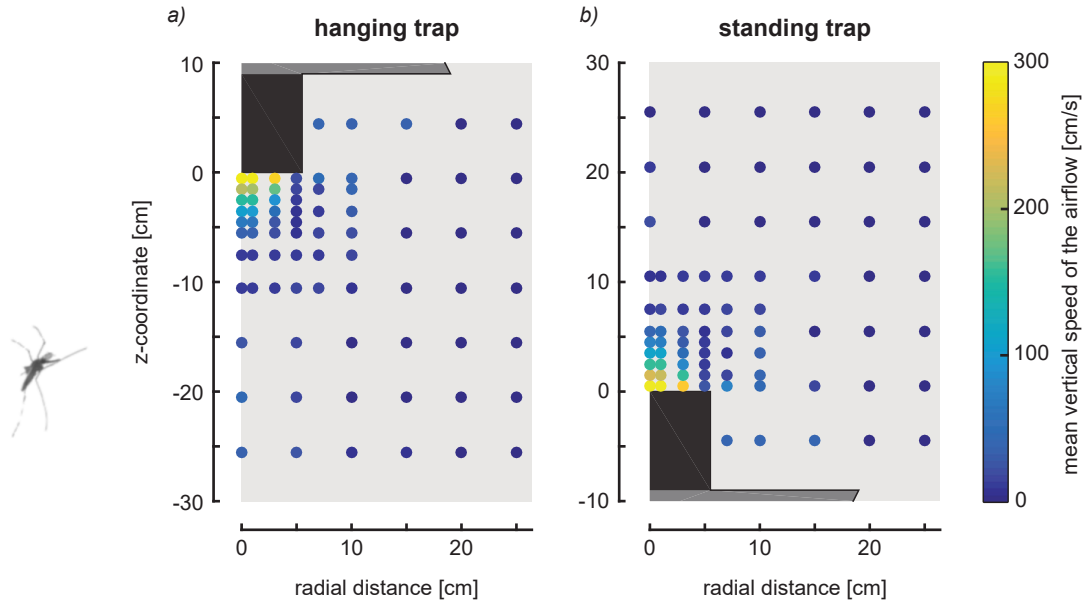d)
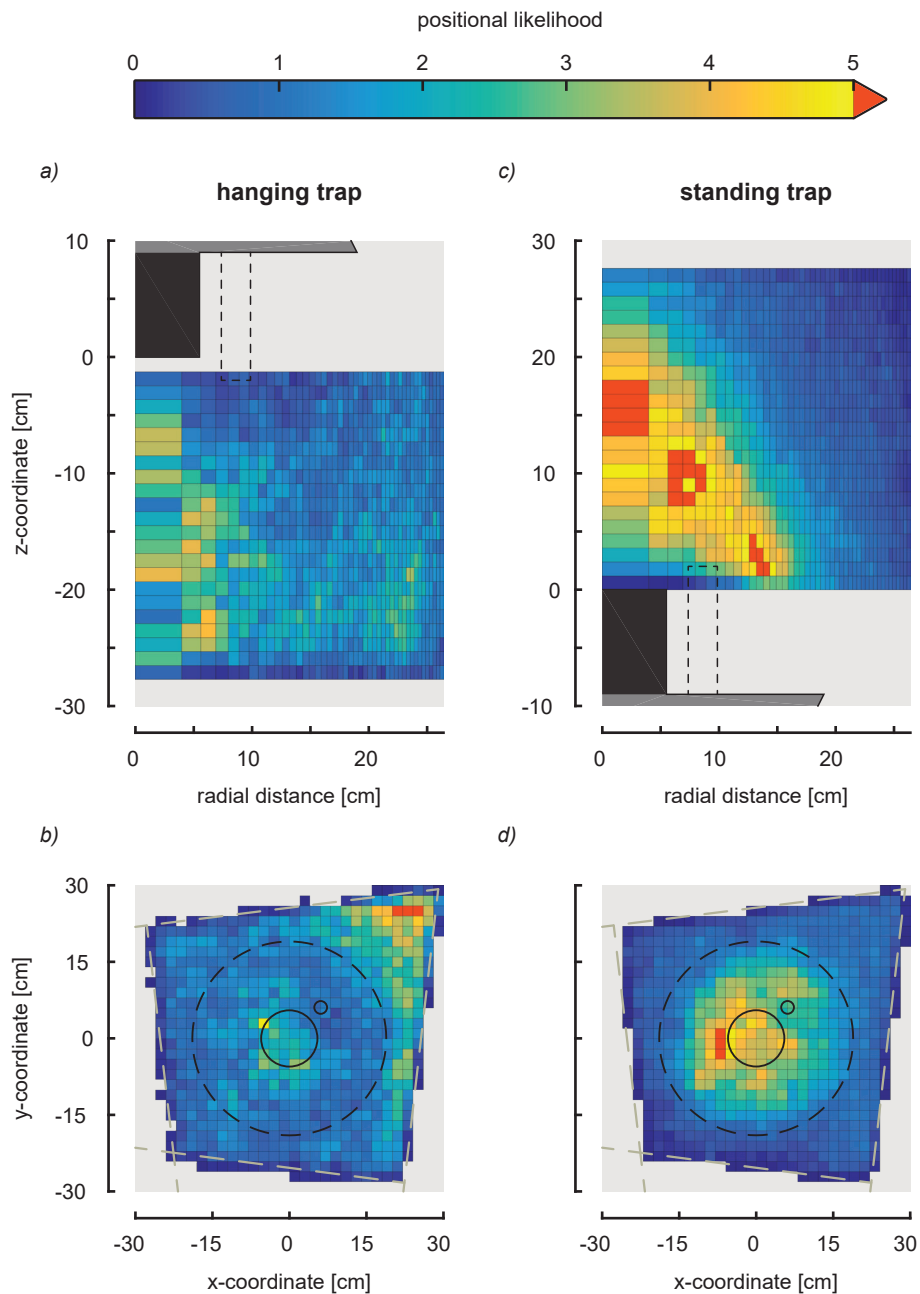
(Caption on the previous page.)

Figure 2.5: The vertical airspeeds produced by the trap.(*a,b*) The vertical airspeed at 76 points around the hanging trap (*a*) and the standing trap (*b*), as colour-coded according to the colour-bar to the right. See supplementary Fig. S2.5 for more details.

very high at the mouth of the entry tube (up to 3 m.s⁻¹), but these speeds rapidly decreased when moving away from the trap entrance. As a result, the region in front of the tube where the airflow is more than 1.5 m.s⁻¹ is only 3 cm high and 10 cm wide. This suggests that for a mosquito to be inevitably captured by the inward-directed airflow, it needs to pass very close to the trap entrance. A comparison of the vertical airspeeds around the standing and hanging trap (Fig. 2.5 and S2.5) shows that trap orientation has a relatively small effect on airflow dynamics, suggesting that a possible ground effect below the hanging trap is mostly negligible.

2.3.4 Mosquito flight dynamics

Based on all flight trajectories, we determined the translational flight speeds, angular speeds and accelerations of mosquitoes around the hanging and standing trap (supplementary materials, Fig. S2.1). The mosquitoes flying around the standing trap flew faster, had higher turn rates as expressed by higher angular speeds, and they produced higher body accelerations than those around the hanging trap ($p < 0.001$, see supplementary materials, Table S2.1).

The two-dimensional distribution of the translational speeds of mosquitoes flying around the standing and hanging traps were similar (Fig. 2.6*a,b,c,d*). Mosquitoes had their highest mean ground speeds (up to 0.5 m s⁻¹) near the trap entrance, whereas in both trap orient-
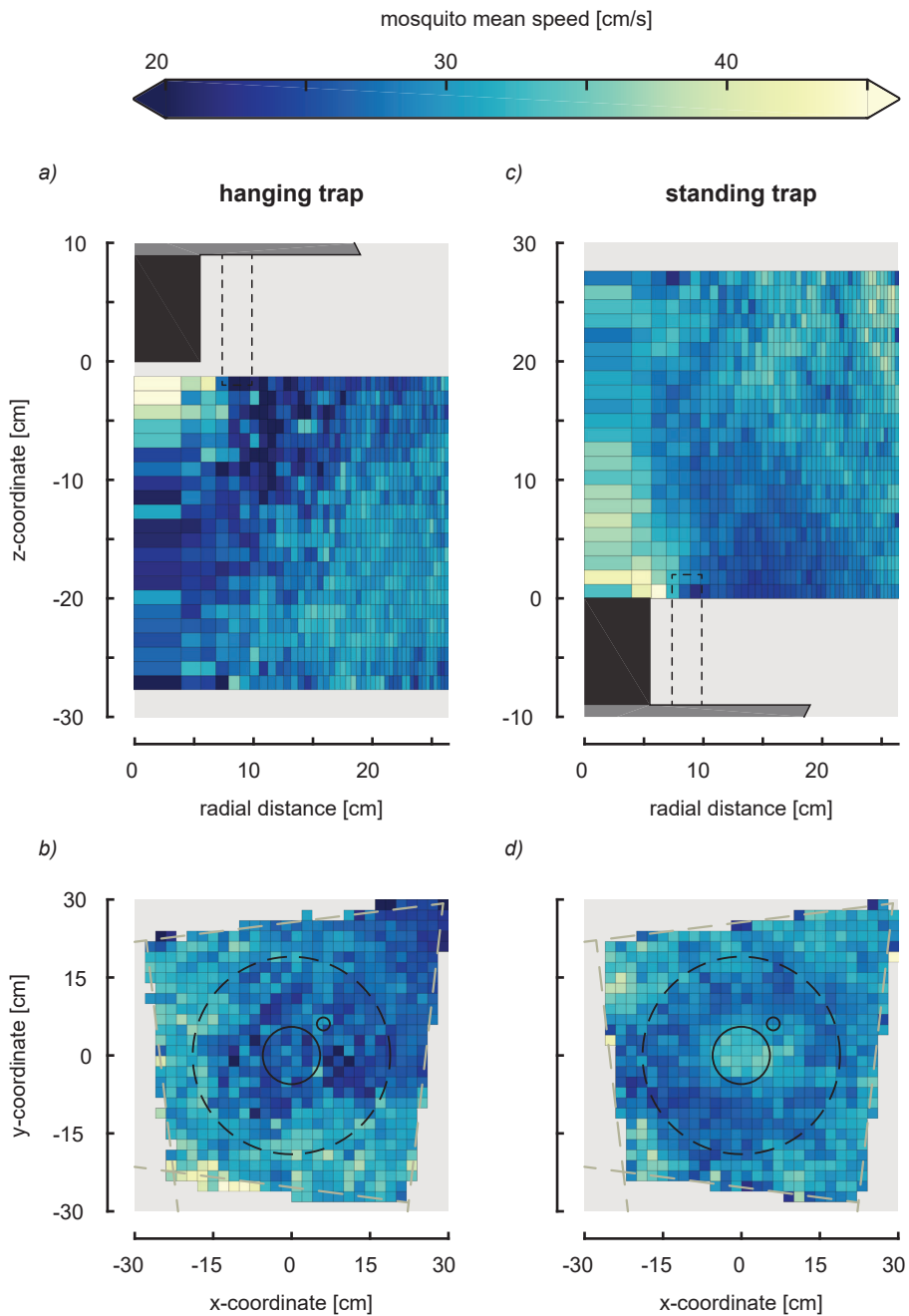
Figure 2.6: The average translational flight speed (*a-d*) and angular flight speed (*e-h*) of mosquitoes flying around the two traps. The top row shows the vertical-radial heat-maps, and the bottom row shows heat maps in the horizontal plane. (*a-d*) The average translational flight speed relative to the ground of mosquitoes flying around the hanging trap (*a,b*) and standing trap (*c,d*) are scaled according to the colour bar above (*a,c*). *Rest of the figure on the next page.*
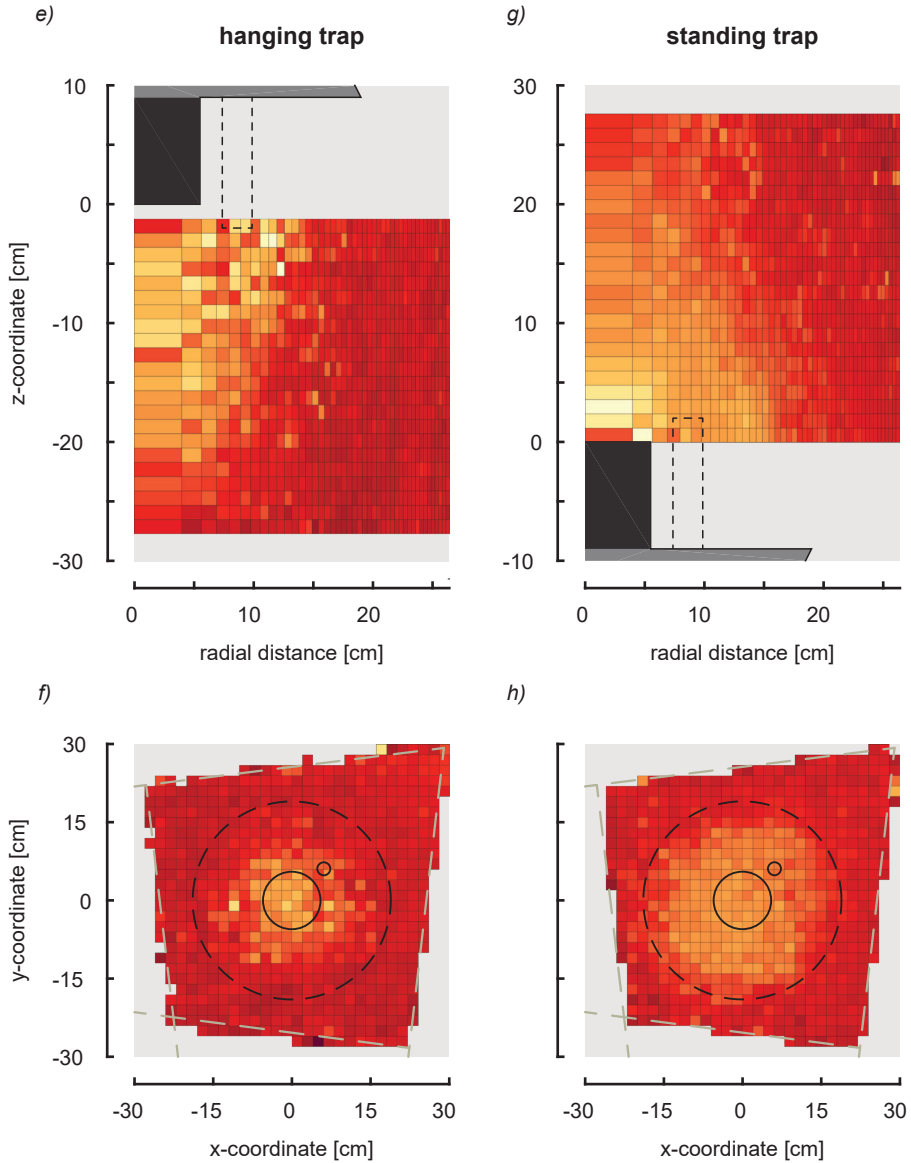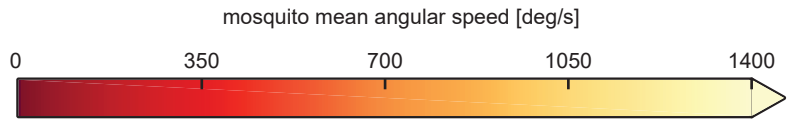
(*e-h*) The average angular flight speed of mosquitoes flying around the hanging trap (*e,f*) and standing trap (*g,h*) scaled according to the colour bar above (*e,g*). Standard errors and track number heat maps are shown in supplementary Fig. S2.6.

ations they had their lowest mean speeds at a radial distance of 10 to 20 cm from the entry tube. At both these regions with increased and reduced translational speeds, the angular speeds were high (Fig. 2.6*e,f,g,h*).

Figure 2.7: Averaged velocity vector fields and streamlines of mosquitoes flying around the hanging trap (*a*) and the standing trap (*b*).Each vector consists of the average velocity in the radial and vertical directions of all mosquitoes that flew within a cell of 24x24 mm. All velocity vectors that resulted from fewer than 5 de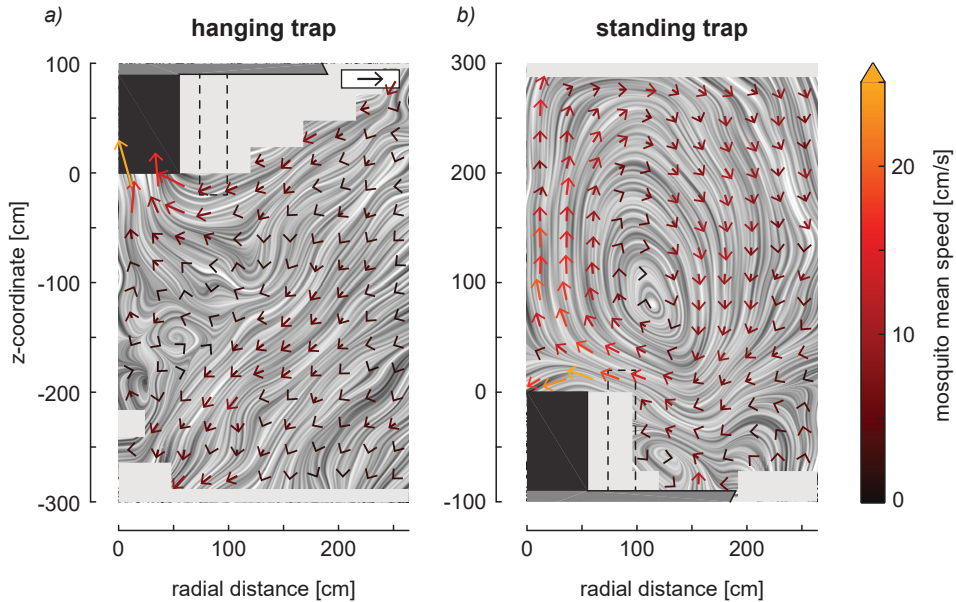tected tracks were discarded. Each velocity vector was scaled according to the black vector on the top right of panel (*a*) with magnitude 0.25 m.s^{-1}, and coloured according to the bar on the right. Standard errors and track number heat maps are shown in supplementary Fig. S2.7.

In contrast with the relatively high similarity in absolute translational and angular flight speeds around the traps, the velocity fields around the traps were strikingly different (Fig. 7). The pattern of mosquito streamlines near the hanging trap suggests that two regions can be identified, separated by a diagonal that runs from the top right to the bottom left of the velocity field. On average, mosquitoes that flew below this diagonal continued to fly downwards and away from the trap, whereas those flying above this border would initially fly downward, but when they got close to the trap entrance, they turned towards the trap entrance and got caught. Example flight tracks of mosquitoes within these two regions are in Fig. 2*a* and supplementary materials, movie S1.

Around the standing trap, mosquitoes followed a more complex circulating flight dynamic. On average mosquitoes entered the filmed volume by flying down towards the trap platform, after which they turned towards the black entry tube. When they were above the tube, mosquitoes either got caught by entering the trap, or they escaped capture by accel-

erating upwards. After flying upwards for approximately 20 cm, on average they turned around and started to fly again downwards towards the trap platform, thus completing the loop. Two typical examples of mosquitoes performing such a circulating flight manoeuvre can be seen in Fig. 2*b* and supplementary materials, movie S2.

As for the hanging trap, we also identified the capture and escape regions for the standing trap based on the distributions of mosquito streamlines. The area for which the streamlines end at the trap entrance is much smaller for the standing trap than for the hanging trap, suggesting that mosquitoes need to approach the standing trap entry tube more closely before being captured than for the hanging trap.

As expected, accelerations of mosquitoes flying around the trap were highest near the trap entrance (Fig. 8*a,b* and supplementary materials, Fig. S6). Around both traps, the mosquitoes flying close to the tube entrance tended to accelerate upwards, despite the oppositely oriented airflow for capture of the different traps. This means that the mosquitoes flying near the entry tube of the standing trap, accelerated in the direction opposite to the airflow direction, and thus avoided capture. On the other hand, the mosquitoes flying near the hanging trap also accelerated upwards, but in this case it was in the same direction as the airflow, and thus these mosquitoes flew straight into the mouth of the trap.

2.3.5 Distribution of the capture probability

The distribution of the capture probability is remarkably different for mosquitoes flying around the two oppositely oriented traps (Fig. 8*c,d*). Mosquitoes that approached the entry tube of the hanging trap within a 10 cm radius have a 75% chance of being caught, whereas for the standing trap mosquitoes need to enter the single cell directly above the entry tube for the likelihood of being caught to reach 75%. We reconstructed the three-dimensional volume within which more than 75% of detected mosquito tracks resulted in captures by revolving the two-dimensional heat-map around the axis of symmetry. For the hanging trap, this volume was 17.5 times larger than for the standing trap (supplementary materials, Table S1).

Figure 2.8: The distribution of average vertical accelerations of mosquitoes flying in the vicinity of the traps, and the distribution of the capture probability of mosquitoes flying around the traps. The top row shows data for the hanging trap, and the bottom row shows standing trap data. (*a,b*) The average vertical accelerations of mosquitoes expressed by the vertical-radial heat map, as colour-coded according to the bar above (*a*). (*c,d*) Vertical-radial heat maps of the percentage of tracks that led to capture. The purple region represents the volume within which more than 75% of the tracks led to capture. Standard errors of the heat maps of *(a, b)* are shown in supplementary Fig. S8. Top-down views of (*a–d*) are shown in the supplementary Fig. S9 and S10.

a)

mean vertical acceleration [m.s^{-2}]

c)

capture probability

b)

d)
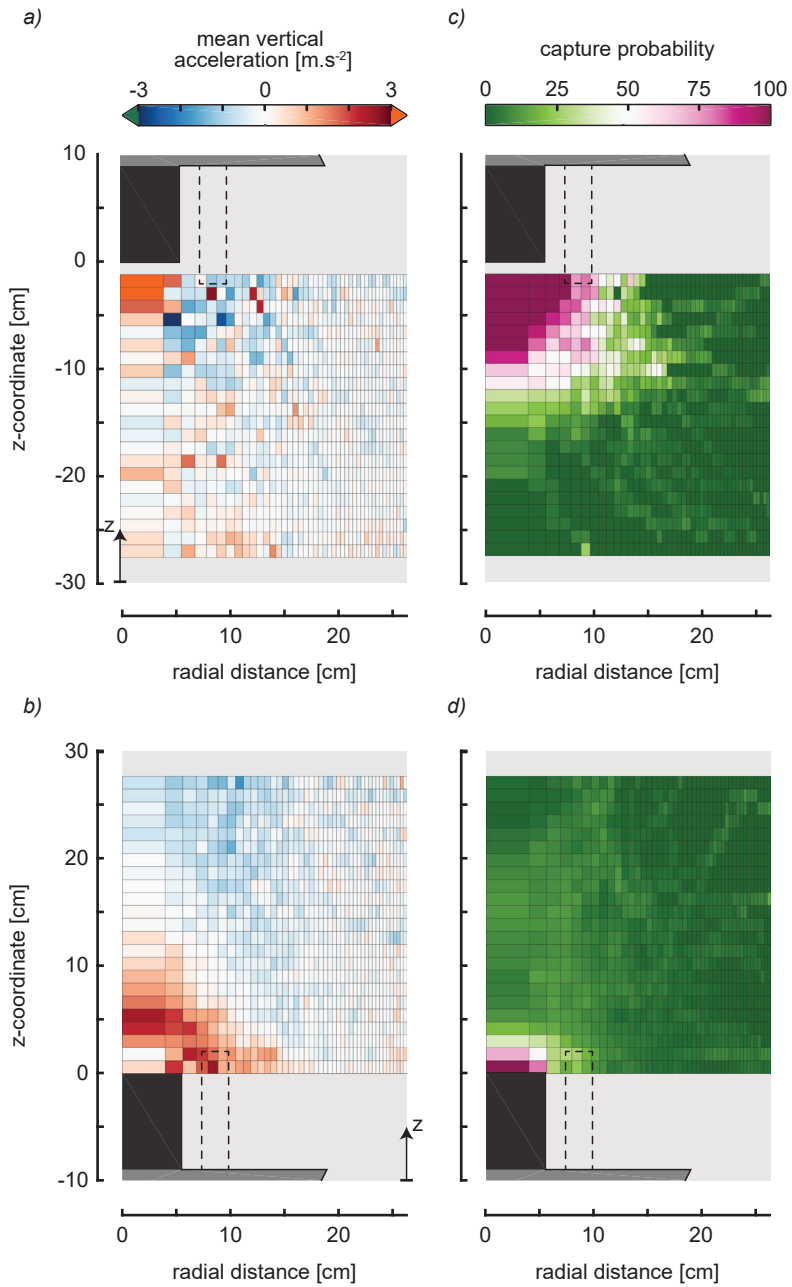
(Caption on the previous page.)

2.4 Discussion

We reconstructed three-dimensional flight tracks from stereoscopic high-speed videos of mosquitoes flying around an odour-baited trap set in two different orientations. The resulting high number of detected tracks was essential to dissect the flight behaviour of mosquitoes around the traps as it allowed the computation of the average flight dynamics throughout the complete region of interest. To study how these dynamics vary in space and as a function of trap orientation, we visualized these three-dimensional flight dynamics using two-dimensional heat maps and vector fields. For this, we assumed that the average flight behaviour of mosquitoes around the trap was axis-symmetric with respect to the axis of symmetry of the trap, which was confirmed as almost all top-down heat maps showed exclusively axis-symmetric patterns.

The only deviation from this symmetry was an off-centred volume under the hanging trap within which mosquitoes had a high probability of being present (Fig. 4b,d). Mosquitoes might have been attracted to this region because of an accumulation of odours and CO_2 in this corner, or because a shadow was casted here by the hanging trap. But because top-down views of all other metric presented in this paper did not show a bias towards this area, we cannot conclusively determine the cause of this accumulation. Additionally, we observed a small reduction in activity near the CO_2 pipe of both traps (Fig. 4b,d and supplementary materials, Fig. S11a), suggesting that mosquitoes were avoiding this region, possibly due to increased CO_2 concentrations or airflow anomalies near the shortened CO_2 pipe (van Breugel et al., 2015; Lacey et al., 2014; McMeniman et al., 2014; Spitzen et al., 2008). Note that both the increased activity of mosquitoes at the off-centred volume under the hanging trap and the reduced activity near the CO_2 pipe had a relative small effect on the flight pattern of mosquitoes in the near vicinity of the trap (Fig. 6 and Fig. S11b, respectively), suggesting that the assumption of axis-symmetric flight behaviour around the trap is still valid.

Beside these small anomalies, the heat-maps of positional likelihood of the mosquitoes (Fig. 4), and of mean flight speed and mean angular speed (Fig. 6) contribute some new elements concerning the short-range attractiveness of the studied odour-baited traps. Indeed, with the exception of the previously described regions, the volumes where mosquito activity was the highest, are also where their mean flight speeds and mean angular speeds were the highest, suggesting that these mosquitoes were performing casting behaviour and might thus have been host-seeking. This is consistent with findings of a previous study whereby host-seeking mosquitoes increased their flight tortuosity in the proximity of a host (Spitzen et al., 2013). Given that the used odour-baited trap has been shown to be successful in attracting host-seeking mosquitoes (Hiscox et al., 2014; Homan et al., 2016), we hypothesise that the majority of mosquitoes flying close to the traps were attracted by the trap, despite that random encounters with the traps likely also occurred.

The question remains as to what particular sensory cues trigger the search behaviour within the highly-unsteady airflow conditions around the trap. For example, mosquitoes

have been found to surge upwind more easily in airflow well mixed with odours and in turbulent CO_2 plumes (Dekker et al., 2001; Geier et al., 1999). To answer this question, an extensive study of the airflow turbulence levels and three-dimensional distributions of CO_2 and odour would be required (Cooperband and Cardé, 2006b).

2.4.1 Stereotypical mosquito flight dynamics

The flight dynamics of mosquitoes around the two oppositely-oriented traps were strikingly different but also highly stereotypical and repeatable (Fig. 7). Near the hanging trap setup, mosquitoes flew on average down towards the ground. But if they flew within a range of approximately 10 centimetres from the trap entry tube during this downward flight, they would turn and start to fly upwards, and as a consequence likely be caught by the trap. Mosquitoes flying around the standing trap showed a very different, circular flight pattern. These mosquitoes would initially also fly downwards when entering the filmed volume, but in this case towards the trap platform instead of the ground. When they came close to the entry tube, they would also turn and start to fly upwards, which resulted in most cases in a successful escape from the trap. After this manoeuvre, they would turn around and again start to fly downwards towards the trap platform, completing the circular flight pattern. For the standing trap, mosquitoes had to approach the entry tube much closer in order to be captured than for the hanging trap (Fig. 8c,d).

Because the trap-induced airspeeds were very similar between the traps (Fig. 5, S5), the large differences in flight dynamics around the two traps must be the result of a difference in behavioural response towards the two oppositely-oriented traps. Here, we hypothesise that these flight patterns are the result of two stereotypic behaviours in host-seeking mosquitoes: 1) mosquitoes that approached a trap tended to also fly downwards to the ground, and 2) mosquitoes that came close to the traps changed their flight direction by rapidly accelerating upwards, possibly reacting to adverse high-velocity airflow cues or to a lack of short-range host cues. This set of behaviours can explain the complex flight patterns observed around the traps, as well as the differences in flight patterns around the oppositely-oriented traps.

2.4.2 Upwind- and downward-directed approach flights

Upon entering the observed volume and despite inverse trap airflow, mosquitoes flew on average downwards, as well as towards the axis of symmetry of the trap, for both traps (Fig. 7). While doing so, they had low angular speeds and low positional likelihood (Fig. 4). Thus, mosquitoes did not remain long in the flight volume for this approach phase. As a result of the downward orientation, mosquitoes naturally flew towards the standing trap, whereas they tended to fly away from the hanging trap.

This flight behaviour is very similar to that described in female mosquitoes seeking a human host. Female *Anopheles* mosquitoes preferred to land on human body parts that

were closest to the ground, which they found by flying downwards and upwind by tracking odours and convective air currents produced by that host (Dekker et al., 1998; De Jong and Knols, 1996) When approaching an odour source, *Aedes aegypti* mosquitoes flew towards the ground to inspect visually-intriguing objects (van Breugel et al., 2015; Hawkes and Gibson, 2016). The similarity in flight patterns of our mosquitoes flying near the trap with those described in the literature, suggest that our mosquitoes performed a similar host-seeking behaviour. In our case, the upwind and downward flight behaviour might have been triggered by the detection of increased concentrations of odours, CO_2 and airflow turbulence, but the importance of visual cues cannot be excluded as possible light conditions differences have not been investigated.

2.4.3 Fast upward-directed flight manoeuvres

The second phase of mosquito flight dynamics takes place in the near vicinity of the trap entry tube. It starts at the boundary between the high-speed airflow volume a few centimetres from the visually contrasting entry tube and the volume where attracted mosquitoes are host-seeking. Here, on average, mosquitoes were found to quickly turn by accelerating and flying upward. For the mosquitoes that flew below the hanging trap, these rapid upward flight manoeuvres often led to capture, whereas the mosquitoes that flew above the standing trap, accelerated away from the trap and thus mostly escaped successfully.

Similar fast upward-directed flight behaviours have been described previously for other host-seeking insects (Hawkes and Gibson, 2016; Thorsteinson et al., 1965; Townes, 1962). Host-seeking *Anopheles* mosquitoes tended to fly quickly upwards after inspecting black tiles on the ground (Hawkes and Gibson, 2016), and horse and deer flies tend to fly upwards after having inspected potentially interesting visual cues (Thorsteinson et al., 1965; Townes, 1962). In fact, the Malaise trap and the Manitoba fly trap have both been designed to trap such upward flying insects (Thorsteinson et al., 1965; Townes, 1962).

The question remains about what sensory cues trigger these rapid upward flight manoeuvres near the trap. This could be the absence of short-range host cues such as heat or moisture (Cardé, 2015; Hawkes and Gibson, 2016), or the flight manoeuvre could be the result of positive phototaxis, reaction to visual cues, or to avoid/evade the high-speed airflow regions. The upward flying mosquitoes in the shadow of the hanging trap flew towards its black entry tube, whereas mosquitoes flew away from the black entry tube of the standing trap. Therefore, positive phototaxis as well as reaction to visual cues most likely do not explain these manoeuvres. Thus, these upward manoeuvres were probably either the result of the absence of short-range host cues, or they might have been executed to avoid or evade the high-speed airflow regions induced by the traps.

Should these upward-directed flights be evasive manoeuvres, then mosquitoes did not use information about the direction of the airflow to steer away from a potential threat, as all manoeuvres were directed upwards regardless of the direction of the airflow. This

makes these manoeuvres strikingly different from the evasive manoeuvres described in flying fruit flies, hawkmoths and hummingbirds, that are directed away from the danger (Cheng et al., 2016; Muijres et al., 2014), or downwards towards the ground (Corcoran and Conner, 2016). Horse flies, on the other hand, have also been shown to fly upwards after inspecting potential hosts (Thorsteinson et al., 1965; Townes, 1962). Because mosquitoes and horse flies both feed on terrestrial animals, these upward-directed evasive or avoidance manoeuvres might be particularly successful for such animals.

The stereotypical upward accelerating manoeuvres of our mosquitoes also explain the large difference in capture dynamics between the oppositely-oriented traps. The air volume around the trap entrance within which 75% or more of the mosquitoes were caught, $V_{75\%}$, was 17.5 times larger for the hanging trap than for the standing trap (Fig. 8c,d). For the standing trap, this $V_{75\%}$ volume overlays well with the region within which the airspeeds directed into the entry tube were more than 1.5 m.s^{-1} (Fig. 5), but for the hanging trap the $V_{75\%}$ volume extended well outside this high airspeed region. In flow tunnel experiments it has been demonstrated that mosquitoes are able to fly against airflow with speeds of up to 1.5 m.s^{-1} (Kennedy, 1940), and thus mosquitoes caught by the standing trap were most likely sucked downwards into the trap, as they were unable to accelerate upward fast enough to avoid capture. Because the $V_{75\%}$ volume underneath the hanging trap extended well beyond the region with high suction airspeeds, many of the mosquitoes captured by the hanging trap must have actively flown into the entry tube when performing an upward-directed flight manoeuvre.

2.4.4 Combining the two stereotypical flight behaviours

The flight dynamics observed near the two traps can be interpreted as a combination of the upwind- and downward-directed approach flights and the fast upward-directed evasive manoeuvres. Although alternative behavioural explanations of the observed flight dynamics are possible, the here-described flight behaviours have previously been identified in host-seeking insects (van Breugel et al., 2015; Dekker et al., 1998; Hawkes and Gibson, 2016; Thorsteinson et al., 1965; Townes, 1962), and the combination of these two behaviours explain well the striking differences in flight dynamics around the oppositely-oriented traps (Fig. 9). The upwind- and downward-directed flight behaviours illustrate why mosquitoes tended to fly away from the hanging trap, and towards the horizontal platform of the standing trap; the fast upward-directed flight manoeuvres caused mosquitoes to fly towards the capture entrance of the hanging trap and away from the standing trap, and thus also explains the larger capture region around the hanging trap (Fig. 8). After the upward flight movement away from the standing trap, these mosquitoes switched back to the downward-directed flight pattern, explaining the advent of the circular flight path, and why mosquitoes remained near the standing trap for a longer time.
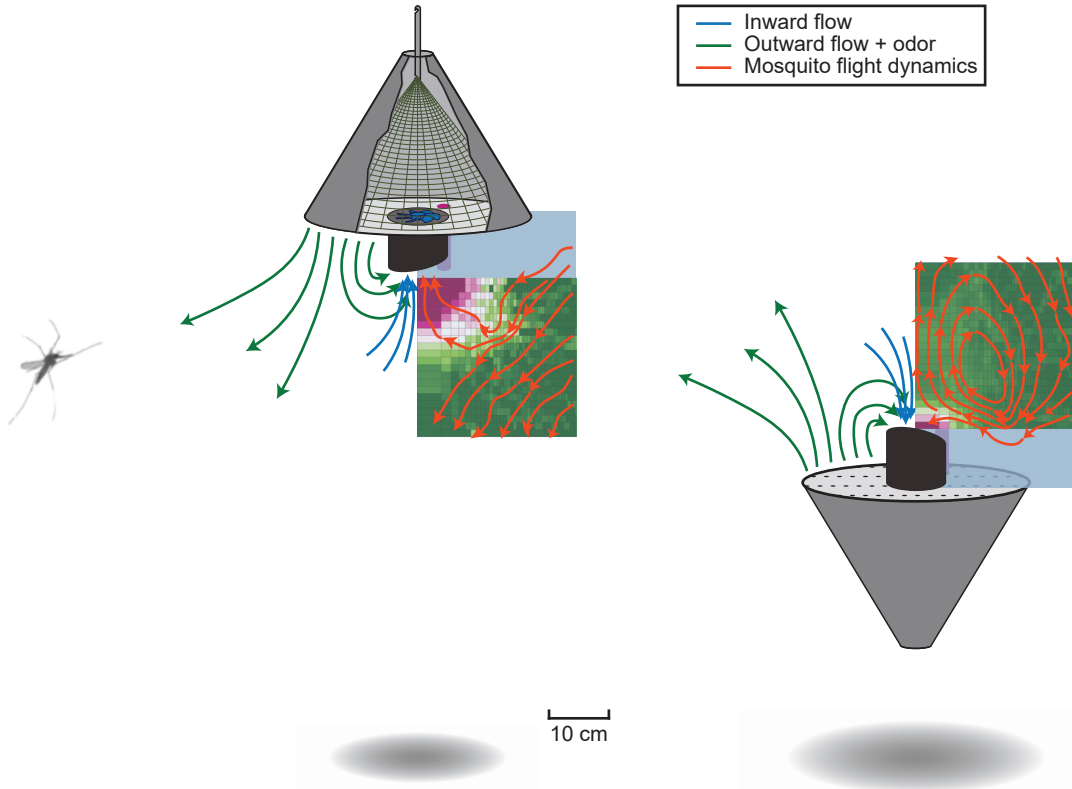
Figure 2.9: The average flight tracks and capture percentage of mosquitoes around the two traps, and an artist impression of airflow induced by the traps. The mean flight tracks (in red) are determined from the streamlines in Fig. 7, and details about the capture percentage distribution (heat map) are shown in Fig. 8*c,d*.

2.4.5 The flight behaviour of mosquitoes explains trap efficiency

Our results suggest that the standing trap has a higher short-range attractiveness, as expressed by both a higher number of detected flight tracks (N_{track}/N_{trial}) and larger flight duration per trial (T_{track}/T_{trial}) for mosquitoes flying around the standing trap. In contrast, the hanging trap has a better capture mechanism because the air volume around the trap entrance within which 75% or more of the mosquitoes were caught, $V_{75\%}$, was more than 17 times larger for the hanging trap compared to the standing trap. However, both the percentage of released mosquitoes caught and the percentage of flight tracks that led to capture ($R_{mosquitoes}$ and R_{tracks}, respectively) were higher for the standing trap. Although $R_{mosquitoes}$ and R_{tracks} were not significantly different between the traps, this suggests that the less efficient capture mechanism of the standing trap was more than compensated by its superior short-range attractiveness. In this way, the greater number of mosquitoes captured by the standing trap seems to be not only because it attracts more mosquitoes to

its vicinity, as was previously suggested (Cooperband and Cardé, 2006a), but also because mosquitoes remained near the standing trap for a longer period of time.

These results, and especially the differences in capture efficiency, would need to be verified in field experiments, where the wind and light conditions would likely impact trap finding by the mosquitoes as well as their use of visual cues. In addition, the fact that our experiments were performed in an enclosed environment, where the proportion of random encounters might have been relatively high, may have impacted our results. However, such random encounters would probably only increase the background noise on the observed flight dynamics and should not result in distinct flight patterns. Finally, height differences might have affected how easily mosquitoes were finding the trap, and hence the trapping efficacy (Hiscox et al., 2014). This subject would deserve to be studied in dedicated experiments.

Besides contributing to the expansion of general knowledge on mosquito flight behaviour, our results help to understand the short-range attractiveness and the capture mechanism of odour-baited traps. This new insight could be used to develop novel trap designs with improved trapping efficiency. Thus, in our opinion, such trap design process would greatly benefit from the use of iterative testing of traps in studies similar to this one. Because the Suna trap is already part of a successful vector control system (Homan et al., 2016), it is likely that the resulting trap improvements would make a valuable contribution to the fight against vector-borne disease.

Data accessibility

The datasets supporting this article are available in supplementary materials database S1 and S2.

Competing interests

The authors declare no competing or financial interests.

Author contributions

Conceived and designed the experiments: FTM AH JS. Performed the experiments: JAvE. Developed the automatic mosquito tracking algorithm: MJL. Analysed the data: AC. Wrote the paper: AC FTM JLvL. All authors read and commented on the manuscript and gave their final approval for publication.

Acknowledgements

for their donation of the Suna traps.

Funding

References

Baker, T. C. and Haynes, K. F. (1987). Manoeuvres used by flying male oriental fruit moths to relocate a sex pheromone plume in an experimentally shifted wind-field. *Physiol. Entomol.* **12**, 263–279.

Bhalala, H. and Arias, J. R. (2009). The Zumba mosquito trap and BG-Sentinel trap: Novel surveillance tools for host-seeking mosquitoes. *J. Am. Mosq. Control Assoc.* **25**, 134–139.

Bouguet, J.-Y. Camera calibration toolbox for matlab.

Cabral, B. and Leedom, L. C. (1993). Imaging vector fields using line integral convolution. In *Proc. 20th Annu. Conf. Comput. Graph. Interact. Tech. - SIGGRAPH '93*, pp. 263–270.

Cardé, R. T. (2015). Multi-cue integration: How female mosquitoes locate a human host. *Curr. Biol.* **25**, R793–r795.

Cardé, R. T. and Willis, M. A. (2008). Navigational strategies used by insects to find distant, wind-borne sources of odor. *J. Chem. Ecol.* **34**, 854–866.

Cheng, B., Tobalske, B. W., Powers, D. R., Hedrick, T. L., Wethington, S. M., Chiu, G. T. C. and Deng, X. (2016). Flight mechanics and control of escape manoeuvres in hummingbirds. I. Flight kinematics. *J. Exp. Biol.* **219**, 3518–3531.

Coetzee, M., Hunt, R. H., Wilkerson, R., Torre, A. D., Coulibaly, M. B. and Besansky, N. J. (2013). Anopheles coluzzii and anopheles amharicus, new members of the anopheles gambiae complex. *Zootaxa* **3619**, 246–274.

Cooperband, M. F. and Cardé, R. T. (2006a). Comparison of plume structures of carbon dioxide emitted from different mosquito traps. *Med. Vet. Entomol.* **20**, 1–10.

Cooperband, M. F. and Cardé, R. T. (2006b). Orientation of Culex mosquitoes to carbon dioxide-baited traps: Flight manoeuvres and trapping efficiency. *Med. Vet. Entomol.* **20**, 11–26.

Corcoran, A. J. and Conner, W. E. (2016). How moths escape bats: predicting outcomes of predator-prey interactions. *J. Exp. Biol.* **219**, 2704–2715.

Cribellier, A., van Erp, J. A., Hiscox, A., Lankheet, M. J., van Leeuwen, J. L, Spitzen, J. and Muijres, F. T. (2018). Flight behaviour of malaria mosquitoes around odour-baited traps: Capture and escape dynamics. *R. Soc. Open Sci.* **5**.

Cynthia, A. ColorBrewer.

De Jong, R. and Knols, B. G. (1996). Selection of biting sites by mosquitoes. *CIBA Found. Symp.* pp. 89–103.

Dekker, T. and Cardé, R. T. (2011). Moment-to-moment flight manoeuvres of the female yellow fever mosquito (Aedes aegypti L.) in response to plumes of carbon dioxide and human skin odour. *J. Exp. Biol.* **214**, 3480–3494.

Dekker, T., Geier, M. and Cardé, R. T. (2005). Carbon dioxide instantly sensitizes female

yellow fever mosquitoes to human skin odours. *J. Exp. Biol.* **208**, 2963–2972.

Dekker, T., Takken, W. and Carde, R. (2001). Structure of host odour plumes influences catch of Anopheles gambiae ss and Aedes aegypti in a dual choice olfactometer. *Physiol. Entomol.* **26**, 124–134.

Dekker, T., Takken, W., Knols, B. G. J., Bouman, E., Van de Laak, S., de Bever, A. and Huisman, P. W. T. (1998). Selection of biting sites on a human host by Anopheles gambiae s.s., An. arabiensis and An. quadriannulatus. *Entomol. Exp. Appl.* **87**, 295–300.

Edman, J. D. and Scott, T. W. (1987). Host defensive behaviour and the feeding success of mosquitoes. *Int. J. Trop. Insect Sci.* **8**, 617–622.

Farajollahi, A., Kesavaraju, B., Price, D. C., Williams, G. M., Healy, S. P., Gaugler, R. and Nelder, M. P. (2009). Field efficacy of BG-Sentinel and industry-standard traps for Aedes albopictus (Diptera: Culicidae) and West Nile virus surveillance. *J. Med. Entomol.* **46**, 919–925.

Ferguson, H. M., Dornhaus, A., Beeche, A., Borgemeister, C., Gottlieb, M., Mulla, M. S., Gimnig, J. E., Fish, D. and Killeen, G. F. (2010). Ecology: A prerequisite for malaria elimination and eradication. *PLoS Med.* **7**, 1–7.

Geier, M., Bosch, O. J. and Boeckh, J. (1999). Influence of odour plume structure on upwind flight of mosquitoes towards hosts. *J. Exp. Biol.* **202**, 1639–1648.

Gibson, G. (1995). A behavioural test of the sensitivity of a nocturnal mosquito, Anopheles gambiae, to dim white, red and infra-red light. *Physiol. Entomol.* **20**, 224–228.

Gillies, M. T. and Wilkes, T. J. (1972). The range of attraction of animal baits and carbon dioxide for mosquitoes. Studies in a freshwater area of West Africa. *Bull. Entomol. Res.* **61**, 389–404.

Hatze, H. (1988). High-precision three-dimensional photogrammetric calibration and object space reconstruction using a modified DLT-approach. *J. Biomech.* **21**, 533–538.

Hawkes, F. and Gibson, G. (2016). Seeing is believing: the nocturnal malarial mosquito Anopheles coluzzii responds to visual host-cues when odour indicates a host is nearby. *Parasites and Vectors* **9**, 320.

Hawkes, F. M., Dabiré, R. K., Sawadogo, S. P., Torr, S. J. and Gibson, G. (2017). Exploiting Anopheles responses to thermal, odour and visual stimuli to improve surveillance and control of malaria. *Sci. Rep.* **7**, 17283.

Hiscox, A., Otieno, B., Kibet, A., Mweresa, C. K., Omusula, P., Geier, M., Rose, A., Mukabana, W. R. and Takken, W. (2014). Development and optimization of the Suna trap as a tool for mosquito monitoring and control. *Malar. J.* **13**, 257.

Homan, T., Hiscox, A., Mweresa, C. K., Masiga, D., Mukabana, W. R., Oria, P., Maire, N., Pasquale, A. D., Silkey, M., Alaii, J. et al. (2016). The effect of mass mosquito trapping on malaria transmission and disease burden (SolarMal): a stepped-wedge cluster-randomised trial. *Lancet* **388**, 1193–1201.

Jawara, M., Smallegange, R. C., Jeffries, D., Nwakanma, D. C., Awolola, T. S., Knols, B. G. J., Takken, W. and Conway, D. J. (2009). Optimizing odor-baited trap methods for collecting mosquitoes during the malaria season in the Gambia. *PLoS One* **4**.

Kawada, H., Honda, S. and Takagi, M. (2007). Comparative laboratory study on the reaction of Aedes aegypti and Aedes albopictus to different attractive cues in a mosquito trap. *J. Med. Entomol.* **44**, 427–432.

Kennedy, J. S. (1940). The visual Responses of flying mosquitoes. *Proc. Zool. Soc. London* **109 A**, 221–242.

Kline, D. L. (2002). Evaluation of various models of propane-powered mosquito traps. *J. Vector Ecol.* **27**, 1–7.

Kline, D. L., Bernier, U. R. and Hogsette, J. A. (2012). Efficacy of three attractant blends tested in combination with carbon dioxide against natural populations of mosquitoes and biting flies at the lower suwannee wildlife refuge. *J. Am. Mosq. Control Assoc.* **28**, 123–127.

Kovesi, P. (2015). Good colour maps: How to design them. *Comput. Sci.* pp. 1–42.

Kuhn, H. W. (1955). The Hungarian method for the assignment problem. *Nav. Res. Logist. Q.* **2**, 83–97.

Lacey, E. S., Ray, A. and Cardé, R. T. (2014). Close encounters: Contributions of carbon dioxide and human skin odour to finding and landing on a host in Aedes aegypti. *Physiol. Entomol.* **39**, 60–68.

Lazzari, C. R. (2009). Chapter 1 Orientation towards hosts in haematophagous insects: An integrative perspective. In *Adv. In Insect Phys.*, volume 37, pp. 1–58. Elsevier Ltd.

McMeniman, C. J., Corfas, R. A., Matthews, B. J., Ritchie, S. A. and Vosshall, L. B. (2014). Multimodal integration of carbon dioxide and other sensory cues drives mosquito attraction to humans. *Cell* **156**, 1060–1071.

Muijres, F. T., Chang, S. W., van Veen, W. G., Spitzen, J., Biemans, B. T. T., Koehl, M. A. R. and Dudley, R. (2017). Escaping blood-fed malaria mosquitoes minimize tactile detection without compromising on take-off speed. *J. Exp. Biol.* **220**, 3751–3762.

Muijres, F. T., Elzinga, M. J., Melis, J. M., Dickinson, M. H., Florian T. Muijres, 1 Michael J. Elzinga, 1 Johan M. Melis, 1, . M. H. D. and Avoiding (2014). Flies evade looming targets by executing rapid visually directed banked turns. *Science (80-.).* **344**, 172–7.

Raji, J. I. and DeGennaro, M. (2017). Genetic analysis of mosquito detection of humans. *Curr. Opin. Insect Sci.* **20**, 34–38.

Schmied, W. H., Takken, W., Killeen, G. F., Knols, B. G. J. and Smallegange, R. C. (2008). Evaluation of two counterflow traps for testing behaviour-mediating compounds for the malaria vector Anopheles gambiae s.s. under semi-field conditions in Tanzania. *Malar. J.* **7**, 230.

Spitzen, J., Smallegange, R. C. and Takken, W. (2008). Effect of human odours and positioning of CO2 release point on trap catches of the malaria mosquito Anopheles gambiae sensu stricto in an olfactometer. *Physiol. Entomol.* **33**, 116–122.

Spitzen, J., Spoor, C. W., Grieco, F., ter Braak, C., Beeuwkes, J., Van Brugge, S. P., Kranenbarg, S., Noldus, L. P. J. J., van Leeuwen, J. L. and Takken, W. (2013). A 3D analysis of flight behavior of Anopheles gambiae sensu stricto malaria mosquitoes in response to human odor and heat. *PLoS One* **8**, 1–12.

Takken, W. and Verhulst, N. O. (2013). Host preferences of blood-feeding mosquitoes. *Annu. Rev. Entomol.* **58**, 433–453.

Thorsteinson, A. J., Bracken, G. K. and Hanec, W. (1965). The orientation of horse flies and deer flies (Tabanidae, Diptera): III. the use of traps in the study of orientation of Tabanids in the field. *Entomolia Exp. Appl.* **8**, 189–192.

Townes, H. (1962). Design For A Malaise Trap. *Proc. Entomol. Soc. Washingt.* **64**, 253 – 262.

van Breugel, F. and Dickinson, M. H. (2014). Plume-tracking behavior of flying drosophila emerges from a set of distinct sensory-motor reflexes. *Curr. Biol.* **24**, 274–286.

van Breugel, F., Riffell, J., Fairhall, A. and Dickinson, M. H. (2015). Mosquitoes use vision to associate odor plumes with thermal targets. *Curr. Biol.* **25**, 2123–2129.

van Loon, J. J. J. A., Smallegange, R. C., Bukovinszkiné-Kiss, G., Jacobs, F., De Rijk, M., Mukabana, W. R., Verhulst, N. O., Menger, D. J. and Takken, W. (2015). Mosquito attraction: crucial role of carbon dioxide in formulation of a five-component blend of human-derived volatiles. *J. Chem. Ecol.* **41**, 567–73.

Vinauger, C., Lahondère, C., Wolff, G. H., Locke, L. T., Liaw, J. E., Parrish, J. Z., Akbari, O. S., Dickinson, M. H. and Riffell, J. A. (2018). Modulation of host learning in Aedes aegypti mosquitoes. *Curr. Biol.* **28**, 333–344.e8.

2

Flight behaviour of malaria mosquitoes around odour-baited traps: capture and escape dynamics

Antoine Cribellier[1], Jens A. van Erp[1], Alexandra Hiscox[2], Martin J. Lankheet[1], Johan L. van Leeuwen[1], Jeroen Spitzen[2], Florian T. Muijres[1]

[1] Experimental Zoology Group, Wageningen University & Research, Wageningen, The Netherlands

[2] Laboratory of Entomology, Wageningen University & Research, Wageningen, The Netherlands

Consisting of:

- List of symbols

- Table S2.1

- Legends of the databases S2.1 and S2.2

- Legends of the videos S2.1 and S2.2

- Supplementary Figures S2.1–S2.11

List of symbols

symbol	units	description
N_{trials}	[-]	number of trials for the standing or hanging trap
T_{trials}	[min]	recording duration for all trials for the standing or hanging trap
N_{tracks}	[-]	number of reconstructed flight tracks
T_{track}	[s]	duration of a flight track
L_{track}	[cm]	length of a flight track
$N_{captured}$	[-]	number of captured mosquitoes
$R_{mosquitoes}$	[-]	percentage of released mosquitoes that were captured
R_{tracks}	[-]	percentage of recorded tracks that led to capture
$f_{captures}$	[min^{-1}]	capture frequency: the number of captures per minute flight duration
$V_{75\%}$	[cm^3]	volume within which more than 75% of detected flight tracks resulted in captures
U	[m.s^{-1}]	linear speed of a flying mosquito
α	[degrees.s^{-1}]	angular speed of a flying mosquito
a	[m.s^{-2}]	acceleration of a flying mosquito

Legends of the supplementary datasets

The datasets can be found here: `https://doi.org/10.1098/rsos.180246`

Database S2.1: Mosquito tracks around the standing and hanging trap and additional experimental metadata. The three-dimensional tracks of the flying mosquitoes were computed from our stereoscopic recordings using the tracker described in the materials and methods. Flight tracks are described as the x, y, z coordinates in centimetres of the mosquito at each video frame. Coordinates are in the world reference frame as defined in Fig. 2.1, with z oriented vertically up, and its origin at the centre of the funnel entrance (at 54.5 cm above the floor for the standing trap, and 81 cm for the hanging trap).

Database S2.2: Airflow speeds around the standing and hanging trap. The speeds have been measured with a hotwire anemometer (tetso 405i) at 76 locations within a two-dimensional vertical plane oriented perpendicularly to the open trapdoor in the trap entrance and at the opposite side of the CO_2 pipe. In the database, airspeed measurements of more than 45 s (at 1 Hz) are documented in meters per second with their respective radial (r) and vertical (z) coordinates in centimetres in the reference frame as defined in Fig. 2.5. The origin of this reference frame is set to the centre of the funnel entrance (at 59.2 cm above the floor for the standing trap, and 81 cm for the hanging trap).

Legends of the supplementary videos

The videos can be found here: `https://doi.org/10.1098/rsos.180246`

Video S2.1: Stereo recordings of flying mosquitoes around the hanging trap and localisation results of two-dimensional tracking (in red). The videos were recorded at 90 frames-per-second and replay is at 30 frames-per-second, so video playback is slowed down

Table S2.1: Statistical results of the comparison between the standing and hanging trap. Given the non-normality of the parameter distributions, p-values have been computed using non-parametric Wilcoxon rank sum tests. *p*-values of 0.05 and smaller are in bold.

parameter	trap orientation	n	mean	standard deviation	median	Q1	Q3	*p*-value
N_{trials}	standing	-	21	-	-	-	-	-
[-]	hanging	-	32	-	-	-	-	
T_{trials}	standing	-	315	-	-	-	-	-
[min]	hanging	-	480	-	-	-	-	
N_{tracks}	standing	-	1673	-	-	-	-	-
[-]	hanging	-	897	-	-	-	-	
T_{track}	standing	1673	1.51	1.65	0.99	0.44	1.86	<0.001
[s]	hanging	897	0.89	0.89	0.66	0.36	1.11	
L_{track}	standing	1673	36.05	36.81	26.19	9.97	47.50	<0.001
[cm]	hanging	897	18.38	18.49	13.53	7.29	23.15	
N_{tracks}/N_{trials}	standing	21	79.67	24.14	75	61.25	87.25	<0.001
[-]	hanging	32	28.03	10.94	27.5	20	33	
T_{track}/T_{trials}	standing	21	8.00	2.14	7.84	6.43	9.05	<0.001
[-]	hanging	32	1.66	0.76	1.53	1.18	1.91	
$N_{captured}$	standing	21	2.95	1.47	3	2	3.25	<0.001
[-]	hanging	32	0.78	1.13	0	0	1	
$R_{mosquitoes}$	standing	21	29.52%	14.65%	30%	20%	32.5%	<0.001
[-]	hanging	32	7.81%	11.28%	0%	0%	10%	
R_{tracks}	standing	21	3.89%	2.06%	3.75%	2.39%	4.86%	0.025
[-]	hanging	32	2.83%	4.13%	0%	0%	4.35%	
$f_{captures}$	standing	21	1.52	0.74	1.18	0.96	1.98	0.35
[min^{-1}]	hanging	32	1.66	2.13	0	0	3	
$V_{75\%}$	standing	-	228.08	-	-	-	-	-
[cm^3]	hanging	-	3991.40	-	-	-	-	
U	standing	226742	23.94	12.63	22.46	15.37	30.15	<0.001
[cm.s^{-1}]	hanging	71519	20.74	9.22	20.47	14.26	26.65	
α	standing	226742	545.06	620.52	367.72	194.76	674.14	<0.001
[degrees.s^{-1}]	hanging	71519	344.54	416.05	230.65	130.18	408.71	
a	standing	226742	2.32	1.94	1.78	0.97	3.11	<0.001
[m.s^{-2}]	hanging	71519	1.43	1.29	1.05	0.61	1.78	

three times. The tracks shown are the same as the ones presented in Fig. 2.2*a*.

Video S2.2: Stereo recordings of flying mosquito around the standing trap and localisation results of two-dimensional tracking (in red). The videos were recorded at 90 frames-per-second and replay is at 30 frames-per-second, so video playback is slowed down three times. The tracks shown are the same as the ones presented in Fig. 2.2*b*.
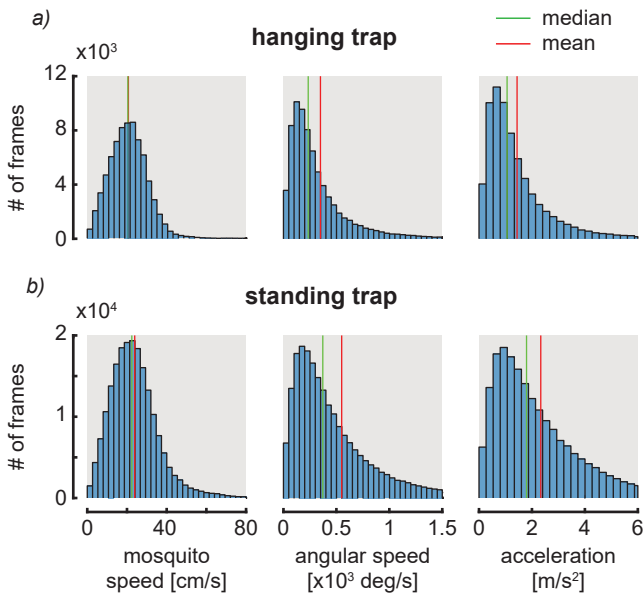
Figure S2.1: Histograms of translational flight speed, rotational flight speed and accelerations throughout all recorded tracks around the hanging trap (*a*) and the standing trap (*b*). Mean and median values are depicted by the red and green lines, respectively.

a1)   **cells: 6x6 mm**

a2)   **6x12 mm**

a3)   **12x12 mm**

a4)   **24x24 mm**

z-coordinate [cm]

radial distance [cm]

positional likelihood
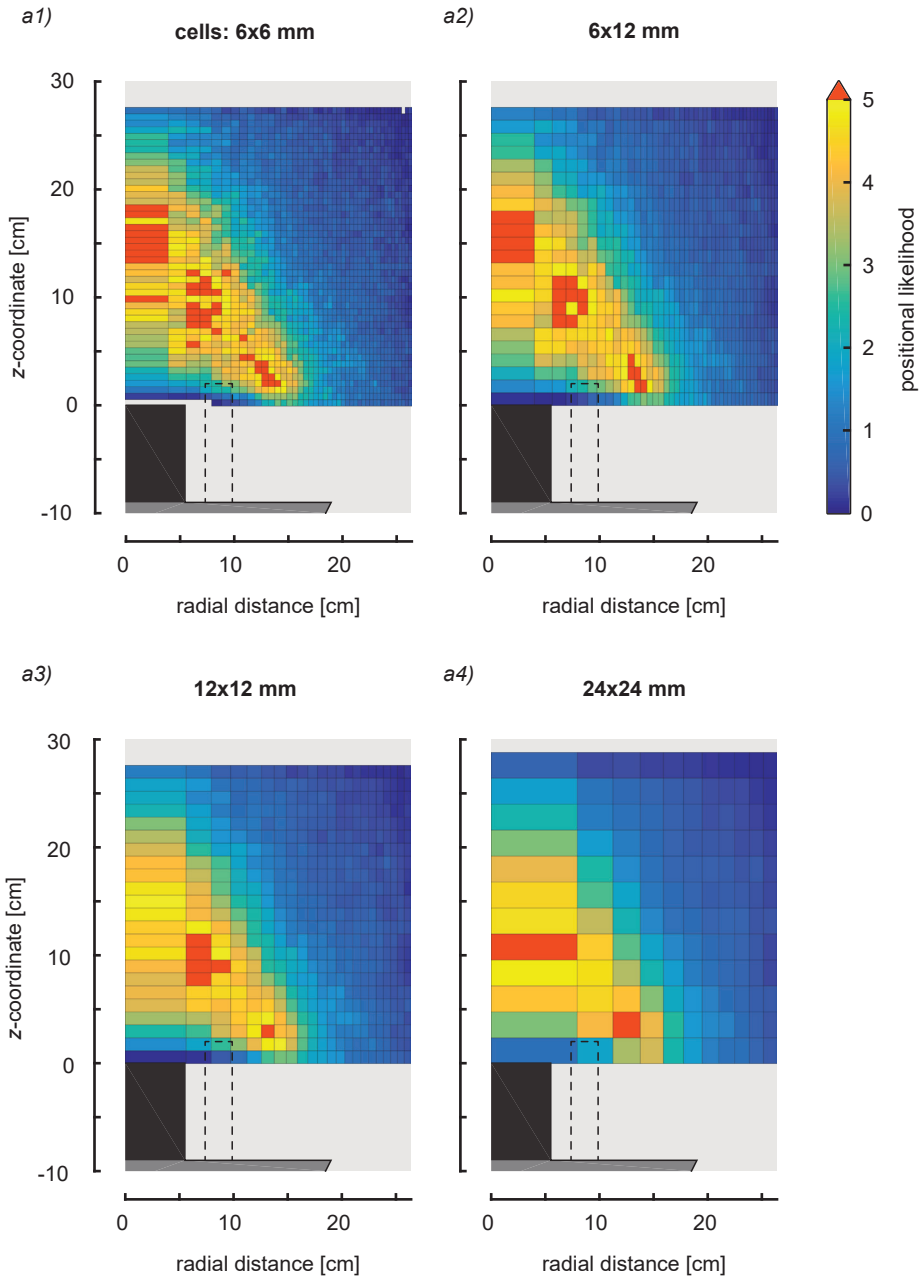
(Caption on the next page.)

Figure S2.2: Sensitivity analysis of positional likelihood for mean cross-sectional area of cells. Radial heat maps of the positional likelihood of mosquitoes around the standing trap with different mean cross-sectional area of cells. In order to give all three-dimensional cells the same volume, cell width varies in the radial direction. Above each panel, the corresponding mean cross-sectional area of the cells is written as the mean width x height. We did not find a dependence of our main results on cell mean cross-sectional area. Finally, 6x12 mm cells were chosen to have a volume of 114.04 cm^3 to obtain pertinent cell sizes compared to the entrance tube diameter and to allow clearly defined results. Similarly, cells of top-down views (Fig. 2.4, 2.5, S2.3 and S2.4) were given a constant rectangular volume of 112 cm^3 (length x width x height: 20x20x280 mm) similar to the constant volume of the previously describe rings.

a1)

# of tracks: 100

a2)

200

b1)

b2)
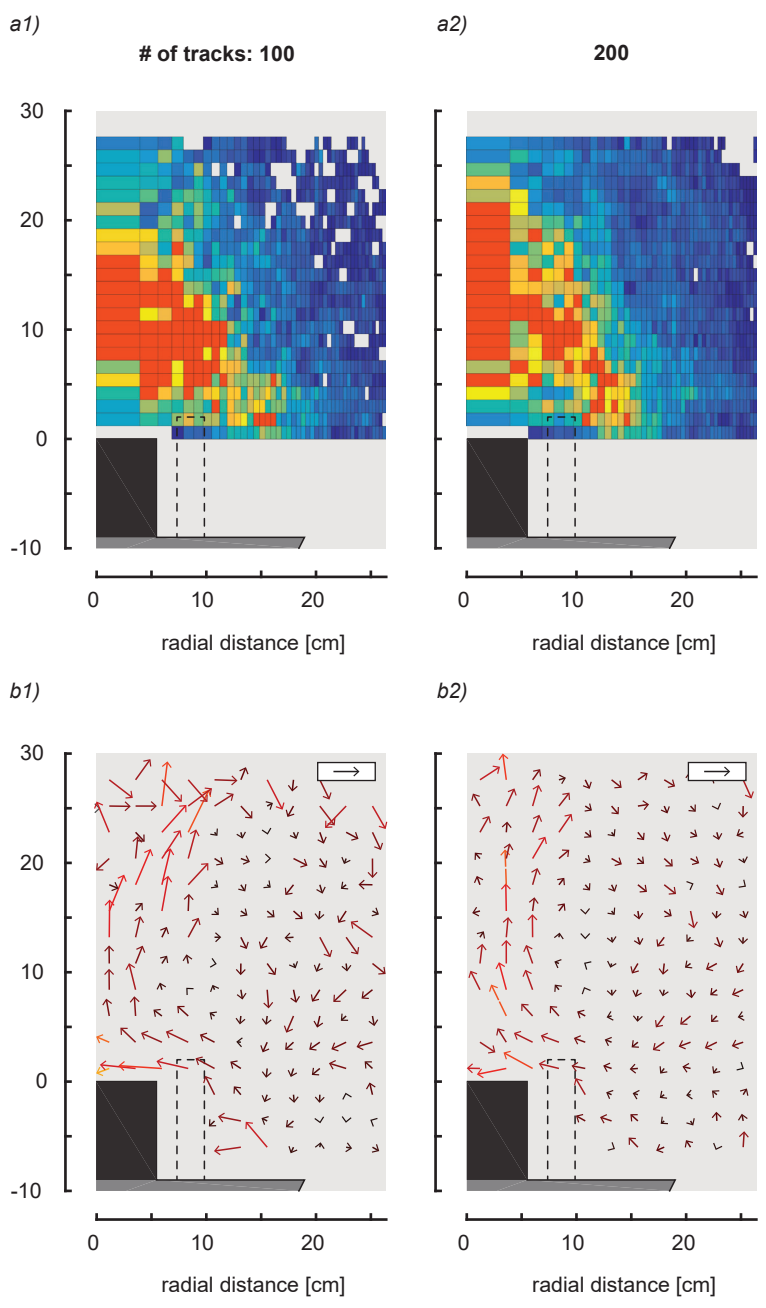
(Caption on the next pages.)
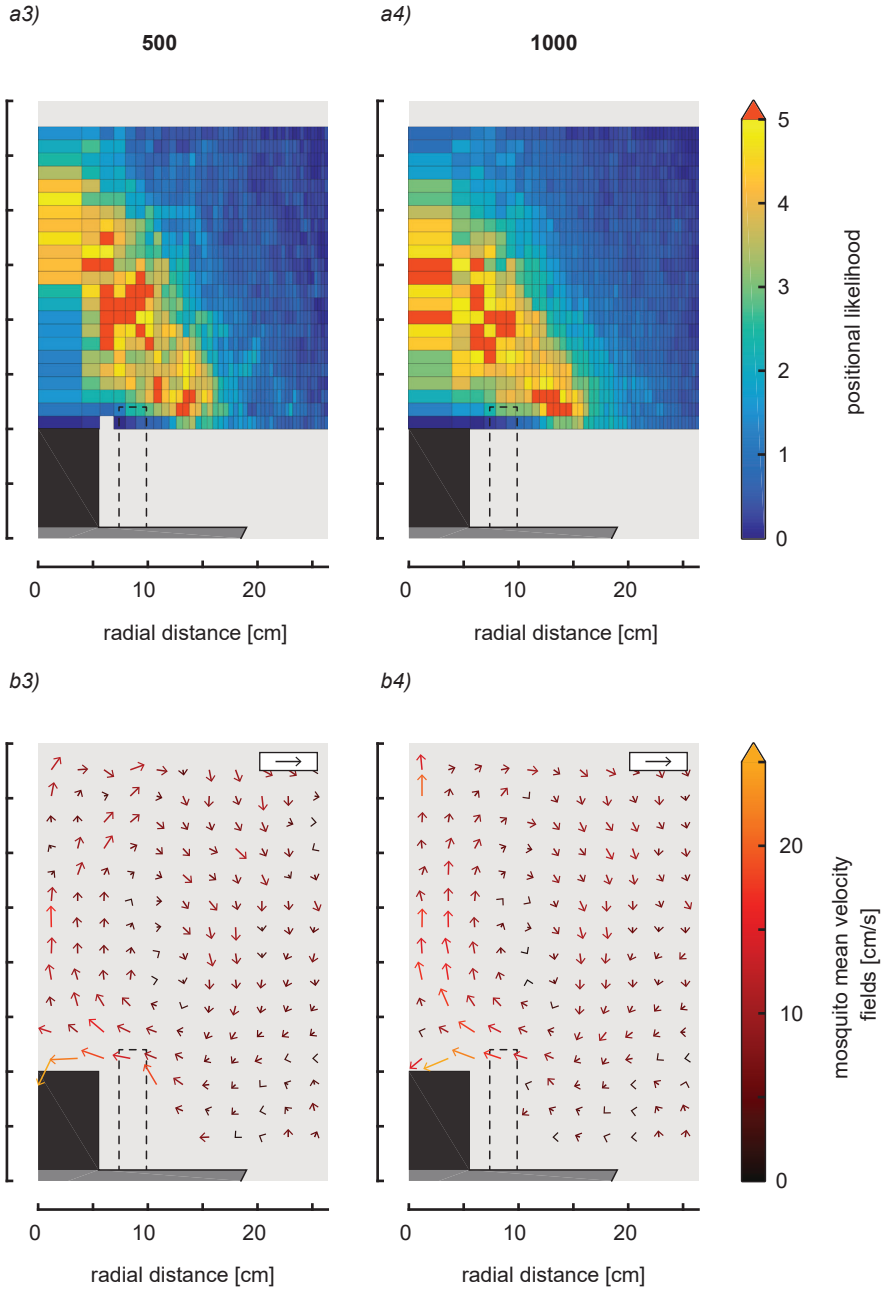
Figure S2.3: Sensitivity analysis of positional likelihood and velocity field for the number of recorded tracks. Radial heat maps of the positional likelihood (*a*) and mean velocity fields (*b*) around the standing trap for 100, 200, 500 and 1000 randomly chosen flight tracks. As expected, the variance of the results are anti-correlated with the number of analysed tracks. However, we did not find any other dependence on the number of analysed tracks when it is greater than 500. All velocity vectors that resulted from fewer than 5 detected tracks were discarded, and the cells were then left empty.

a1)

**hanging trap
1st half**

a2)

**hanging trap
2nd half**

b1)

b2)

(Caption on the next page.)

a3)

**standing trap
1ˢᵗ half**

a4)

**standing trap
2ⁿᵈ half**

positional likelihood

b3)

b4)

mosquito mean velocity
fields [cm/s]

radial distance [cm]

radial distance [cm]
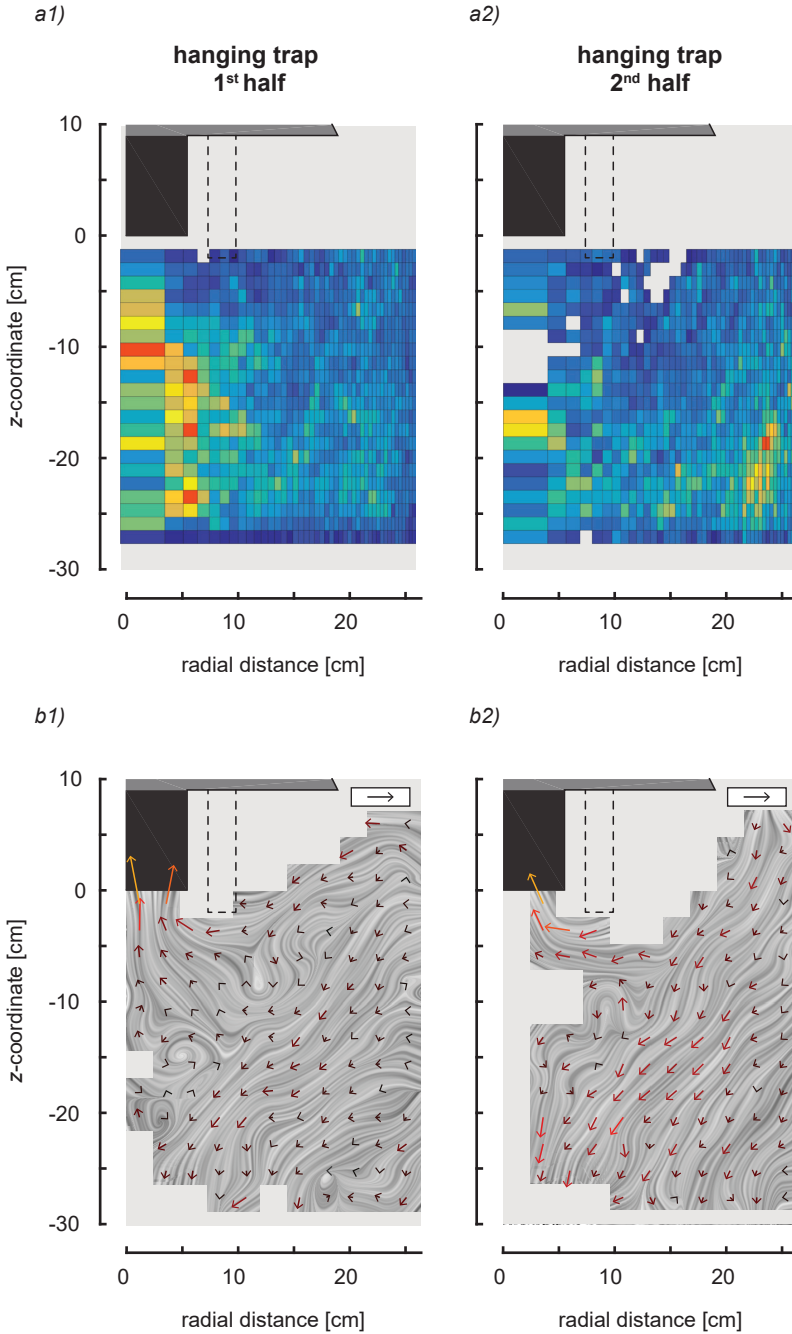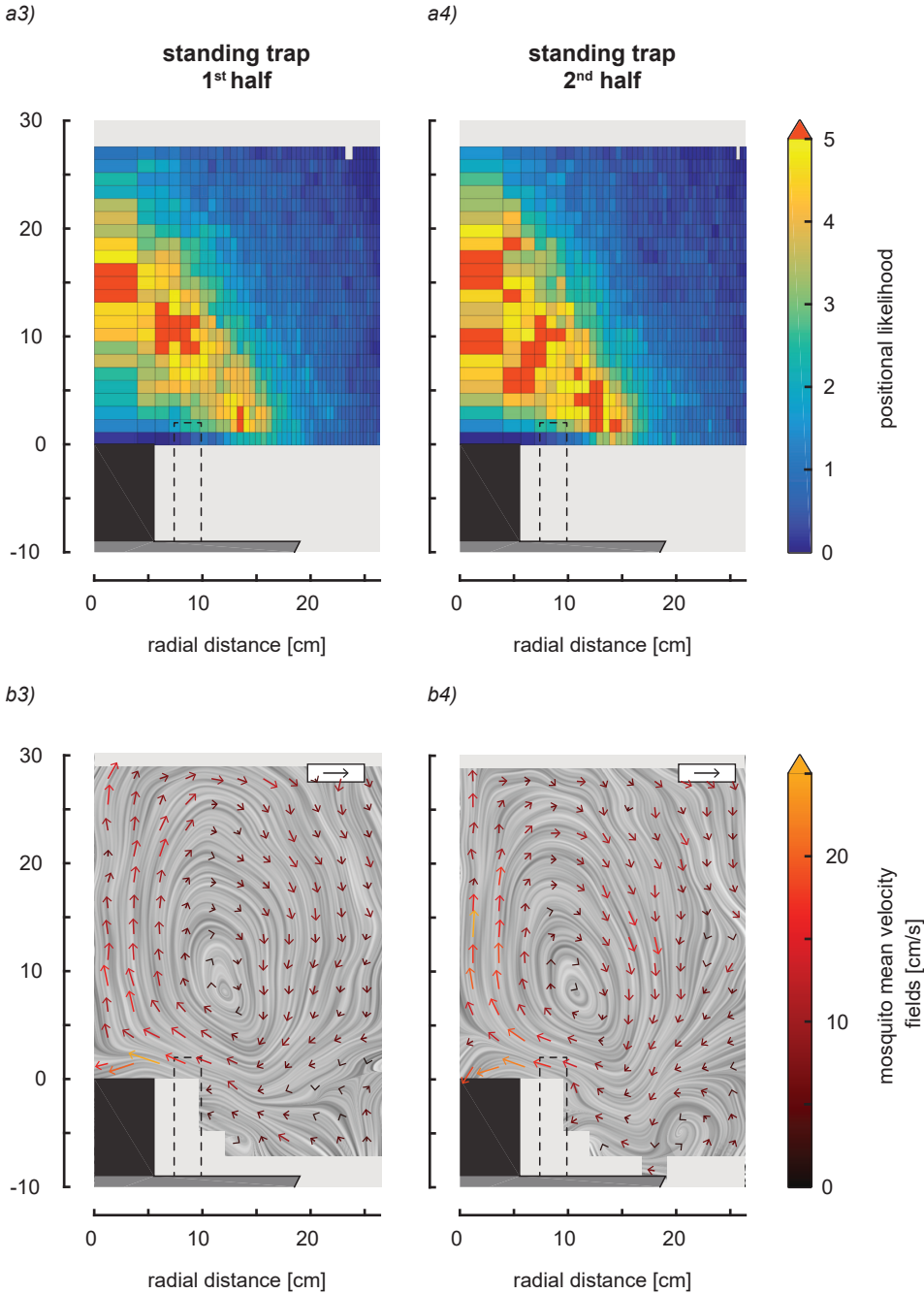
Figure S2.4: Comparison between the flight dynamics of the first and second 50% of tracks throughout the experiments. Positional likelihood (*a*) and velocity fields *(b)* of mosquito tracks that started before (1ˢᵗ half) or after (2ⁿᵈ half) the time threshold separating the total number of recorded tracks in two. This time threshold has been found equal to 4.46 min for the hanging trap and to 4.13 min for the standing trap. The results suggest that flight behaviour around the traps does not change over time within the time duration of our experiments.
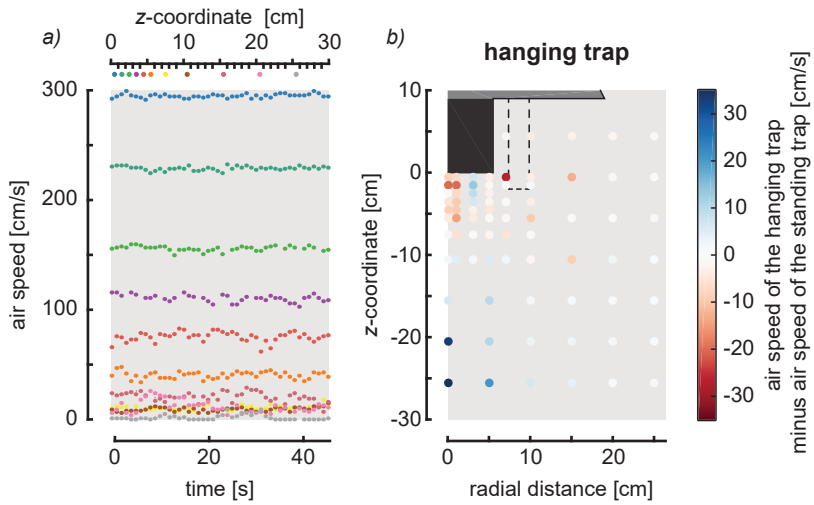
Figure S2.5: Additional data on the airflow measurement around the traps. (*a*) Measurements of the airflow speed at different heights above the centre of the standing trap ($r = 0$ mm). (*b*) Differences between the measured airflow speed below the hanging trap and above the standing trap.

95% confidence intervals of
mosquito mean speed [cm/s]

a) **hanging trap**

c) **standing trap**

b)

d)

Figure S2.6: 95% confidence intervals (standard error∗1.96) of the average translational flight speed (*a-d*) of mosquitoes flying around the two traps. The top row shows the vertical-radial heat maps, and the bottom row shows heat maps in the horizontal plane. The corresponding average translational flight speeds are show in Fig. 2.6.

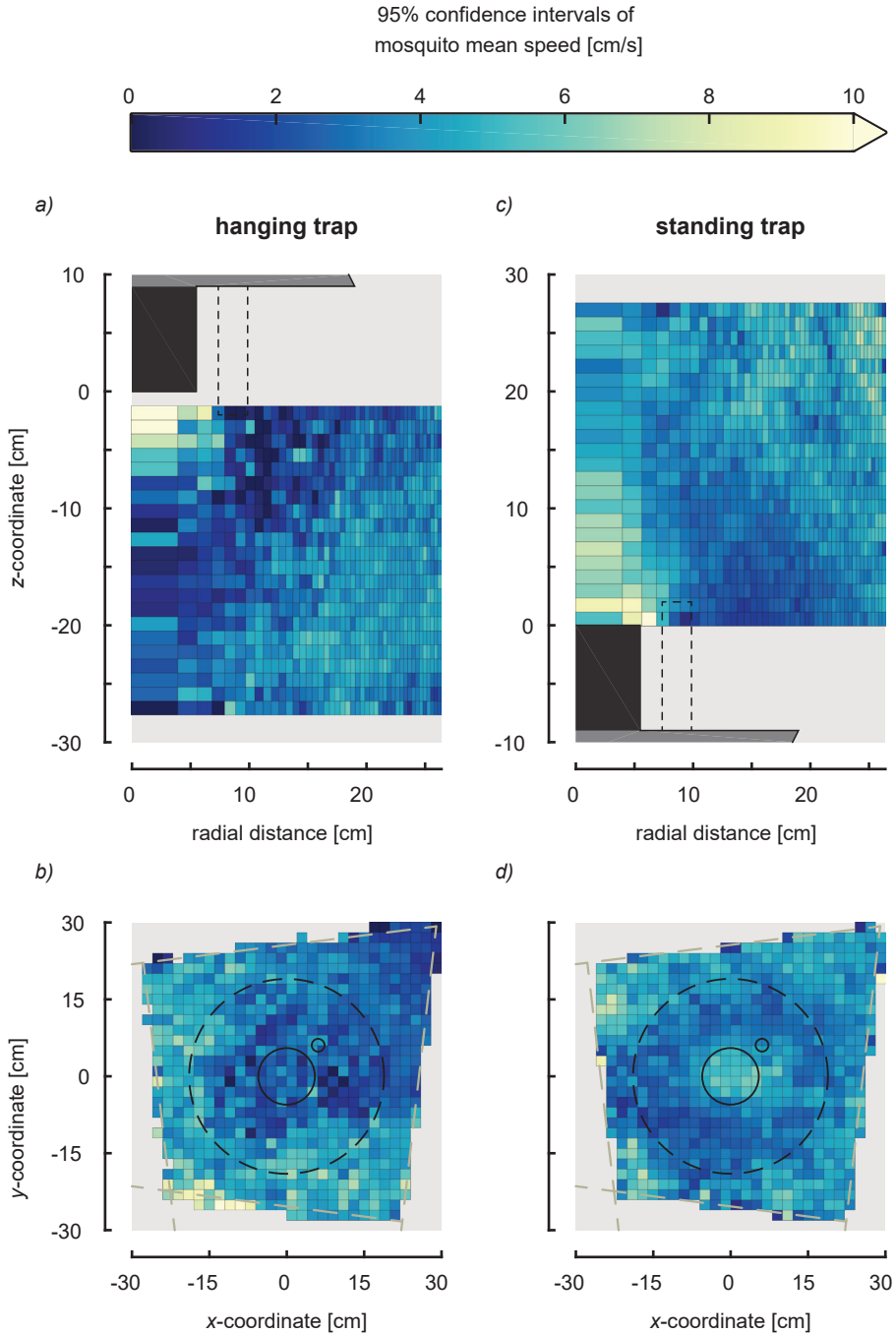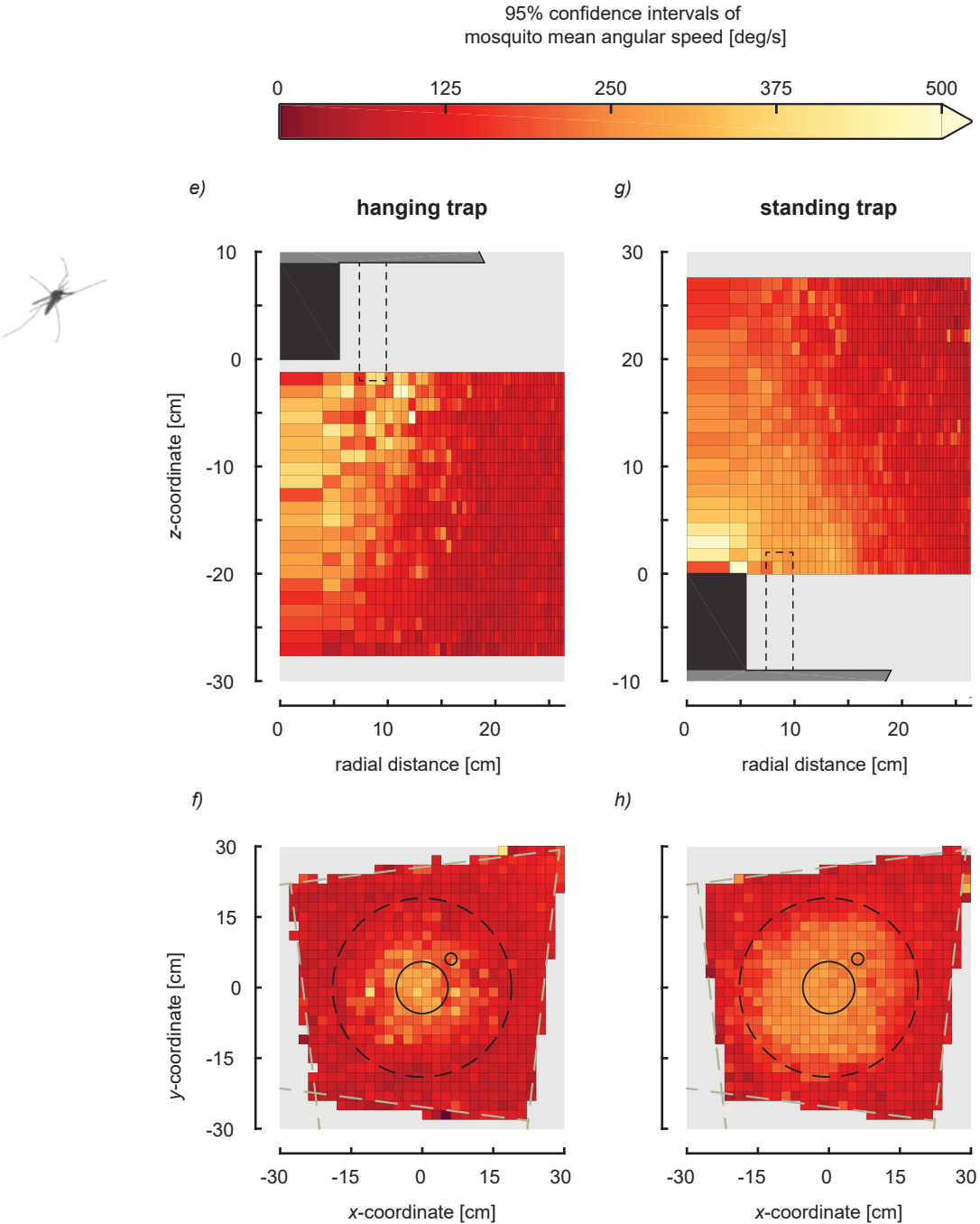**Figure S2.6: 95% confidence intervals (standard error∗1.96) of the average angular flight speed (*e-h*) of mosquitoes flying around the two traps.** The top row shows the vertical-radial heat maps, and the bottom row shows heat maps in the horizontal plane. The corresponding average angular flight speeds are show in Fig. 2.6.
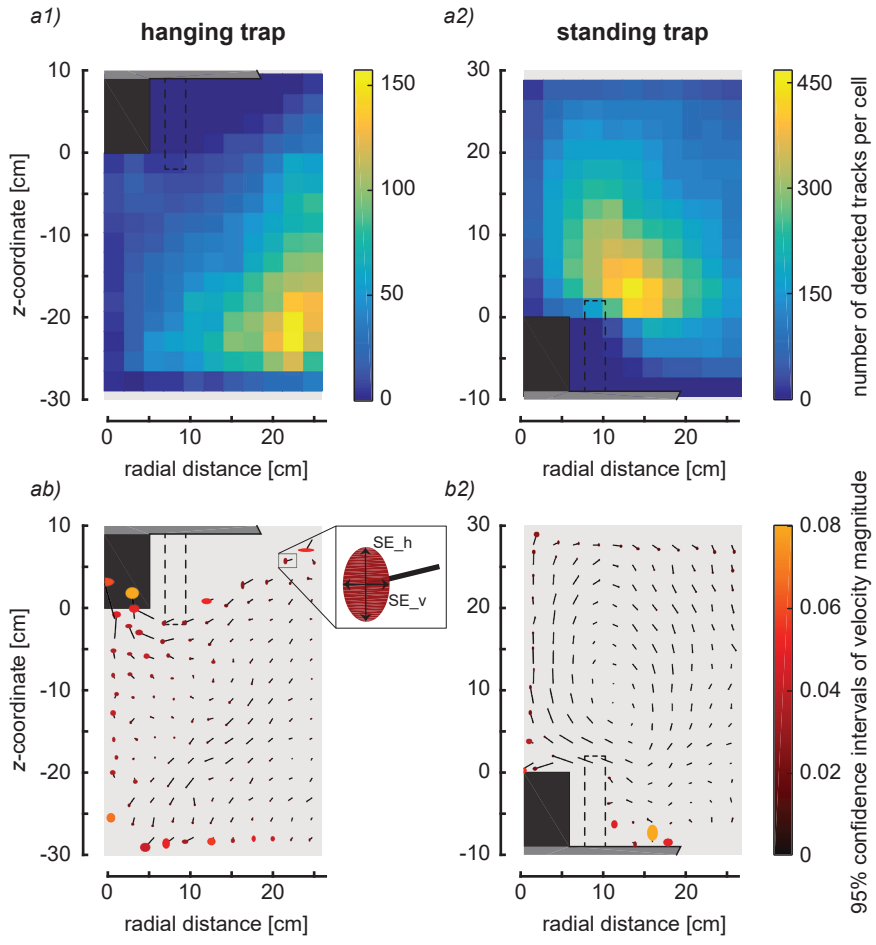
Figure S2.7: Additional data related to mosquito track location and mean velocity fields. (*a*) Radial plane heat maps of the number of tracks detected in each cell around the hanging and standing trap. (*b*) 95% confidence intervals in the vertical and horizontal directions (SE_v and SE_h, respectively) of each velocity vector corresponding to the mean velocity fields in Fig. 2.5. The cells are the same as those used for Fig. 2.5 and have a constant cell cross-section of 24x24 mm.
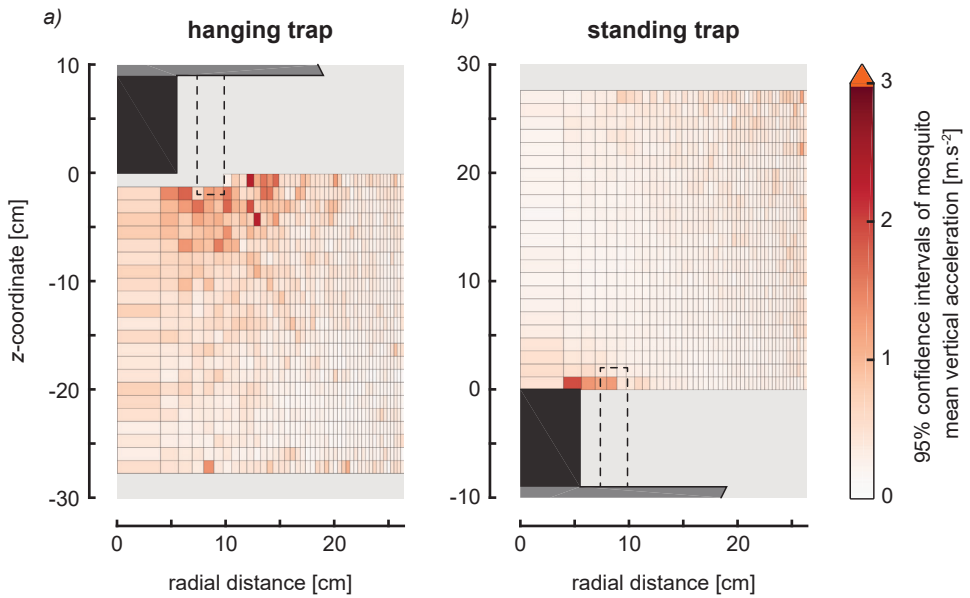
Figure S2.8: Distribution of the 95% confidence intervals of the average vertical accelerations of mosquitoes flying in the vicinity of the hanging trap *(a)* and the standing trap *(b).* The corresponding average vertical accelerations of mosquitoes are shown in the Fig. 2.6.
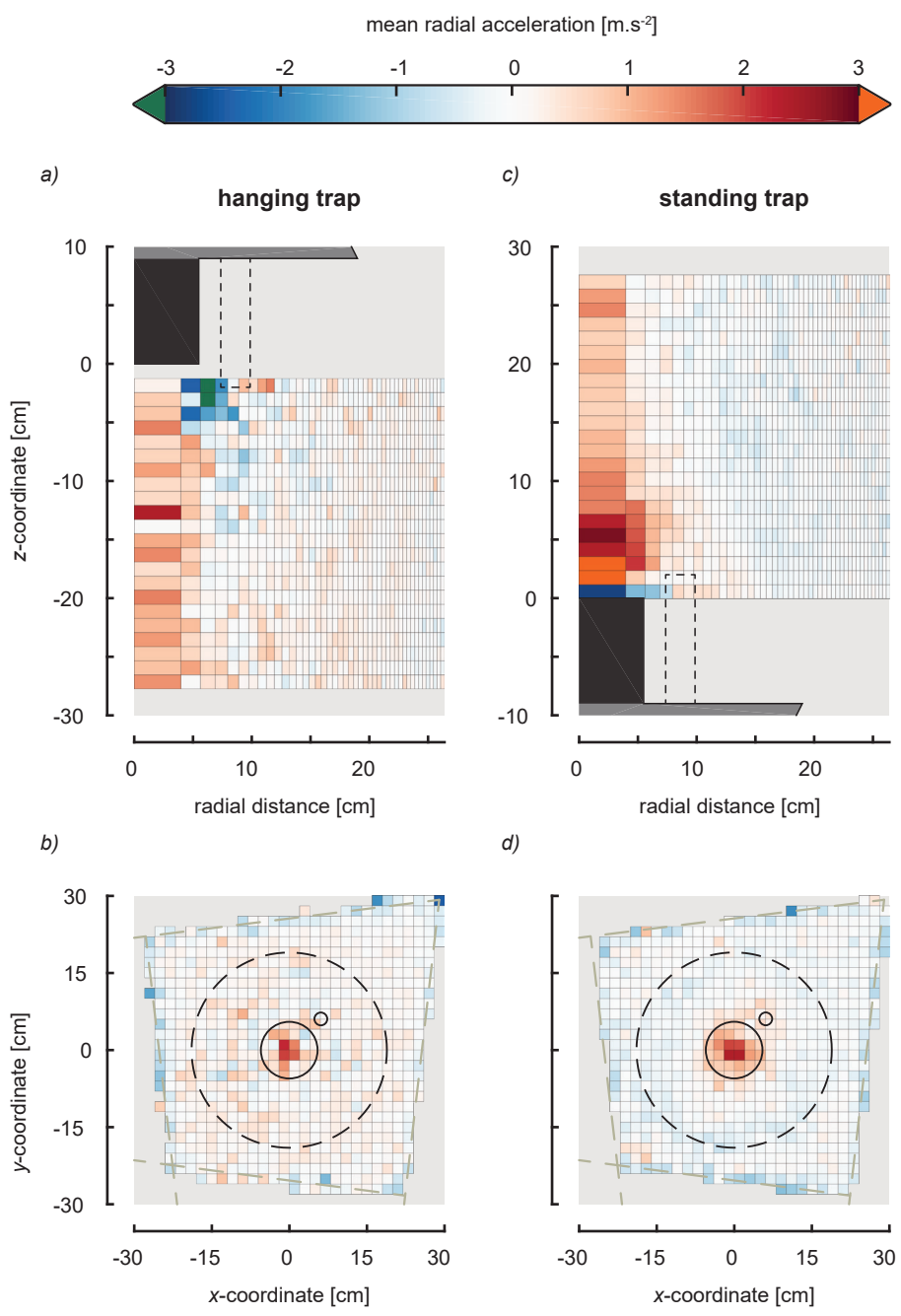
Figure S2.9: The mean radial acceleration of mosquitoes around the hanging and standing traps.
(*a-d*) Radial and top-down views of the mean flight acceleration of mosquitoes along the *r*-axis.
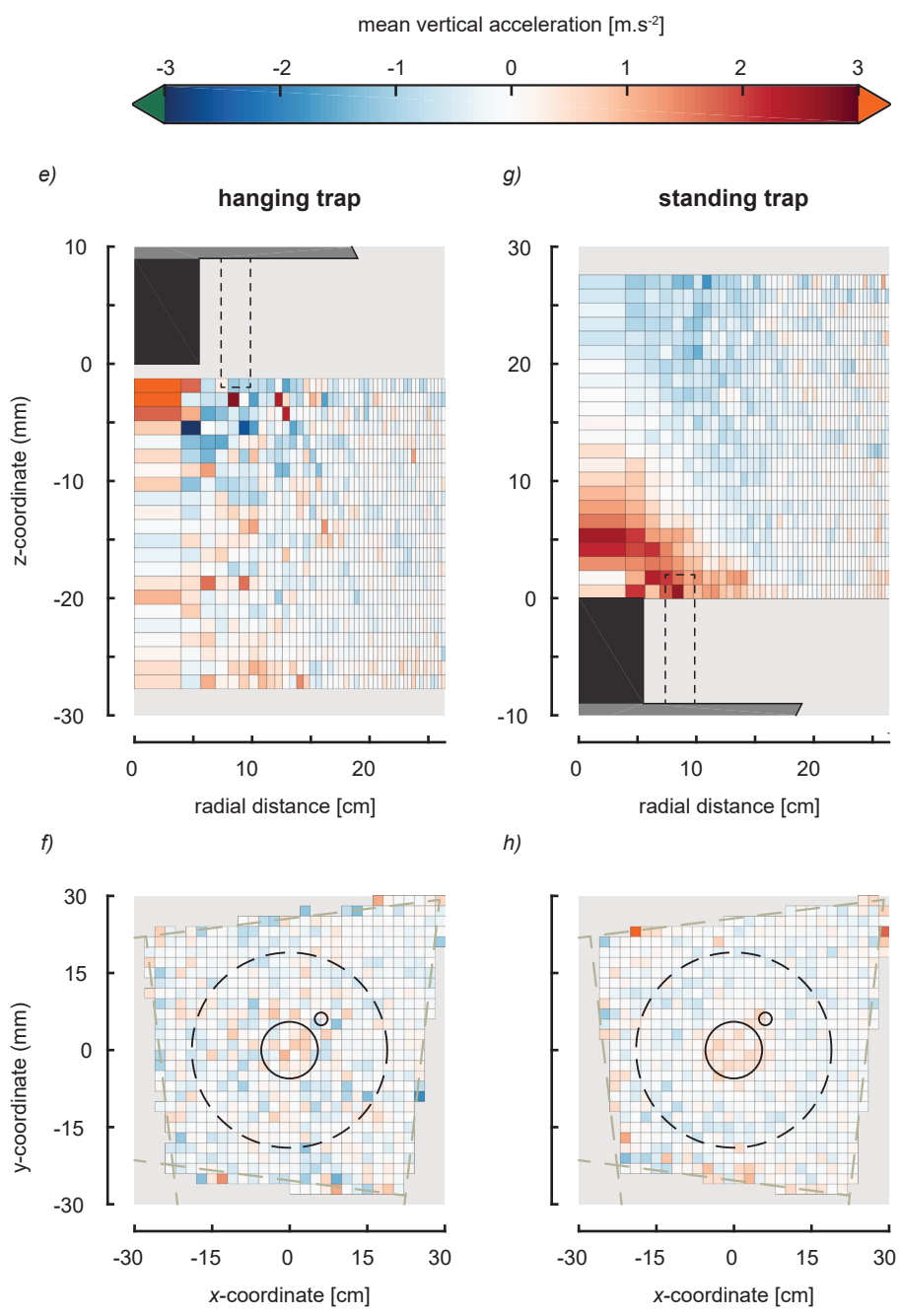
Figure S2.9: The mean vertical acceleration of mosquitoes around the hanging and standing traps.
(*e-h*) Radial and top-down views of the mean flight acceleration of mosquitoes along the *z*-axis.
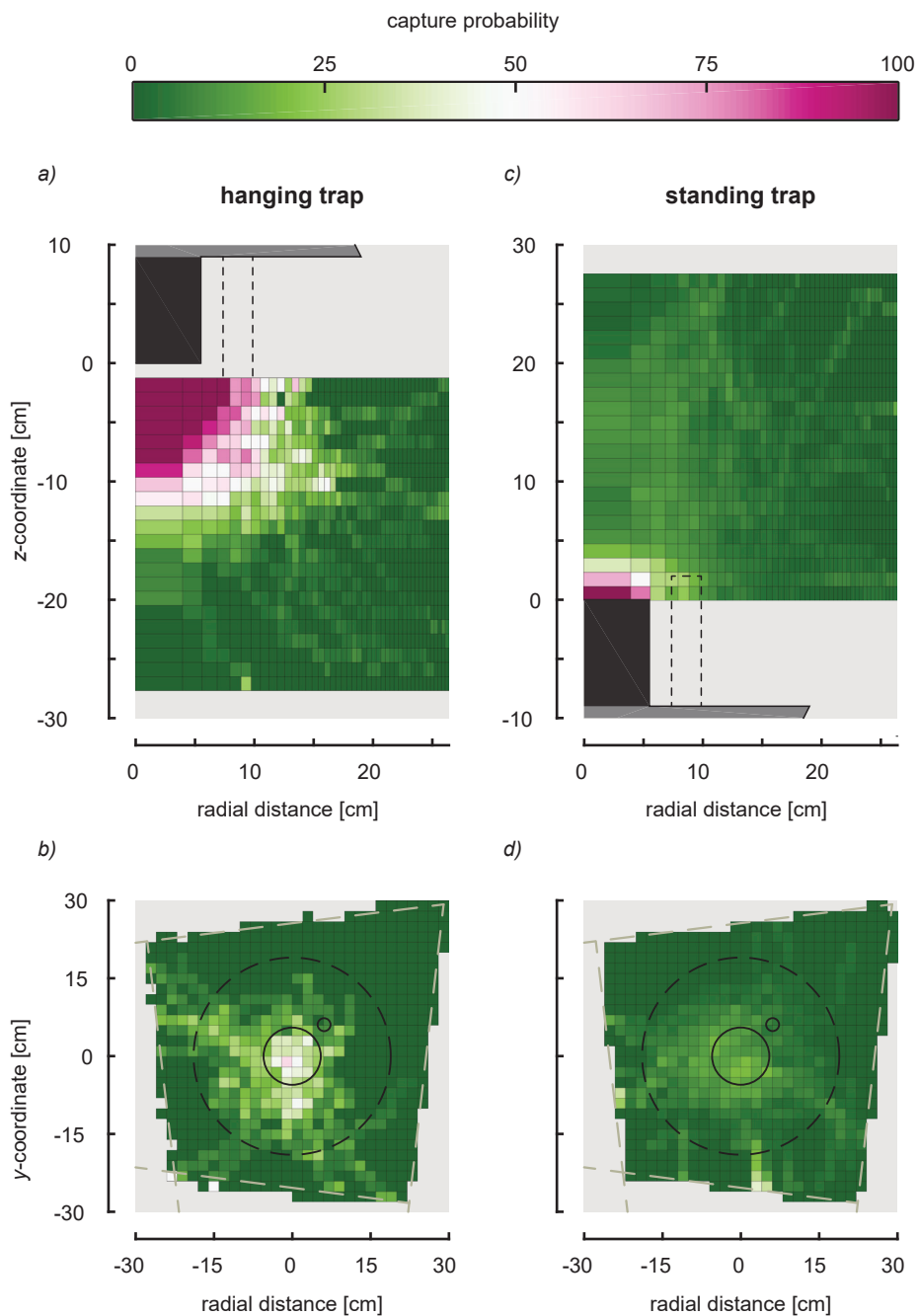
Figure S2.10: Heat maps of the capture probability. Radial views (*a,c*) and top-down views (*b,d*) of the ratio between tracks that led to capture versus those that did not, around the standing trap (*a,b*) and hanging trap (*c,d*). The purple region corresponds to the volume within which more than 75% percent of the tracks led to capture.

a1)

hanging trap

a2)

**hanging trap
close to the CO$_2$ pipe**

b1)

b2)
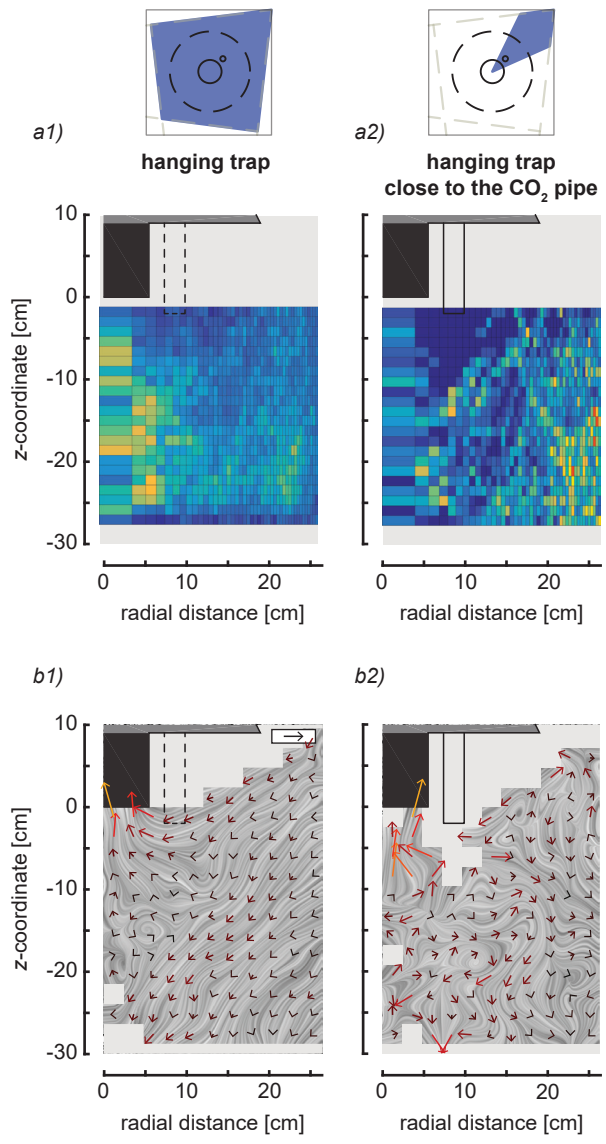
(Caption on the next pages.)
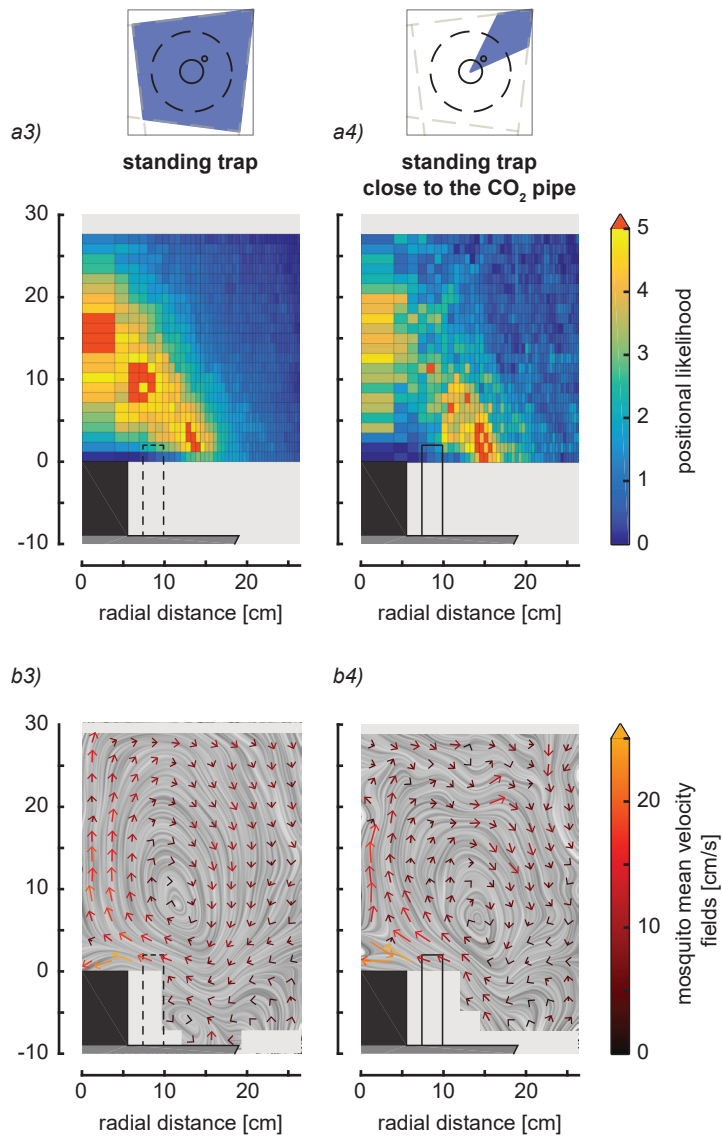
Figure S2.11: Likelihood of mosquito position (*a*) and averaged velocity vector fields (*b*) around the CO$_2$ funnel and around the complete trap (as indicated on the top of each column). For the results around the CO$_2$ pipe, the region was bound by an angle of +/- 20 degrees.
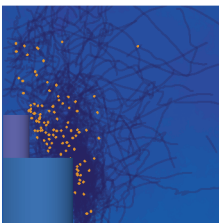
Chapter 3 ————————————————————————————

Lure, retain, and catch malaria mosquitoes. How heat and humidity improve odour-baited trap performance

Antoine Cribellier[1], Jeroen Spitzen[2], Henry Fairbairn[1,3], Cedric van de Geer[1,2,3,4], Johan L. van Leeuwen[1], Florian T. Muijres[1]

[1] Experimental Zoology Group, Wageningen University & Research, Wageningen, The Netherlands

[2] Laboratory of Entomology, Wageningen University & Research, Wageningen, The Netherlands

[3] Faculty of Industrial Design Engineering, Delft University of Technology, Delft, The Netherlands

[4] Ifakara Health Institute, Ifakara, Tanzania

——

———————————————————————

Abstract

When seeking a human for a blood meal, mosquitoes use several cues to detect and find their hosts. From this knowledge, counter-flow odour-baited traps have been developed that use a combination of CO_2, human-mimicking odour, visual cues and circulating air-flow to attract and capture mosquitoes. Initially developed for monitoring, these traps are now also being considered as promising vector control tools. The traps are attractive to host-seeking mosquitoes, but their capture efficiency is low. It has been hypothesized that the lack of short-range host cues, such as heat and increased local humidity, often prevent mosquitoes from getting close enough to get caught; this lack might even trigger avoidance manoeuvres near the capture region. This study investigated how close-range host cues affect the flight behaviour of *Anopheles* female malaria mosquitoes around odour-baited traps, and how this affects trap capture performance. For this, a novel counter-flow odour-baited trap was developed, the M-Tego. In addition to the usual CO_2 and odour-blend, this trap can provide the short-range host cues, heat and humidity. Systematically adding or removing these two cues, it was tested how this affected the trap capture percentages and flight behaviour. First, capture percentages of the M-Tego with and without short-range host cues to the BG-Suna trap were compared, in both laboratory and semi-field testing. Then, machine-vision techniques were used to track the three-dimensional flight movements of mosquitoes around the M-Tego. With heat and humidity present, the M-Tego captured significantly more mosquitoes as capture percentages almost doubled. Comparing the flight behaviour around the M-Tego with variable close-range host cues showed that when these cues were present, flying mosquitoes were more attracted to the trap and spent more time there. In addition, the M-Tego was found to have a better capture mechanism than the BG-Suna, most likely because it does not elicit previously observed upward avoiding manoeuvres. Results suggest that adding heat and humidity to an odour-baited trap lures more mosquitoes close to the trap and retains them there longer, resulting in higher capture performance. These findings support the development of control tools for fighting mosquito-borne diseases such as malaria.

3.1 Introduction

Anthropophilic mosquitoes are vectors of dangerous diseases such as dengue fever and malaria, hence their host-seeking behaviour has been studied thoroughly (Gmp/who, 2019). Mosquitoes rely on the detection of CO_2 and volatile odours to find human hosts (Dekker and Cardé, 2011; McMeniman et al., 2014). Then, like many other insects, mosquitoes perform a so-called cast and surge strategy to fly towards the odour source [2,4-6]; they surge upwind when detecting an odour plume and cast crosswinds if they lose the plume. Finally, mosquitoes inspect visually contrasting objects and initialize landing in the presence of short-range host cues, such as heat or increased local humidity (van Breugel et al., 2015; Cardé, 2015; Hawkes and Gibson, 2016; McMeniman et al., 2014; Olanga et al., 2010; Raji and DeGennaro, 2017; Spitzen et al., 2013; Vinauger et al., 2019).

Based on this knowledge on mosquito host-seeking behaviour, odour-baited traps have been developed (Cooperband and Cardé, 2006b; Hiscox et al., 2014; Jawara et al., 2009). These traps usually combine CO_2, a bait mimicking human skin odours, and visual contrasts to attract mosquitoes (Hawkes et al., 2017; Hiscox et al., 2014). Most odour-baited traps have a single fan to generate a counter flow to dissipate the odour away from the trap, and capture mosquitoes by sucking them into the trap (Cooperband and Cardé, 2006b; Cribellier et al., 2018; Hiscox et al., 2014). Odour-baited traps can attract many mosquito species and have been used successfully for years as research tools for monitoring mosquito populations (Bhalala and Arias, 2009; Hiscox et al., 2014). Recently, these traps have been considered as tools for integrated vector management, and used effectively in the field as such (Homan et al., 2016). In the context of the recent worldwide slowdown of decrease in malaria cases, which is thought to be partly induced by the increasing mosquito resistance against widely used insecticides (Gmp/who, 2019), such novel insecticide-free vector control tools are a promising alternative.

Understanding capture mechanisms of traps and flight dynamics around these traps is essential for further improvement of capture performance of the system. But only a few studies looked at mosquito flight behaviour in the vicinity of odour-baited traps. First, Cooperband and Carde analysed three-dimensional flight tracks of two *Culex* mosquito species flying towards CO_2-baited traps in a semi-field tent (Cooperband and Cardé, 2006a). They showed that differences in capture percentages between the traps correlated with changes in the observed flight dynamics of mosquitoes.

More recently, Cribellier *et al*. reconstructed thousands of three-dimensional flight tracks of malaria mosquitoes (*Anopheles coluzzii*) interacting with the BG-Suna trap (Biogents, Germany) in its default hanging position and in an opposite standing orientation (Cribellier et al., 2018). The standing orientation made the studied BG-Suna analogous to a BG-Sentinel trap (Biogents, Germany), which has been developed for capturing *Aedes* mosquitoes. The standing BG-Suna was found to be more attractive and overall performed better than the hanging BG-Suna. However, only the standing BG-Suna elicited upward avoiding manoeuvres from mosquitoes flying above its inlet. Such avoiding behaviour may be due to the lack of short-range host cues or be mediated by the high-speed suction flow generated by the traps (Amos et al., 2020; Cribellier et al., 2018). As a result, only a low percentage of flight trajectories near the trap led to capture in both trap orientations (Cribellier et al., 2018). Despite the fact that the BG-Suna trap seems to have a relatively low capture efficiency, long-term employment in the field resulted in significant reductions in mosquito populations and a decrease in malaria incidence (Homan et al., 2016). Follow-up studies confirmed these findings on mosquito flight dynamics around traps. Batista *et al*. found that *Anopheles arabiensis* follow similar flight patterns below the BG-Malaria trap (Batista et al., 2019). This trap is adapted from an upside-down BG-Sentinel to trap anopheline mosquitoes. Finally, by studying the flight behaviour of *Aedes aegypti* around the BG-Sentinel, Amos *et al*. also observed upward avoidance responses near the trap inlet, and confirmed that tested traps showed low capture efficiency (Amos et al., 2020).

Several mosquito traps use short-range host cues such as heat and humidity to increase capture performances (Cooperband and Cardé, 2006a; Kline, 2002). Odour-baited CDC-type traps (Centers for Disease Control, USA) were found to capture significantly higher numbers of *Aedes*, *Anopheles* and *Culex* mosquitoes when generating heat using a 50W moist heating pad (Kline and Lemire, 1995). Mosquito Magnet traps run on propane gas that is catalytically converted to produce CO_2, heat, and moisture (Cooperband and Cardé, 2006a). And heat was found to be a crucial cue to elicit the landings of anopheline mosquitoes necessary for the Human Decoy Trap (HDT) (Hawkes et al., 2017; Howlett, 1910; Spitzen et al., 2013). This adhesive trap uses a combination of CO_2 and odour provided from people or cattle in a nearby tent, with visual cues and heat generated by a black container filled with warm water (surface temperature of $35 \pm 5°C$) (Abong'O et al., 2018; Hawkes et al., 2017). Despite their good capture performance, these traps have a number of practical drawbacks for potential use as vector control tools against *Anopheles* mosquitoes. The CDC-type traps with a heating pad require high electric power input for generating heat. The Mosquito Magnet traps are expensive and distribution to malaria-endemic countries would be more than challenging. The HDT trap requires live bait as well as the warming up of a large quantity of water at high temperature ($\sim 80°C$) (Abong'O et al., 2018).

It is still unknown how adding heat and increased local humidity to odour-baited traps affects mosquito flight behaviour near the trap entrance. This study tested the hypothesis that without close-range host cues such as heat and humidity, mosquitoes often do not get close enough to odour-baited traps to get caught, resulting in a low capture efficiency. This was done by studying the flight behaviour of *Anopheles* mosquitoes around a new counter-flow odour-baited trap, the M-Tego. This trap was developed by the authors in order to be able to generate both heat and humidity in addition to the CO_2, odour blend and visual cues that are usually implemented in odour-baited traps. Additionally, the M-Tego is easy to transport and maintain and as such, has the potential for a wide use in vector control programmes (Homan et al., 2016). As a benchmark, the capture percentage of the M-Tego was compared to the ones of the standing BG-Suna trap in both laboratory and semi-field conditions. The M-Tego without or with additional cues was found to capture significantly more mosquitoes than the standing BG-Suna in the laboratory and in semi-field conditions.

To investigate why such high capture percentages were observed, the flight behaviour of mosquitoes around the M-Tego was recorded, with or without short-range host cues. Despite high similarities between flight behaviour around the BG-Suna and the M-Tego, it was found that, if additional host cues were present, flight activity greatly increased in a region around the rim of the odour outlet. Finally, contrary to what has been found for the BG-Suna, avoidance behaviours of mosquitoes were not observed above the M-Tego. This lack of avoidance manoeuvres may explain why the M-Tego even without additional host cues had higher capture percentages than the BG-Suna. These results are promising for integrated vector control programs to improve human health and welfare.

3.2 Materials and methods

3.2.1 Experimental animals

For all laboratory experiments at Wageningen University, female *Anopheles coluzzii* mosquitoes were used. These came from a laboratory-reared colony that originated from Suakoko, Liberia in 1987. The colony is housed in the Laboratory of Entomology (Wageningen University & Research, The Netherlands) with a clock shifted 12h light : 12h dark cycle, and at fixed temperature of 27 °C and relative humidity of 70%. Adults were kept in Bug-Dorm (MegaView Science Co. Ltd., Taiwan) cages (30×30×30 cm) and fed sugar water solution with 6% glucose. Additionally, they were blood-fed daily with human blood (Sanquin, Nijmegen, The Netherlands) using a membrane feeding system (Hemotek, Discovery Workshop, UK). Female mosquitoes could lay their eggs on wet filter papers that were then moved to plastic trays filled with water. Emerging larvae were fed with Liquifry No. 1 fish food and TetraMin Baby (Tetra Ltd, UK). Finally, new pupae were placed in new Bug-Dorm cages to emerge. Males and females were kept together so they could mate. Non-blood-fed adult females (age = 9.8 ± 1.4 days (mean ± std)) were collected between 12 and 16 hours before experiments.

Semi-field experiments in Tanzania were done using 3 to 8 days old *Anopheles gambiae s.s.* female mosquitoes. These mosquitoes were reared under standard insectary conditions of 27 ± 5 °C (room temperature), 40-100% relative humidity and a 12L:12D cycle. Larvae were fed *ad libitum* on TetraMin fish flakes (Tetra Ltd., UK). Adult mosquitoes were kept in metal cages (30x30x30 cm) and fed *ad libitum* on a 10% glucose solution. Female mosquitoes used for the rearing were blood-fed with cow blood using a membrane feeding system (Hemotek).

3.2.2 Odour-baited traps

The traps used in these experiments were the BG-Suna (Biogents, Germany) and prototypes of the new M-Tego trap (PreMal b.v., The Netherlands). The BG-Suna was used in a standing orientation, thus mimicking the BG-Sentinel, as this position was found to have a better capture efficiency and attractiveness than the hanging BG-Suna (Cribellier et al., 2018; Visser et al., 2020). In both traps, an odour source containing MB5 blend was used to simulate human skin odour (van Loon et al., 2015; Visser et al., 2020), and CO_2 to simulate human breath. For the laboratory experiments, CO_2 was provided using a pressurized canister, and consisted of a mixture of 5% CO_2 with 95% air at a flow rate of 200 ml/min. For the semi-field tests, CO_2 was produced using a mixture of 17.5 g of yeast and 500 g of molasses in 2 L of water (Mweresa et al., 2014; Smallegange et al., 2010). As in Cribellier *et al.* (Cribellier et al., 2018) the CO_2 pipe of the BG-Suna was shortened and the top of the inlet was levelled to minimize blind spots of the cameras.

The M-Tego is a novel trap developed by the authors (see author contributions for de-

tails) at Wageningen University (The Netherlands) in collaboration with industrial designers from Delft University of Technology (The Netherlands) (see Fig. S3.1). In this study, prototypes of this novel trap were used, from here on those prototypes will be referred to as M-Tego traps. The M-Tego trap uses a similar counter-flow principle as the BG-Suna to attract and capture mosquitoes, and both traps use the same brushless 12V dc fan. With a diameter of 30 cm and a height of 38.8 cm, the M-Tego is smaller than the BG-Suna trap that has a diameter of 52 cm and a total height of 39 cm. Its inlet is slightly higher than that of the BG-Suna (9.5 cm *vs* 8.3 cm with levelled inlet) but both inlets have the same diameter of 11 cm. The M-Tego has a foldable black polyester tarpaulin bag (70 g per sq m, Gamma, The Netherlands), which makes transportation easier, as well as an HDPE insect net (Howitec, The Netherlands) on the top of the tarpaulin bag, to allow the outward circulation of the odour-saturated air. Additionally, the M-Tego uses an inlet module with an integrated catching cage that simplifies the removal of caught mosquitoes (see supplementary Fig. S3.1). These design decisions improve user-friendliness and aim to reduce fabrication costs, which is beneficial for a vector control tool in rural Africa. To generate heat similar to that produced by a human body (37°C), the M-Tego uses a 2-m Nichrome wire (diameter 0.5 mm) wrapped around the top of its inlet. The heater has an electric power requirement of 9.6 W (12 V and 0.8 A)). Finally, the trap can be filled with 1 L of warm water at 40°C to increase local relative humidity and temperature. The wire is not in contact with the water and thus cannot warm it up. Instead, the water needs to be warmed up passively during the day or using exterior means.

3.2.3 Experimental setups

Three experiments were performed. First, in dual choice testing in the laboratory, two traps were placed next to each other in a flight tent. Mosquitoes were released in the tent where they were free to fly around the two traps. Using this set-up, trap capture percentages were compared to each other. Secondly, semi-field experiments were performed inside three large screen houses in Tanzania. In each screen house, one of the tested traps was placed next to a replicate of a rural African house. The numbers of released mosquitoes that were captured by each trap were then compared. Third, to study the flight behaviour of mosquitoes around the M-Tego, with or without additional host cues, their flight trajectories were tracked in the laboratory in the vicinity of the trap using machine vision techniques.

3.2.4 Dual-choice experiments

The goals of the dual-choice tests were, first, to benchmark the capture performance of the M-Tego by comparing it to the well-established BG-Suna and, secondly, to quantify the effect of adding short-range host cues on the capture performance of the M-Tego. Five trap conditions were tested *versus* the same BG-Suna: the BG-Suna #2 (control), the M-

Tego without additional cues, the M-Tego with heat, the M-Tego with warm water, and the M-Tego with heat and warm water.

The dual-choice tests were performed in a netting cage of 2.9×2.5×2.5 m (Howitech, The Netherlands, see supplementary Fig. S3.2) inside a climate-controlled room (ambient temperature = 26.1 ± 0.9 °C (mean ± std), and relative humidity = 72.9% ± 3.9%). On each side of the cage, a trap could be placed above the centre of a 1 × 1 m horizontal white ground plate. These two plates were placed in front of two 1 × 2 m vertical white plates and next to each other, separated by another 1 × 2 m vertical plate. All traps were placed in the cage such that the top of the trap inlet was at a height of 54.5 cm, in order to be consistent with our previous study (Cribellier et al., 2018). During the experiments, the room was illuminated only by a single nightlight (0.4 W), placed above the centre of the cage.

Each trap was equipped with a MB5 odour source (OS1 or OS2) and placed on the left or right side of the cage. The position of the traps (left or right) and the odour source used (OS1 or OS2) were chosen following a quasi-randomized planning where all combinations of conditions were tested at least seven times. See supplementary database S1 for a summary of all test conditions.

Before each experiment, the traps and the experimental set-up were cleaned using a 15% ethanol solution. All handling of the materials and mosquitoes was done wearing nitrile gloves to minimize the risk of skin odour contamination. After setting up the traps, 50 mosquitoes were released from a holding container on the opposite side inside the netting cage by pulling a string outside of the cage. Then, the experimenter left the room. Mosquitoes could then choose to fly around their preferred trap. After 20 minutes, the experimenter re-entered the room, closed the traps, killed the remaining mosquitoes in the cage using an electric mosquito zapper and cleaned the cage with a vacuum cleaner. Each trap capture bag was then placed in a freezer to kill captured mosquitoes, which were manually counted later. Relative humidity and temperature inside the room were recorded before and after each trial using a weather station (TFA Dostmann/Wertheim, Kat. Nr. 30.5015). Four such dual-choice trials were done during each experimental morning, which coincided with the dark period of night-active mosquitoes.

3.2.5 Semi-field testing

To verify the results of the dual-choice laboratory tests, the capture percentage of the BG-Suna and the M-Tego with or without heat and warm water in semi-field experiments were compared. These experiments were performed at the Ifakara Health Institute (Ifakara, Tanzania) during the first week of November 2018. For the experiments, three screen houses of 10×10 m each were used with a slightly scaled-down house inside (see Fig. S3.3). These houses were built from local materials such as bricks, corrugated sheet metal, straw or mud. Three traps were tested each experimental night, a BG-Suna, a M-Tego without additional host cues and an M-Tego with heat and warm water. The tested traps were placed outside

the houses, with their inlet pipe at a height of 65 cm. The fact that this height is higher than the one in the laboratory experiments (65 vs. 54.5 cm) might have resulted in a small overall difference in capture performances (Hiscox et al., 2014). However, it is unlikely that it would have affected the comparative results between traps. The M-Tego traps were hung from the house, whilst the BG-Suna was placed in a metal wire frame on the ground. The traps were cleaned before use with 70% ethanol and handled with gloves afterwards. Each trap was powered using a 12 V car battery and contained an MB5 odour source. CO_2 was produced using 5.5 L plastic containers with a yeast and molasses mixture, which was placed next to each trap, and replaced daily. Inside each house, a set-up with CO_2, a MB5 blend and a fan (same as used in the traps) was placed below a bed net to simulate human presence. The fan was positioned such that it produced an airflow that directed the odour and CO_2 towards the nearest window. Screen houses were cleaned before and after the experiments. Only natural (moon) light was illuminating the screen house during the night.

Before each trial, each trap was equipped with one of three MB5 odour sources (OS3, OS4 or OS5), and placed inside one of the three screen houses. The odour source and the screen house used for each trap were changed following a quasi-randomized planning (see supplementary database S2). The M-Tego with short-range host cues was then filled with 0.7 L of water from a water bottle that stood in direct sunlight during the day (temperature = 39.7 ± 0.5°C, n = 2). At the start of the experiment, a release pot containing 200 females *An. gambiae s.s.* was placed in the corner of each screen house and the mosquitoes were released manually, at approximately 18:00 hours. The experiment ended around 06:20 the following morning. Captured mosquitoes were killed by moving the capture bag or pot out of the trap and placing them in direct sunlight for a day. The desiccated mosquitoes were manually counted.

The mean run-time of the experiments was 12 hours and 23 minutes (± 22 minutes). At the start of the experiment, the ambient air temperature was 32.4 ± 1.4°C and ambient relative humidity of the air was 38.1 ± 4.7%. The next morning, the ambient air temperature was 22.9 ± 0.8°C and ambient relative humidity was 78.0 ± 6.0%.

3.2.6 Mosquito flight tracking experiments

To study the flight behaviour of mosquitoes around the M-Tego with or without additional host cues, mosquitoes were tracked around the traps in the same netted cage as used for the dual-choice tests (ambient temperature = 24.9 ± 0.7°C and relative humidity = 73.7 ± 3%). The experimental procedure was identical to the dual-choice experiments, except for the following differences. A single M-Tego was placed on the right side of the dual-choice setup and a single MB5 odour source was used inside the trap (OS1). Four trap conditions were tested, the M-Tego without additional cues, the M-Tego with heat, the M-Tego with warm water, and the M-Tego with heat and warm water. Each experimental morning, all conditions were tested using as quasi-randomized planning (see supplementary database S1).
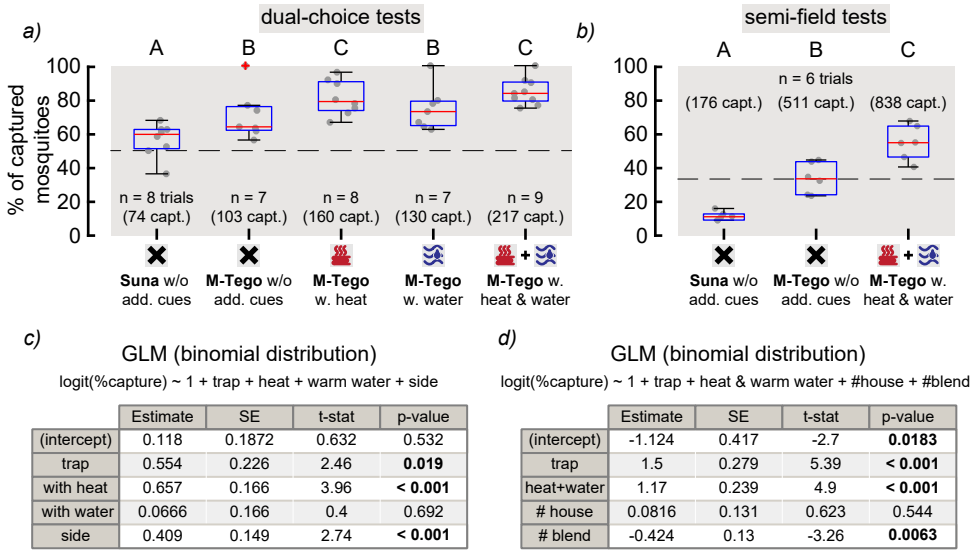
Figure 3.1: Comparing capture performance of the BG-Suna and the M-Tego, with and without close-range host cues. (*a,b*) Capture percentage of the BG-Suna and the M-Tego with or without additional host cues against a second BG-Suna in dual-choice tests (*a*) and in separated screen houses in semi-field tests (*b*). Dashed line shows expected percentage if no differences existed between the traps. Letters above box plots indicate results that did not differ significant (GLM, p > 0.05). Total numbers of captures per condition are indicated in parentheses. (*c,d*) Formula and results of the minimal GLM used to model variation of capture percentages in *a* and *b*, respectively.

Three infrared-enhanced cameras (Basler acA2040-90umNI) with Kowa 12.5 mm lenses (LM12HC f1.4) were used for the tracking (Fig. 3.2), which synchronously recorded images at temporal resolution of 90 frames per second and a spatial resolution of 1,024×1,024 pixels. Cameras were synchronized using pulses from an Arduino Uno board. Because mosquitoes cannot see infrared light (Gibson, 1995), the tracking set-up was illuminated using two infrared light-emitting-diode (LED) lamps (Bosch Aegis SuperLed, 850 nm, 10° beam pattern – SLED10-8BD). Lens distortions were corrected using pictures of a chequerboard pattern. Calibration was done daily using a single LED manually waved inside the filmed volume to find DLT (direct linear transformation) coefficients (Cabral and Leedom, 1993). Alignment was done with a calibration device with four LEDs that were consecutively blinking at various known three-dimensional positions. The real-time three-dimensional tracking software Flydra (version 0.20.19) was used to track the three-dimensional positions, velocities and accelerations of flying mosquitoes within a three-dimensional space of approximately 1x1x1 m around the trap (Straw et al., 2011). For each experiment, mosquito flight trajectories were recorded for 20 minutes, but the first 3 minutes were used for tracker initialization. The remaining 17 minutes were used for the analysis.
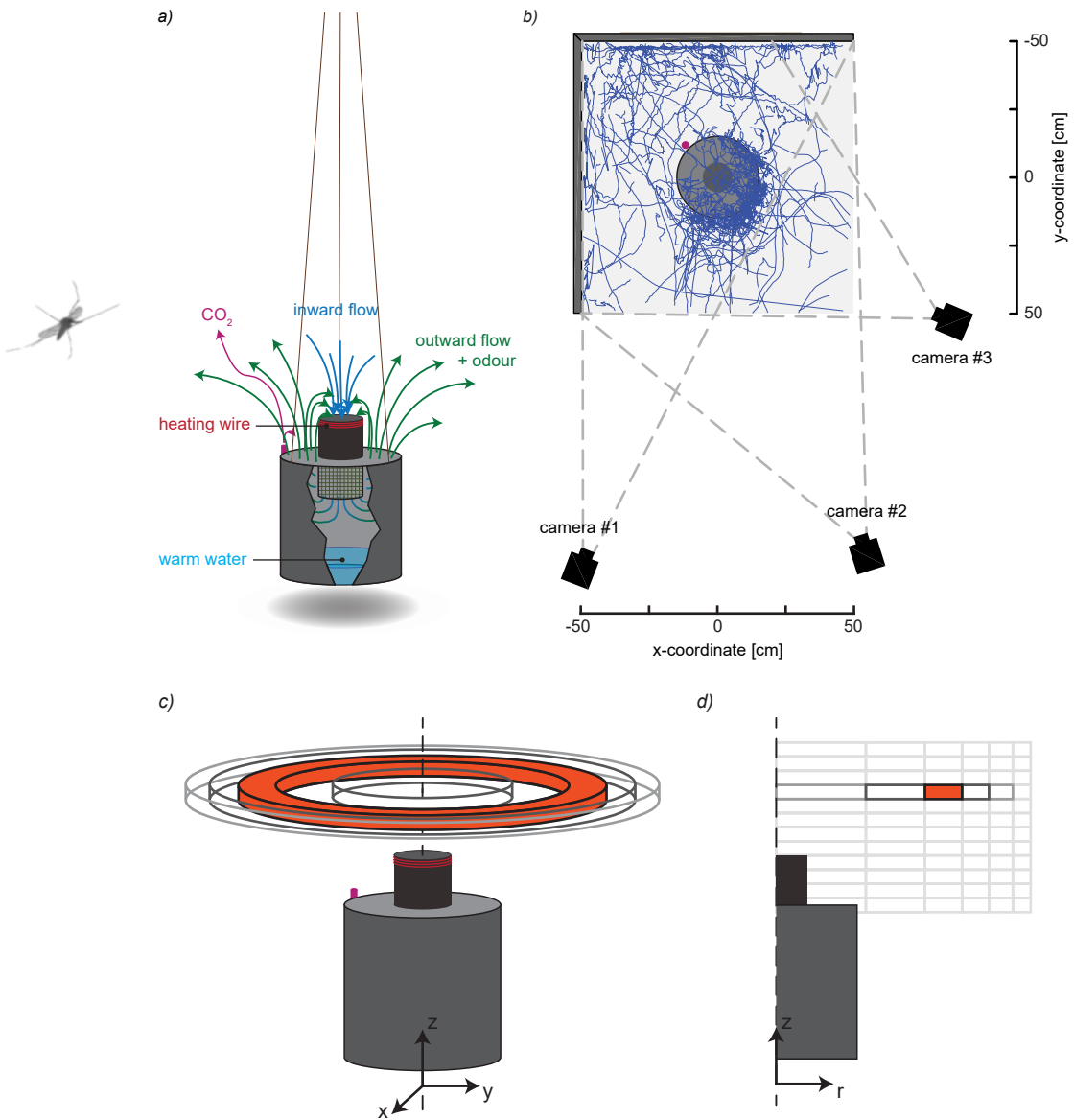
Figure 3.2: Experimental setup of the mosquito-tracking experiments, and analysis method for visualizing the three-dimensional flight dynamics in two-dimensional heat maps. (*a*) Schematic of the M-Tego with a removed slice to make the inside visible. The fan inside the inlet generates a circulating airflow by sucking air inside (blue arrows), mixing it with the odour blend and CO_2, and then pushing air away from the trap (green arrows). Additionally, the trap can be filled with 1 L of warm water and heat can be generated by a Nichrome heating wire at the top of the inlet. (*b*) Top-down view of the experimental setting used for recording mosquito flight behaviour around the M-Tego. The filmed region is delimited by the angles of view of the 3 cameras (dashed grey lines). Flight tracks recorded during one trial are visualized in blue. *Rest of the caption on the next page.*

(*c*,*d*) Method for projecting three-dimensional rings around the trap (*c*) into two-dimensional surfaces (*d*). (*c*) The filmed volume was divided in three-dimensional rings of equal volume and centred around the trap axis of symmetry. (*d*) Each ring is projected into a cell in a two-dimensional parametric space comprising the vertical position (z-coordinate) and the radial distance to the trap's axis of symmetry. In this way, heat maps of various metrics have been computed to visualize flight behaviour.

3.2.7 Analysis of three-dimensional flight tracks

All the flight dynamics analyses were done using Matlab 2018b (MathWorks). Mosquitoes could enter and exit the filmed three-dimensional space several times per trial, therefore individuals could not be identified. Filtering of tracked points was based on the covariance matrices estimated by the extended Kalman filter used for three-dimensional reconstruction by Flydra. Three-dimensional points with too high estimated standard deviation of either their position or speed were considered as outliers and deleted. When two or fewer consecutive video frames had missing values in the three-dimensional tracks, they were linearly interpolated. If more than two consecutive frames had missing values, the trajectory was divided in two separate tracks. Finally, tracks shorter than 10 video frames in length were deleted. For all frames of each computed three-dimensional track, linear and angular flight speeds as well as linear accelerations were computed (as in (Cribellier et al., 2018)).

To systematically analyse the flight behaviour of mosquitoes around the M-Tego trap, the visualization technique developed by (Cribellier et al., 2018) was used: based on the verified assumption that the three-dimensional flight behaviour is on average axially symmetric around the trap axis of symmetry, the three-dimensional flight movements can be projected onto a two-dimensional sub-space (Cribellier et al., 2018). For this, the three-dimensional space was divided into multiple three-dimensional rings centred around the M-Tego axis of symmetry (Fig. 3.2*a*,*c*). Within each ring, all relevant flight dynamics metrics (such as mean flight speed) were computed. Results were visualized by projecting the metric value in each ring onto a two-dimensional parametric space with the radial and vertical positions as coordinates (Fig. 3.2*d*). All rings had a constant volume to allow metric comparison. In addition, all metric results were visualized using two-dimensional heat maps from a top-down view and from a side view close to the background walls (see supplementary Figs S5, S7, S9 and S12). For these the three-dimensional space around the trap was divided into vertical and horizontal columns, respectively.

For each tested condition, the following metrics were computed in all cells (rings or columns) around the trap: the positional likelihood of mosquitoes in each cell (Figs 3*a*,*d*, 4*a*), the average time spent in a cell, the average flight velocity, flight speed, upward acceleration, angular speed, and capture probability.

The capture probability of a mosquito flying in a specific cell is defined as the number of tracks in that cell that ended by a capture divided by the total number of tracks detected in the cell. The positional likelihood of mosquitoes in a cell is defined as the normalized probability of a mosquito to fly in a cell (i.e., a horizontal ring projected in the

two-dimensional parametric space). This metric allows the identification of regions of high flight activity. The positional likelihood P_i of mosquitoes to fly in cell i, was computed as $P_i = \frac{n_i}{N} \times I$, where N is the sum of the length of all tracks in the filmed three-dimensional space (i.e. the total number of frames), n_i is the sum of the length of the parts of these tracks with mosquitoes flying in cell i, and I is the total number of cells within the three-dimensional space. In this way, if flight behaviour was random and the number of tracks was high, the positional likelihood heat-maps would be uniform with a value of 1. The average time spent by mosquitoes in a cell is defined as the total time spent by all mosquitoes in a cell divided by the number of tracks detected in that cell. Because the positional likelihood in a cell is equivalent to the normalized total time spent by all mosquitoes in a cell, the average time spend is a good metric to weight the measure of positional likelihood. For details about the other metrics, see (Cribellier et al., 2018).

To test how close-range cues affected the flight dynamics of mosquitoes, the difference in each metric between treatments were computed by subtracting the results distribution around the M-Tego without additional cues from the treatments with heat and/or warm water (Fig. 3.4).

3.2.8 Statistical analysis

For all statistical tests, generalized linear models (GLM) were used. For each test, the minimal model was determined by successively removing the least significant predictors from the model until all remaining predictors were significant (p-value <0.05). We then chose the GLMs with the lowest AIC (Akaike Information Criterion) values (see supplementary Table S3.1).

For the dual choice experiments, a GLM with a binomial distribution, logit link function and estimated dispersion (Verhulst et al., 2015) was used. The response variable of the GLM was the capture percentage, defined as the ratio between number of captures by one trap and the number of captures by both traps. The predictors for the full model were: trap (BG-Suna or M-Tego), with or without heat, with or without warm water, mean humidity, mean temperature. Location (left or right side) and the odour source used in the trap (OS1 or OS2) were also included as random effects. When determining the minimal model, the predictors of interest "trap", "heat" and "warm water" in the model were always kept.

For the semi-field experiment, a GLM with a binomial distribution, logit link function and estimated dispersion was also used. The response variable of the GLM was the capture percentage, defined as the ratio between number of captures of one trap and the total number of captures of all traps across all three screen houses. The full model predictors were trap (BG-Suna or M-Tego), with/without heat and warm water, mean humidity, mean temperature, day of the experiment, house number (H1, H2 or H3), and the odour source used in the trap (OS3, OS4 or OS5).

To compare the flight behaviour of the mosquitoes around the M-Tego trap with or

without host cues, three doughnut-shaped volumes were defined around the top rims of the trap with various radii of their tube ($r = \left[\frac{1}{2}, \frac{3}{4}, 1\right] \times \left(r_{bag} - r_{inlet}\right)$, with r_{bag} and r_{inlet} being, respectively, the radius of the tarpaulin bag and radius of the inlet of the trap). The positional likelihood of mosquitoes to be tracked inside these volumes as well as how long on average they stayed inside for each trial was then computed (Fig. 3.6). Because mosquitoes were not tracked during the dual-choice and semi-field experiments, these two metrics could not be used as covariate in the previously described models. GLMs with a gamma distribution, negative inverse link function and estimated dispersion were used to model how these two metrics varied as a function of the presence of heat and warm water. Full model predictors were with heat (yes or no), with warm water (yes or no), mean humidity, mean temperature, volume of the doughnut and age in days of the adult female mosquitoes.

3.3 Results

3.3.1 Capture efficiency of the traps

A total of 39 dual-choice trials were performed in the laboratory (Fig. 3.1*a*) and 907 female mosquitoes were caught by the traps, for a total of 1,950 released mosquitoes (more details in the supplementary database S3.1). Here, the capture performance of the M-Tego with various additional short-range host-cues was compared to that of the BG-Suna (Fig. 3.1). The M-Tego without additional short-range host-cues captured on average 70.8% ± 13.6% (mean ± std, 7 trials) of the total number of mosquitoes captured by the M-Tego and BG-Suna combined, which was significantly higher than the capture percentage of the BG-Suna in control experiments (GLM, p = 0.019). Adding heat to the M-Tego significantly increased this capture percentage to 81.1% ± 9.7% of all captured mosquitoes (GLM, p <0.001, 8 trials). The M-Tego with only warm water captured 74.8% ± 12% (7 trials) of all captured mosquitoes, and the M-Tego with both warm water and heat captured 83.8% ± 7.3% (7 trials), but the effect of adding warm water to the M-Tego (with (9 trials) or without heat (7 trials)) was not significant (GLM, p = 0.692). On average the M-Tego without additional cues and with heat captured 2.4 and 4.3 as many mosquitoes than the competing BG-Suna.

A total of six tests were performed in semi-field conditions (Fig. 3.1*b*) in which the capture performance of the BG-Suna, the M-Tego without additional cues and the M-Tego with warm water and heat were compared. 3,600 female mosquitoes were released, of which a total of 1,525 were caught (see supplementary database S3.2 for details). The M-Tego without additional host cues captured on average 33.8% ± 8.3% of all mosquitoes captured by the three traps, the M-Tego with warm water and heat captured 54.7% ± 9.4% of these mosquitoes, and the BG-Suna captured only captured 11.5% ± 2.4% of all captured mosquitoes (Fig. 3.1*b*). The capture percentages of all three traps differed significantly from each other (GLM, p <0.001, Fig. 3.1), showing that on average the M-Tego without and with additional cues captured 2.9 and 4.7 as many mosquitoes than the BG-Suna, respectively.

3.3.2 Flight dynamics around the M-Tego

The flight dynamics of mosquitoes around the M-Tego trap were monitored, with or without additional host cues for a total of 18 hours and 25 minutes (65 trials). During these trials, 3,250 mosquitoes were released, 13,618 flight trajectories were reconstructed, and 1,335 of these tracks led to capture. The number of tracks per trial that were identified to result in a capture was highly correlated with the number of mosquitoes caught inside the traps (1,600 mosquitoes in total, correlation coefficient = 0.937). This suggests that the detection of tracks leading to capture was good.

From all these tracks, various heat maps were computed to visualize the average flight behaviour of the mosquitoes around the traps (Figs 3-5). Positional likelihood around the M-Tego without additional cues was similar to the ones observed above the BG-Suna (Cribellier et al., 2018). Near both traps, mosquitoes were likely to be found flying in a cone-shaped region close to the traps (Fig. 3.3). Their positional likelihood was especially high close to the rim of the top surface where odour is released. Despite this similarity in positional likelihood, the average flight dynamics around the BG-Suna and the M-Tego traps exhibited clear differences. Although mosquitoes had similar flight paths towards the inlets of both traps, only mosquitoes flying above the BG-Suna exhibited an upward-directed avoiding behaviour (Fig. 3.3*b,e*). This difference is highlighted by the heat maps representing mean vertical acceleration (Fig. 3.3*c,f*). Indeed, mosquitoes close to the M-Tego inlet were on average only accelerating downward (i.e., when being caught), while above the BG-Suna mosquitoes were also found to avoid capture by accelerating upwards (Cribellier et al., 2018). Flight paths in other regions near the M-Tego do not show any clear directional patterns (Fig. S3.7).

Two distinct behavioural regions can be defined based on the spatial distributions of the remaining computed flight metrics around the M-Tego (Fig. 3.5*b-e*). In the first region, just above and around the trap tarpaulin bag, mosquitoes had on average lower flight speeds and higher angular speeds (Fig. 3.5*b,d*) than in the rest of the filmed volume. In the second region, above the trap inlet, mosquito flew faster and produced on average higher accelerations (Fig. 3.5*b, c*). In this last region, the capture probability was also the highest (Fig. 3.5*e*), meaning that most tracks detected there led to capture.

3.3.3 Effect of heat and warm water on flight behaviour

To compare the flight behaviour of mosquitoes around the M-Tego with or without additional host cues, heat maps of their positional likelihood (Fig. 3.4*a*) and time spent close to the traps (Fig. 5*a*) were computed. On these heat maps, a higher flight activity was observed close to the M-Tego when additional host cues were added. By adding heat to the M-Tego, the positional likelihood around the rim of the trap increased by 79.0% ± 49.5%; when adding warm water, the positional likelihood increased by 98.3% ± 52.3%; when adding both heat and warm water, the positional likelihood around the trap rim was

increased by 171.1% ± 79.5% (GLM with p <0.001, Fig. 3.6*d*, *f*). Additionally, mosquitoes have been found to fly on average 21.2% ± 38.5% longer in this region if the trap generated heat, 12.6% ± 36.5% longer if warm water was added to the trap, and 37.3% ± 46.0% longer if both cues were present (GLM, p >0.03, Fig. 3.6*e*, *g*). The spatial distribution of the remaining computed flight metrics did not vary if heat or warm water were added to the M-Tego (see supplementary Fig. S3.10–S3.12).

3.4 Discussion

The main hypothesis examined in this study was that due to a lack of the close-range host cues heat and humidity, mosquitoes do not approach counter-flow odour-baited traps closely enough, thus resulting in low capture efficiency. To systematically test this hypothesis, a novel trap was developed, the M-Tego, to provide these close-range host cues. First, the capture performance of this M-Tego with or without additional cues to that of the standing BG-Suna were compared in dual-choice tests and semi-field experiments. The flight behaviour of female mosquitoes around this M-Tego trap with or without additional heat and humidity were also compared.

It was found that, when the close-range host cues heat and humidity were present, more mosquitoes were lured to a region close to the rim of the trap tarpaulin bag. Mosquitoes were also observed to stay longer in this region where flight activity was high. This increase in mosquito attraction and time spent in this region when short-range host cues were present correlates with the concomitant increase in capture percentages.

These results are consistent with previous findings showing that heat and increased local humidity are important short-range host cues used by mosquitoes (Hawkes et al., 2017; Kline and Lemire, 1995; Olanga et al., 2010; Spitzen et al., 2013). Several odour-baited traps such as the HDT or CDC-type traps were shown to have increased capture rate when generating heat (Hawkes et al., 2017; Kline and Lemire, 1995). Heat and increased local humidity have been classified as short-range cues because they cannot be detected from more than one metre, and work in synergy with host odour and CO_2 to trigger landing behaviour (McMeniman et al., 2014; Spitzen et al., 2013). As such, it is not surprising that such cues are crucial for adhesive traps like the HDT because they only capture mosquitoes that land (Hawkes et al., 2017). However, counter-flow traps capture mosquitoes while they fly, and therefore the function of short-range host cues for these traps was previously not clear. Then again, the higher flight activity observed near the trap tarpaulin bag would suggest that landing on the bag occurred more often when these cues were present (Hawkes et al., 2017).

Similar behavioural changes were observed when adding a heat source and warm water to the M-Tego. This occurred even though the heat source was placed on the top of the trap inlet while the warm water was inside the tarpaulin bag. This suggests that the circulating airflow allowed an approximately homogeneous mixing of the warmed air around the trap. This is confirmed by measurements (Fig. S3.15) showing similar temperature increases in
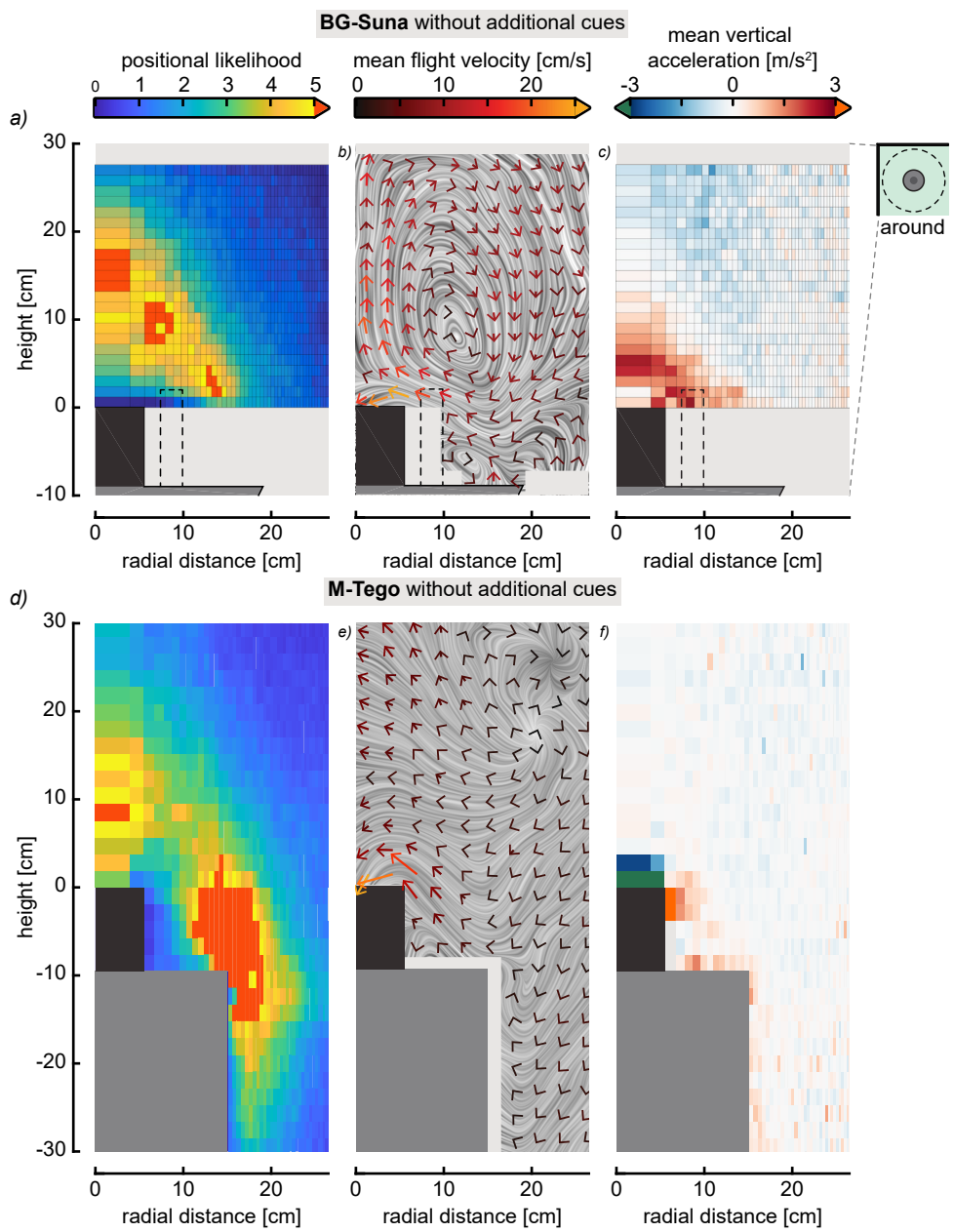
Figure 3.3: Comparison of the flight dynamics of mosquitoes around the BG-Suna and the M-Tego.
(*a*,*d*) Heat maps of the positional likelihood of mosquitoes flying around (*a*) the BG-Suna (from Cribellier *et al.* 2018) and (*d*) the M-Tego without additional host cues. The positional likelihood P_i in a cell *i* is defined as the normalized probability of mosquitoes to fly inside a given three-dimensional ring around the trap (average cell size = 19 x 3 mm). Random flight behaviour would result in a uniform probability equal to 1 throughout the filmed volume. *Rest of the caption on the next page.*

(*b,e*) Average velocity fields and streamlines of mosquitoes flying around (*b*) the BG-Suna and (*e*) the M-Tego without additional host cues. Each vector consists of the average velocity in the radial and vertical direction of all mosquitoes that flew in a cell (size = 27.5 x 27.5 mm). All velocity vectors resulting from fewer than 20 tracks were discarded. Streamlines are shown using line integral convolution (LIC). (*c,f*) Heat maps of the average vertical acceleration of mosquitoes flying around (*c*) the BG-Suna, and (*f*) the M-Tego without additional cues.
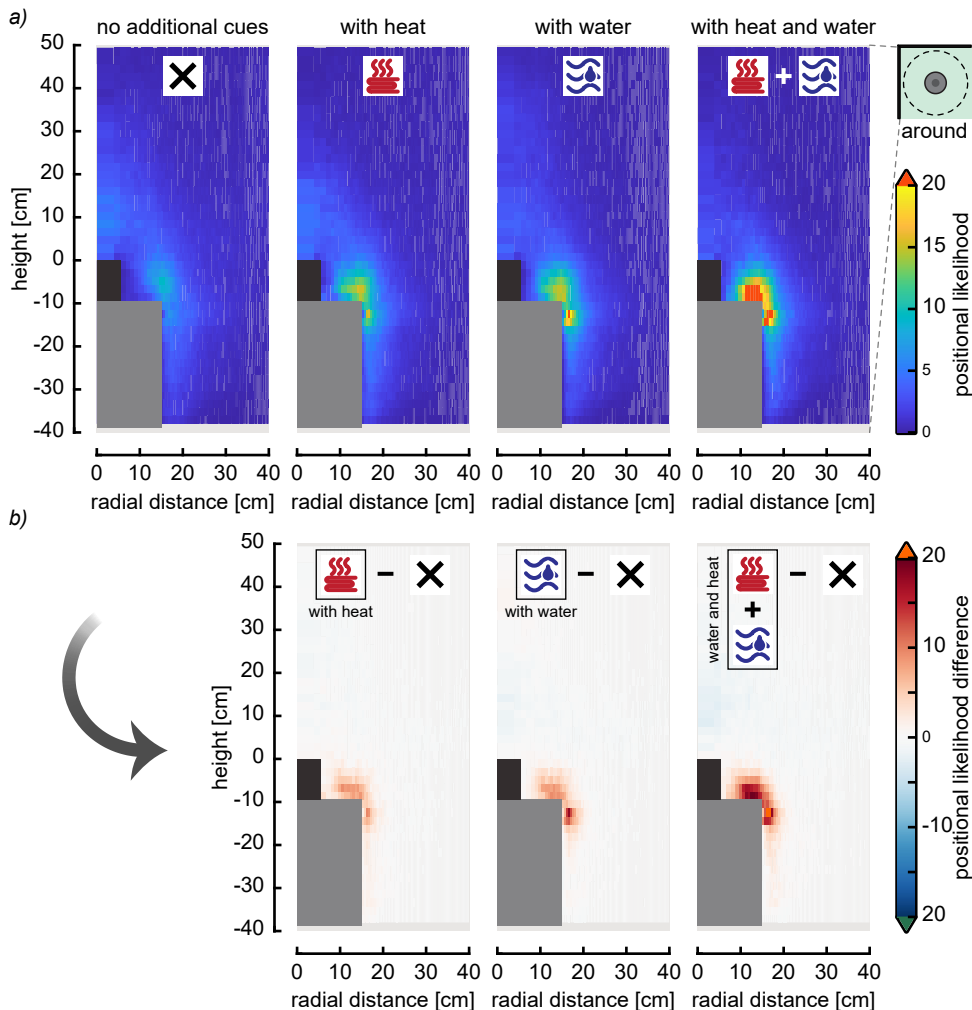
Figure 3.4: Spatial distribution of the positional likelihood of mosquitoes flying around the M-Tego with and without additional cues. (*a*) Radial - vertical heat maps of the positional likelihood around the M-Tego with various combinations of additional host cues. The positional likelihood P_i in a cell *i* is defined as the normalized probability of mosquitoes to fly inside a given three-dimensional ring around the trap. Random flight behaviour would result in a uniform probability equal to 1 throughout the filmed volume. Average cell size = 19 x 3 mm. (*b*) Difference between the heat maps of positional likelihood around the M-Tego with various additional host cues (heat and/or water) and the heat maps of positional likelihood around the M-Tego without additional host cues.
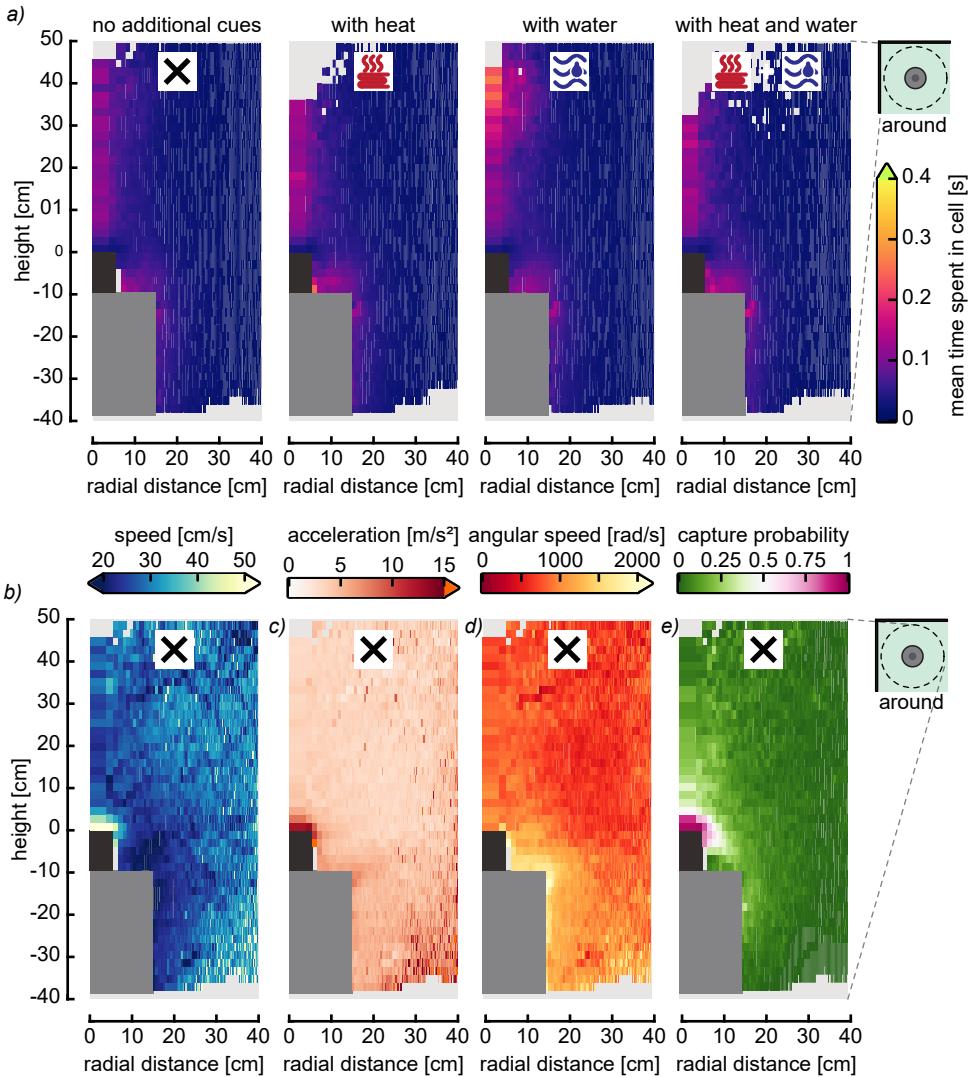
Figure 3.5: Heat maps of various flight dynamics metrics of mosquitoes flying around the M-Tego.
(*a*) Heat maps of the average time spent by mosquitoes around the M-Tego with various combinations of additional host cues. (*b–e*) Heat maps of the average flight speed, average acceleration, average angular speed and capture probability of mosquitoes flying around the M-Tego (without additional cues). Cells with fewer than 20 tracks have been masked. Average cell size = 19 x 3 mm. See supplementary Fig. S3.10–S3.12 for additional heat-maps of these metrics.

the full volume above the trap bag.

Results suggest that there is a saturation effect of adding heat and warm water on the change of flight activity near the trap (Fig. 3.6*f*), e.g., the benefit of adding both cues together is not the sum of their separate benefits. Moreover, despite including both sensory cues (heat and humidity), the benefit of adding warm water to the M-Tego was not clearly
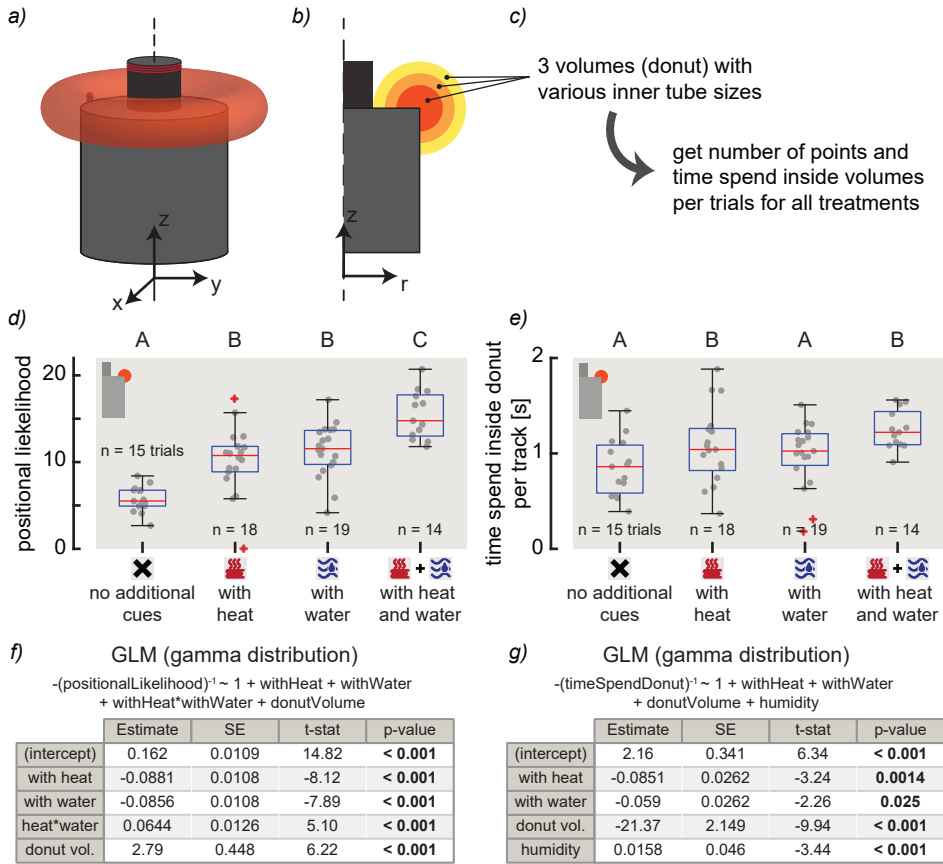
Figure 3.6: The positional likelihood and time spent in the donut-shaped region close to the trap edge, and how these differed for traps with variable additional host cues. (*a–c*) Method description, showing (*a*) a three-dimensional view of the donut shaped volume used to compare flight behaviour around the trap, (*b*) a transverse section through three donuts with variable radii, and (*c*) the method explanation for the comparison between the different treatments. (*d–g*) Statistical results for the largest donut-shaped volume (yellow in *b*), using 7153 tracks. Results for the two smaller volumes are shown in supplementary Fig. S3.13. (*d*) Box plots of the positional likelihood inside the largest donut-shaped volume (yellow in *b*) of mosquitoes flying around the various traps with or without additional cues. Each datapoint shows the result of a single trial. (*e*) Box plot of the average time spend inside the largest volume (yellow in *b*) by mosquitoes flying around the different traps with various additional cues. (*d,e*) Each datapoint shows the result of a single trial, and different letters above each box plot indicate significance difference between treatment (GLM, p < 0.05). (*f,g*) Formula and results of the generalized linear mixed models (GLM) used to model the metrics from panel d and e, respectively.

established because this addition of warm water was not found to significantly increase capture percentages of the M-Tego in laboratory conditions, but resulted in increased flight activity and time spent near the trap. A higher difference between the local humidity and ambient humidity might have resulted in significant difference in trapping performances. Thus, future research could investigate the effects of such differences between local and ambient values of temperature and relative humidity on capture performance, as well as how

mosquito flight dynamic is affected by changes in the position of local heat and humidity sources.

To generate short-range host cues in the field, it is probably easier to use a heat source rather than warm water. The latter requires more labour as water needs to manually be warmed up, and evaporated water needs to be replaced. Also, small water bodies may attract mosquitoes to oviposit, and access to water needs to be carefully restricted. In addition, warming up water requires most likely more energy than directly using a heat source on the trap. Passive heating solutions may need to be considered to reduce energy consumption.

In all experiments, the heat source was powered using the same 12V energy source used for the fan. The Nichrome heating wire used 9.6W, and because the fan only used 3.4W, adding the heating wire increased the power requirement of the trap by 282%. This power requirement may need to be lowered if the M-Tego is to be powered using solar panels in rural areas without a power grid.

Still, the M-Tego presents several advantages as a potential vector control tool against malaria. Like other counter-flow odour-baited traps, it uses artificial bait, and does not need to draw odours from living organisms such as humans or cattle. This greatly improves usability and repeatability, which are important when used as a monitoring tool. The M-Tego is easy to transport thanks to its small size, it has high modularity and can be folded like the BG-Sentinel, and its catch pot is easier to remove and empty than commonly used capture bags. Finally, despite having similar designs, the M-Tego without additional host cues captures between 2.4 to 2.9 as many *Anopheles* mosquitoes than the standing BG-Suna.

There was one striking difference in the flight dynamics of mosquitoes around the M-Tego when compared to the previously studied standing BG-Suna. Mosquitoes were found to elicit upward manoeuvres resulting in escapes above the inlet of the standing BG-Suna (Cribellier et al., 2018) and the BG-Sentinel (Amos et al., 2020). Such manoeuvres were not observed above the M-Tego. This difference might help explain the superior capture percentages of M-Tego compared to the standing BG-Suna, even when no additional close-range host cues were present. Despite similarities between the two traps, the design of the M-Tego distinguished itself by its materials, its smaller size and the use of a transparent net through which the odour is released, instead of perforated hard plastic (see supplementary Fig. S3.1). Therefore, the slightly different visual cues and airflow generated by the M-Tego may explain the lack of avoidance behaviour. The airflow speeds measured around the M-Tego were similar to the ones measured around the BG-Suna (see supplementary Fig. S3.15 and (Cribellier et al., 2018)). However, it is possible that the fine net of the M-Tego resulted in a different turbulence level of the airflow, which might have changed how mosquitoes perceived the air movements (Geier et al., 1999). The exact reason for this capture performance difference needs to be investigated further.

Except for the differences in flight behaviour near the trap inlet, the mosquito flight dynamics around the M-Tego were very similar to what has been observed around the stand-

ing BG-Suna and BG-Sentinel (Amos et al., 2020; Cribellier et al., 2018). However, because the cameras covered a larger volume than previous studies, it was possible to study the flight behaviour around the full trap and close to the back walls (see supplementary Figs S5, S7, S9 and S12). Similarly to what was observed for the standing BG-Suna and the BG-Sentinel, the flight activity was the highest close to the M-Tego, where mosquitoes had lower flight speed and higher angular speed (Amos et al., 2020; Cribellier et al., 2018). Such flight characteristics suggest that mosquitoes were host-seeking in this region (Spitzen et al., 2013). Additionally, mosquitoes had high average flight speeds and accelerations in the region close to the inlet, and where the capture probability was high. Moreover, the size and shape of this capture region were similar to the ones of the capture region of the standing BG-Suna (Cribellier et al., 2018). These similarities are not surprising considering that the two traps generate similar odour cues and airflow speeds (see supplementary Fig. S3.15).

3.4.1 Conclusions

By tracking mosquitoes in the vicinity of the newly developed M-Tego trap, their interaction with this odour-baited trap was described. Even though the role played by warm water is still ambiguous, adding a heat source to the trap resulted in large and significant increases in capture performance of the M-Tego in both laboratory and semi-field conditions. The results of this study suggest that these increases are due to a rise of flight activity close to the rim of the odour-release surface of the trap. The presence of the close-range host cues heat and increased humidity caused mosquitoes to approach the trap more often, and it retained mosquitoes for a longer period close to the trap. The combination of more approaches and increased retainment most likely explain the up to 129% increase in capture performance of the M-Tego with close-range host cues, compared to the M-Tego without such cues.

Additionally, in contrast to what was observed above the standing BG-Suna and BG-Sentinel (Amos et al., 2020; Cribellier et al., 2018), it was shown that the average mosquito did not exhibit upward avoiding manoeuvres when flying above the M-Tego. This important difference could explain the 140% to 190% increase in capture performance of the M-Tego without additional host cues, relative to the standing BG-Suna.

This study showed that adding close-range host cues to odour-baited traps can greatly increase their capture performance. This knowledge may help the development or improvement of vector control tools and strategies, especially for malaria vectors. In addition, this study showed that the M-Tego has the potential to be valuable for the monitoring and control of *Anopheles* mosquitoes.

Symbols and abbreviations

GLM   generalized linear model

AIC   Akaike information criterion

std   standard deviation

P_i positional likelihood of mosquitoes in a cell i

N sum of the length of all tracks in the filmed volume (i.e. the total number of frames)

n_i sum of the length of the parts of these tracks with mosquitoes flying in the cell i

I total number of cells within the filmed volume

r_{bag} radius of the trap bag

r_{inlet} radius of the inlet of the trap

Declarations

Ethics approval and consent to participate

Human blood used to rear the main mosquito colony was obtained from the blood bank (Sanquin, The Netherlands) where donors filled out an informed consent.

Consent for publication

Not applicable

Availability of data and materials

The datasets generated and analysed during the current study are available in the following Dryad repository: doi:10.5061/dryad.k6djh9w47

Competing interests

H.F. is a co-founder of PreMal b.v. that sells the M-Tego trap. To avoid conflicts of interest, he did not participate in analysing the results. A.C., F.M. and J.S. are part of the advisory board of PreMal b.v., but have no financial competing interests.

Authors' contributions

A.C., J.S. and F.T.M. conceived and designed the experiments. H.F. performed the experiments at Wageningen University. C.v.G. performed the semi-field experiments in Ifakara. The M-Tego was designed by H.F. and A.C., with the advice of F.T.M., J.S. and J.L.v.L. A.C. analysed the data, and wrote the first draft of the manuscript. F.T.M., J.S. and J.L.v.L. co-wrote the manuscript. All authors read and commented on the manuscript and gave their final approval for publication.

3

References

Abong'O, B., Yu, X., Donnelly, M. J., Geier, M., Gibson, G., Gimnig, J., Ter Kuile, F., Lobo, N. F., Ochomo, E., Munga, S. et al. (2018). Host Decoy Trap (HDT) with cattle odour is highly effective for collection of exophagic malaria vectors. *Parasites and Vectors* **11**, 533.

Amos, B. A., Staunton, K. M., Ritchie, S. A. and Cardé, R. T. (2020). Attraction versus capture: Efficiency of BG-Sentinel trap under semi-field conditions and characterizing response behaviors for female Aedes aegypti (Diptera: Culicidae). *J. Med. Entomol.* .

Batista, E. P. A., Mapua, S. A., Ngowo, H., Matowo, N. S., Melo, E. F., Paixão, K. S., Eiras, A. E. and Okumu, F. O. (2019). Videographic analysis of flight behaviours of host-seeking Anopheles arabiensis towards BG-Malaria trap. *PLoS One* **14**, e0220563.

Bhalala, H. and Arias, J. R. (2009). The Zumba mosquito trap and BG-Sentinel trap: Novel surveillance tools for host-seeking mosquitoes. *J. Am. Mosq. Control Assoc.* **25**, 134–139.

Cabral, B. and Leedom, L. C. (1993). Imaging vector fields using line integral convolution. In *Proc. 20th Annu. Conf. Comput. Graph. Interact. Tech. - SIGGRAPH '93*, pp. 263–270.

Cardé, R. T. (2015). Multi-cue integration: How female mosquitoes locate a human host. *Curr. Biol.* **25**, R793–r795.

Cooperband, M. F. and Cardé, R. T. (2006a). Comparison of plume structures of carbon dioxide emitted from different mosquito traps. *Med. Vet. Entomol.* **20**, 1–10.

Cooperband, M. F. and Cardé, R. T. (2006b). Orientation of Culex mosquitoes to carbon dioxide-baited traps: Flight manoeuvres and trapping efficiency. *Med. Vet. Entomol.* **20**, 11–26.

Cribellier, A., Spitzen, J., Fairbairn, H., van de Geer, C., van Leeuwen, J. L. and Muijres, F. T. (2020). Lure, retain, and catch malaria mosquitoes. How heat and humidity improve odour-baited trap performance. *Malar. J.* **19**, 1–16.

Cribellier, A., van Erp, J. A., Hiscox, A., Lankheet, M. J., van Leeuwen, J. L., Spitzen, J. and Muijres, F. T. (2018). Flight behaviour of malaria mosquitoes around odour-baited traps: Capture and escape dynamics. *R. Soc. Open Sci.* **5**.

Dekker, T. and Cardé, R. T. (2011). Moment-to-moment flight manoeuvres of the female yellow fever mosquito (Aedes aegypti L.) in response to plumes of carbon dioxide and human skin odour. *J. Exp. Biol.* **214**, 3480–3494.

Geier, M., Bosch, O. J. and Boeckh, J. (1999). Influence of odour plume structure on upwind flight of mosquitoes towards hosts. *J. Exp. Biol.* **202**, 1639–1648.

Gibson, G. (1995). A behavioural test of the sensitivity of a nocturnal mosquito, Anopheles gambiae, to dim white, red and infra-red light. *Physiol. Entomol.* **20**, 224–228.

Gmp/who (2019). World Malaria Report 2019. Technical report.

Hawkes, F. and Gibson, G. (2016). Seeing is believing: the nocturnal malarial mosquito Anopheles coluzzii responds to visual host-cues when odour indicates a host is nearby. *Parasites and Vectors* **9**, 320.

Hawkes, F. M., Dabiré, R. K., Sawadogo, S. P., Torr, S. J. and Gibson, G. (2017). Exploiting Anopheles responses to thermal, odour and visual stimuli to improve surveillance and control of malaria. *Sci. Rep.* **7**, 17283.

Hiscox, A., Otieno, B., Kibet, A., Mweresa, C. K., Omusula, P., Geier, M., Rose, A., Mukabana, W. R. and Takken, W. (2014). Development and optimization of the Suna trap as a tool for mosquito monitoring and control. *Malar. J.* **13**, 257.

Homan, T., Hiscox, A., Mweresa, C. K., Masiga, D., Mukabana, W. R., Oria, P., Maire, N., Pasquale, A. D., Silkey, M., Alaii, J. et al. (2016). The effect of mass mosquito trapping on malaria transmission and disease burden (SolarMal): a stepped-wedge cluster-randomised trial. *Lancet* **388**, 1193–1201.

Howlett, F. M. (1910). The influence of temperature upon the biting of mosquitoes. *Parasitology* **3**, 479–484.

Jawara, M., Smallegange, R. C., Jeffries, D., Nwakanma, D. C., Awolola, T. S., Knols, B. G. J., Takken, W. and Conway, D. J. (2009). Optimizing odor-baited trap methods for collecting mosquitoes during the malaria season in the Gambia. *PLoS One* **4**.

Kline, D. L. (2002). Evaluation of various models of propane-powered mosquito traps. *J. Vector Ecol.* **27**, 1–7.

Kline, D. L. and Lemire, G. F. (1995). Field evaluation of heat as an added attractant to traps baited with carbon dioxide and octenol for Aedes taeniorhynchus. *J. Am. Mosq. Control Assoc.* **11**, 454–456.

McMeniman, C. J., Corfas, R. A., Matthews, B. J., Ritchie, S. A. and Vosshall, L. B. (2014). Multimodal integration of carbon dioxide and other sensory cues drives mosquito attraction to humans. *Cell* **156**, 1060–1071.

Mweresa, C. K., Omusula, P., Otieno, B., van Loon, J. J., Takken, W. and Mukabana, W. R. (2014). Molasses as a source of carbon dioxide for attracting the malaria mosquitoes Anopheles gambiae and Anopheles funestus. *Malar. J.* **13**, 1–13.

Olanga, E. A., Okal, M. N., Mbadi, P. A., Kokwaro, E. D. and Mukabana, W. R. (2010). Attraction of Anopheles gambiae to odour baits augmented with heat and moisture. *Malar. J.* **9**, 6.

Raji, J. I. and DeGennaro, M. (2017). Genetic analysis of mosquito detection of humans. *Curr. Opin. Insect Sci.* **20**, 34–38.

Smallegange, R. C., Schmied, W. H., Van Roey, K. J., Verhulst, N. O., Spitzen, J., Mukabana, W. R. and Takken, W. (2010). Sugar-fermenting yeast as an organic source of carbon dioxide to attract the malaria mosquito Anopheles gambiae. *Malar. J.* **9**, 292.

Spitzen, J., Spoor, C. W., Grieco, F., ter Braak, C., Beeuwkes, J., Van Brugge, S. P.,

Kranenbarg, S., Noldus, L. P. J. J., van Leeuwen, J. L. and Takken, W. (2013). A 3D analysis of flight behavior of Anopheles gambiae sensu stricto malaria mosquitoes in response to human odor and heat. *PLoS One* **8**, 1–12.

Straw, A. D., Branson, K., Neumann, T. R. and Dickinson, M. H. (2011). Multi-camera real-time three-dimensional tracking of multiple flying animals. *J. R. Soc. Interface* **8**, 395–409.

van Breugel, F., Riffell, J., Fairhall, A. and Dickinson, M. H. (2015). Mosquitoes use vision to associate odor plumes with thermal targets. *Curr. Biol.* **25**, 2123–2129.

van Loon, J. J. J. A., Smallegange, R. C., Bukovinszkiné-Kiss, G., Jacobs, F., De Rijk, M., Mukabana, W. R., Verhulst, N. O., Menger, D. J. and Takken, W. (2015). Mosquito attraction: crucial role of carbon dioxide in formulation of a five-component blend of human-derived volatiles. *J. Chem. Ecol.* **41**, 567–73.

Verhulst, N. O. N. N. O., Bakker, J. W. J. and Hiscox, A. (2015). Modification of the Suna Trap for Improved Survival and Quality of Mosquitoes in Support of Epidemiological Studies. *J. Am. Mosq. Control Assoc.* **31**, 223–232.

Vinauger, C., van Breugel, F., Locke, L. T., Tobin, K. K., Dickinson, M. H., Fairhall, A. L., Akbari, O. S. and Riffell, J. A. (2019). Visual-olfactory integration in the human disease vector mosquito Aedes aegypti. *Curr. Biol.* **29**, 2509–2516.e5.

Visser, T. M., De Cock, M. P., Hiwat, H., Wongsokarijo, M., Verhulst, N. O. and Koenraadt, C. J. (2020). Optimisation and field validation of odour-baited traps for surveillance of Aedes aegypti adults in Paramaribo, Suriname. *Parasites and Vectors* **13**, 1–14.

3

Lure, retain, and catch malaria mosquitoes. How heat and humidity improve odour-baited trap performance

Antoine Cribellier[1], Jeroen Spitzen[2], Henry Fairbairn[1,3], Cedric van de Geer[1,2,3,4], Johan L. van Leeuwen[1], Florian T. Muijres[1]

[1] Experimental Zoology Group, Wageningen University & Research, Wageningen, The Netherlands

[2] Laboratory of Entomology, Wageningen University & Research, Wageningen, The Netherlands

[3] Faculty of Industrial Design Engineering, Delft University of Technology, Delft, The Netherlands

[4] Ifakara Health Institute, Ifakara, Tanzania

Consisting of:

- Legends of the databases S2.1, S2.2, and S2.3 and of the table S2.1

- Supplementary figures S3.1–S3.15

Legends of the supplementary datasets and table

The datasets can be found at: `https://doi.org/10.1186/s12936-020-03403-5`

Database S2.1: Experimental conditions and results from the dual-choice testing and the mosquito flight tracking in the laboratory (Wageningen, the Netherlands).

Database S2.2: Experimental conditions and results from the semi-field experiments (Ifakara, Tanzania).

Database S2.3: Mosquito flight tracks around the M-Tego with or without additional host cues and experimental metadata. Matlab .mat file with the three-dimensional tracks of the flying mosquitoes were obtained as described in the materials and methods. Flight tracks were described as the x, y, z coordinates in meters of the mosquito at each video frame. Coordinates are in the world reference frame as defined in Fig. 3.1, with z oriented vertically up, and its origin at the centre of the trap inlet.

Table S2.1: Table with generalized linear models (GLM) results and model selection criterions used to select the models presented in the manuscript.
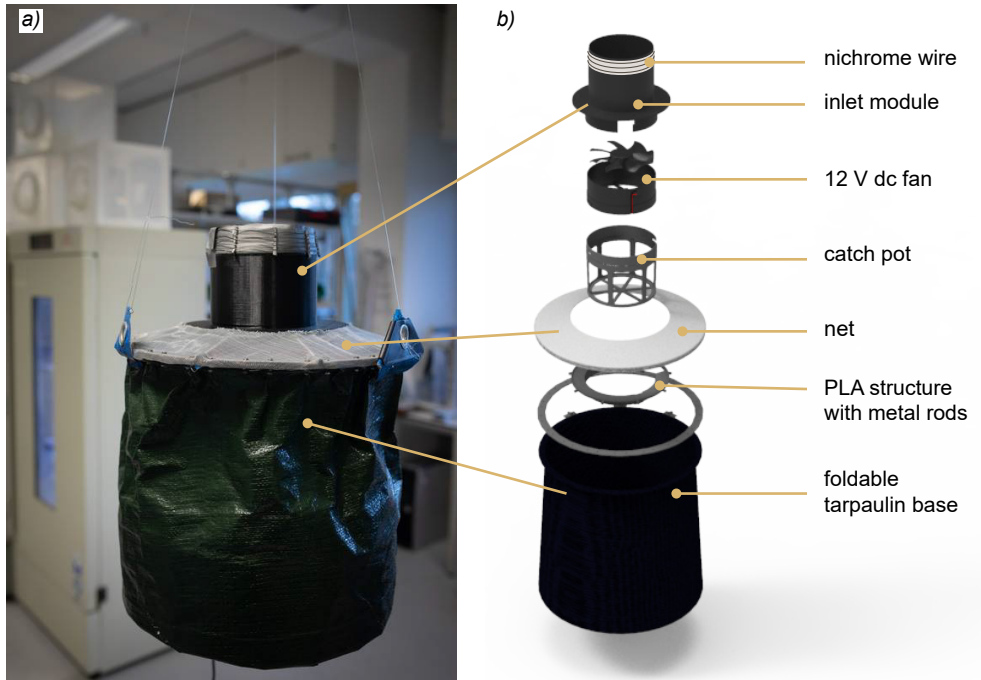
Figure S3.1: Pictures and exploded view of the M-Tego prototype mosquito trap. (*a*) Picture of the M-Tego trap used during the experiments (Photo by Sven Menshel). (*b*) Exploded view of the trap showing its various parts.
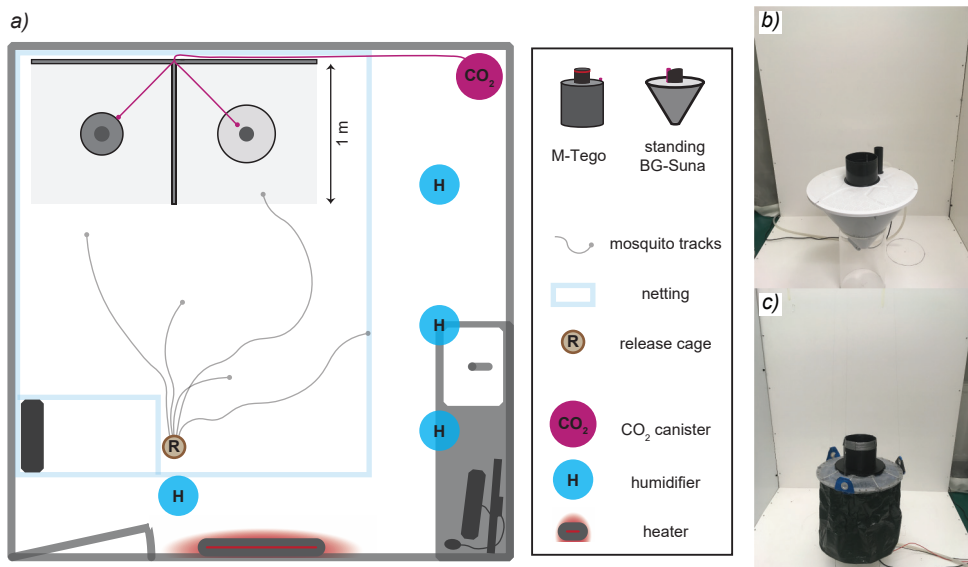
Figure S3.2: Experimental setup used for the dual-choice experiments. (*a*) Top-down view of the room used for the laboratory experiments at Wageningen University (Wageningen, The Netherlands). Two traps (standing BG-Suna or M-Tego) were placed on the left and right of the dual-choice setup (alternated between replicates). The traps were separated by a vertical white wall. A MB5 blend was placed inside each of the traps and both were connected to the CO_2 canister. Several humidifiers and one heater were regulating the relative humidity and temperature in the room. (*b*) BG-Suna placed in the left side of the setup. (*c*) M-Tego placed in the right side of the setup.
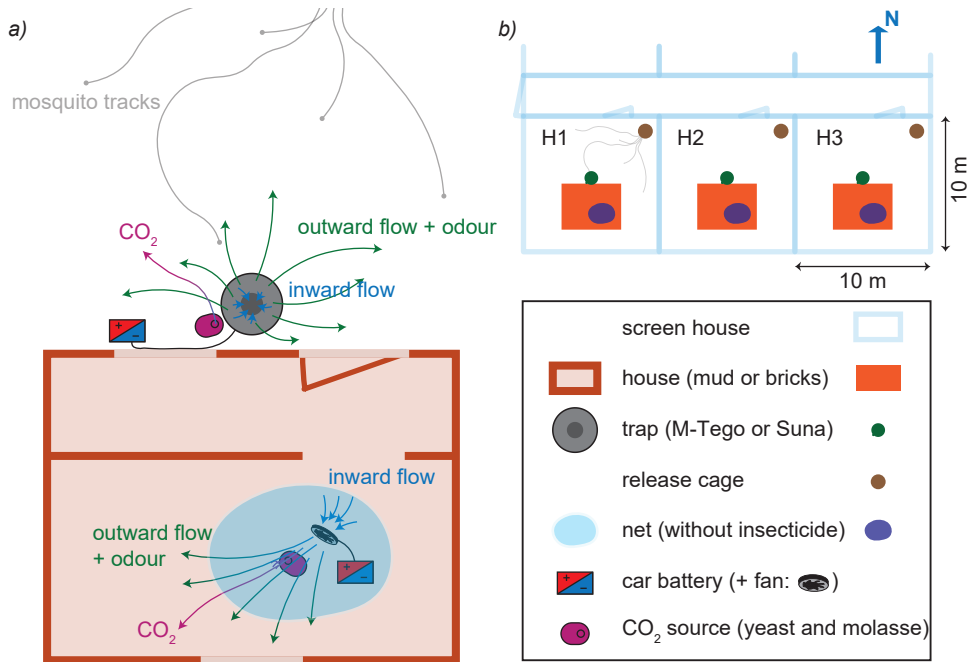
Figure S3.3: Experimental setup of the semi-field experiments. (*a*) Top-down view of the setup inside one screen house at Mosquito City in Ifakara (Tanzania). A standing BG-Suna or M-Tego was placed outside the house. Inside the bed net in the house, we placed a fan with an MB5 blend and a molasses-based CO_2 source to mimic human presence. (*b*) Top-down view of all three screen houses used in the semi-field experiments.
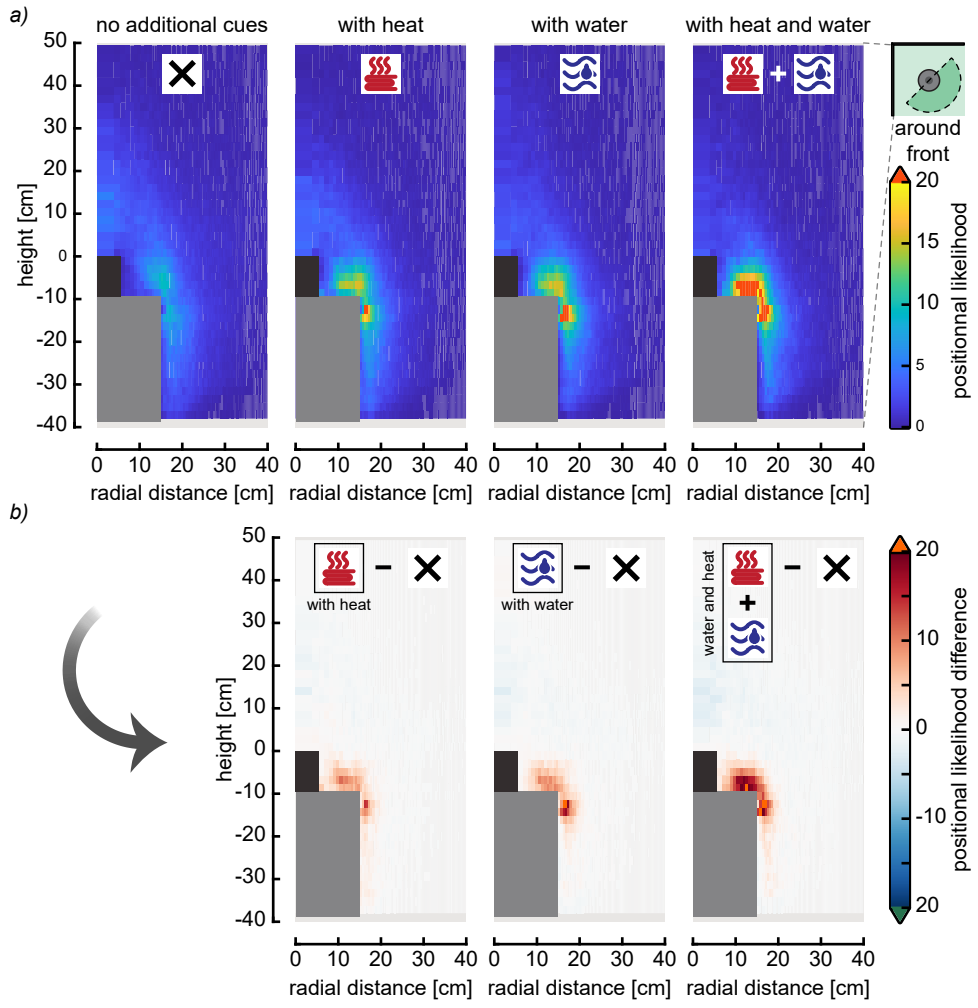
Figure S3.4: Spatial distribution of the positional likelihood of mosquito flying around the M-Tego with or without additional cues (half the volume, as indicated in the top right of *a*). (*a*) Radial - vertical heat maps of positional likelihood around the M-Tego with or without additional host cues. As indicated in the top right of a, all heat maps have been computed on only half the volume to avoid overlapping with blind spots behind the trap. (*b*) Difference between the heat maps of positional likelihood around the M-Tego with additional host cues (heat and/or water) and the heat maps of positional likelihood around the M-Tego without additional host cues. Average cell size = 19 x 3 mm.
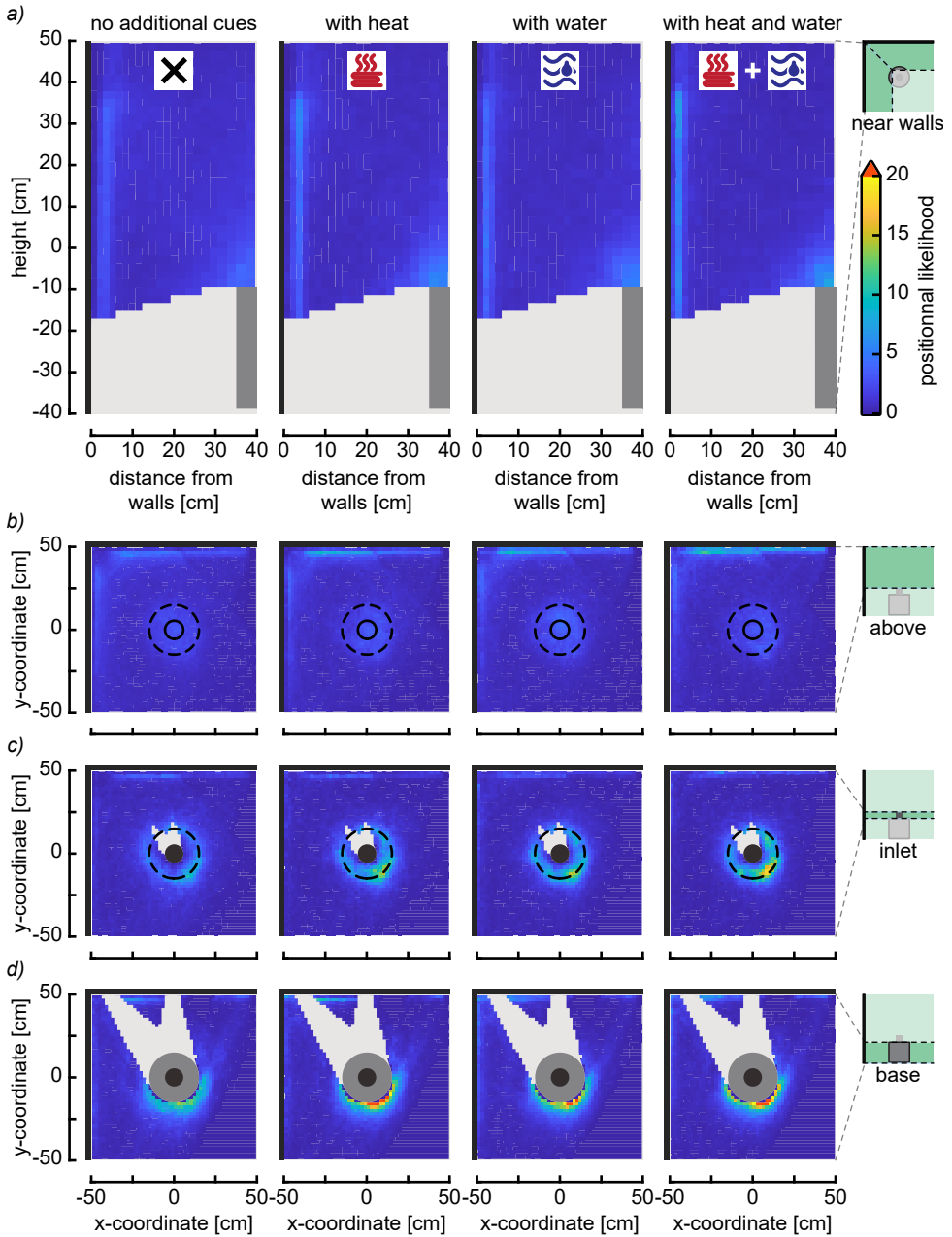
Figure S3.5: Positional likelihood of mosquito flying within various volumes around the M-Tego with or without additional cues (volumes around the trap are indicated on the right). (*a*) Vertical heat maps of positional likelihood close to the walls behind the various conditions, as indicated on the top right. (*b,c,d*) Top-down view of the positional likelihood above the trap inlet (*b*), at the inlet height (*c*) and around the trap base (*d*). Average cell size = 19 x 19 mm.

a)
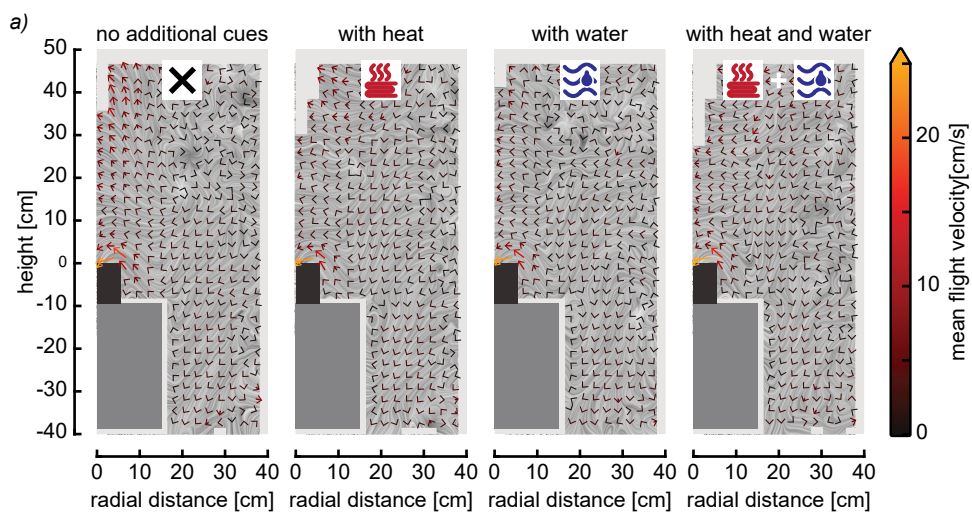
Figure S3.6: Average velocity fields and streamlines of mosquitoes flying around the M-Tego with or without additional host cues (cues as indicated by the symbols). (*a*) Vectors show the average velocity fields in the radial and vertical direction each cell of average size 27.5 x 27.5 mm. Velocity vectors resulting from fewer than 20 tracks were discarded. Streamlines were computed using LIC (Line Integral Convolution).
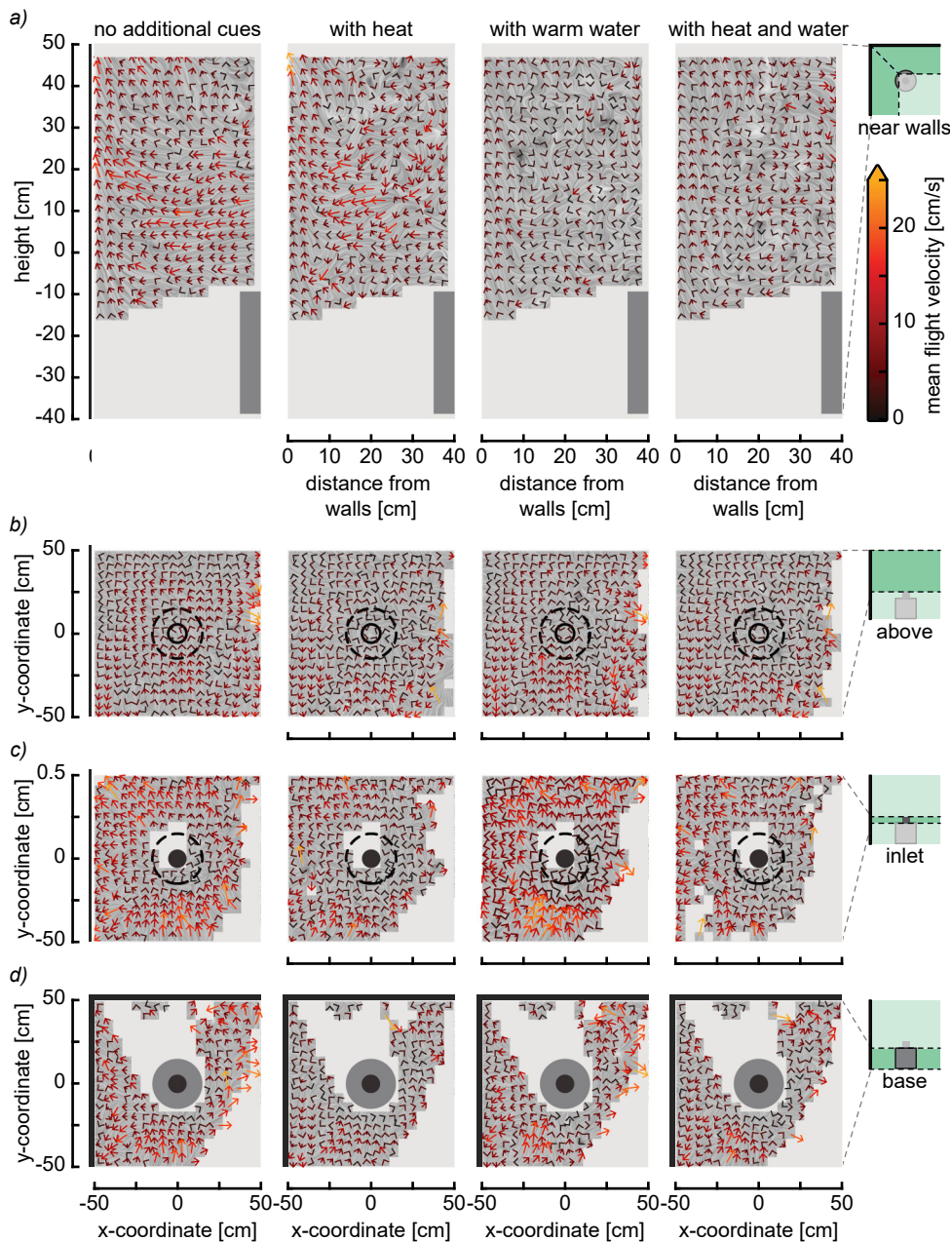
Figure S3.7: Average velocity fields and streamlines of mosquitoes flying within various volumes around the M-Tego with or without additional cues (volumes around the trap are indicated on the right in dark green). (*a*) Vertical view of the average velocity fields close to the walls. Each vector consists of the average velocity in that cell of average size 27.5 x 27.5 mm. All velocity vectors resulting from less than 20 tracks were discarded. Streamlines were computed using LIC (Line Integral Convolution). (*b,c,d*) Top-down velocity fields above the trap inlet (*b*), at the inlet height (*c*) and around the trap base (*d*). Cell size is 55 x 55 mm.
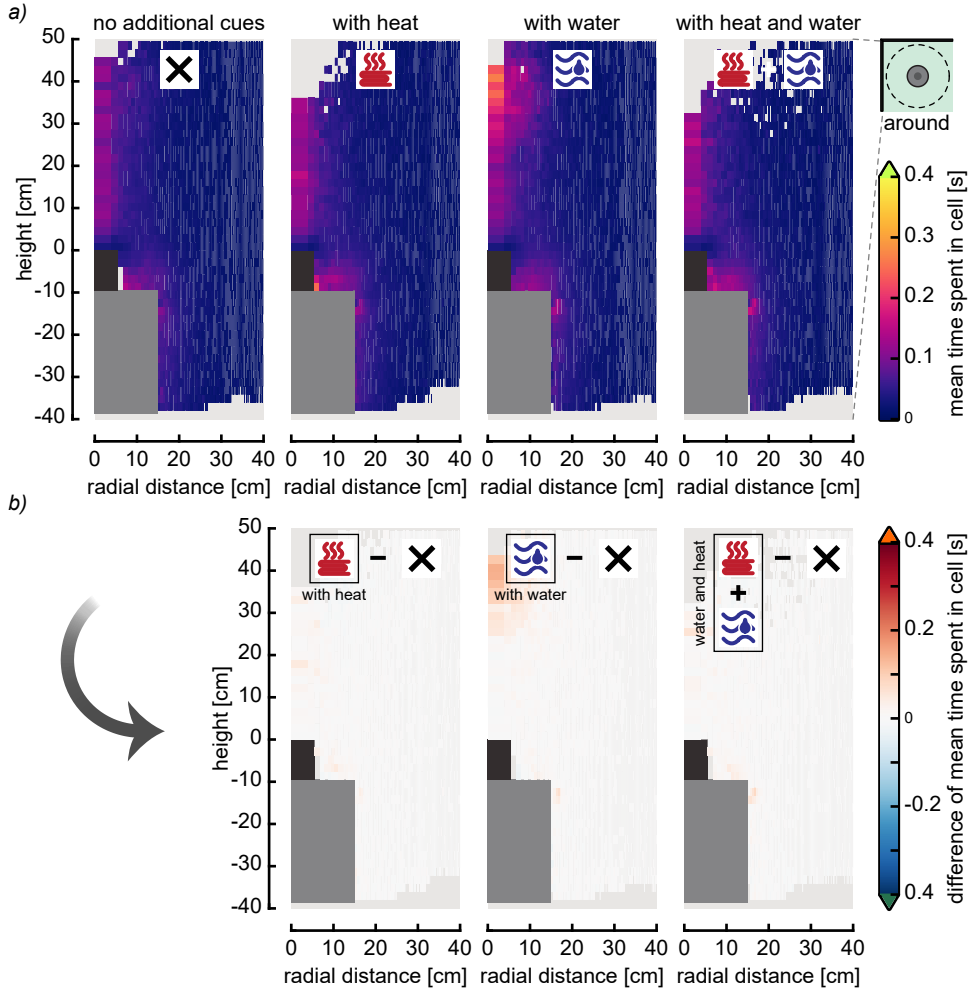
Figure S3.8: Spatial distribution of time spent by mosquitoes around the M-Tego with or without additional cues. (*a*) Radial - vertical heat maps of the average time spend by mosquitoes around the M-Tego with or without additional host cues. (*b*) Difference between the heat maps of time spend around the M-Tego with additional host cues (heat and/or water) and the heat maps of time spend around the trap without additional host cues. Average cell size = 19 x 3 mm.
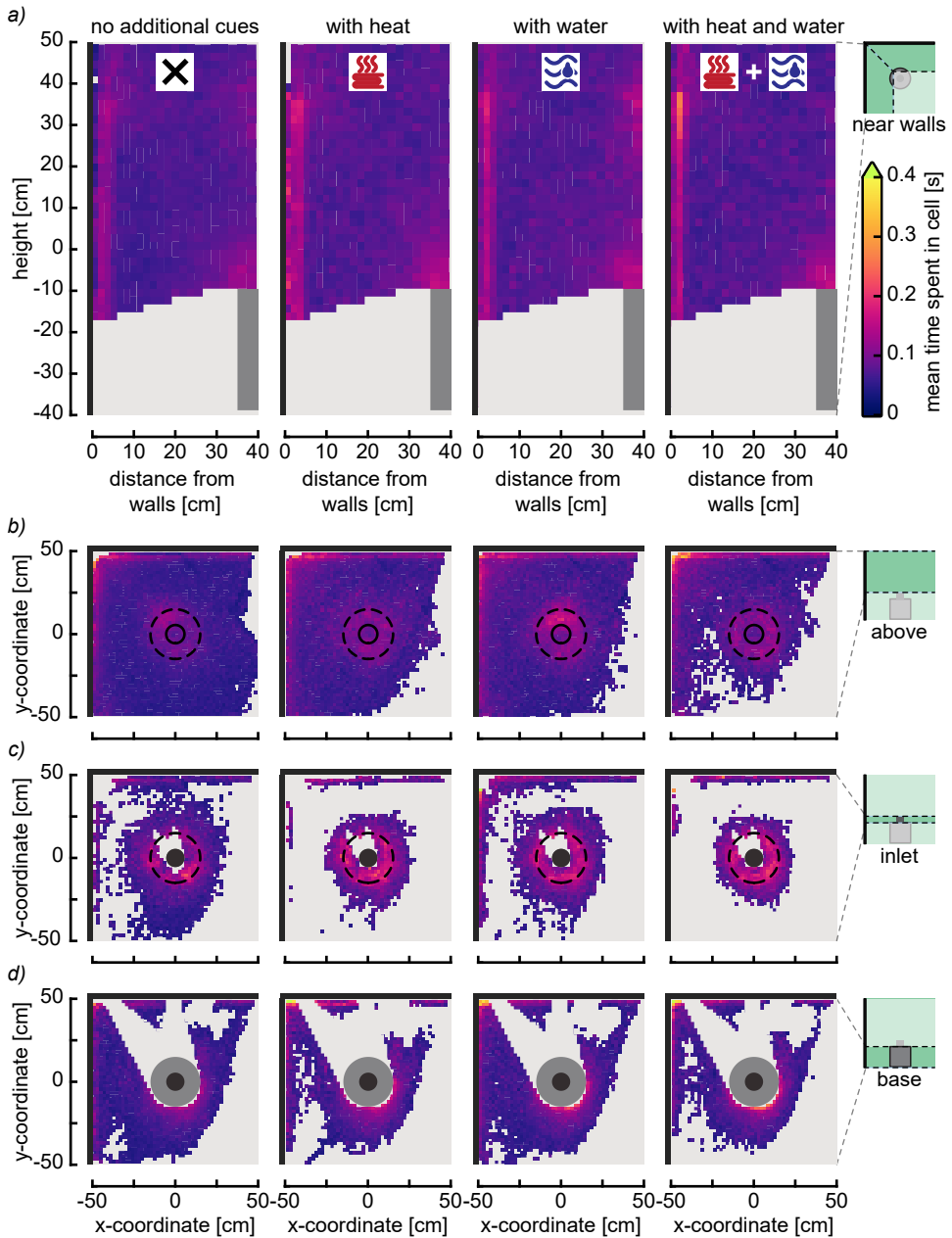
Figure S3.9: Spatial distribution of time spent by mosquitoes within various volumes around the M-Tego with or without additional cues (volumes around the trap are indicated on the right in dark green). (*a*) Vertical heat maps of the average time spend by mosquitoes close to the walls behind the traps. (*b,c,d*) Top-down view of the average time spend by mosquitoes above the trap inlet (*b*), at the inlet height (*c*), and around the trap base (*d*). Average cell size = 19 x 19 mm.
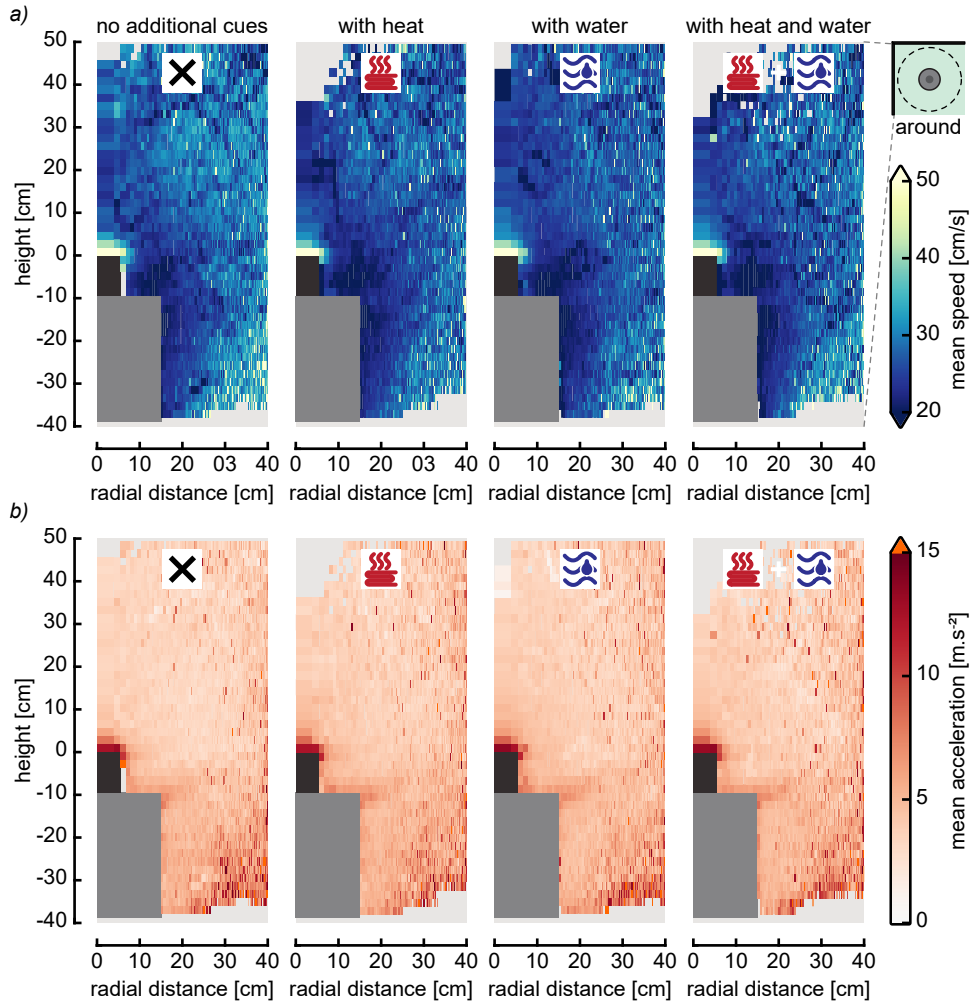
Figure S3.10: Spatial distribution of flight speed and vertical acceleration of mosquitoes flying around the M-Tego with or without additional cues. (*a*) Radial - vertical heat maps of the average flight speed around the M-Tego with or without additional cues. (*b*) Radial - vertical heat maps of the average acceleration of mosquitoes flying around the M-Tego with or without additional cues. Average cell size = 19 x 3 mm.
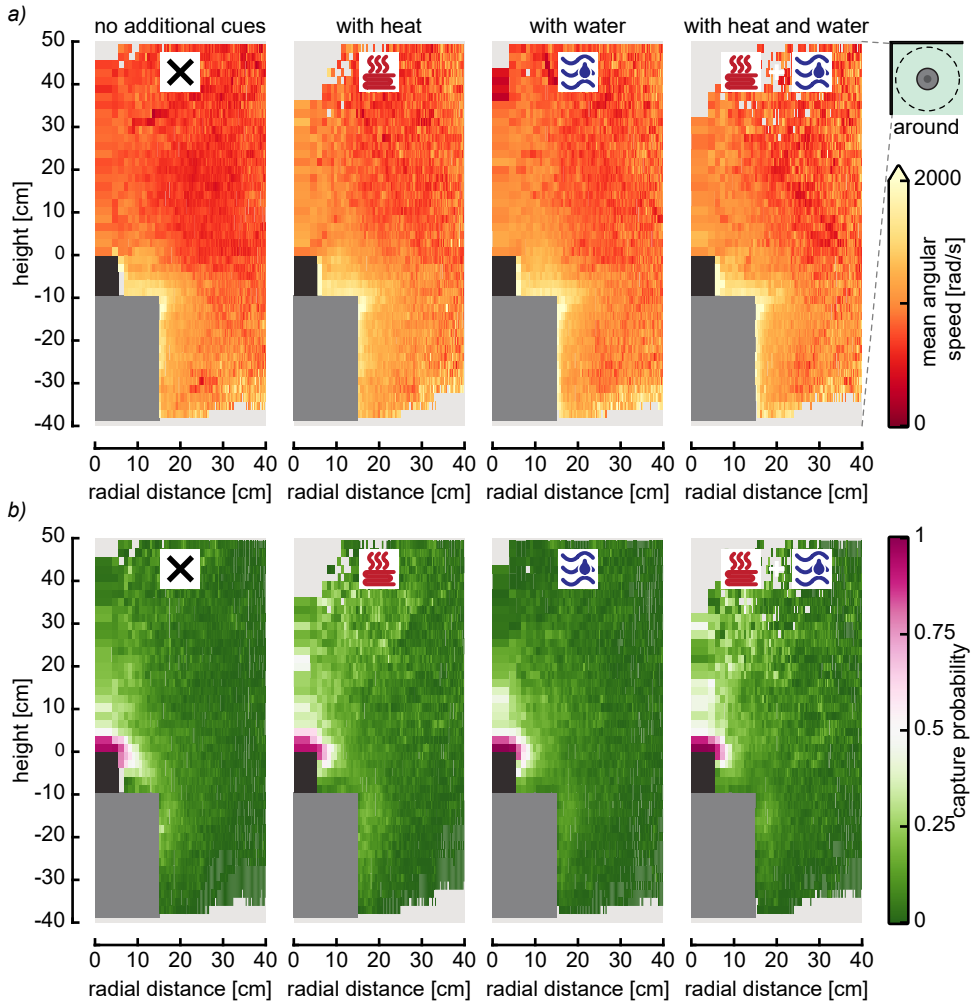
Figure S3.11: Spatial distribution of angular flight speed and capture probability of mosquitoes flying around the M-Tego with or without additional cues. (*a*) Radial - vertical heat maps of the average angular speed of mosquitoes. (*b*) Radial - vertical heat maps of mosquitoes capture probability around the M-Tego with or without additional cues. Average cell size = 19 x 3 mm.
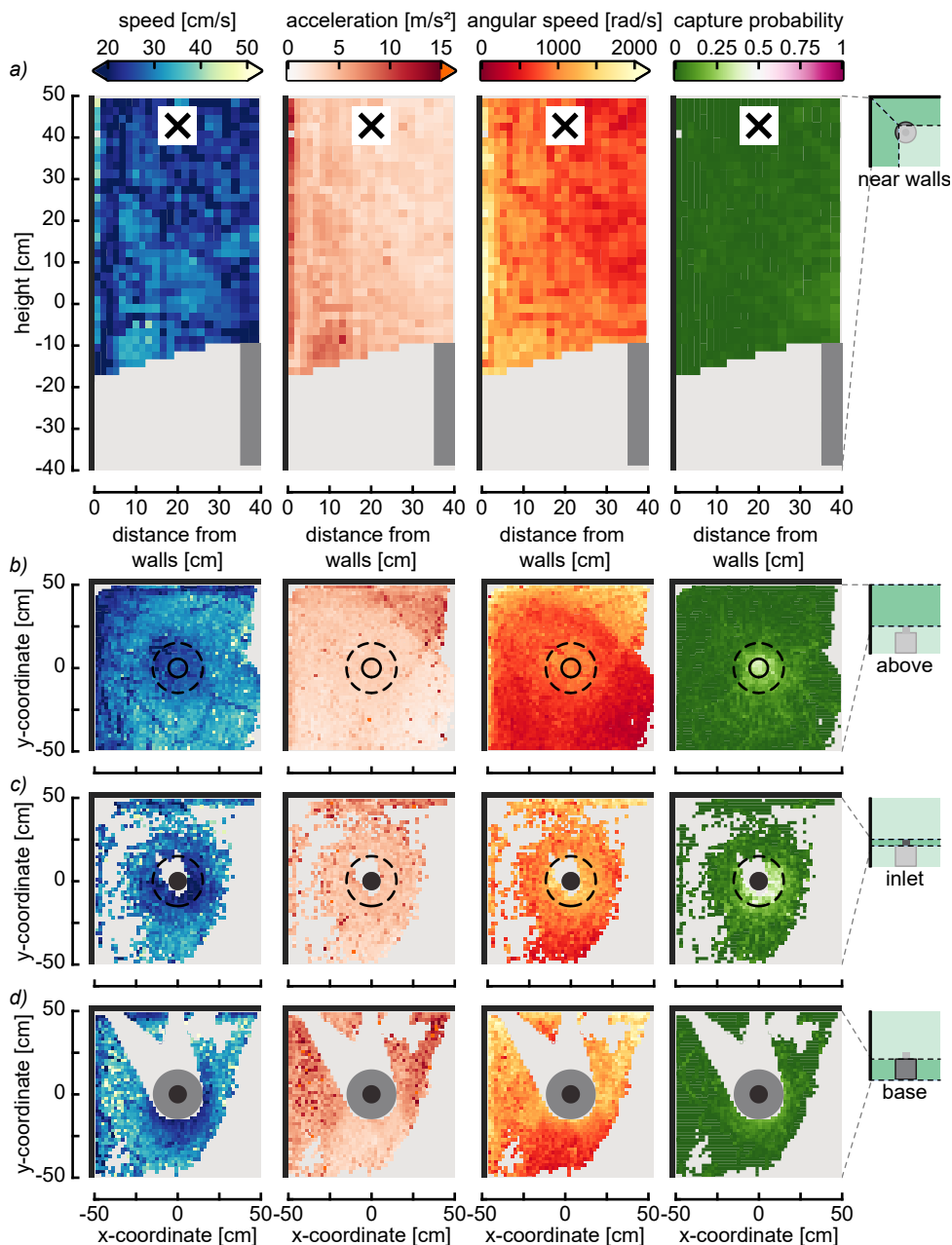
Figure S3.12: Spatial distribution of various flight dynamics metrics of mosquitoes flying within various volumes around the M-Tego without additional cues (volumes around the trap are indicated on the right in dark green). (*a*) Vertical heat maps of average flight speed, average acceleration, average angular speed and capture probability near the wall. (*b,c,d*) Top-down view of these metrics above the trap inlet (*b*), at the inlet height (*c*) and around the trap base (*d*). Average cell size = 19 × 19 mm.
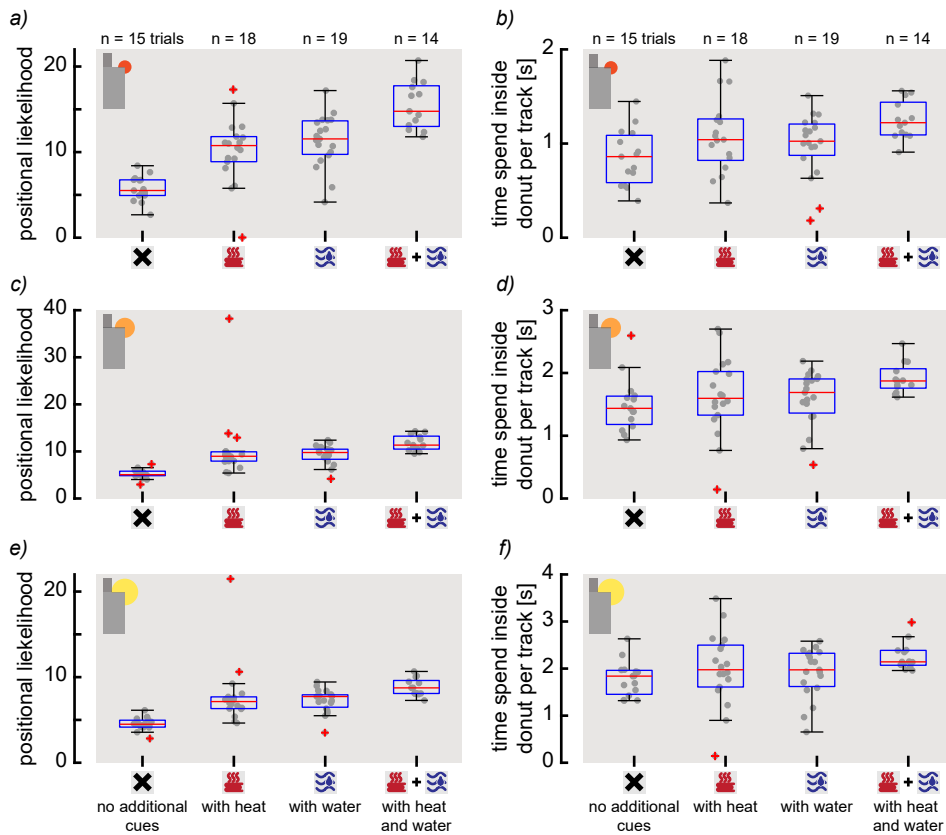
Figure S3.13: Positional likelihood and time spent by mosquitoes in the donut-shaped region close to the trap edge. (*a,c,e*) Box plots of the percentage of points detected inside three volumes of various sizes over the total number of detected points for each trial and in function of if the trap was with or without additional cues. (*b,d,f*) Box plots of the average time spend by mosquitoes inside the three donuts of various sizes for each trial and in function of if the trap was with or without additional cues. The number of tracks used for computing both metrics were 7153 (*a,b*), 9011 (*c,d*) and 10565 (*e,f*).
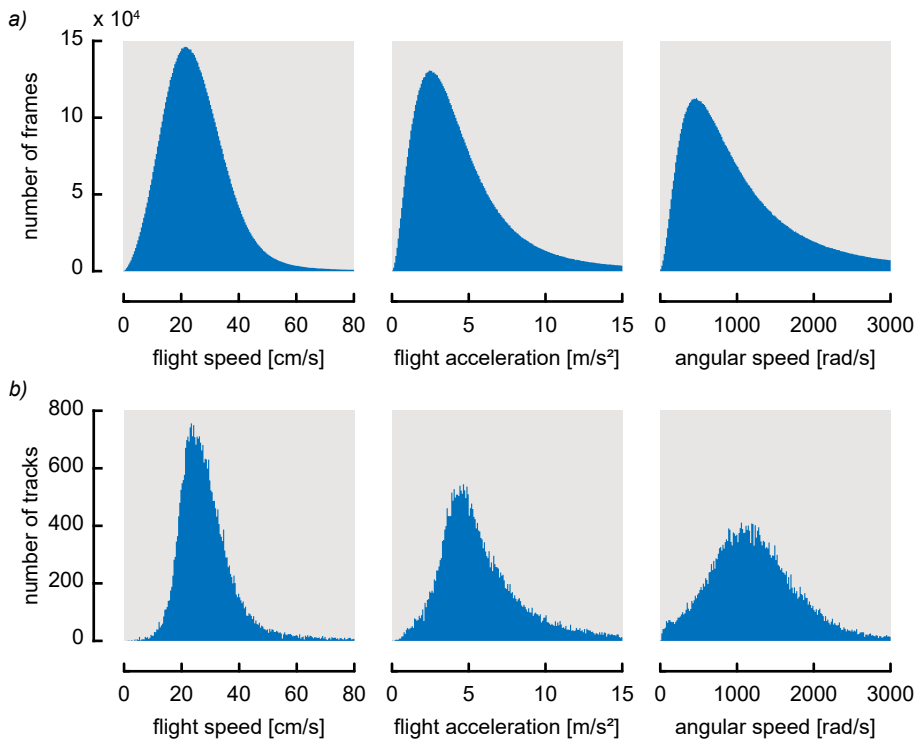
Figure S3.14: Histograms of several flight metrics around the M-Tego. Histograms of mosquito flight speed, acceleration and angular speed for all recorded frames (*a*) or averaged per tracks (*b*).
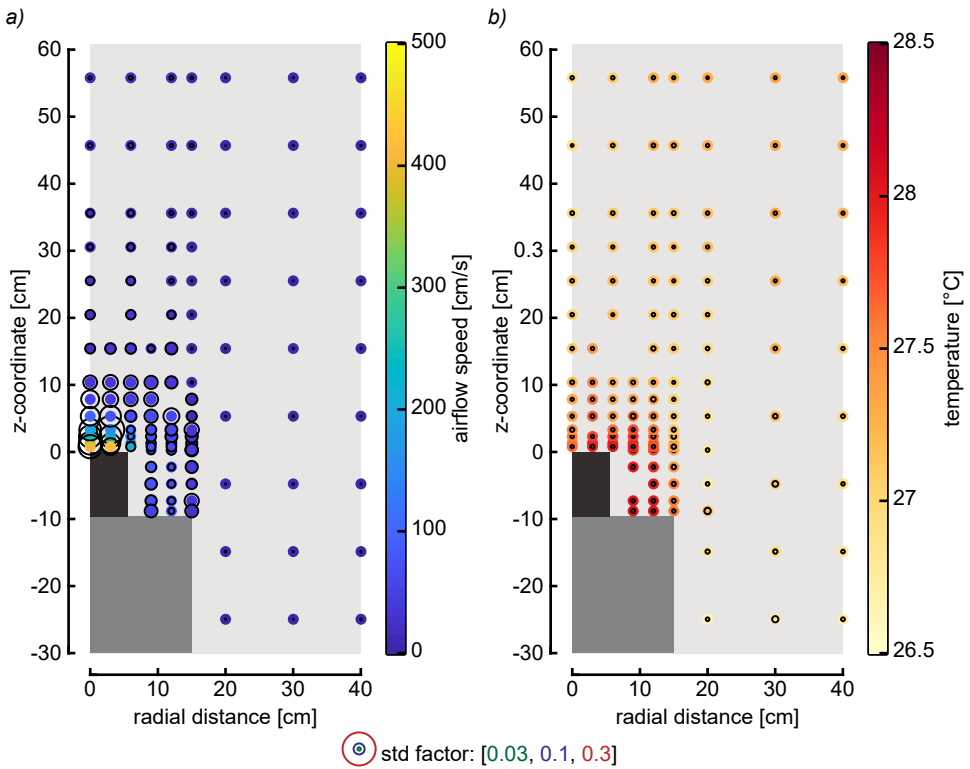
Figure S3.15: Airflow and temperature measurements around the M-Tego. (*a*) airspeeds generated by the M-Tego at various position around the trap. These airspeeds have been computed from the vertical and radial airspeeds measured with a hotwire anemometer (tetso 405i). These are similar to the ones measured around the BG-Suna (Cribellier et al., 2018). (*b*) Temperature generated by the nichrome wire on the top of the M-Tego inlet (with fan turned on). These temperatures have been measured at various positions around the trap. Standard deviations are shown using circles of various sizes (the legend is showing corresponding factors).
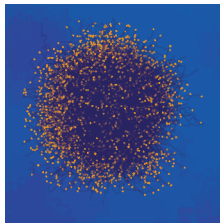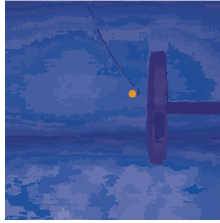
Chapter 4 ————————————————————————————

Diurnal and nocturnal mosquitoes escape looming threats using distinct flight strategies under various light conditions

Antoine Cribellier[1], Andrew D. Straw[2], Jeroen Spitzen[3], Remco P.M. Pieters[1], Johan L. van Leeuwen[1], Florian T. Muijres[1]

[1] Experimental Zoology Group, Wageningen University & Research, Wageningen, The Netherlands

[2] Institute of Biology I and Bernstein Center Freiburg, University of Freiburg, Freiburg, Germany

[3] Laboratory of Entomology, Wageningen University & Research, Wageningen, The Netherlands

Abstract

Flying insects have developed the ability to rapidly evade approaching objects such as predators and swatting hands. This is particularly relevant for blood-feeding insects like mosquitoes that routinely need to avoid defensive actions of their blood-hosts. To minimize the chance of being swatted, a mosquito can use two different strategies: exhibit an unpredictable flight path or maximize its escape manoeuvrability. Here, we studied how flight unpredictability and escape manoeuvrability affects the escape performance of day-active and night-active mosquitoes (*Aedes aegypti* and *Anopheles coluzzii*, respectively). We used a multi-camera high-speed videography system to track how freely flying mosquitoes respond to a rapidly approaching mechanical swatter, in four light intensities ranging from dark to overcast daylight conditions. Results show that both species exhibit enhanced escape performance in their respective natural light condition (daylight for *Aedes* and dark for *Anopheles*). To achieve this, they also use strikingly different behaviours. The escape performance of *Anopheles* at night is explained for 90% by its unpredictable erratic flight behaviour, whereas the increased escape performance of *Aedes* in overcast daylight compared to sunrise is due to its enhanced escape manoeuvrability. This shows that both day and night active mosquitoes adapt their flight behaviour to light intensity such that their escape performance is maximum in their natural blood-feeding conditions, and when these defensive actions by their blood-hosts occur most. Because *Aedes* and *Anopheles* mosquitoes are major vectors of several deadly human diseases, this knowledge can be used to optimize vector control methods for these specific species.

4.1 Introduction

To complete their life cycle, hematophagous female mosquitoes need to forage, mate, find, approach and feed from a blood host for egg development, and lay their eggs. Because mosquitoes are vectors of many deadly human diseases, their blood-host seeking behaviour has been studied thoroughly (van Breugel et al., 2015; Cardé, 2015; Dekker et al., 2005; McMeniman et al., 2014). In contrast, the direct interaction of a mosquito with a defensive blood-host or an attacking predator has been studied relatively little.

To get a blood meal, female mosquitoes need to interact with blood hosts such as humans, cattle or birds. Because mosquitoes are both a nuisance to hosts and vectors of many deadly diseases such as malaria and yellow fewer, these hosts can exhibit defensive behaviours such as swatting, pecking, or tail swishing to kill, push away or discourage them (Darbro and Harrington, 2007; Edman et al., 1984; Edman and Scott, 1987; Matherne et al., 2018; Reid et al., 2014; Walker and Edman, 1985). Additionally, flying mosquitoes can be attacked by predators such as dragonflies, birds or bats (Medlock and Snow, 2008; Roitberg et al., 2003; Yuval and Bouskila, 1993). Many of these animals have advanced attacking strategies like minimizing changes in the visual angle to their target either to follow or intercept their prey (Pal, 2015). Dragonflies approach their prey from below (Mischiati et al., 2015; Olberg et al., 2007), and camouflage into immobile distant objects during the attack

(Mizutani et al., 2003). Bats use a comparable motion-camouflage strategy (Ghose et al., 2006). However, it is not known if mosquitoes exhibit counter-strategies against such attacks.

To successfully escape from looming threats produced by defensive blood-hosts or predators, a flying mosquito might rely on two types of behaviours, so-called 'protean' movements or evasive manoeuvres. In this context, protean behaviours can be defined as an unpredictable or erratic flight behaviour that prevents the predator or host from predicting in detail the position or (re)actions of the flying mosquito (Humphries and Driver, 1970; Moore et al., 2017). While protean behaviours are probably the most widespread anti-predator strategy, their effect on escape performance has been studied very little (Humphries and Driver, 1970; Richardson et al., 2018). If exhibited continuously or in risky situations (e.g. while host seeking), such behaviour could be seen as an insurance against attacks that might be difficult to detect or avoid by the mosquito.

Secondly, to avoid a threat, mosquitoes might exhibit evasive manoeuvres such as the ones observed in insects and birds when attacked by visual looming targets (Cheng et al., 2016; Muijres et al., 2014; Santer et al., 2012). Such manoeuvres are usually directed away from the danger (Muijres et al., 2014), or in the case of some moths, towards safety zones at the flank of the attacking bats (Corcoran and Conner, 2016). Similar to horse flies, female mosquitoes make fast upward manoeuvres after encountering specific host cues or airflow conditions (Cribellier et al., 2018; Hawkes and Gibson, 2016; Thorsteinson et al., 1965; Townes, 1962), suggesting that these manoeuvres might be examples of such evasive manoeuvres.

To detect a threat, a mosquito might rely on its complex sensory system. It is well known that mosquitoes are able to detect CO_2, body odours, visual cues and heat generated by a nearby blood host (van Breugel et al., 2015; Cardé, 2015; McMeniman et al., 2014). Amongst these sensory cues, the presence of CO_2 or body odour could trigger a protean flight behaviour, but only looming visual cues could be used to detect an incoming attack. Recent studies suggest that mosquito hearing, for long thought to only be used during mating behaviour (Cator et al., 2009; Dou et al., 2021), might also inform them about their hosts or predators before an attack (Fournier et al., 2013; Menda et al., 2019). And it is possible that mosquitoes use their mechanoreceptors (antennas and sensible hairs) to detect and react to the air movements generated by an attacker (Fuller et al., 2014). Such an airflow-mediated response has already been described in ground-dwelling insects such as praying mantis and crickets (Chapman and Webb, 1999; Dupuy et al., 2012; Triblehorn and Yager, 2006), and could be an alternative to vision mediated response in low light intensities. This would be particularly relevant for night-active mosquitoes.

Additionally, it is possible that, to escape, mosquitoes simply go with the (air)flow, i.e. passively use the air gust produced by the attack. Such hypothesis seems to be the intuitive assumption on which was based the design of flies swatter made of perforated materials. However such passive usage of the air gust produced by an attack remain to be described

in the scientific literature.

Knowledge is also lacking concerning how environmental conditions affect threat detections and escape performances of mosquitoes and of other insects. Because using vision is potentially the fastest way to detect a threat, light condition is probably the most important factor that can influence the success rate of escapes (Combes et al., 2012). Therefore, we expect that diurnal mosquitoes will rely principally on vision to detect a threat in bright light conditions. But nocturnal mosquitoes flying in pitch darkness cannot rely on vision to detect a threat, and thus, to escape they may rely principally on passive use or detection of the air gust produced by a looming object. Alternatively, these night-active mosquitoes might rely more on distinct protean behaviour to increase their escape performance. Therefore, comparing escape performances of day-active and night-active mosquitoes in various light conditions should inform us on how this activity difference has influenced each of their escape strategies.

In this paper, we studied the escape dynamics of female mosquitoes being attacked by a looming object. For that, we used a real-time videography-based mosquito tracking system to track the 3D movements of mosquitoes flying freely in a flight arena (Fig. 4.1). Based on the position and velocity of the flying mosquito we automatically triggered a 10 cm diameter mechanical swatter to simulate the attack of a human hand, generating both visual and air movement cues. By varying the light intensity inside the flight-arena from dark night-time conditions to overcast daylight conditions, we studied the effect of light conditions on the escape performance of the mosquito. Finally, we performed this study with both night-active malaria mosquitoes (*Anopheles coluzzii*) and day-active *Aedes aegypti*. This allowed us to test how escape performance differed between species that are specialized in blood-feeding in dark night conditions and daylight conditions, respectively.

Our results show that the night active *Anopheles* mosquitoes maximized their escape performance in dark conditions, whereas the day-active *Aedes* mosquito showed enhanced escape performance in overcast daylight compared to sunrise. These are the conditions in which both species are naturally blood-feeding, and thus can expect defensive attacks from blood-hosts. This suggests that both diurnal and nocturnal mosquitoes have optimized their escape flight behaviour for the conditions in which they are most at risk. Our detailed analysis of the flight kinematics shows that this is achieved using distinct mechanisms. *Anopheles* flying in the dark relies primarily on their protean erratic flight behaviour to avoid the swatter, whereas *Aedes* flying in overcast daylight depict a relative increase in escape

Figure 4.1: Experimental setup and conditions. (*a-c*) Schematics showing the experimental setup where free flying mosquito behaviours were recorded in real time using 5 infra-red enhanced cameras. The swatter (orange) was triggered to attack a mosquito if this one was predicted to fly in the middle of the flight-arena. (*d*) Kinematics of the swatter. (*e*) Examples of two tracks (one escape and one collision), as well as details on how the swatter was triggered. The predicted position was based on mosquito initial position and velocity. (*f*) Position over time of all tracked mosquitoes and the swatter. (*g*) Experimental conditions. During mosquito active phase, the light condition was changed according to a semi-random planning (see supplementary Fig. S4.1).

a)

b)

c)

d)

e)

example of: escape | collision
position at trigger | initial velocity (20 cm/s)

swatter (▬) was trigerred when mosquito predicted position (+) was inside the sphere of interest (●).

f)

swatter kinematics

mosquito trajectories

g)

Anopheles coluzzii

Day | Night | trial #1 | trial #2 | trial #3 | Night | Day

dark (≈ 0.02 cd/m²) | twilight (≈ 0.35 cd/m²) | sunrise (≈ 29 cd/m²) | overcast (≈ 781 cd/m²)

Aedes aegypti

Night | Day | trial #1 | trial #2 | trial #3 | Day | Night

time after start of normal light condition [hours]

(Caption on the previous page.)

manoeuvrability compared to sunrise conditions.

The here-studied mosquito species together are the two most dangerous insect species, because they are vectors of a range of human diseases including malaria, yellow fever, Zika and dengue. Therefore, our results can be useful for optimizing or developing species specific trapping systems.

4.2 Results

We recorded the flight behaviour of mosquitoes during 54 experimental trials of 160 minutes in length each (144 hours in total). These trials consisted of 18 controls during which the mechanical swatter was turned off, and 36 trials with the mechanical swatter turned on. Half of these trials were performed on *Anopheles* mosquitoes in the dark, twilight and sunrise light conditions, and the other half were performed on *Aedes* in the twilight, sunrise and overcast conditions. See supplementary Fig. S4.1 for details.

For all trials combined, the mechanical swatter was triggered 13,730 times, whereby 3,666 triggers occurred in the control experiments and 10,064 triggers occurred in the experiments with an activated swatter. For the control experiments, triggering did not activate the swatter, but we did simulate virtual swatter movements and the resulting virtual collisions between mosquito and swatter. These virtual hits occurred in 543 of the cases, whereas real collisions between mosquito and swatter was observed 780 times. This shows that without the swatter activated 15% of the mosquitoes that approached the swatter were hit virtually, and with the swatter activated, 8% of the approaching mosquitoes were hit (Fig. 4.2*a*).

Thus, with the swatter turned off 85% of the mosquitoes were not virtually hit, which suggests that protean flight behaviour might be important for mosquitoes to avoid a looming object. Turning on the swatter reduced the hit percentage by a factor two, suggesting that also swatter-induced mosquito movements are important.

Using a combined statistical and mechanistic modelling of the mosquito flight dynamics, we investigated how the studied mosquito species adjust their flight dynamics to optimize their escape performance. We did this in four steps.

1. First, we determined how the chance of being hit by the mechanical swatter differed between species, light conditions and swatter activation (on/off).

2. Second, we studied how protean flight behaviour affected the escape performance.

3. Third, we determined how the swatter-induced escape manoeuvre dynamics affected escape performance.

4. Finally, we quantified the relative contributions of protean flight behaviour and escape manoeuvre dynamics to the overall escape performance.

For each step of the analysis, we used Bayesian Generalized Linear Models (B-GLM) to determine how the results varied between species, light conditions and with swatter activation.

4.2.1 Modelling the probability of being hit by the mechanical swatter

Using a Bayesian Generalized Linear Model (B-GLM), we first tested how the probability of being hit by the swatter varied between species, light conditions and swatter activation (Fig. 4.2*d-i*). Here, we modelled light as a binary variable, either the light condition during which each species naturally host-seeks (dark for *Anopheles* and overcast daylight for *Aedes*), or the other light conditions combined. From here-on we will refer to these as the reference light conditions and the altered light conditions, respectively. The minimal model obtained after doing a forward selection procedure contained four predictors, swatter activation (on/off), species, and reference light versus altered light (modelled as the interactions between *Anopheles* or *Aedes* with the light condition). An effect was found to be significant (i.e. null-hypothesis rejected) if the 89% Highest Density Interval (HDI) of the standardized effect size (SES) was found completely outside of the Region Of Practical Equivalence (ROPE = [-0.1, 0.1]) (Fig. 4.2*g-i*).

The model confirms that mosquitoes had a significantly lower chance of being hit when the swatter was triggered than of being virtually hit when the swatter was turned off (SES mode = -0.63, HDI = [-0.72 −0.52]; Fig. 4.2*d,g*). Additionally, *Aedes* mosquitoes had a collision probability of 7.0 % which was found significantly lower than the 13.6 % chance of being hit of *Anopheles* mosquitoes (SES mode = -0.75, HDI = [-0.85 -0.62]; Fig. 4.2*e,h*). This effect had a high effect size comparable to the effect size of turning the swatter on or off. Finally, *Anopheles* mosquitoes were significantly less likely to be hit by the swatter if they were flying in their reference dark conditions (SES mode = 0.42, HDI = [0.30 0.54]; Fig. 4.2*f,i*). A comparable trend in reference versus altered light was observed for *Aedes* mosquitoes, but this was not significant (Fig. 4.2*i*). We tested why this was the case by comparing estimated means of hit probabilities between light conditions (Fig. 4.2*j,k*). This shows that with the swatter activated, *Aedes* mosquitoes had significantly lower hit percentages in overcast daylight and twilight, compared to the intermediate sunrise condition (Fig. 4.2*k*); sunrise and overcast did not differ significantly between each other. (Fig. 4.2*f*). For *Anopheles* the hit percentages are consistently lower in the reference dark condition (Fig. 4.2*j,k*).

4.2.2 The unpredictable flight behaviour of mosquitoes explains the low probability of being hit by the swatter

In our experiments we programmed the swatter to be activated when a mosquito was on a collision course with the moving swatter, based on the position and velocity of the mosquito (Fig. 4.3*a-c*). Still, among all trials with the swatter activated, the probability of a

a) % collision probability (over triggers)

= 1 trial

virtual hits

n = number of triggers

n = 10064

n = 3666

swatter off on

b) ☐ swatter off

n = 972 + 549

n = 525

n = 904

n = 404 + 312

dark twilight sunrise overcast

c) 🟧 swatter on

■ *Anopheles*
■ *Aedes*

n = 1841 + 2024

n = 1805

n = 1546

777 + 2071

dark twilight sunrise overcast

Bayesian GLM (Bernoulli distribution)

$$\text{logit}(P(hit)) \approx \beta_0 + \beta_1 * piston\_on + \beta_2 * species + \beta_{3.1} * Anopheles*light\_cdt + \beta_{3.2} * Aedes*light\_cdt$$

d) % collision probality (over triggers)

x543   x780

— mode
▨ HDI

virtual hits

x3123   x9284

swatter off   swatter on

e) x837   x486

x5607   x6800

Anopheles   *Aedes*

f) % x252   x1071
x147   x1176

x2198   x10209
x2183   x10224

Anopheles in 🌙
or *Aedes* in 🟡

all remaining conditions

g) null-hypothesis rejected*

-0.8 -0.6 -0.4 -0.2   0

β_1 (standardized slope for piston on)

h) null-hypothesis rejected*

-1 -0.8 -0.6 -0.4 -0.2 0

β_2 (standardized slope for species)

i) no conclusion null-hyp. rejected*

-0.2   0   0.2 0.4 0.6 0.8

β_3 (standardized slope for interaction of *Anopheles* or *Aedes* with light condition)

*the null-hypothesis is rejected if the 89% HDI (■) is outside the ROPE (▨ ▨)

j) % 🟦 swatter off

collision probability (over triggers)

**

**

dark

overcast

twilight sunrise

-5   0   5   10
log of luminance [cd/m²]

k) % 🟧 swatter on

collision probability (over triggers)

**

dark

overcast

wilight

sunrise

**

**

**null hypothesis rejected

-5   0   5   10
log of luminance [cd/m²]

(Caption on the next page.)

Figure 4.2: Mosquito collision probability. (*a–c*) Collisions percentage (number of collisions over the number of triggers) during the tested conditions. With swatter off, virtual collisions were counted. Because *Anopheles* and *Aedes* are flying very little in respectively overcast daylight and dark, no experiments were done with these conditions. (*d–h*) Results of the Bayesian-GLM used to model how mosquito collision probability varied with the experimental conditions. Each panel is a slice plot showing the effect of one of the predictors. The distributions are estimates of the mean of the collision probability for a given condition. Each panel show the effect of one of the predictors for the entire dataset. Red crosses indicate data points used in the B-GLM. (*f*) *Anopheles* mosquitoes were hit less often than usual while flying in the dark. (*g–i*) Distributions of the means of the standardized slopes β_1, β_2 and β_3. Here, all slopes differ significantly from zero. More on null-hypothesis testing is provided in the supplementary Fig. S4.2. (*j,k*) Bayesian estimation of the means of mosquitoes collision probability in the various experimental conditions. Histograms of the associated standardized effect sizes can be found in supplementary Fig. S4.3.

mosquito being hit by the swatter was on average 7%. And even with the swatter turned off, the virtual hit percentage remained on average below 14%.

Here, we tested whether these low amounts of (virtual) hits were the result of an unpredictable flight behaviour of mosquitoes. For this, we first quantified how and how much the flying mosquitoes deviated over time from their predicted flight path (Fig. 4.3). The temporal dynamics of the distance between mosquito and disk (Fig. 4.3*d*) shows that the average mosquito was flying at a minimal distance of more than 6 cm from the swatter, and that this was even the case when the swatter was turned off. This explains why most mosquitoes are not being hit (when the distance reduces to zero).

To explain why most mosquitoes did not get closer to the swatter, we calculated the distance to the predicted position throughout all analysed flights (Fig. 4.3*c*). For the cases when the swatter was not activated, the distance to the predicted position increases approximately linearly with time, directly after the moment of triggering (Fig. 4.3*e*). At the moment when the virtual (non-activated) swatter would reach its most forward position (time t=0 s), this distance of the average mosquito to its predicted position was 8 cm.

With the swatter turned on, the distance to the predicted position initially increases with time similar to the control case, but closely before the swatter reaches the mosquito this distance rapidly increases (Fig. 4.3*e*). As a result, at t=0 s the distance of the average mosquito being attacked by the swatter was 11 cm, 36% larger than for the control. This rapid increase in distance to the predicted position for the active swatter case can be explained by the simultaneous sharp rise in escape velocity of these mosquitoes (Fig. 4.3*f*).

These results thus show that the active swatter causes a rapid increase in distance to the initial prediction position of the mosquito, but this explained only 36% of this total distance. The additional 64% of this deviation was also present when the swatter was not activated, showing that the unpredictability of the flight path is a major component in explaining the low hit percentages observed in our study.

Fast and curvy flight paths prior to swatter activation reduce the chance of being hit

To determine what flight kinematics characteristics are responsible for this protean flight behaviour, we characterized each flight prior to swatter activation using the mean linear and angular flight speed at the moment of triggering ($U_{initial}$ and $\theta_{initial}$, respectively; Fig. 4.4*a*). We then used a B-GLM to determine how these free flight characteristics affect the probability of being hit by both the activated and virtual swatter (Fig. 4.4). The minimal model showed that both flight speed and angular speed were significantly negatively correlated with the probability of being hit by the real and virtual swatter. For both the linear and angular speed, the chance of being hit rapidly reduces with increasing magnitude, and the effect is larger when the swatter is turned off (Fig. 4.4*b,c*).

To study how variations in the initial flight speed affected the flight unpredictability, we tested how the temporal dynamics of distance from the predicted flight path varied with linear and angular flight speed (Fig. 4.4*g* and 4.4*h*, respectively). This shows that faster flying mosquitoes deviated more from their predicted flight paths (Fig. 4.4*g*), but this distance did not vary with angular speed (Fig. 4.4*h*). It is thus still unknown what is the mechanisms responsible for the effect of angular speed on the chance of being hit.

Anopheles and Aedes mosquitoes use different mechanisms to maximize their protean flight behaviour

The distribution of linear and angular speeds (Fig. 4.4*d*) suggests that there is a trade-off between high linear speeds and high angular speeds, and thus mosquitoes could adjust their flight dynamics to maximize of the two. We tested whether this is the case using B-GLMs with which we modelled how the initial linear and angular flight speeds varied between species, with light conditions and with time during the experimental trial (Fig. 4.5). Because we were here interested in the protean flight behaviour, we performed this analysis on the control flights only, when the swatter was turned off.

Comparing the flight characteristics between the species shows that, relative to *Aedes* mosquitoes, *Anopheles* mosquitoes fly with a 20% higher angular speed and a 13% lower linear flight speed (Fig. 4.5*c,f*). This suggests that the two species of mosquitoes achieve a high protean flight behaviour using two distinct mechanisms: the night-active *Anopheles* mosquitoes fly slowly with curved flight paths, and the day-active *Aedes* mosquitoes fly significantly faster but with a straighter flight path. The temporal dynamics of the distance to the predicted position for the two species shows that the faster flying *Aedes* mosquitoes deviate more from the predicted position than the slower flying *Anopheles* mosquitoes (Fig. 4.5*i*). At the moment when the virtual swatter would reach maximum extension ($t=0$ s) this distance is on average 50% larger for *Aedes* mosquitoes than for Anopheles (12 cm and 8 cm, respectively).

Because the mosquitoes could vary their protean flight behaviour throughout the day,
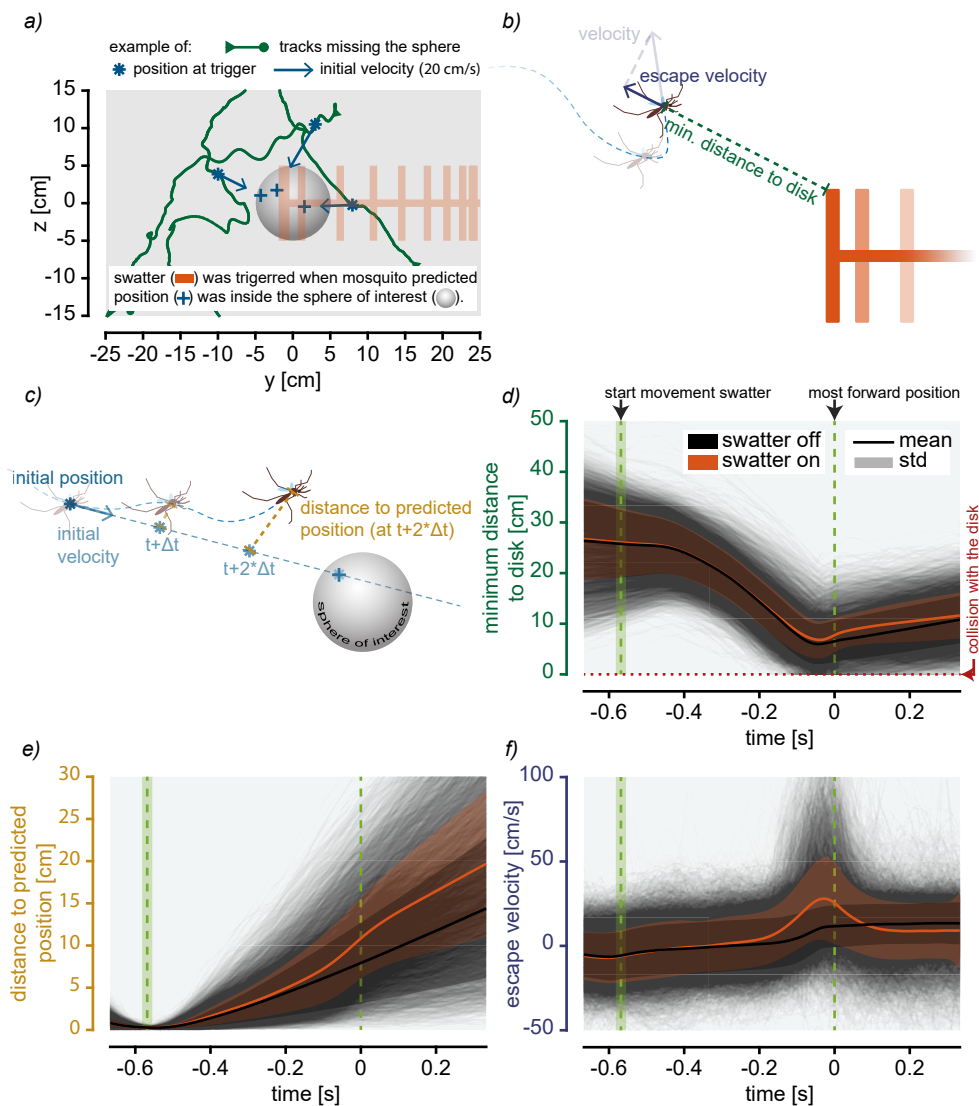
Figure 4.3: Most of the time, mosquitoes are missed by the swatter. (*a*) Examples of mosquito tracks completely missing the sphere of interest despite having been predicted to fly inside (blue crosses). (*b*) Schematic showing how the minimum distance to the disk and the escape velocity are defined as a function of the positions of the swatter and the mosquito. (*c*) Schematic showing how the Euclidian distance between the initially predicted position and the actual mosquito position is defined. The predicted position was calculated by assuming a constant flight velocity. (*d–f*) Variation over time of mosquito minimum distance to disk, distance to predicted position and escape velocity for all tracks. Here is shown the mean and std of all track recorded either while the swatter was turned off or on.

and in response to previous interactions with the swatter, we also tested how linear and angular flight speed varied with time during the experimental trial (Fig. 4.5*d*). Although we did see trends with time for both linear and angular flight speeds, none of these trends

Bayesian GLM (Bernoulli distribution)

$$logit(P(hit)) \approx \beta_0 + \beta_1 * mean\_initial\_speed + \beta_2 * mean\_initial\_angular\_speed$$
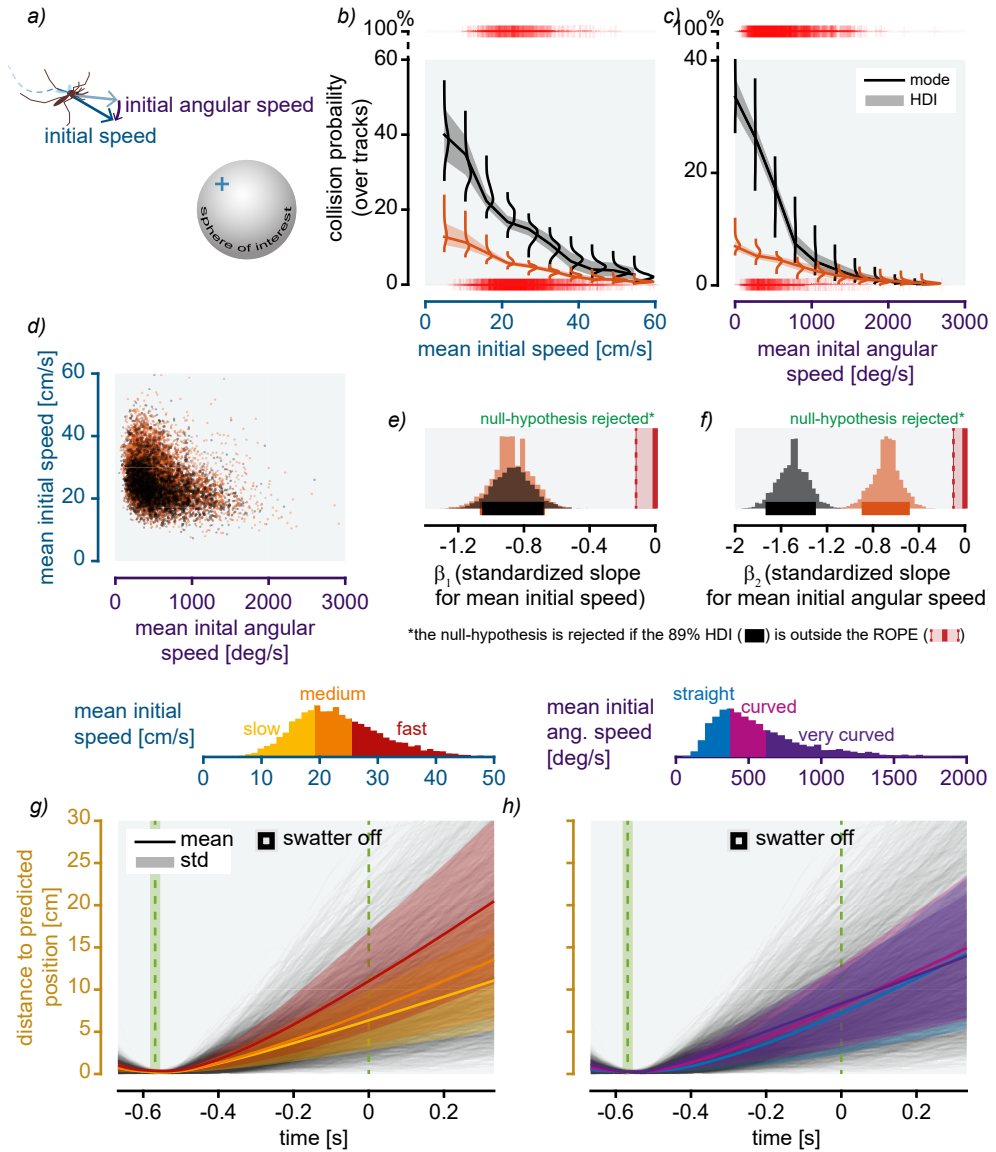
Figure 4.4: Initial flight conditions influence the probability of being hit. (*a*) Schematic showing how mosquito initial flight speed and angular speed are defined. (*b,c*) Results from the B-GLMs used to model how the probability of collisions of tracks is correlated with initial flight metric if the swatter was turned off or on. Each panel is a slice plot to show the effect of one of the predictors. The distributions are estimates of the mean of the collision probability for a given condition. (*d*) mean initial speed versus mean initial angular speed for all tracks with the swatter turned on or off. (*e,f*) Distributions of the means of the standardized slopes β_1 and β_2. Here, all slopes HDIs are found to be outside the ROPE (i.e. significant). *Rest of the caption on the next page.*

148

(*g,h*) Distribution of the mean initial speed and angular speed were respectively into 3 or 2 groups of the same size (one third or one half of the complete dataset). These groups were then given labels (e.g. slow, medium and fast) and the mean and std of each group were plotted over time. Here we see that initially fast-flying mosquitoes are found to deviate faster from their predicted course.

were significant (Fig. 4.5*g*).

Finally, we tested how linear and angular flight speed varied with light conditions for the two species (Fig. 4.5*e,h*). This shows that *Anopheles* mosquitoes fly faster in their reference light condition (dark) than in the altered conditions. For *Aedes* mosquitoes we observed a similar trend of higher flight speeds in the reference light condition (overcast daylight), but the difference was not significant. The angular speed did not differ significantly between the reference and altered light conditions.

The temporal dynamics of the distance to the predicted position for *Anopheles* mosquitoes is larger in the dark (reference light) than in the altered light condition (Fig. 4.5*f*). At the moment when the virtual swatter would reach maximum extension (t=0 s), this distance is on average 40% larger in the dark than for the other conditions combined (7 cm and 4 cm, respectively). This shows that the increased flight speed in the dark increases the protean unpredictability of the flying *Anopheles* mosquitoes.

4.2.3 Both mosquito species exhibit fast swatter-induced evasive manoeuvres more often in brighter light conditions

Following our analysis on the protean flight behaviour, we studied how flying mosquitoes responded to the looming swatter, using all analysed mosquito flights with activated swatter (Fig. 4.6). For this, we used a Hidden Markov Model (HMM) trained on the temporal dynamic of escape velocities (Fig. 4.3*b*) throughout these flight manoeuvres to categorize each flight track into one of three types: flight tracks that ended in a swatter hit, flight tracks that include a slow escape manoeuvre, and flight tracks with a fast escape. Based on this characterization, we estimated the probability that the swatter triggered a fast escape P_{escape}, and how this varied between species, active and inactive swatter, and with varying light conditions (Fig. 4.6). The probability that a virtual swatter triggered a fast escape was lower than 1%, showing that the Hidden Markov Model produced practically no false positive fast escapes (Fig. 4.6*a*). In contrast, probability that a real swatter triggered a fast escape was 20%. Because many flights do not get close to the swatter (Fig. 4.3*d*), these percentages are not surprising.

Applying a B-GLM to these data shows that *Anopheles* mosquitoes have a 43% higher chance of exhibiting fast escape than *Aedes* (Fig. 4.6*e,h*). Also, fast escape probability is positively correlated with the logarithm of light condition luminance, whereby P_{escape} increases with light intensity from 14% in the dark to 25% in overcast daylight (Fig. 4.6*f,i*). Finally, fast escape probability did not differ significantly between the reference and altered light conditions, for both species (Fig. 4.6*g,j*).

a)

b)

log(mean init. ang. speed) $\approx \beta_0 + \beta_1 *$ species $+ \beta_2 *$ time
$+ \beta_{3.1} *$ Anopheles*light_cdt

log(mean initial speed) $\approx \beta_0 + \beta_1 *$ species $+ \beta_2 *$ time
$+ \beta_{3.2} *$ Aedes*light_cdt

Bayesian GLM (gamma distribution)

c)

d)

e)

f)

g)

h)

i)

f)
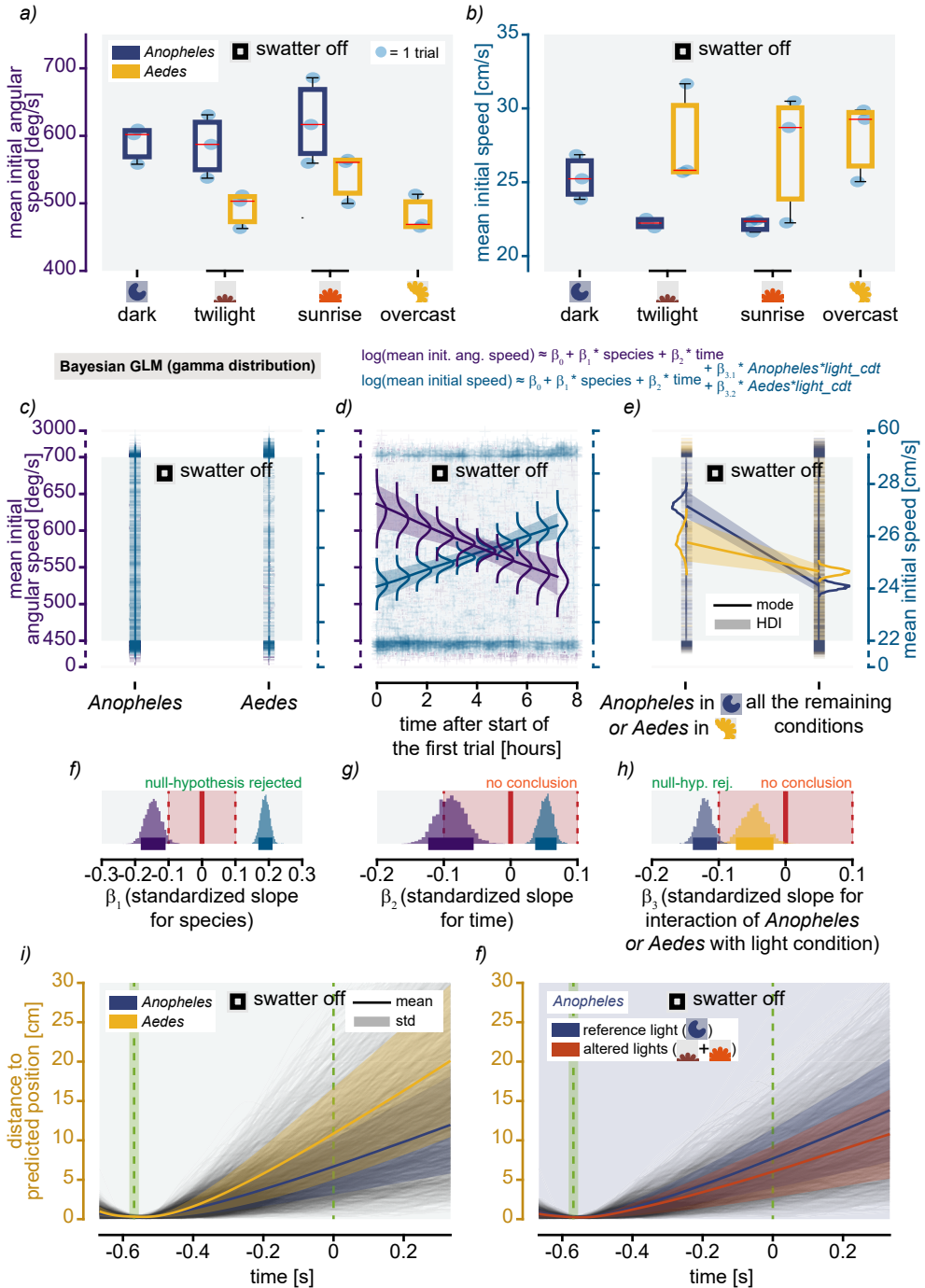
(Caption on the next page.)

Figure 4.5: Initial speed varies with experimental conditions. (*a,b*) Mean initial speed and angular speed of mosquitoes during the tested conditions (swatter off). (*c–e*) Results from the B-GLMs used to model how the mean initial flight speed and angular speed are correlated with experimental conditions (swatter off). Each panel is a slice plot to show the effect of one of the predictors. The distributions are estimates of the mean of the collision probability for a given condition. (*f–h*) Distributions of the means of the standardized slopes β_1, β_2 and β_3. (*i*) Distance to predicted position of *Anopheles* and *Aedes* mosquitoes when the swatter was turned off. *Anopheles* mosquitoes were deviating less from their initial course than *Aedes* mosquitoes.

4.2.4 The escape strategies of day and night active mosquitoes varies differently with light conditions

Mosquitoes thus rely both on protean flight behaviour and escape manoeuvrability to avoid a rapidly looming object (Fig. 4.5 and 4.6, respectively). In this analysis section, we tested how the relative contribution of both behaviours affect escape performance, and how this differs between species and light conditions (Fig. 4.7).

For this, we quantified escape performance of the flying mosquito using its distance from the predicted location at time $t=0$ s, when the swatter reached its maximum extension (Fig. 4.3*c,e*). For the control trials without the swatter activated, this deviation distance is the result of only the protean flight behaviour, and for the trials with an active swatter the distance is the result of both the protean flight behaviour and the escape manoeuvre. As a result, the deviation distances tend to be higher when the swatter is turned on, for all conditions (Fig. 4.7*a-c*).

By applying a B-GLM to these data, we found that the distance from the predicted position was on average 45% higher when the swatter was turned on (Fig. 4.7*d,g*), and it was 63% higher for *Aedes* than for *Anopheles* (Fig. 4.7*e,h*). Additionally, *Anopheles* mosquitoes deviated more from their predicted path when they flew in the dark than in the other light conditions (Fig. 4.7*f,i*). A similar trend was found for *Aedes* mosquitoes, but the effect size was too low to be found significant (Fig. 4.7*f,i*).

These results are very much in line with the results of the B-GLM used to model the probability of being hit by the swatter (Fig. 4.2), suggesting that the deviation from predicted position is a good metric to describe mosquitoes escape performance. We therefore used this parameter to study what were the relative contributions of protean flight behaviour and escape manoeuvrability on the overall escape performance (Fig. 4.7*j-l*).

To quantify this, we defined the relative contribution of the protean behaviour on the escape performance as $R_{protean} = d_{off}/d_{on}$, where d_{off} and d_{on} are the distances of the mosquito at $t=0$ s from its predicted location for the case with the swatter turned off and on, respectively. We quantified $R_{protean}$ for all tested conditions based on the corresponding d_{off} and d_{on} modelled using our B-GLM (Fig. 4.7*j-l*, see materials and methods for details). Note that deviation distance d_{off} is the result of only the protean flight behaviour, and distance d_{on} is the result of both the protean flight behaviour and the escape manoeuvre. Thus, a high $R_{protean}$ suggests high contribution of protean behaviour to escape

a)

b)

c)

d)

e)

f)

g)

h)

i)

j)

$$\text{logit}(P(esc)) \approx \beta_0 + \beta_1 * species + \beta_2 * log(luminance) + \beta_{3.1} * Anopheles*light\_cdt + \beta_{3.2} * Aedes*light\_cdt$$

Bayesian GLM (Bernoulli distribution)
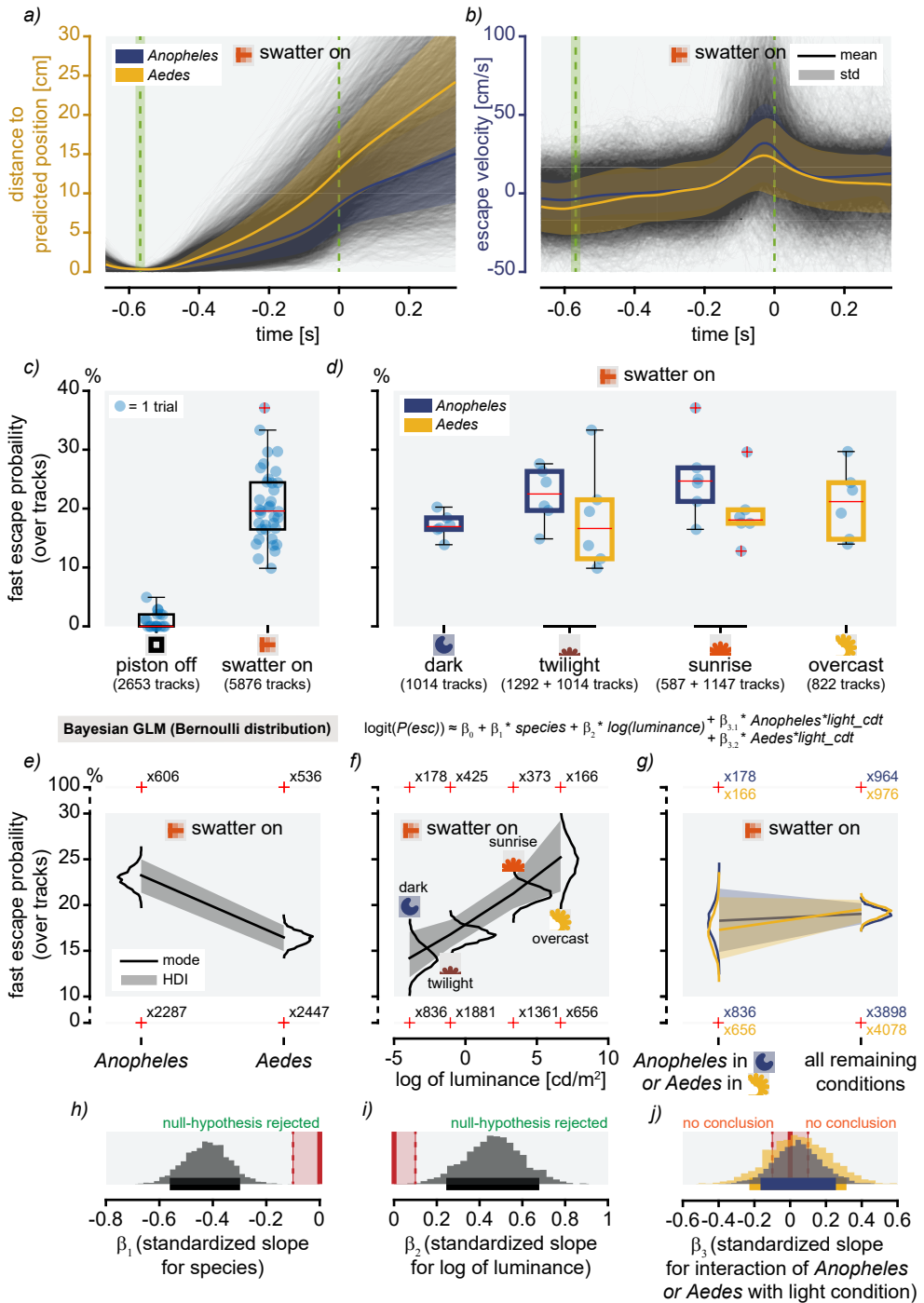
(Caption on the next page.)

Figure 4.6: Mosquito fast escape probability changes with species and light conditions. (*a,b*) Distance to predicted position and escape velocities of *Anopheles* and *Aedes* mosquitoes with the swatter triggered. *Anopheles* mosquitoes were deviating less from their initial course, but exhibited higher escape velocities than *Aedes* mosquitoes. (*c,d*) Percentage of tracks that were at some point in the fast escape state during the tested conditions over the total number of tracks that were not hit by the swatter. (*e-g*) Results of the Bayesian-GLM used to model how mosquito fast escape probability varied with the experimental conditions when the swatter was triggered. Each panel is a slice plot to show the effect of one of the predictors. The distributions are estimates of the mean of the collision probability for a given condition. (*h-j*) Distributions of the means of the standardized slopes β_1, β_2 and β_3. Here, β_1 and β_2 are found to be significantly different from zero.

performance, and a low R_{protean} suggests high contribution of escape manoeuvrability to escape performance.

The average *Anopheles* mosquito was found to have a significantly higher mean R_{protean} in the dark (90%) than in twilight (75%) or in sunrise (79%). This suggests that *Anopheles* mosquitoes achieved enhanced escape performance in the dark due to their increased protean flight behaviour. *Aedes* mosquitoes have the lowest R_{protean} in the overcast daylight condition (78%) and the highest R_{protean} in sunrise (89%). This suggests that *Aedes* mosquitoes achieved the enhanced escape performance in overcast daylight condition compared to sunrise due to increased their escape manoeuvrability in overcast, which reduces R_{protean}.

4.3 Discussion

Here, we studied the escape performance of flying mosquitoes by testing how freely flying mosquitoes avoid being hit by an automated mechanical swatter. The mechanical swatter simulated a looming threat similar in size to a human hand and generated both visual cues and air movements. To quantify the escape performance of the flying mosquitoes, we used real-time videography tracking to reconstruct the three-dimensional flight paths of the mosquitoes before, during and after the attack. Based on the resulting escape dynamics, we tested how the attacked mosquitoes rely on their flight path unpredictability and escape manoeuvrability to maximize escape performance. Finally, we studied how this differed between day active and night active mosquitoes, and how escape dynamics varied with light intensities ranging from dark to overcast daylight.

4.3.1 Simulating a realistic attack

Of all 10,064 swatter attacks only 8% lead to a collision between mosquito and swatter, highlighting the surprisingly high escaping performance of the flying mosquitoes. In our experiments, we triggered the mechanical swatter based on the prediction that a mosquito would fly in a sphere of interests when and where the swatter would finish its swatting motion (Fig. 4.1*e*). Therefore, at the triggering time, the swatter was on an intercepting course with the mosquito. This is quite similar to how humans and dragonflies have been

a)

b) ☐ swatter off

- Anopheles
- Aedes

c) ▪ swatter on

Bayesian GLM (gamma distribution)

$$\log(dist\_pred\_pos) \approx \beta_0 + \beta_1 * piston\_on + \beta_2 * species + \beta_{3.1} * Anopheles*light\_cdt + \beta_{3.2} * Aedes*light\_cdt$$

d)

— mode

HDI

e)

f)

swatter off   swatter on

Anopheles   *Aedes*

Anopheles in 🌙 *or Aedes* in   all the remaining conditions

g)   null-hypothesis rejected

β_1 (standardized slope for piston on)

h)   null-hypothesis rejected

β_2 (standardized slope for species)

i)   null-hyp. rejected   no conclusion

β_3 (standardized slope for interaction of *Anopheles* or *Aedes* with light condition)

j)   ☐ swatter off ▪ swatter on

— mode   HDI

k) *Anopheles*

l) *Aedes*

(Caption on the next page.)

Figure 4.7: Mosquito deviation from their predicted paths varies with experimental conditions. (*a-c*) Mean final distance to predicted flight path of mosquitoes during the tested conditions (all tracks without collisions). (*d-f*) Results from the B-GLMs used to model how the mean final distance to predicted path varied with experimental conditions (all tracks without collisions). Each panel is a slice plot to show the effect of one of the predictors. The distributions are estimates of the mean of the collision probability for a given condition. (*g-i*) Distributions of the means of the standardized slopes β_1, β_2 and β_3. (*j*) Bayesian estimation of the means of *d(off/on)* the ratio of the distance to predicted position when the swatter was turned off over when it was on (all tracks without collisions). We expect *d(off/on)* = 100% if turning on the swatter doesn't have any effect on how much mosquitoes deviated from their predicted flight path. (*k,l*) Standardized effect size of the comparisons of the estimated means of panel (*j*). *Anopheles* mosquitoes flying the dark had a significantly higher ratio *d(off/on)* than when flying in twilight or sunrise. For *Aedes*, only the difference between overcast an sunrise was found to be significant.

found to attack moving targets (Mischiati et al., 2015; Mrotek and Soechting, 2007; Nakata et al., 2020; Soechting and Flanders, 2008; Wiederman et al., 2017), although they both use more complex prediction model than used here. Indeed, our constant-speed motion model is based solely on the instantaneous position and velocity of the mosquito and the movement latency of the swatter, whereas humans and dragonflies are continuously updating their predictions (Brenner and Smeets, 2018; Zhao and Warren, 2015). However, updating a prediction is not always possible (e.g. when the target is occluded), and will always be limited by neuromuscular delays (Mrotek and Soechting, 2007). Due to the mechanical single degree-of-freedom of our swatter, such complex prediction update was not possible. This might have resulted in lower attack success rates as for a real attack, but the standardized swatting dynamics allowed us to more precisely assess the effect of treatment on escape performance. Also, the use of our mechanical swatter instead of simpler visual looming targets allowed for the generation of more realistic range of cues than in previous studies (Card, 2012; Muijres et al., 2014).

4.3.2 Mosquitoes have a high escape performance due to their erratic flight behaviour

A surprising result of this study is the finding that, during control experiments where the swatter was off, only 13% of mosquitoes would have been hit by the virtual swatter, despite all of these mosquitoes being initially on a collision course (Fig. 4.2*d*). This hit percentage can be explained by the combination of the relatively high movement latency of the swatter (367.5 ms), and the unpredictable nature of the flight trajectories of the mosquitoes. Indeed, our analysis of the control experiments showed that after triggering the virtual swatter mosquitoes deviated quickly from their predicted paths, which often resulted in avoiding the danger without performing an evasive manoeuvre (Fig. 4.3*e*). In this way, such flight behaviour would work as a kind of protean insurance against attacks that could be difficult to detect or be avoided (Humphries and Driver, 1970). Because the predators and hosts of mosquitoes have been found to wait for optimal conditions before eliciting an attack (Lin and Leonardo, 2017; Mrotek and Soechting, 2007), such erratic flight behaviour should also reduce the chance of attack initialisation.

Additionally, the chance of being hit by the swatter was found to be lower for mosquitoes that flew faster and with a higher angular speeds prior to the attack (Fig. 4.4*b* and 4.4*c*, respectively). This, coupled with the mosquito flight dynamics (Fig. 4.4*g*,*h*), indicates that flight unpredictability is modulated by the mosquitoes using their linear and angular flight speeds. By definition, these two variables cannot be considered as protean *sensu stricto*, as they do not describe behaviour randomness; instead, linear and angular flight speed most likely function as an amplification factor that increases the effect of an underlying unpredictability in the flight behaviour (Fig. 4.4*g*,*h*). These results are in line with previous findings showing that human targeting accuracy is best predicted by an interaction between the speed and turn angle of the target (Richardson et al., 2018). Thus, by flying faster or with sharper angles, mosquitoes decrease the chance of being hit or caught by an attacker.

Finally, despite recent examples of learning and habituation among mosquitoes (Baglan et al., 2017; Vinauger et al., 2018), our results were inconclusive about the effect of time after the start of the experiments on mosquito escape behaviour (as shown in Fig. 4.5*d* and by the fact that time related predictors were otherwise left out of our models). Nevertheless, these aspects of mosquito escapes are important to understand, especially if we want to improve current vector control strategies (Batista et al., 2019; Cribellier et al., 2018), and therefore they would need to be tackled by future studies.

4.3.3 Rapid escape manoeuvres are induced by both airflow and visual cues produced by the looming object

To study the swatter-induced escape manoeuvre dynamics, we used a Hidden Markov Model (HMM) to identify flight tracks that included rapid escape manoeuvres (Fig. 4.6, and supplementary Fig. S4.8). For the control experiments in which the swatter was not activated, fast escapes occurred in less than 1% of the recorded flight tracks (Fig. 4.6*c*), which shows that the identified fast escapes were indeed describing real escape manoeuvres induced by the swatter movement.

With the swatter turned on, we observed a fast escape in 19% of the recorded tracks (Fig. 4.6*c*). Thus, not all mosquitoes attacked by the swatter performed a rapid evasive manoeuvre, which can be explained by the highly protean nature of mosquito flight behaviour. In the control experiments, 85% of the flying mosquitoes are not hit by the virtual swatter (Fig. 4.1*a*), and thus, in the experiments with the swatter activated, a similar percentage would not need to perform an evasive manoeuvre to avoid a hit.

Comparing the hit percentage between the control and active swatter experiments (Fig. 4.1*a*) shows that the evasive manoeuvres reduced the chance of being hit by approximately a factor two (from 15% to 7% between the experiments with a virtual and real swatter, respectively). Thus, the fast escapes observed in 19% of the recorded flight tracks were very effective in increasing the overall escape performance of the ~15% mosquitoes at risk of being hit.

Based on the temporal dynamics of the escape velocity of mosquitoes attacked by the swatter (Fig. 4.3*f* and *6b*) we see that the fast escapes mostly happened just before the moment when the swatter entered the sphere of interest, where the mosquito was predicted to flight. Thus, the swatter-induced escape manoeuvre when the swatter was close to the mosquito. At these close distances, the swatter-induced airflow is expected to be high, and thus the question remains of whether these swatter-induced rapid escapes are active responses by the mosquito or whether the mosquito is simply pushed away by this airflow. Our B-GLM analysis of the escape manoeuvres shows that the fast escape probability is strongly affected by light intensity (Fig. 4.6*f,i*). Mosquitoes flying in overcast daylight intensity performed significantly more escape manoeuvres than in the dark, with an average escape probability of 25% in overcast and 15% in the dark. Thus, visual detection of the swatter is an important factor in triggering an escape manoeuvre, showing that rapid escapes are at least for a large part performed actively in bright light conditions. Because rapid escapes still occur in 15% of flights in full darkness, the airflow induced by the swatter are also partly responsible for the rapid manoeuvre dynamics of the attacked mosquitoes. More research is needed to determine whether the swatter-induced airflow triggered an active manoeuvre, or whether these are fully- passive airflow-induced movements.

4.3.4 Day-active Aedes mosquitoes exhibit higher escape performance than night-active Anopheles

Our general analysis showed that both tested mosquito species, the night-active *Anopheles coluzzii* and day-active *Aedes aegypti*, rely on protean flight behaviour and escape manoeuvrability to avoid being swatted. But they do this in strikingly different ways. The chance of being hit by the swatter was twice as high for *Anopheles* mosquitoes than for *Aedes*, irrespectively of the light conditions or whether the swatter was turned on or off (Fig. 4.2*d*). This was explained by the higher flight path unpredictability of *Aedes*, quantified by their higher deviation from their predicted flight path (Fig. 4.5*i*). *Aedes* mosquitoes achieve this higher unpredictability by flying faster than *Anopheles* prior to the attack (Fig. 4.5*c*). Interestingly, *Anopheles* mosquitoes fly slower but with higher angular speeds than *Aedes*, suggesting that they increase their protean flight behaviour using a different mechanism (Fig. 4.5*c*). In contrast with the higher protean performance of *Aedes* mosquitoes, *Anopheles* mosquitoes being attacked by the swatter performed a higher number of rapid escape manoeuvres than *Aedes* mosquitoes (Fig. 4.6*e*). *Anopheles* mosquitoes are night-active and thus need to navigate complex environments with limited or sometimes a complete lack of visual feedback. To be able to do this, they might be forced to fly consistently at relatively low flight speeds, and as a result their protean performance is reduced compared to the faster flying *Aedes* mosquitoes. Our results suggest that *Anopheles* mosquitoes partly compensate for their reduced protean performance by flying with higher angular speeds and by responding more strongly to the looming object.

4.3.5 In the dark, night-active Anopheles mosquitoes have the highest escape performance

A very striking result of our study is that *Anopheles* mosquitoes were least likely to be hit when flying in the dark condition (0.0201 cd/m²), despite the greatly reduced visual cues compared to the other tested light conditions (Fig. 4.2*f*). This suggests that these night-active mosquitoes adjust their flight behaviour in such a way that they maximize their escape performance in the light condition in which they are most at risk of being attacked.

Comparing the escape performance of *Anopheles* in the control experiments and swatter activated experiments (Fig. 4.2*j* and 4.2*k*, respectively), shows that (virtual) collision probability is particularly low in the control experiments, with the swatter turned off. This suggests that *Anopheles* primarily increases its escape performance in the dark by increasing its protean flight behaviour. This is confirmed by the striking increase in flight speed of *Anopheles* in the dark compared to the other light conditions (Fig. 4.5*b,e*). This contrast with the increases with light intensity of mosquitoes chance of exhibiting fast escapes, regardless of species (Fig. 4.6*f*). Thus, *Anopheles* displayed enhanced escape performance in darkness, most likely due to their strong increase in protean flight behaviour achieved by flying at higher baseline speeds. As a result, in the dark, the escape performance of *Anopheles* mosquitoes, expressed by the deviation from the predicted flight path, is explained for 90% by their protean behaviour (Fig. 4.7*j*).

4.3.6 Day-active Aedes mosquitoes show enhanced escape performance in overcast daylight

In contrast with *Anopheles*, the day-active *Aedes* mosquitoes exhibit the lowest collision probabilities in the brightest tested light conditions (Fig. 4.2*c*). Although the collision probability in overcast daylight was not significantly different from the other light conditions combined (Fig. 4.2*f,i*), it was significantly lower than in sunrise conditions with the swatter turned on (Fig. 4.2*k*). This suggests that the day-active *Aedes* mosquitoes also adjust their flight behaviour in function of the light condition in which they are at risk of being attacked, in order to maximize their escape performance.

The escape performance of *Aedes* in the control experiments with the swatter turned off did not change with light intensity (Fig. 4.2*j*, respectively), showing that *Aedes* mosquitoes did not modulate escape performance with light by varying their protean flight behaviour. This was confirmed by the equally non-significant change in linear and angular flight speed of *Aedes* with varying light conditions (Fig. 4.5). This suggests that *Aedes* mosquitoes flying in overcast daylight exhibit enhanced escape performance compared to sunrise due to the increase in escape manoeuvrability, which we showed to increase with light intensity (Fig. 4.6*f*). Surprising, *Aedes* also exhibits increased escape performance in the lowest tested twilight condition compared to sunrise. With our analysis on both the protean flight behaviour and escape manoeuvrability, we could not explain this effect. Finally,

we determined how the deviation of *Aedes* mosquitoes from their predicted flight path is affected relatively by protean behaviour and escape manoeuvrability, in different light conditions (Fig. 4.7*j*). Our results confirmed that *Aedes* mosquitoes exhibit enhanced escape performance in overcast daylight, most likely due to their increase in escape manoeuvrability (lower relative protean flight behaviour contribution).

4.3.7 Day-active and night-active mosquitoes escape differently in varying light conditions

Comparing the escape dynamics of night-active *Anopheles* and day-active *Aedes* mosquitoes shows that these two species respond very differently to changes in light condition. *Aedes* does not change its baseline flight speed with varying light brightness, and thus its protean flight behaviour remains similar among all tested light conditions. In contrast, night-active *Anopheles* fly at significantly higher flight speeds in the dark, compared to the other tested light conditions, enhancing their protean flight behaviour in the darkness. Because escape manoeuvrability partly depends on visual detection of the looming object, escape performance increases with light intensity. As a result, *Aedes* mosquitoes have the highest escape performance in the brightest light condition (overcast). And this despite the fact that the eyes of *Anopheles* mosquitoes seem to be better adapted to low light conditions (Land et al., 1999).

Comparing the relative contribution of protean behaviour and escape manoeuvrability to escape performance between *Anopheles* and *Aedes* highlights these differences in behaviour very well (Fig. 4.7*j-l*). *Anopheles* mosquitoes show a striking increase in how much they rely on protean behaviour in the dark compared to the other conditions, whereas 90% of the escape performance is explained by baseline erratic flight behaviour. In contrast, in twilight and sunrise *Aedes* mosquitoes rely on a higher contribution of protean behaviour than *Anopheles*, but when transitioning from sunrise to overcast daylight the contribution of escape manoeuvrability rapidly increases (reduced protean contribution), resulting in a concomitant enhanced escape performance.

These combined results thus suggest that both day and night active mosquitoes have optimized their flight behaviour such that their escape performance is maximized in the light condition in which they naturally seek blood-hosts, and are thus most at risk of being swatted by such defensive host.

4.3.8 Conclusion

Flying mosquitoes attacked by a looming object possess a good escape performance, due to both their highly unpredictable flight paths and their highly successful escape manoeuvres. Flight path unpredictability is modulated by both the linear and angular speed of the flying mosquito; escape manoeuvres are triggered by both visual cues and the airflow induced by the attacker. The night-active *Anopheles* mosquitoes exhibited maximum escape per-

formance in the dark, whereas day-active *Aedes* showed enhanced escape performance in maximum light intensity. Thus, for both species escape performance is highest in the light conditions in which they naturally exhibit host-searching behaviour. Finally, *Aedes* had better escape performance than *Anopheles* due to their greater unpredictability, which we interpret as a protean insurance against the increased risks of being active during the day.

Authors' contributions

AC and FTM conceived and designed the experiments. AC and RP designed and build the experimental setup. AS developed the real time tracking software flydra and provided support for integrating it in the experimental setup. AC designed and build the automatic experimental system. AC performed the experiments. AC analysed the data. FTM, JS and JLvL provided support for the analysis. AC wrote the first draft of the manuscript. All authors commented the manuscript. All authors read and approved the final manuscript.

Declaration of Interests

The authors declare no competing or financial interests.

4.4 Material and Methods

4.4.1 Experimental animals

In our experiments, we used female *Anopheles coluzzii* and *Aedes aegypti* mosquitoes. *Anopheles coluzzii* mosquitoes came from a colony that originated from Suakoko, Liberia in 1987. The colony of *Aedes aegypti* mosquitoes (Rockefeller strain) was obtained via Bayer AG Monheim, Germany in 2015. Both colonies are housed in the Laboratory of Entomology (Wageningen University & Research, The Netherlands) with a shifted clock 12h light:12h dark cycle. Mosquitoes were reared at fixed temperature of 27 °C and relative humidity of 70%. Adults were kept in BugDorm cages (30 × 30 × 30 cm, MegaView Science Co. Ltd., Taiwan). They had constant access to 6% glucose sugar water solution and were blood-fed daily with human blood (Sanquin, Nijmegen, The Netherlands) using a membrane feeding system (Hemotek, Discovery Workshop, UK). In the cages, female

mosquitoes had access to wet filter papers for egg-laying. Upon collection, eggs were dried for 3 days after which they were moved to plastic larval trays filled with 27°C water containing a few drops of Liquifry No. 1 fish food (Interpet, UK). Emerging larvae were fed with TetraMin Baby (Tetra Ltd, UK). The handling of pupae differed slightly between the two species. *Anopheles* pupae were placed directly in new BugDorm cages to emerge, whereas *Aedes* pupae stayed in their larvae trays covered with nylon netting material. Twice a week, emerged *Aedes* adults were vacuumed to new BugDorm cages. Males and females were kept together so they could mate. Non-blood-fed adult females (age = 7.6 ± 2.3 days (mean ± std)) were used in our experiments.

4.4.2   The flight arena

In this study, we filmed free flying mosquitoes in a custom-made octagonal flight arena (50x50x48cm (height x width x length)) with transparent Plexiglas walls (see Fig. 4.1*a*). A visible light panel (20x48cm) with 176 LEDs (OSLON SSL 80°, CS8PM1.PM) was positioned above the flight arena. Multiple polyester neutral density filters of 0.8 ND (LEE filters, Panavision Inc.) were used to stop down the light intensity of four LEDs to mimic twilight condition. Additionally, 4 infrared light panels (3x 20x48cm + 1x 50x50cm) with a total of 600 LEDs (OSLON Black Series (850 nm) 150°, SFH 4716A) were set around the flight-arena. The spectrums of the light conditions used in our experiments were measured and can be found in the supplementary Fig. S4.5. Because mosquitoes cannot see infrared light (Gibson, 1995), the infrared light panels were used for backlighting flying mosquitoes. Mosquitoes could then be tracked in real time using Flydra (version 0.20.30)(Stowers et al., 2017; Straw et al., 2011) and the live footage from 5 enhanced infrared cameras (Basler acA2040-90umNIR). To each camera were attached one 12.5 mm lens (Kowa LM12HC F1.4). A pixel-binning of 3 was used resulting in a recording resolution of 680x680px and a framerate of 90 fps. Lens distortions were corrected using a backlighted print of a chequerboard pattern (OpenCV, 2014).

To simulate an attacking threat, we build a swatter made of a 1 cm diameter black aluminium shaft and a transparent plexiglass disk with a diameter of 10 cm and a thickness of 1 cm, thus similar in size to a human hand size. In addition, an either clear or black mesh (Ornata plus 95135, howitec.nl) was covering the disk. These meshes were used to allow the variation of the generated visual cues independently to changes of the amount of air movement generated by either solid or perforated transparent Plexiglas disks. The results presented in this paper are excluding data using the hollow disk in order to focus on the effect of light conditions on mosquito flight behaviours.

The swatter (disk + shaft) was moved by a 50 cm long-toothed belt axes (drylin ZLW-1660-G0BW0-D0A3B-0A0A-500) powered by an AC servo motor (Schneider Electric Lexium BCH2 LD0433CA5C). The servo motor was controlled by a programmable motion servo driver (Schneider Electric Lexium LXM28A) programmed using the software SoMove 2 (Schneider Electric). The swatter kinematic (Fig. 4.1*d*), was designed to have a peak velocity

of around 1 m/s. This kinematic was based on preliminary experiments of human swatting hanging ping-pong balls and quantified data on mosquito flight speed that generally does not exceed 1 m/s (Cooperband and Cardé, 2006; Cribellier et al., 2018; Dekker and Cardé, 2011; Spitzen et al., 2013). The airflow velocity generated by the attack was quite similar to the one generated by an attacking bat (Triblehorn and Yager, 2006).

The temperature and relative humidity inside the experimental room were controlled by a previously described climate system (Spitzen et al., 2013). To facilitate air circulation and cleaning inside the flight arena, there was circular holes in the front (diameter of 17.4 cm) and back (diameter of 43.7 cm) plexiglass panels. These holes were closed using easily removable HDPE insect screenings (Howitec, The Netherlands). On the floor of the flight arena, we placed visual markers, randomly shaded grey squares printed on a plasticized paper sheet. Finally, a sensor recording local temperature and relative humidity (AM2302, ASAIR) was also placed inside the flight arena. Microcontroller boards (Arduino UNO) and custom-made scripts were used to communicate with the sensor, to trigger the swatter movement and to change the light condition from a nearby Linux computer. The setup was automated with the Robotic Operation System (ROS version Kinetic Kame).

4.4.3 Experimental procedure

In the late afternoon before each experimental day, the flight-arena was cleaned using a 15% ethanol solution and paper towels. Calibration was done by tracking a manually waved single LED inside the flight-arena. Then the new calibration was aligned to the flight arena coordinate system using a calibration device made of 8 LEDs positioned at various known three-dimensional locations. The flight arena was then closed. 50 female mosquitoes were transferred from a rearing cage to a release cage, which was then plugged to the side of the flight-arena. All handling of the mosquitoes and of the materials was done wearing nitrile gloves to avoid skin odour contamination. A dedicated Python 2.7 script was started to automatically run consecutive experiments with the different light conditions the succeeding day. By removing a metal mesh door, the mosquitoes could enter the flight arena and the experimenter left the room at 6 p.m. ± 1.2 hours. The first experimental trial started 11.2 ± 3 hours later the following morning,

Upon the start of the Python script controlling the experimental conditions, the light condition was set to follow the mosquito's normal light cycle in the rearing. Then the first experimental light condition was set, either at 2:30 a.m. for *Anopheles* mosquitoes (during their night phase) or at 8 a.m. for *Aedes* mosquitoes (during their day phase), in order to give mosquitoes two hours buffer time to adjust to their active phase. Three different light conditions were tested consecutively every day, each during an experimental window of 160 minutes. The order of these light conditions was changed following a quasi-randomized planning (see supplementary Fig. S4.1). The three light conditions tested for *Anopheles* mosquitoes were dark (visible light turned off), twilight and sunrise, whereas the ones for *Aedes* mosquitoes were twilight, sunrise and overcast, resulting in an overlap of two light

conditions between the two species (Fig. 4.1g and supplementary Fig. S4.1). Neither *Anopheles* or *Aedes* were recorded flying in respectively overcast or dark because of their observed low flight activity in those light conditions.

Real-time estimations of mosquito positions and velocities were used to compute their predicted positions 367.5 ms in the future. Such latency corresponds to the time the swatter takes to be around halfway towards its most forward position. If the predicted position was found to be inside a sphere of interest, defined as a 10 cm diameter sphere in the centre of the flight arena, the swatter was triggered (Fig. 4.1e). After one second, the swatter was moved back to its initial position and a delay of 10 seconds was respected before any new trigger of the swatter. During post-processing, mosquito initial positions and mean initial velocities (i.e. at trigger time) were used to filter out tracks that were not predicted to be inside the sphere of interest when the swatter would reach its most forward position. Thus, for the rest of the analysis, we only kept the tracks that were predicted to be entirely in the sphere of interest during the second half of the swatter movement (-157.5 to 0 ms).

When all the experiments of the day were finished, the experimenter came back into the room. A vacuum cleaner was plugged to the flight arena in place of the handling cage, and was used to capture all mosquitoes while avoiding potential escapes. The captured mosquitoes were left inside the vacuum cleaner to desiccate. Finally, the disk and mesh attached to the swatter rod were changed according to the previously mentioned plan (supplementary Fig. S4.1) for the next experimental day.

4.4.4 Analysis of three-dimensional flight tracks

Pre-processing was done using Python 2.7. For each trigger, collisions were manually identified by looking at the two-dimensional tracking results of the side cameras. A mosquito track with a collision was labelled as such when the tracked points of the swatter were intercepting the track. By projecting the swatter's three-dimensional shape into the two-dimensional view of each camera, the two-dimensional points of the swatter were filtered out for each trigger. The three-dimensional tracks of all mosquitoes were then reconstructed again, thus optimizing tracking performance near the swatter.

The rest of the analysis was done using Matlab R2019b. A first filtering of outlying three-dimensional points was done using the covariance matrices estimated by the extended Kalman filter used by the Flydra tracker. Then, less than four points long segments of mosquito tracks were filtered out, and segments that were separated by more than 15 missing points were divided in two different tracks. Remaining missing values were interpolated using the modified Akima piecewise cubic Hermite method (makima, Matlab). Then, in order to analyse only complete manoeuvres, we filtered out all the tracks that were not starting at least 60 frames before the most forward position of the swatter was reached (t = 0 s on Fig. 4.2–4.7). Similarly, except for collisions, we filtered out tracks that ended less than 30 frames after the time when the swatter reached its most forward position. Finally,

three-dimensional tracks were smoothed using a Savitzky-Golay filter with a moving window of five frames. Mosquito velocities and accelerations over time were computed using a second order derivate central finite difference scheme. Initial and final values were estimated respectively using forward and backward finite difference schemes. The angular flight speed was computed as in (Cribellier et al., 2018). Then, the distance between the nearest point on the swatter disk was estimated using the synchronized position of the swatter over time (Fig. 4.3*b*). The escape speed was defined and computed by projecting mosquito speed over time on the moving line between the nearest point on the swatter and mosquito three-dimensional position (see Fig. 4.4*a*). The initial mean and standard deviation (std) of flight speed or angular speed were computed over the 11 frames around the frame at which the swatter was triggered. Finally, to see how much mosquitoes deviated from their initial trajectory, for each point in time we computed the Euclidian distance between their current position and the predicted position based on their initial position and initial mean velocity (Fig. 4.3*c*). And the mean final Euclidian distance to predicted position of each mosquito was computed over the 11 frames around the frame at which the swatter reached its most forward position.

To be able to compare the chance of being hit by the swatter with or without potential mosquito responses (i.e. with the swatter on or off), collisions with a virtual swatter were predicted. These virtual collisions were estimated by computing if and when mosquito flight tracks would have crossed the path of the swatter (here virtual), assuming it had been triggered according to the triggering rules defined earlier.

4.4.5 Statistical analysis

Various Bayesian generalized linear models (B-GLM) were used in this study to model mosquito flight behaviour and escape performances. We used Bayesian statistics mainly because of its conceptual clarity, whereas in Frequentist statistics there are common misconceptions about important concepts like p-values and confidence intervals (e.g. interpreted as credibility intervals). Additionally, the Bayesian approach provides richer results by giving the probability distributions of the estimated parameters as well as an intuitive way of testing the null-hypothesis (see next paragraph). Finally, in Bayesian statistics there is no need for multiple testing correction (Dienes, 2011; Kruschke, 2010).

In Bayesian statistics, before estimating the posterior distribution of a parameter mean (e.g. the slope of a statistical model), our prior knowledge of this distribution needs to be defined (Kruschke, 2013). For this study, we had no prior knowledge of the standardized estimated mean parameters, therefore we used diffuse priors with a wide normal distribution (mean = 0 and std = 100). Then, the posterior distribution of the parameter is estimated by updating the prior distribution with new data (e.g. experimental results). This is computationally costly, and was done using JAGS which use Markov chain Monte Carlo (MCMC) (Plummer, 2003). Finally, null-hypothesis testing was done using the "HDI+ROPE decision rule" (Kruschke and Liddell, 2018), where the null-hypothesis is

rejected if the 89% Highest Density Interval (HDI) of the standardized parameter is outside the Region of Practical Equivalence (ROPE = [-0.1, 0.1]). The 89% HDI being defined as the interval in which all the points have a higher probability density than points outside. The ROPE is defined as the range around zero (i.e. the null-hypothesis) where, if estimated there, a parameter would be found to have "practically no effect". Thus, to reject the null-hypothesis, the HDI of an estimated parameter must fall outside the ROPE (see supplementary Fig. S4.2).

We estimated means of mosquitoes probability of being hit (Fig. 4.2) for each combination of light condition and species using MATJAGS, a Matlab interface for JAGS (Steyvers and Kalish, 2014), and the Matlab Toolbox for Bayesian Estimation (MBE) (Winter, 2016), a Matlab implementation of Kruschke's R code (Kruschke, 2013). To model the probability of being hit we used a Bernoulli distribution and a logistic link function. Then we compared the estimated mean distribution by computing standardized effect sizes. Here we defined the effect size between two groups as the difference of their means divided by the norm of their standard deviations.

For this study, we wrote a B-GLM package based on the two Matlab toolboxes previously mentioned MATJAGS (Steyvers and Kalish, 2014), and MBE (Winter, 2016). JAGS modelling codes were based on examples from (Zuur et al., 2013). Binary response variables (like the probability of being hit *P(hit)*) were modelled using Bernoulli distributions and a logistic link function. Flight metrics, like initial mean speed or mean angular speed, were modelled using gamma distributions and a log link function. To allow the use of the "HDI+ROPE decision rule", we standardized continuous predictors and response variable, by subtracting their mean and dividing them by two standard deviations (instead of one for typical z-scores) (Gelman, 2008). All the other variables were binaries (e.g. was hit = yes/no), and they were only centred (i.e. to have zero mean). In this way, the estimated standardized slopes (i.e. effect sizes) are comparable across all models (Gelman, 2008; Schielzeth, 2010). B-GLMs were selected by applying a forward selection procedure, where compared models are increasingly complex. Additionally, models including interactions between predictors were also compared. The best models were selected using the AIC (Akaike Information Criterion) and BIC (Bayesian Information Criterion). When comparing models of same complexity, we chose the model with the lowest AIC and BIC. When comparing models of different complexity, we selected a more complex model only if it had at the maximum an AIC and a BIC values 10 points inferior to less complex models (Zuur et al., 2013). Finally, we checked that good mixing of chains and low autocorrelation coefficients could be observed.

When determining the minimal B-GLM to model how the probability of being hit *P(hit)* varied in function of the experimental conditions (Fig. 4.2), we used the following predictors: swatter off or on (0 or 1), species (*Anopheles* or *Aedes*), logarithm of light condition luminance (cd/m²), reference (dark for *Anopheles* or overcast for *Aedes*) or altered light (twilight and sunrise), mesh color (black or clear), time after start of first trial, humidity and temperature. In addition, to test for learning effect, we also used the interaction

between the two following predictors: swatter on/off and the time after start of first trial. Finally, in order to check for potential behavioural difference of the two species, and if the predictor species was already in the model, we compared models with interactions between *Anopheles* or *Aedes* with the other remaining predictors (e.g. *Anopheles.*∗time to test if *Anopheles* mosquitoes' behaviour was changing over time). The final set of predictors included in the minimal model were swatter off or on, species and the interaction *Anopheles*∗light condition (altered or reference). To improve clarity and because it didn't change the results, we added the interaction *Aedes*∗light condition to the model shown in Fig. 4.2.

To model how *P(hit)* varied in function of mosquito initial flight state, a minimum B-GLM was determined by using the mean or std of the initial speed or angular speed as predictors (Fig. 4.4*b,c,e,f*). Then we modelled how the predictors left in the minimal model (initial mean of the speed and angular speed) changed with the experimental conditions while the swatter was off and using the same predictors as the ones used for initially modelling *P(hit)*.

To compare mosquito flight behaviour during the manoeuvres, a Hidden Markov model (HMM) was used to classified mosquito behaviour over time (Matlab toolbox by Kevin Murphy (Murphy, 1998)). This HMM allowed us to determine in which of three states each mosquito was at each point in time, just by observing its escape velocity over time (see Fig. S4.8*a*). The probability of being in the states depending only on the previous state. The model was trained on all mosquito tracks recorded with the swatter triggered (i.e. without controls). The initial parameters of the model were found by fitting a mixture of three Gaussians to the distributions of all escape velocities of the tracks (fitgmdist, Matlab). Then a Baum–Welch algorithm, with fixed means and standard deviations, was used to find the unknown parameters of the HMM (see supplementary Fig. S4.8). We labelled the first two states as "cruising" states towards or away from the swatter, and the last one as the "escaping" state (with high escape velocities away from the swatter, supplementary Fig. S4.8*a-d*). The Viterbi algorithm was used to compute the most-likely corresponding sequence of states (see example on Fig. S4.8*a*). Almost all mosquitoes were found to initially be in one of the two cruising states. When the swatter started to move towards the centre of the flight arena, the proportion of mosquitoes in the cruising state away from the swatter grew. Then, around the time when the swatter was halfway towards its most forward position (t = 0), mosquitoes started to get into the fast escape state. The maximum proportion of mosquitoes to be in this state over time was 17.1% and this maximum was reached just before the swatter arrived at its most forward position (supplementary Fig. S4.8*f*). In the rest of the analysis, all the tracks that were predicted at least once to be in this fast escape state were labelled as fast escapes. In this way, each track was put in one of three groups, the collisions, the slow escapes and the fast escapes.

Additionally, the probability of being a fast escape *P(esc)* was modelized with a B-GLM (Fig. 4.6). The minimum model was determined using the same initial predictors as the ones used for modelling *P(hit)*. We observed high autocorrelation and bad mixing of chains with the predictor swatter on or off, most likely because the number of fast escapes was

really low during the controls. Thus it was decided to model *P(esc)* separately for the tracks recorded while the swatter was triggered (Fig. 4.6*e-j*).

In order to confirm and summarize this study findings, we modelized the mean distance to the predicted position when the swatter (virtual or not) reached its most forward position using a B-GLM (Fig. 4.7*d-i*). In order to get the minimal model, we used the same initial predictors as the ones previously described for the B-GLMs of *P(hit)* and *P(esc)*. The predictors included in the minimal model were the same as for the first B-GLM.

Finally, in order to quantify the role of escape manoeuvres (active or passive) in the overall observed unpredictability of mosquito flight path, we defined *d(off/on)* as being the ratio of the distance to predicted position when the swatter was turned off over when it was on. We expect *d(off/on)* to be equal to 1 if mosquitoes (e.g. the distance to predicted position doesn't change if the swatter if off or on). We estimated means of *d(off/on)* for each combination of light condition and species using Bayesian estimation (Fig. 4.7*j-k*) (Kruschke, 2013). To model *d(off/on)* we used a log-normal distribution and estimated the means each combination from a sample of 10000 randomly chosen values of *d(off/on)* out of all the computed *d(off/on)* values. Then we compared the estimated mean distribution by computing standardized effect sizes.

4

References

Baglan, H., Lazzari, C. and Guerrieri, F. (2017). Learning in mosquito larvae (Aedes aegypti): Habituation to a visual danger signal. *J. Insect Physiol.* **98**, 160–166.

Batista, E. P. A., Mapua, S. A., Ngowo, H., Matowo, N. S., Melo, E. F., Paixão, K. S., Eiras, A. E. and Okumu, F. O. (2019). Videographic analysis of flight behaviours of host-seeking Anopheles arabiensis towards BG-Malaria trap. *PLoS One* **14**, e0220563.

Brenner, E. and Smeets, J. B. Continuously updating one's predictions underlies successful interception.

Card, G. M. (2012). Escape behaviors in insects. *Curr. Opin. Neurobiol.* **22**, 180–186.

Cardé, R. T. (2015). Multi-cue integration: How female mosquitoes locate a human host. *Curr. Biol.* **25**, R793–R795.

Cator, L. J., Arthur, B. J., Harrington, L. C. and Hoy, R. R. (2009). Harmonic convergence in the love songs of the dengue vector mosquito. *Science (80-.).* **323**, 1077–1079.

Chapman, T. and Webb, B. (1999). A neuromorphic hair sensor model of wind-mediated escape in the cricket. *Int. J. Neural Syst.* **9**, 397–403.

Cheng, B., Tobalske, B. W., Powers, D. R., Hedrick, T. L., Wethington, S. M., Chiu, G. T. C. and Deng, X. (2016). Flight mechanics and control of escape manoeuvres in hummingbirds. I. Flight kinematics. *J. Exp. Biol.* **219**, 3518–3531.

Combes, S. A., Rundle, D. E., Iwasaki, J. M. and Crall, J. D. (2012). Linking biomechanics and ecology through predator-prey interactions: Flight performance of dragonflies and their prey. *J. Exp. Biol.* **215**, 903–913.

Cooperband, M. F. and Cardé, R. T. (2006). Comparison of plume structures of carbon dioxide emitted from different mosquito traps. *Med. Vet. Entomol.* **20**, 1–10.

Corcoran, A. J. and Conner, W. E. (2016). How moths escape bats: predicting outcomes of predator-prey interactions. *J. Exp. Biol.* **219**, 2704–2715.

Cribellier, A., van Erp, J. A., Hiscox, A., Lankheet, M. J., van Leeuwen, J. L., Spitzen, J. and Muijres, F. T. (2018). Flight behaviour of malaria mosquitoes around odour-baited traps: Capture and escape dynamics. *R. Soc. Open Sci.* **5**.

Darbro, J. M. and Harrington, L. C. (2007). Avian defensive behavior and blood-feeding success of the West Nile vector mosquito, Culex pipiens. *Behav. Ecol.* **18**, 750–757.

Dekker, T. and Cardé, R. T. (2011). Moment-to-moment flight manoeuvres of the female yellow fever mosquito (Aedes aegypti L.) in response to plumes of carbon dioxide and human skin odour. *J. Exp. Biol.* **214**, 3480–3494.

Dekker, T., Geier, M. and Cardé, R. T. (2005). Carbon dioxide instantly sensitizes female yellow fever mosquitoes to human skin odours. *J. Exp. Biol.* **208**, 2963–2972.

Dienes, Z. (2011). Bayesian versus orthodox statistics: Which side are you on? *Perspect. Psychol. Sci.* **6**, 274–290.

Dou, Z., Madan, A., Carlson, J. S., Chung, J., Spoleti, T., Dimopoulos, G., Cammarato, A. and Mittal, R. (2021). Acoustotactic response of mosquitoes in untethered flight to incidental sound. *Sci. Rep.* **11**, 1884.

Dupuy, F., Steinmann, T., Pierre, D., Christidés, J. P., Cummins, G., Lazzari, C., Miller, J. and Casas, J. (2012). Responses of cricket cercal interneurons to realistic naturalistic stimuli in the field. *J. Exp. Biol.* **215**, 2382–2389.

Edman, J. D., Day, J. F. and Walker, E. D. (1984). Field confirmation of laboratory observations on the differential antimosquito behavior of herons. *Condor* **86**, 91.

Edman, J. D. and Scott, T. W. (1987). Host defensive behaviour and the feeding success of mosquitoes. *Int. J. Trop. Insect Sci.* **8**, 617–622.

Fournier, J. P., Dawson, J. W., Mikhail, A. and Yack, J. E. (2013). If a bird flies in the forest, does an insect hear it? *Biol. Lett.* **9**, 20130319.

Fuller, S. B., Straw, A. D., Peek, M. Y., Murray, R. M. and Dickinson, M. H. (2014). Flying Drosophila stabilize their vision-based velocity controller by sensing wind with their antennae. *Proc. Natl. Acad. Sci. U. S. A.* **111**, E1182–e1191.

Gelman, A. (2008). Scaling regression inputs by dividing by two standard deviations. *Stat. Med.* **27**, 2865–2873.

Ghose, K., Horiuchi, T. K., Krishnaprasad, P. S. and Moss, C. F. (2006). Echolocating bats use a nearly time-optimal strategy to intercept prey. *PLoS Biol.* **4**, 865–873.

Gibson, G. (1995). A behavioural test of the sensitivity of a nocturnal mosquito, Anopheles gambiae, to dim white, red and infra-red light. *Physiol. Entomol.* **20**, 224–228.

Hawkes, F. and Gibson, G. (2016). Seeing is believing: the nocturnal malarial mosquito Anopheles coluzzii responds to visual host-cues when odour indicates a host is nearby. *Parasites and Vectors* **9**, 320.

Humphries, D. A. and Driver, P. M. (1970). Protean defence by prey animals. *Oecologia* **5**, 285–302.

Kruschke, J. K. (2010). Bayesian data analysis. *Wiley Interdiscip. Rev. Cogn. Sci.* **1**, 658–676.

Kruschke, J. K. (2013). Bayesian estimation supersedes the t test. *J. Exp. Psychol. Gen.* **142**, 573–603.

Kruschke, J. K. and Liddell, T. M. (2018). The Bayesian New Statistics: Hypothesis testing, estimation, meta-analysis, and power analysis from a Bayesian perspective. *Psychon. Bull. Rev.* **25**, 178–206.

Land, M. F., Gibson, G., Horwood, J. and Zeil, J. (1999). Fundamental differences in the optical structure of the eyes of nocturnal and diurnal mosquitoes. *J. Comp. Physiol. - A Sensory, Neural, Behav. Physiol.* **185**, 91–103.

Lin, H. T. and Leonardo, A. (2017). Heuristic rules underlying dragonfly prey selection and interception. *Curr. Biol.* **27**, 1124–1137.

4

Matherne, M. E., Cockerill, K., Zhou, Y., Bellamkonda, M. and Hu, D. L. (2018). Mammals repel mosquitoes with their tails. *J. Exp. Biol.* **221**, jeb178905.

McMeniman, C. J., Corfas, R. A., Matthews, B. J., Ritchie, S. A. and Vosshall, L. B. (2014). Multimodal integration of carbon dioxide and other sensory cues drives mosquito attraction to humans. *Cell* **156**, 1060–1071.

Medlock, J. M. and Snow, K. (2008). Natural predators and parasites of British mosquitoes–a review. *Eur. Mosq. Bull.* **25**, 1–11.

Menda, G., Nitzany, E. I., Shamble, P. S., Wells, A., Harrington, L. C., Miles, R. N. and Hoy, R. R. (2019). The long and short of hearing in the mosquito Aedes aegypti. *Curr. Biol.* **29**, 709–714.e4.

Mischiati, M., Lin, H. T., Herold, P., Imler, E., Olberg, R. and Leonardo, A. (2015). Internal models direct dragonfly interception steering. *Nature* **517**, 333–338.

Mizutani, A., Chahl, J. S. and Srinivasan, M. V. (2003). Motion camouflage in dragonflies. *Nature* **423**, 604.

Moore, T. Y., Cooper, K. L., Biewener, A. A. and Vasudevan, R. (2017). Unpredictability of escape trajectory explains predator evasion ability and microhabitat preference of desert rodents. *Nat. Commun.* **8**, 1–9.

Mrotek, L. A. and Soechting, J. F. (2007). Target interception: Hand-eye coordination and strategies. *J. Neurosci.* **27**, 7297–7309.

Muijres, F. T., Elzinga, M. J., Melis, J. M., Dickinson, M. H., Florian T. Muijres, 1 Michael J. Elzinga, 1 Johan M. Melis, 1, . M. H. D. and Avoiding (2014). Flies evade looming targets by executing rapid visually directed banked turns. *Science (80-.).* **344**, 172–7.

Murphy, K. Hidden Markov Model (HMM) Toolbox for Matlab.

Nakata, T., Henningsson, P., Lin, H. T. and Bomphrey, R. J. (2020). Recent progress on the flight of dragonflies and damselflies. *Int. J. Odonatol.* **23**, 41–49.

Olberg, R. M., Seaman, R. C., Coats, M. I. and Henry, A. F. (2007). Eye movements and target fixation during dragonfly prey-interception flights. *J. Comp. Physiol. A Neuroethol. Sensory, Neural, Behav. Physiol.* **193**, 685–693.

OpenCV. OpenCV documentation: Camera calibration and 3D reconstruction.

Pal, S. (2015). Dynamics of aerial target pursuit. *Eur. Phys. J. Spec. Top.* **224**, 3295–3309.

Plummer, M. (2003). JAGS: A program for analysis of Bayesian graphical models using Gibbs sampling. In *Proc. 3rd Int. Conf. Distrib. Stat. Comput.*, pp. 1–10.

Reid, J. N., Hoffmeister, T. S., Hoi, A. G. and Roitberg, B. D. (2014). Bite or flight: The response of mosquitoes to disturbance while feeding on a defensive host. *Entomol. Exp. Appl.* **153**, 240–245.

Richardson, G., Dickinson, P., Burman, O. H. P., Pike, T. W., Richardson, G., Dickinson, P. and Burman, O. H. P. (2018). Unpredictable movement as an anti-predator

strategy. *Proc. R. Soc. B Biol. Sci.* **285**.

Roitberg, B. D., Mondor, E. B. and Tyerman, J. G. (2003). Pouncing spider, flying mosquito: Blood acquisition increases predation risk in mosquitoes. *Behav. Ecol.* **14**, 736–740.

Santer, R. D., Rind, F. C. and Simmons, P. J. (2012). Predator versus prey: locust looming-detector neuron and behavioural responses to stimuli representing attacking bird predators. *PLoS One* **7**, e50146.

Schielzeth, H. (2010). Simple means to improve the interpretability of regression coefficients. *Methods Ecol. Evol.* **1**, 103–113.

Soechting, J. F. and Flanders, M. (2008). Extrapolation of visual motion for manual interception. *J. Neurophysiol.* **99**, 2956–2967.

Spitzen, J., Spoor, C. W., Grieco, F., ter Braak, C., Beeuwkes, J., Van Brugge, S. P., Kranenbarg, S., Noldus, L. P. J. J., van Leeuwen, J. L. and Takken, W. (2013). A 3D analysis of flight behavior of Anopheles gambiae sensu stricto malaria mosquitoes in response to human odor and heat. *PLoS One* **8**, 1–12.

Steyvers, M. and Kalish, M. MATJAGS, a Matlab interface for JAGS.

Stowers, J. R., Hofbauer, M., Bastien, R., Griessner, J., Higgins, P., Farooqui, S., Fischer, R. M., Nowikovsky, K., Haubensak, W., Couzin, I. D. et al. (2017). Virtual reality for freely moving animals. *Nat. Methods* **14**, 995–1002.

Straw, A. D., Branson, K., Neumann, T. R. and Dickinson, M. H. (2011). Multi-camera real-time three-dimensional tracking of multiple flying animals. *J. R. Soc. Interface* **8**, 395–409.

Thorsteinson, A. J., Bracken, G. K. and Hanec, W. (1965). The orientation of horse flies and deer flies (Tabanidae, Diptera): III. the use of traps in the study of orientation of Tabanids in the field. *Entomolia Exp. Appl.* **8**, 189–192.

Townes, H. (1962). Design For A Malaise Trap. *Proc. Entomol. Soc. Washingt.* **64**, 253 – 262.

Triblehorn, J. D. and Yager, D. D. (2006). Wind generated by an attacking bat: Anemometric measurements and detection by the praying mantis cercal system. *J. Exp. Biol.* **209**, 1430–1440.

van Breugel, F., Riffell, J., Fairhall, A. and Dickinson, M. H. (2015). Mosquitoes use vision to associate odor plumes with thermal targets. *Curr. Biol.* **25**, 2123–2129.

Vinauger, C., Lahondère, C., Wolff, G. H., Locke, L. T., Liaw, J. E., Parrish, J. Z., Akbari, O. S., Dickinson, M. H. and Riffell, J. A. (2018). Modulation of host learning in Aedes aegypti mosquitoes. *Curr. Biol.* **28**, 333–344.e8.

Walker, E. D. and Edman, J. D. (1985). The influence of host defensive behavior on mosquito (diptera: culicidae) biting persistence. *J. Med. Entomol.* **22**, 370–372.

Wiederman, S. D., Fabian, J. M., Dunbier, J. R. and O'Carroll, D. C. (2017). A pre-

dictive focus of gain modulation encodes target trajectories in insect vision. *Elife* **6**.

Winter, N. GitHub - NilsWinter/matlab-bayesian-estimation: Matlab Toolbox for Bayesian Estimation.

Yuval, B. and Bouskila, A. (1993). Temporal dynamics of mating and predation in mosquito swarms. *Oecologia* **95**, 65–69.

Zhao, H. and Warren, W. H. (2015). On-line and model-based approaches to the visual control of action. *Vision Res.* **110**, 190–202.

Zuur, A. F., Hilbe, J. M. and Ieno, E. N. (2013). *A Beginner's Guide to GLM and GLMM with R*. 253 pp.

4

Supplementary materials _____

Diurnal and nocturnal mosquitoes escape looming threats using distinct flight strategies under various light conditions

Antoine Cribellier[1], Andrew D. Straw[2], Jeroen Spitzen[3], Remco P.M. Pieters[1], Johan L. van Leeuwen[1], Florian T. Muijres[1]

[1] Experimental Zoology Group, Wageningen University & Research, Wageningen, The Netherlands

[2] Institute of Biology I and Bernstein Center Freiburg, University of Freiburg, Freiburg, Germany

[3] Laboratory of Entomology, Wageningen University & Research, Wageningen, The Netherlands

_____

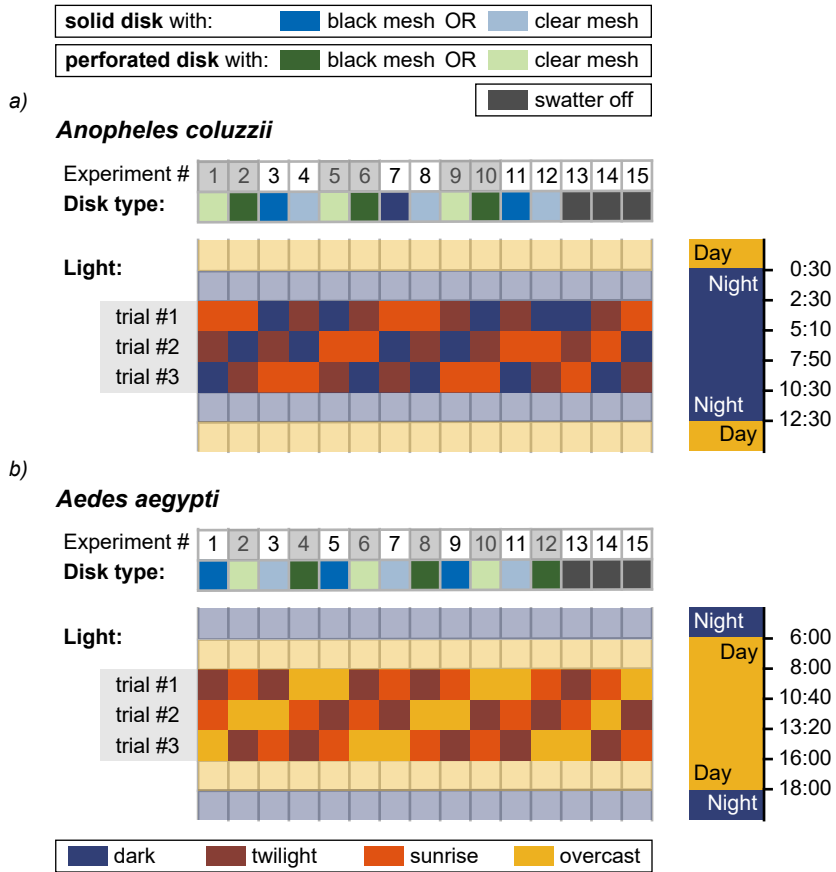**Consisting of:**

- Supplementary figures S4.1–S4.13

Figure S4.1: Experimental conditions. (*a-b*) Experimental planning for *Anopheles* and *Aedes* mosquitoes. The experimental days that haven't been used in this study have been coloured in grey.

Bayesian estimation (null-hypothesis testing) the "HDI+ROPE decision rule"

> the null-hypothesis is rejected if the 89% Highest Density Interval (HDI: ▬) of the standardized parameter is outside the Region of Practical Equivalence (ROPE: ▨)
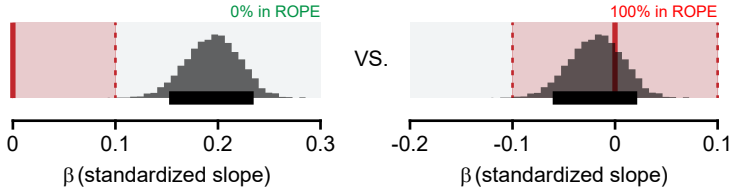
> the null-hypothesis is accepted if the HDI is fully inside the ROPE
> otherwise (e.g. 32% of the HDI is inside the ROPE), no conclusion is made

Figure S4.2: Null hypothesis testing with Bayesian estimation. Examples of two distributions of the estimated mean of a standardized parameter β in black. The null hypothesis is rejected (left) if the Highest Density Interval (HDI) is outside the Region Of Practical Equivalence (ROPE). The null-hypothesis is accepted (right) if the full HDI is inside the ROPE.
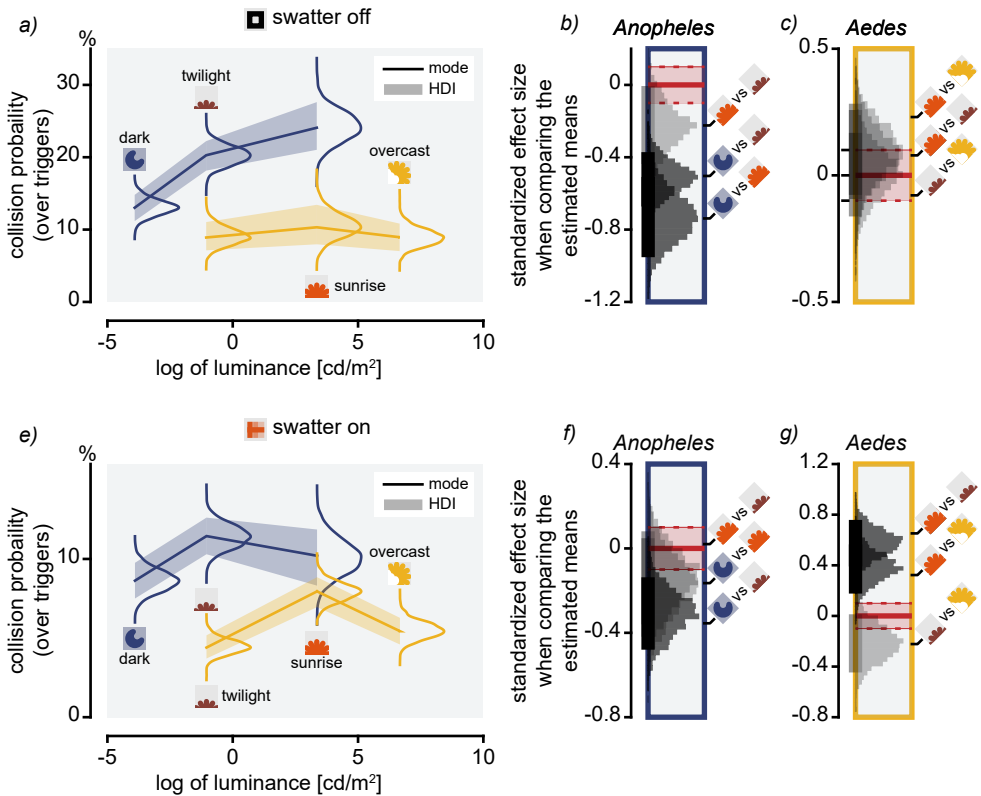
Figure S4.3: Collisions probabilities the various experimental conditions. (*a,d*) Bayesian estimation of the means of mosquitoes collision probability for each combination between species and light conditions. (*b,c,e,f*) Standardized effect size of the comparisons of the estimated means of panels (*a,b*).
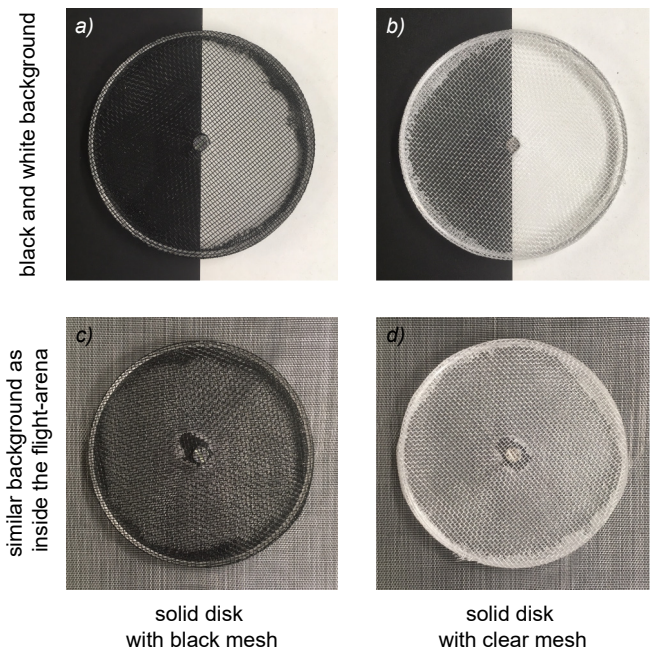
Figure S4.4: Disk with black and clear meshes. Pictures of the disk with black or clear meshes in front of a black and white background (*a-b*) or a background very similar to the one inside the flight arena (*c-d*).
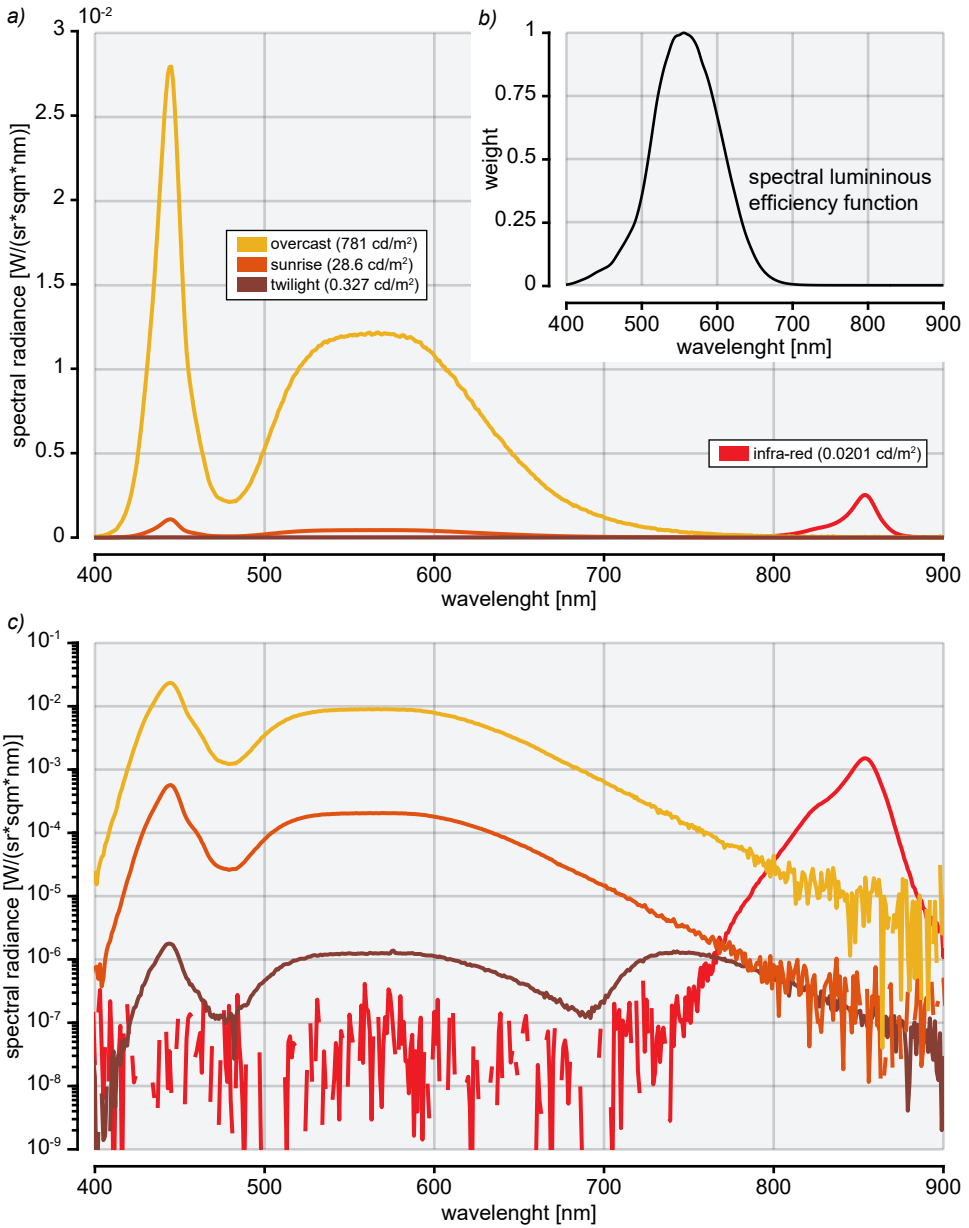
Figure S4.5: Spectrum of various light conditions. (*a*) Spectral radiance of the twilight, sunrise and overcast conditions and of the infrared light measured in the middle of flight arena with a spectrometer (specbos 1211, JETI) and using a diffuse reflector (USRS-99-010-EPV, Labsphere). (*b*) Spectral luminous function of humans (Sharpe et al., 2005) used to compute the luminance of each light condition. (*c*) Spectral radiance of the light conditions in log scale. The low radiance parts of the spectrums appear noisy due to limitation in the range of the radiance that can be measured at the same time.
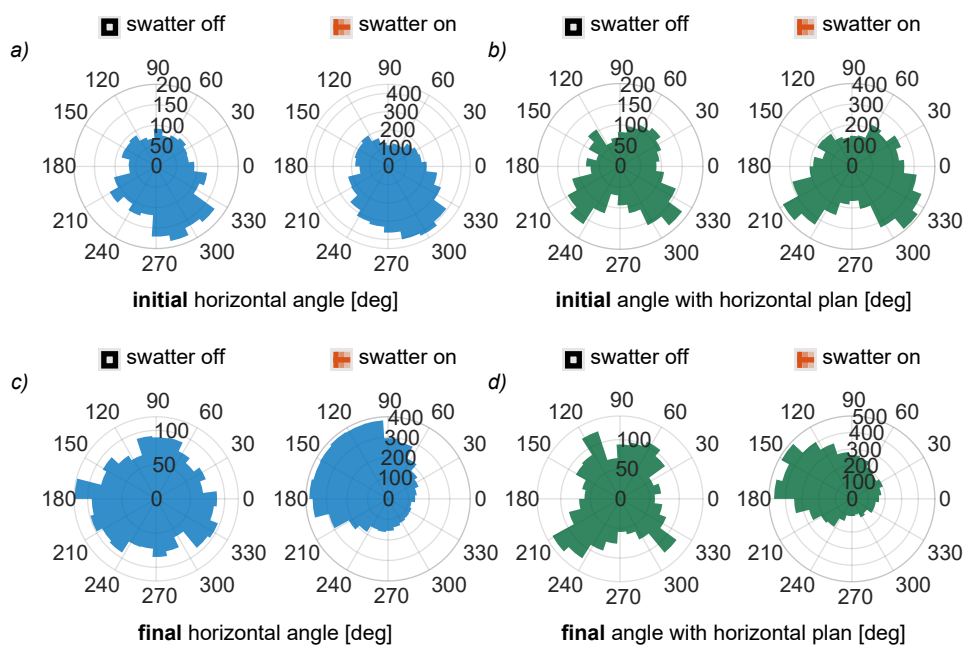
Figure S4.6: Initial and final flight angles. (*a,c*) Rose plots of mosquito flight angle in the horizontal plan at trigger time ((*a*) - initial) and when the swatter reach its most forward position ((*c*) - final). (*b,d*) Rose plots of the initial and final mosquito flight angle with horizontal plan. The swatter is coming from the right (0° angle). Radial scale showing the number of tracks in each bar.
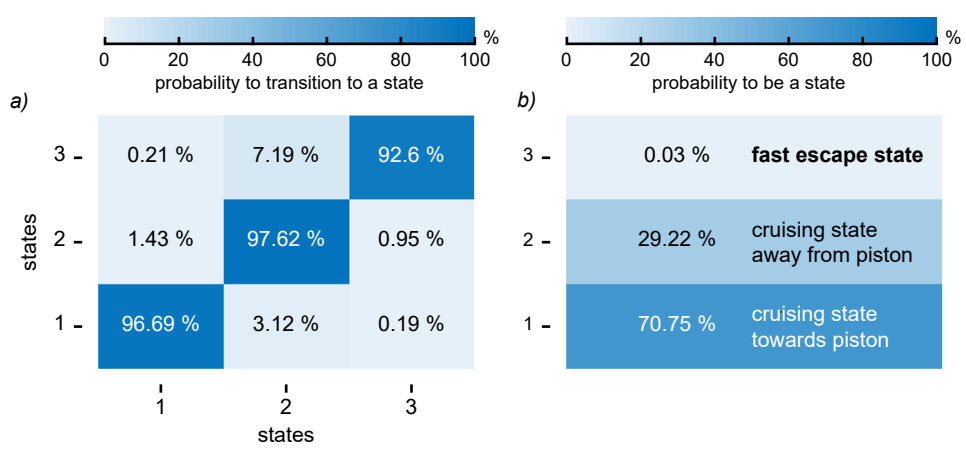
Figure S4.7: Hidden Markov Model parameters. (*a*) Transition matrix. Each number is the probability of transition from the current state (on the abscise) to a new state (on the ordinate). (*b*) Prior probability to be on each one of the three states.
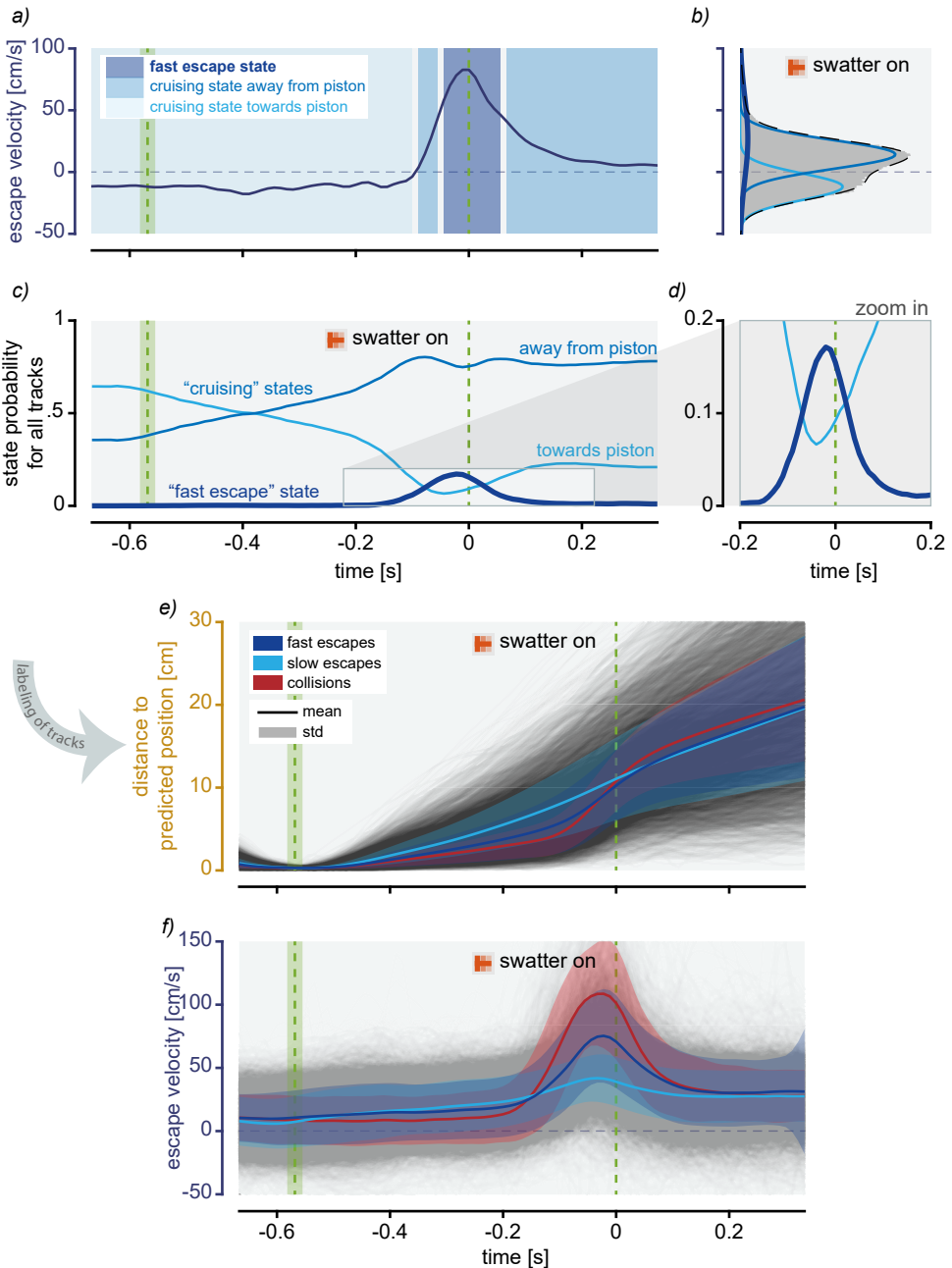
Figure S4.8: Modelling of mosquitoes escape velocities. A Hidden Markov Model (HMM) is used to model how a mosquito flight state changes over time based on its escape velocity. (*a*) An example of variation of a mosquito escape velocity is modelled by a change of its state from initially cruising towards the swatter, then away from the swatter, then escaping fast, and then cruising again away from the swatter. (*b*) Distribution of all escape velocities of the mosquitoes with the Gaussian distribution of the three states used in the HMM. (*c*) Total probability of being in one of the three states over time. (*d*) Zoom-in on the fast escape state probability curve. (*e,f*) If a track was at some point in the fast escape state, it is labelled as the fast escape, otherwise it is labelled as a slow escape. Thus, mosquito distances to the predicted positions and the escape velocity are plotted over time.
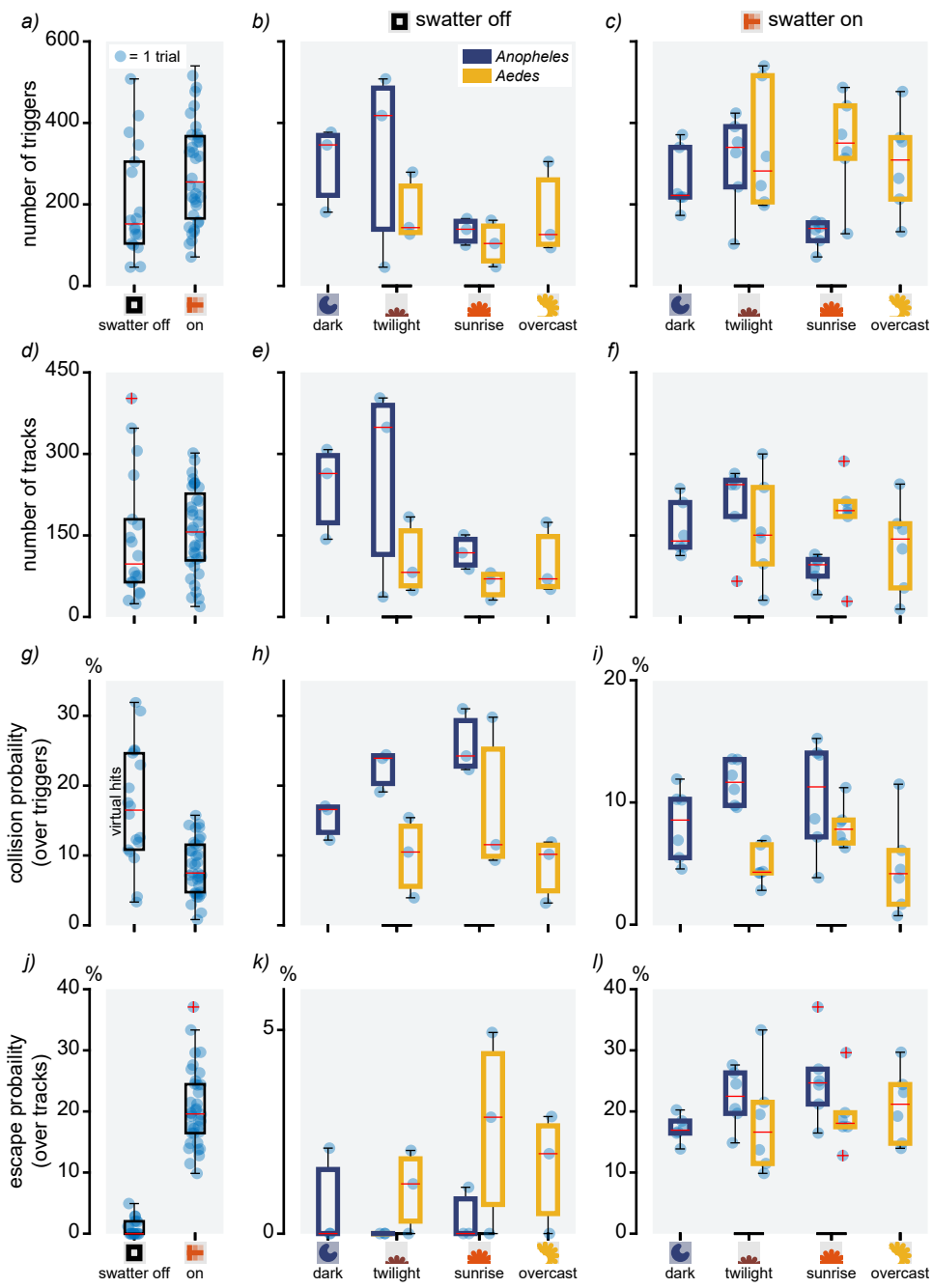
Figure S4.9: Box plots of various parameters. (*a-c*) Number of triggers recorded in the various experimental conditions. (*d-f*) Number of tracks left after filtering. Probability of collision (*g-i*) and of fast escape (*j-l*) for the various experimental conditions.
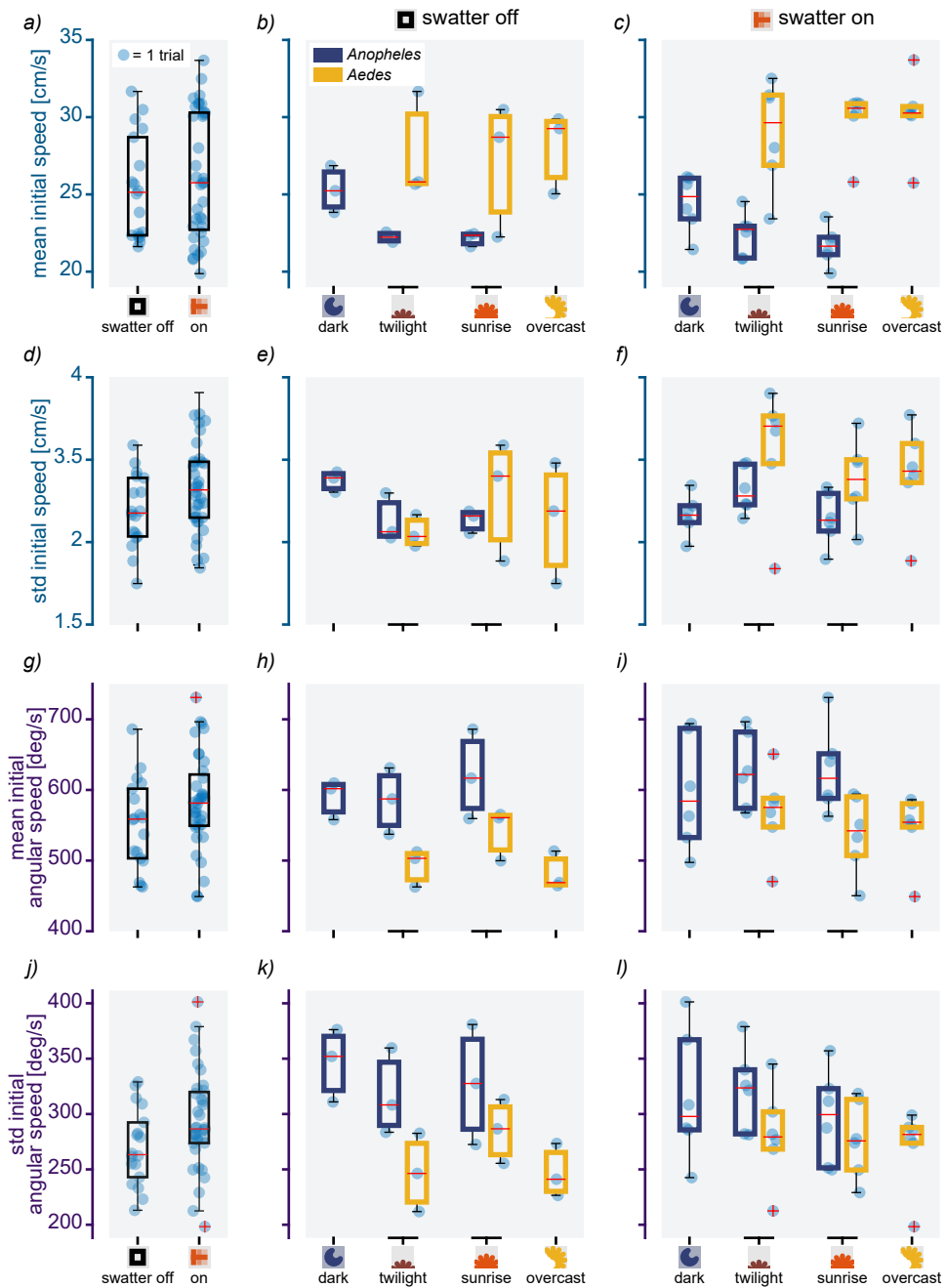
Figure S4.10: Box plots of initial flight metrics. Initial mean and standard deviation of mosquito flight speed (*a-f*) and angular speed (*g-i*) during various experimental conditions.

Bayesian GLM (Bernoulli distribution) $logit(P(hit)) \approx \beta_0 + \beta_1 * mean\_initial\_speed + \beta_2 * mean\_initial\_angular\_speed$
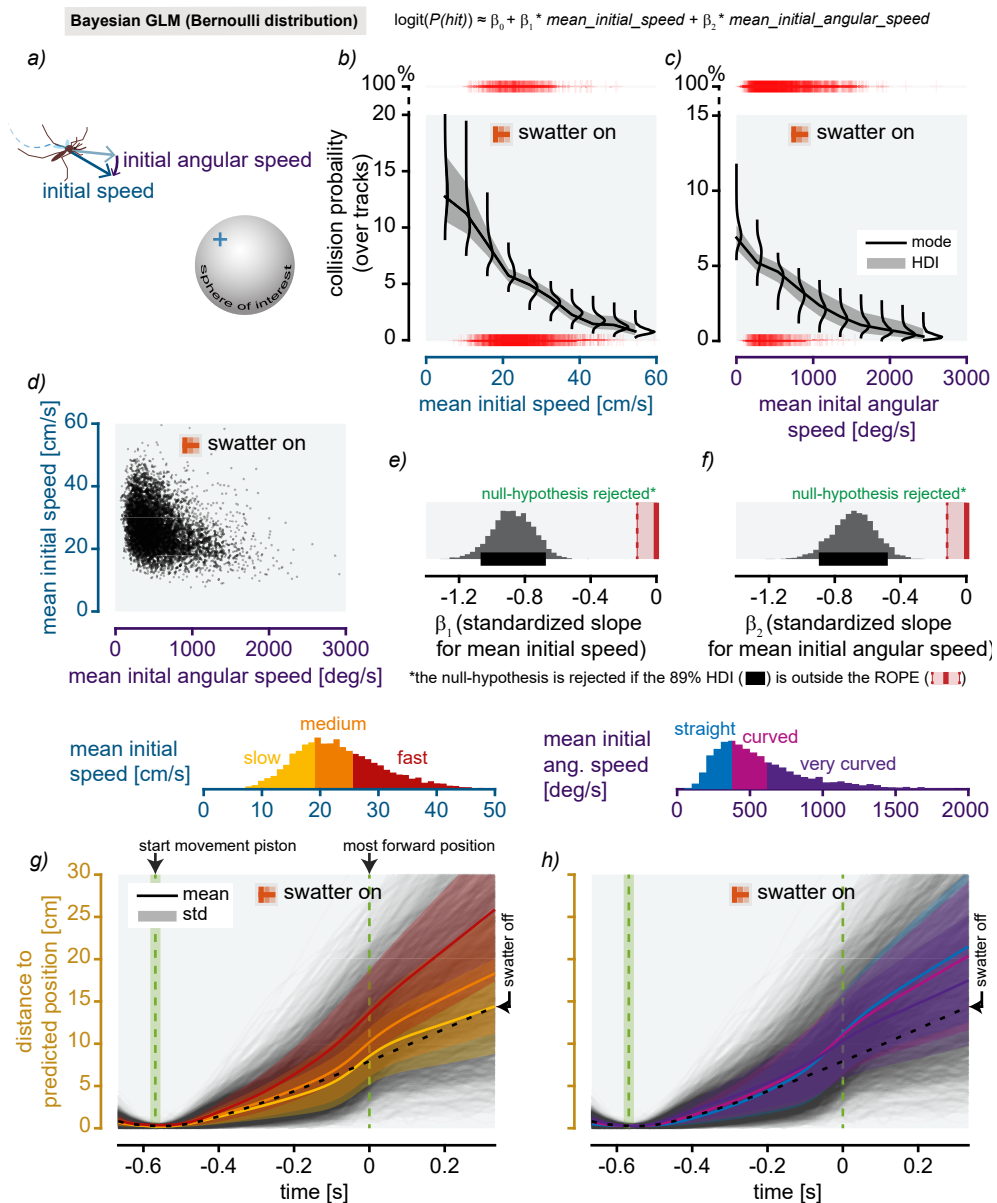
Figure S4.11: How initial flight speed influence the probability of being hit? (*a*) Schematic showing how mosquito initial flight speed and angular speed are defined. (*b-c*) Results from the B-GLMs used to model how the probability of collisions of tracks is correlated with initial flight metric if the swatter was turned on. (*e-f*) Distributions of the means of the standardized slopes $\beta1$ and $\beta2$. Here, all slopes are found to be significantly different from zero. (*d*) mean initial speed versus mean initial angular speed for all tracks with the swatter turned on. (*g-h*) Distribution of the initial mean speed and angular speed were respectively into 3 or 2 groups of the same size (one third or one half of the complete dataset). These groups were then given labels (e.g. slow, medium and fast) and the mean and std of each group were plotted over time.
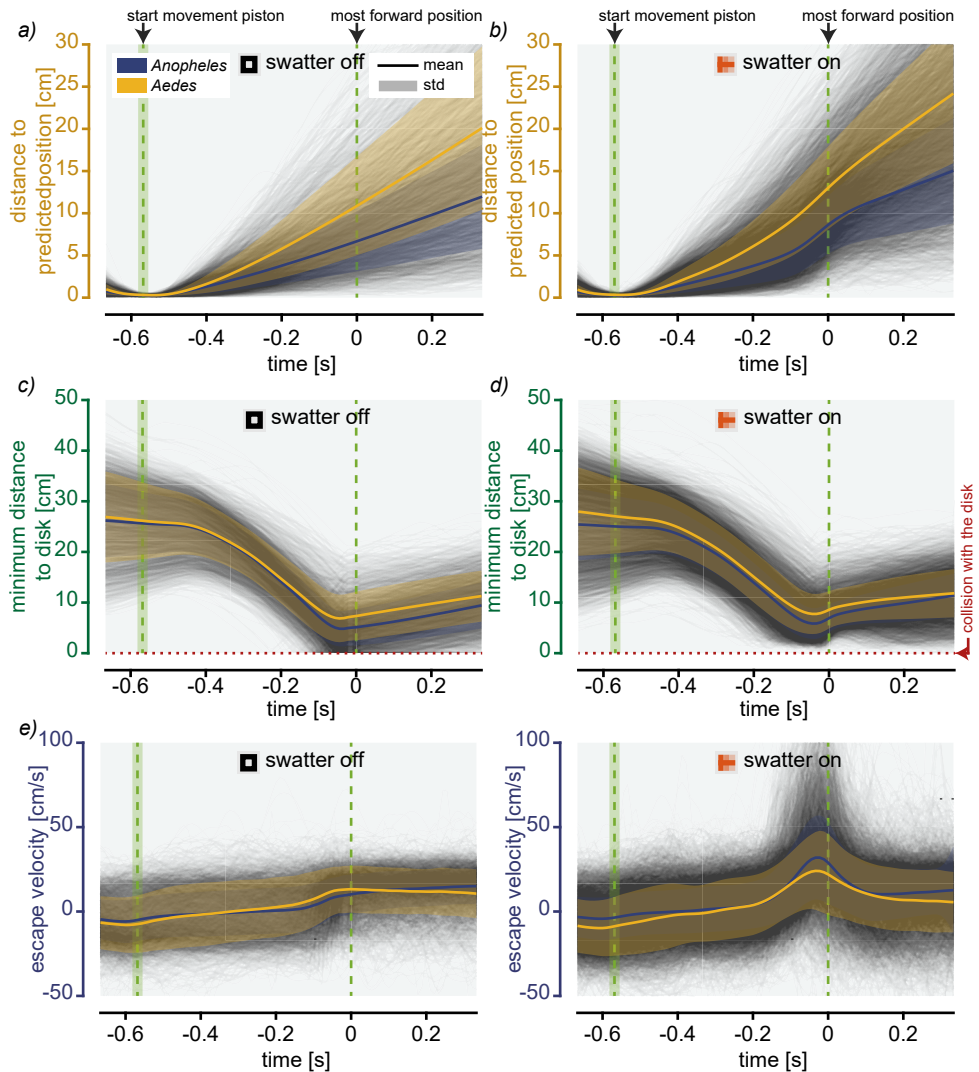
Figure S4.12: Flight metrics over time: *Anopheles* vs. *Aedes*. (*a-b*) Mosquito distance to predicted position over time if the swatter was turned off or on. (*c-d*) Minimum distance to disk over time. (*e-f*) Mosquito escape velocity over time.
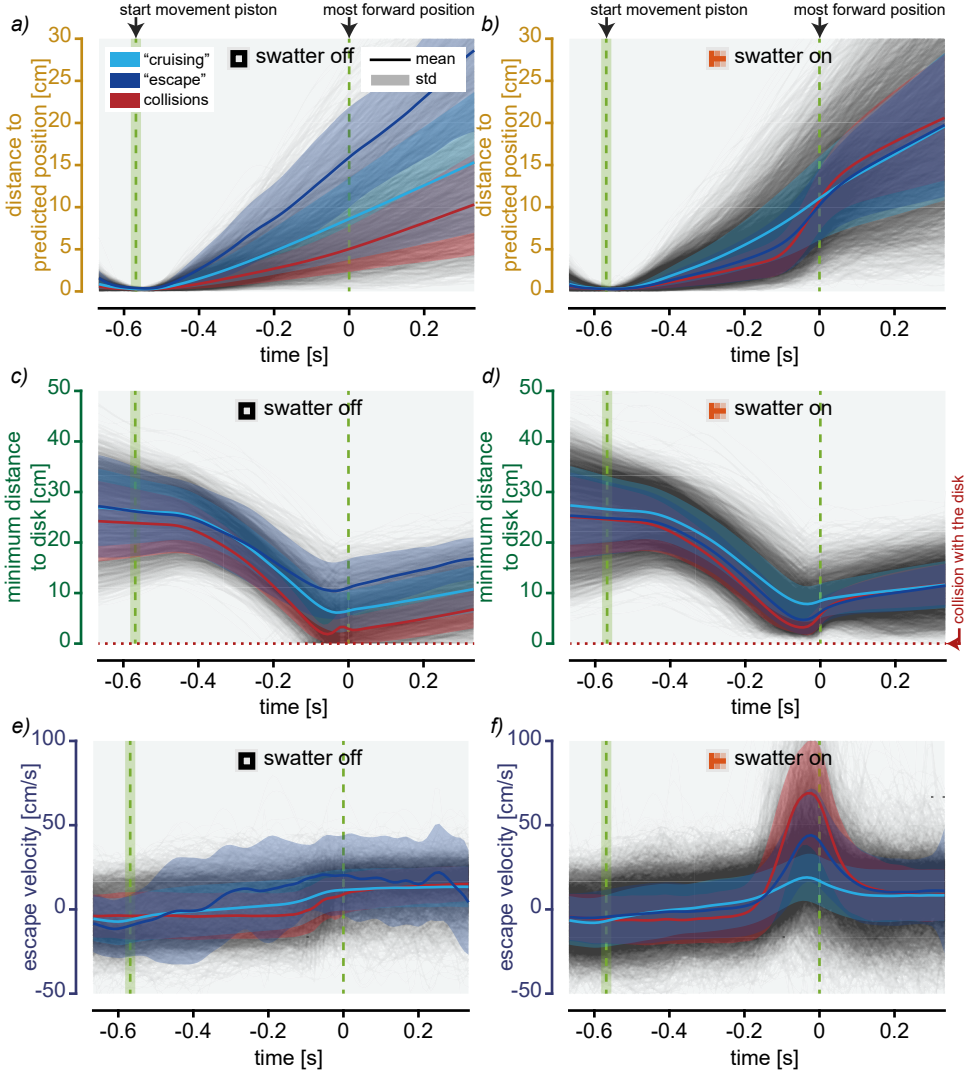
Figure S4.13: Flight metrics over time: Collisions vs. Cruising vs. Escapes. (*a-b*) Mosquito distance to predicted position over time if the swatter was turned off or on. (*c-d*) Minimum distance to disk over time. (*e-f*) Mosquito escape velocity over time.

References

Sharpe, L. T., Stockman, A., Jagla, W. and Jaägle, H. (2005). A luminous efficiency function, V*(λ), for daylight adaptation. *J. Vis.* **5**, 948–968.
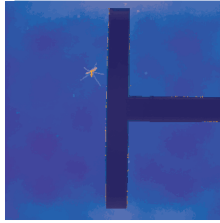
Chapter 5

Mosquitoes escape from being swatted by actively surfing the swatter-induced bow wave

Antoine Cribellier[1], Leonardo Honfi Camilo[1], Pulkit Goyal[1], Florian T. Muijres[1]

[1] Experimental Zoology Group, Wageningen University & Research, Wageningen, The Netherlands

Abstract

When attacked, flying nocturnal insects cannot rely on vision to detect a threat. To evade from predators, insects such as moths, praying mantis or cockroaches rely on other senses such as hearing or airflow-sensing. Some flying insects, such as mosquitoes, also must escape from the defensive behaviour of their blood hosts. Nocturnal malaria mosquitoes are capable of escaping from swatting in the dark, but how they achieve this is still unknown. Here, we show that flying mosquitoes escape from being swatted by using the airflow induced by the attack both passively and actively. By tracking free-flying mosquitoes in real time, we were able to simulate attacks using an automatic mechanical swatter. In both dark and low-light conditions, we showed that the faster the air movements induced by the attack, the less malaria mosquitoes were hit by the swatter. Then, using airflow simulations and measurements of wingbeat kinematics, we estimated the aerodynamic forces involved during the escape manoeuvres. We found that, although seemingly going with the airflow, mosquitoes actively surfed the bow wave induced by the swatter. We estimated that the mosquitoes' active contribution explained about two-thirds of their escape acceleration when the swatter was almost invisible. This indicates that the passive effect of the airflow still significantly contributed to the escaping success of mosquitoes. We anticipate that similar escape strategies must be common in small lightweight insects.

5.1 Introduction

If you have ever been woken up by the buzz of a mosquito, you can probably testify that a flying mosquito is difficult to swat. If a mosquito is found flying near yourself, it's most likely because hematophagous female mosquitoes must interact with their hosts to get the blood meals necessary for egg development (Clements, 1999). This interaction is the reason why anthropophilic mosquitoes can be vectors of many deadly diseases such as malaria, making them the most dangerous animal in the world (Who, 2020). In order to protect themselves, humans developed many vector control tools such as bed nets or traps (Benelli et al., 2016; Hiscox et al., 2014). But before that, and as a natural response to biting nuisance, blood hosts of mosquitoes had already adopted defensive behaviours – such as hand swatting or tail swishing (Darbro and Harrington, 2007; Edman et al., 1984; Edman and Scott, 1987; Matherne et al., 2018; Reid et al., 2014; Walker and Edman, 1985) – to discourage or kill host seeking mosquitoes. Despite the large amount of work done on host seeking behaviours (van Breugel et al., 2015; Cardé, 2015; Dekker et al., 2005; McMeniman et al., 2014), how mosquitoes respond to these defensive strategies has been the subject of only one study (chapter 4).

Recently, we have shown that, when swatted, nocturnal and diurnal mosquitoes exhibited good escape performances (chapter 4). They do so by relying on a combination of so-called protean insurance behaviours (mosquitoes exhibiting unpredictable flight paths) and escape manoeuvres (chapter 4). Also, the relative proportion of these two strategies explaining the escape performance was found to be dependent on light intensity and spe-

cies, most likely in order to adapt to available sensory information. In particular, nocturnal malaria mosquitoes have been found to fly faster in the dark in order to decrease their predictability. Additionally, we found that, with increasing light intensity, mosquitoes exhibited fast escape manoeuvres more often. This suggests that they use visual cues to detect the threat and trigger their escapes. However, the flight dynamics of these escape manoeuvres of mosquitoes have not been studied in detail. And it remains unexplained why mosquitoes often successfully escaped when there was only little or no visual information available.

Escape manoeuvres of mosquitoes have been little studied, but more is known about the escape of flying animals such as hummingbirds, moths or fruit flies. While escaping, these flying animals are usually directing their manoeuvre away from the danger (Cheng et al., 2016; Muijres et al., 2014), or towards safety zones at the flank of the attacker (Corcoran and Conner, 2016). These animals achieve flight by flapping their wings back and forth in order to generate upward lift while relying on unsteady aerodynamic effects (Sane, 2003). Fruit flies, dipterans such as mosquitoes, have been shown to follow the so-called 'helicopter model' when manoeuvring to escape (Muijres et al., 2014). According to this model, while manoeuvring an animal will rotate its whole body in order to redirect the generated aerodynamic force vector in the direction of the intended motion (Dickinson and Muijres, 2016; Ros et al., 2011). Thus, when evading looming targets, fruit flies execute banked turns by pitching their nose-up and rolling on the side opposite to the threat location (Muijres et al., 2014). They do so by modulating kinematic parameters such as wingbeat frequency and amplitude. Among those parameters, wingbeat amplitude is probably the most important as it is key in modulating total flight force, and in regulating body roll. Mosquitoes have wingbeat frequencies and amplitudes (between 350 and 750 Hz and around 40° (Bomphrey et al., 2017; Kim et al., 2021)) that are respectively much higher and much lower than that of fruit flies (~220 Hz and ~140° (Muijres et al., 2017)). Therefore, one could expect mosquitoes to rely on different wing kinematic parameters to control their manoeuvres. Nevertheless, measurements of mosquito kinematics while taking off suggest that they use very similar ways of controlling lift production as fruit flies, notably by modulating their wingbeat amplitude (Muijres et al., 2017).

All previously mentioned escape manoeuvres are fully active manoeuvres, where the animal detects the threat and then triggers the escape. Most of the time, the incoming threat is detected using vision and therefore these manoeuvres have usually been studied by simulating visual looming threats (Muijres et al., 2014; Santer et al., 2012). However, in the dark, insects need to rely on alternative senses such as hearing or mechanoreception. Hearing has been the subject of many studies because of its important role for detecting the attacks of bats. Crickets, praying mantis, and moths were all shown to be capable of hearing the ultrasounds generated by an attacking bat (Ter Hofstede and Ratcliffe, 2016; Hoy et al., 1989; Tauber and Camhi, 1995; Triblehorn et al., 2008). Concerning mosquitoes, hearing was long thought to only be used for mating (Cator et al., 2009), but it has been recently suggested to have the potential to also inform mosquitoes about a host or predator

before being attacked (Fournier et al., 2013; Menda et al., 2019).

Another sensory cue that has the potential to inform insects of an incoming threat is the air gust produced by the attack. Ground dwelling crickets and cockroaches as well as flying praying mantis and tethered cockroaches were all found to be able to detect an attack in such a way (Dangles et al., 2006; Ganihar et al., 1994; Ritzmann, 1984; Triblehorn et al., 2008; Triblehorn and Yager, 2006). However, no example is known amongst small insects such as dipterans. Nevertheless, it is probable that these small insects rely on the air movement generated during an attack to successfully escape from it. This is supported by the wide usage of fly swatters, whose perforated design is based on the intuitive assumption that insects such as flies or mosquitoes can use the airflow induced by an attack to escape successfully. Praying mantis, crickets and cockroaches have been shown to use sensible hairs or cerci in order to trigger their responses (Chapman and Webb, 1999; Dupuy et al., 2012; Ganihar et al., 1994; Triblehorn and Yager, 2006). Small insects could rely on their mechanoreceptors (i.e. Johnston's organs and sensible hairs) to detect the air gust generated by the attack in order to trigger a response (Fuller et al., 2014). Theoretically, these insects could be completely passively pushed away by the airflow. In that case, and because small insects have very low inertia, the air movement would generate a high enough aerodynamic drag force on the insect's body to move it away from danger.

In this study, we investigated if and how a nocturnal mosquito, when swatted, use wind gusts induced by the attack to escape successfully. We did so with two sets of experiments: first, by recording the escape dynamics and kinematics of free flying malaria mosquitoes (*Anopheles coluzzii*) while being attacked by a mechanical swatter roughly the size of a human hand (Fig. 5.1). First, we compared the escape performances of mosquitoes when attacked, in the dark or in low-light conditions. The attacks were simulated by a swatter that generated low visual cues and could induce various amounts of air movements. To do so, we modified the swatter to either generate no sensory cues (i.e. swatter off), low air movement and low visual cues (perforated transparent disk with a clear mesh) or high air movement and low visual cues (solid transparent disk with a clear mesh) (Fig. 5.1*f*).

Figure 5.1: Experimental setup and conditions. (*a*) Schematic of the experimental setup used to record the free-flying behaviour of mosquitoes while being attacked by a mechanical swatter (orange). Mosquitoes illuminated with infrared light were tracked in real time using five Basler cameras. Three Photron cameras were used to film the escape manoeuvres of mosquitoes. The configuration shown here is for the experiment #2 (see supplementary Fig. S5.2 for the configuration of experiment #1). (*b*) Side view of the experimental setup. (*c*) The swatter was triggered to attack if a mosquito was predicted to fly in the middle of the flight-arena. Two mosquito tracks are shown as examples of an escape and a collision. (*d*) Kinematics of the swatter. (*e*) Airflow velocity field resulting from our CFD simulation for $t = -5$ ms before the swatter (full disk) reached its most forward position. (*f*) Experimental conditions for experiment #1. Every experimental night, one out of the three swatter configurations was chosen: the full disk with a clear mesh generated high air movement but low visual cues, the hollow disk with a clear mesh generated less air movement but similar visual cues or the swatter was turned off (no air movement and no visual cues). Then the experiment was run automatically, and the light condition was changed according to a preestablished planning (see supplementary Fig. S5.1). Three light conditions were compared (dark, twilight, and sunrise). (*g*) Experimental conditions for experiment #2. Only the twilight light condition was used and two swatter types (transparent and black) were compared.

a)

top camera

infra red light panel

visible light panel

basler camera

Photron
side camera
(12500 fps)

flight arena

swatter

-45° camera

z

x

y

b)

swatter

c)

escape

collision

position at trigger

initial velocity

swatter (■) was trigerred when mosquito predicted
position (+) was inside the sphere of interest (○).

d)

start movement swatter

most forward position

disk inside sphere
of interest

e)

time = - 0.05s

airflow velocity [cm/s]

f)

swatter off

perforated disk
with clear mesh

solid disk
with clear mesh

one disk per experimental night

dark
(< 0.002 cd/m²)

twilight
(≈ 0.21 cd/m²)

sunrise
(≈ 24 cd/m²)

Day | Night | trial #1 | trial #2 | trial #3 | Night | Day

0:00   2:00   4:40   7:20   10:00   12:00

time after start of dark phase [hours]

g)

solid disk
(transparent)

solid disk
(black)

one disk per experimental night

Day | twilight | Day

0:00   2:00   4:40   7:20   10:00   12:00

time after start of dark phase [hours]

(Caption on the previous page.)

Secondly, using high-speed videography and deep learning, we recorded escape manoeuvres of mosquitoes in detail and estimated their kinematic parameters in order to answer how mosquitoes were achieving their successful escapes. For this, we compared the escapes of mosquitoes while attacked by one of two solid disks (transparent or black) producing almost none to high visual information about the attack. Finally, using a Computational Fluid Dynamics (CFD) simulation of the airflow induced by the swatter movement, we estimated to what extent escape manoeuvres of mosquitoes were explained by passive or active effects.

5.2 Results

5.2.1 How does airflow impact mosquito escape performance?

Our first experiment aimed at answering whether mosquitoes relied on air gusts to escape successfully from a looming threat. For that, we tracked the escape manoeuvres of mosquitoes while being attacked by one of the two different types of swatters. One with a solid disk or one with a perforated disk (see supplementary materials and methods). Based on the recorded tracks, we estimated the escape performance of mosquitoes. We also tracked mosquitoes flight paths during control trials with the swatter turned off. In that case, during our analysis we simulated a virtual swatter to estimate the performances of mosquitoes if no cues from an attack were available.

We recorded 5005 three-dimensional tracks of mosquitoes. Among those tracks, 196 ended up in collisions by the solid disk (out of 1539 tracks), and 415 by the perforated disk (out of 1605 tracks). In addition to those real collisions, we computed that 447 tracks would have been hit by the virtual swatter when the real swatter was not activated (1861 tracks).

Using Bayesian statistics, we estimated the mean collision probabilities of mosquitoes in the various experimental conditions (Fig. 5.2a). First, we noticed that mosquito collision probabilities varied with light conditions with remarkably lower probabilities of being hit when flying in the dark. Previously (chapter 4), we demonstrated that this lowered collision probability results from the higher unpredictability of *Anopheles* mosquitoes when flying in dark than in brighter light conditions. Secondly, we found that for all light conditions, the estimated means of the collisions probabilities of mosquitoes differed between each swatter type (off, perforated or solid), indicating that the more air movement generated by an attack, the smaller is the chance that the mosquito is being hit (Fig. 5.2a,b).

To complete our analysis of this first experiment, we compared their escape velocities and accelerations over time (i.e. away from the swatter) (Fig. 5.2d,e). We found that, when flying away from the swatter that induced the fastest airflow, mosquitoes exhibited both higher escape velocities and accelerations than when escaping from the swatters that induced less or no air movements (perforated or virtual swatter). This suggests that mosquitoes rely on the airflow induced by the attack to successfully escape, but how they used this airflow is still unclear at this point.
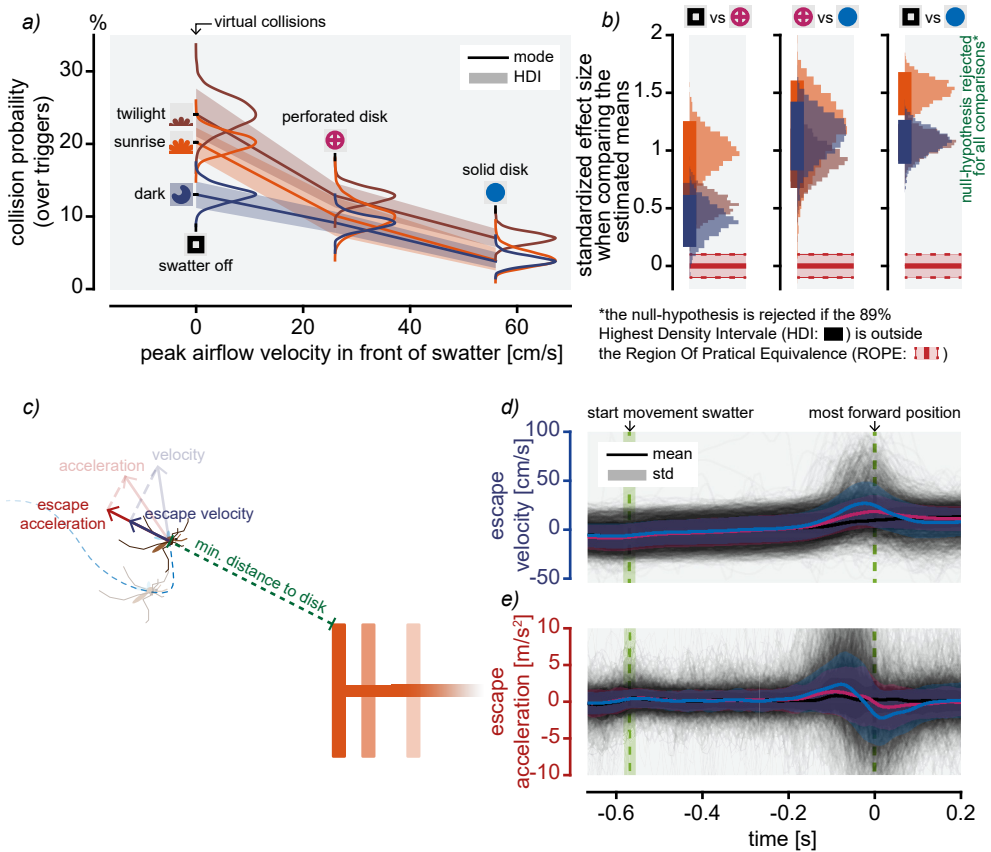
Figure 5.2: Mosquito collision probability and escape dynamics. (*a*) Distributions of the estimated (using Bayesian estimations) means of mosquito collision probability in the various experimental conditions. The mean collision probability of mosquitoes was higher when the swatter was turned off (virtual collisions) than when the mosquitoes were attacked by the hollow disk or full disk. For all light conditions, mosquito collision probabilities decreased with the increasing peak airflow velocities generated by the different swatter (virtual or not). (*b*) Standardized effect sizes were computed to compare the estimated means of panel (*a*). Here, all standardized effect sizes differ significantly from zero. Detailed explanation about null-hypothesis testing is provided in supplementary Fig. S5.3. (*c*) Schematic showing how the instantaneous escape velocity and acceleration of a mosquito is defined as a function of its relative position with the swatter. (*d,e*) Mosquitoes escape velocities and accelerations over time (excluding tracks that resulted in collisions). Mosquitoes are accelerating more and are flying faster when escaping from the solid swatter than from the perforated swatter.

5.2.2 How do mosquitoes escape from a looming threat?

Our second experiment aimed at answering how mosquitoes use the airflow induced by an attack to successfully escape. For this goal, we added high-speed cameras (12500 fps) to our setup to be able to record escape manoeuvres of mosquitoes in detail (Fig. 5.1*a*). This allowed us to track the kinematics of their body and of both of their wings. Additionally, we simulated the airflow generated by the swatter movement using CFD simulations (Fig. 5.1*e*, and see supplementary Fig. S5.10–S4.12). This allowed us to investigate the role that the air-

flow played in mosquito escapes. Finally, in this second experiment, we untangled the effect of air gusts from the effect of visual cues on escape performances by comparing two swatters: one with a ne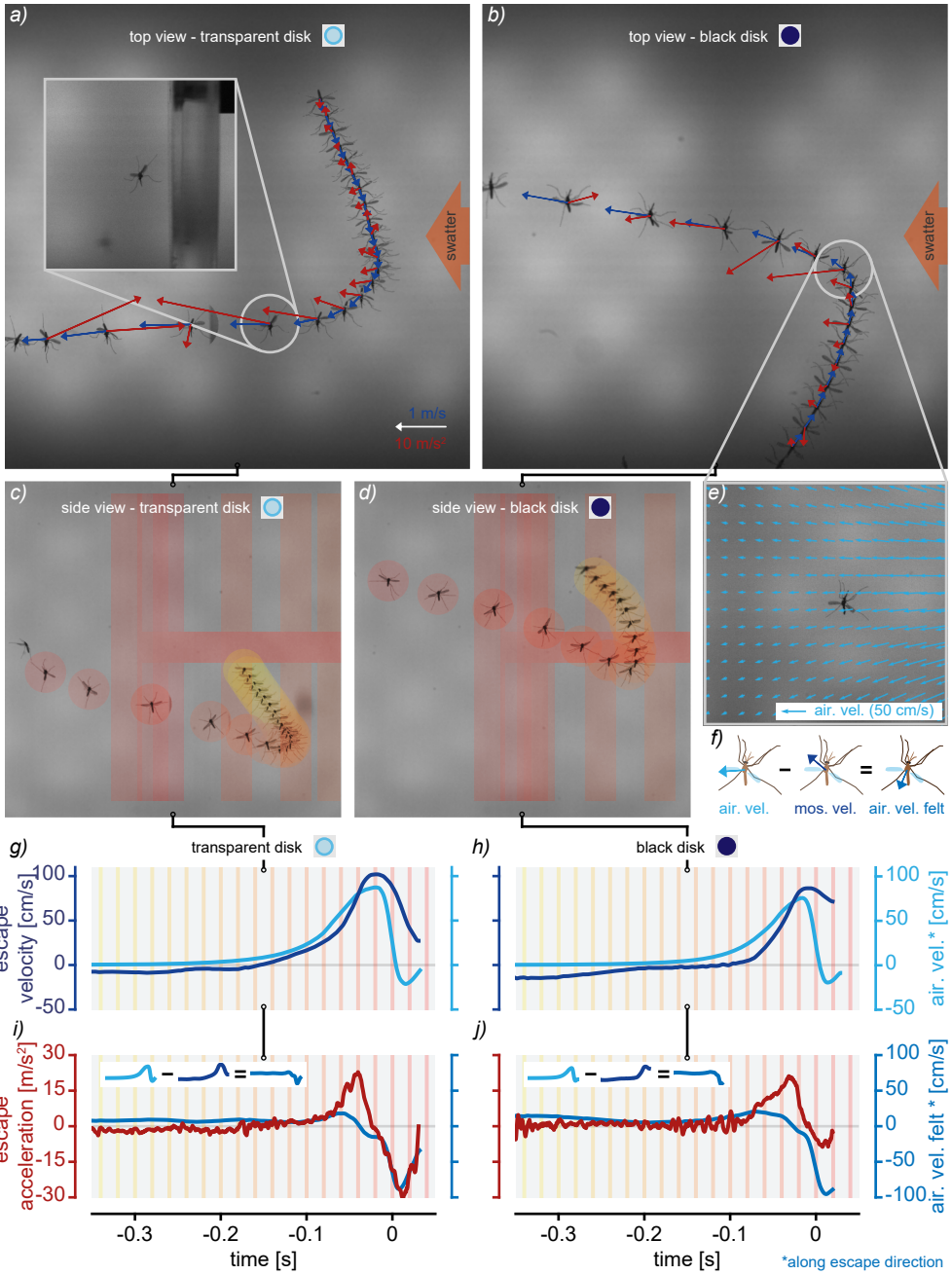arly invisible transparent disk and one with a black disk that was strongly contrasting with the background (see supplementary Fig. S5.4).

We recorded 775 swatter attacks, of which 14% resulted in a collision (with the swatter) and were left out of the following analysis. After filtering of the badly tracked manoeuvres, there were respectively 237 and 257 of manoeuvres left for the transparent and black disk, respectively.

5.2.3 Describing escape manoeuvres of mosquitoes

To understand how mosquitoes manoeuvre when escaping, it can be useful to first look at selected examples. In Fig. 5.3, we present photo montages of two typical examples of such manoeuvres, one when a mosquito escaped from the transparent disk and one when another escaped from the black disk. In both of those examples, mosquitoes entered the filmed volume from aside, then rapidly accelerated and rolled away from the swatter. All the mosquitoes that escaped successfully were heading away from the attack at the end of the swatter movement. However, not all manoeuvres looked similar. Therefore, we divided all tracks into three groups depending on initial heading when entering the filmed volume. These groups showed the mosquitoes attacked from the front, from the side or from the back (Fig. 5.4). Mosquitoes attacked from the back exhibited the smallest escape (ground) velocities and accelerations, whereas mosquitoes attacked from the front exhibited the highest escape velocities and accelerations (Fig. 5.4c,e). On average, mosquitoes of all groups had a nearly constant body yaw during the manoeuvres and similarly rolled towards the side opposite of the attack (Fig. 5.4h,j). However, they exhibited very different body pitch dynamics (Fig. 5.4i). Mosquitoes attacked from their side exhibited on average very little changes in body pitch, whereas mosquitoes attacked from the front or back respectively pitched up or down, towards the same direction as the airflow (i.e. away from the attack). These results suggest that the helicopter model apply to manoeuvring mosquitoes, because by rotating their body in this way, mosquitoes are redirecting their aerodynamic force vector and consequently accelerate in the direction away from the attack.

Figure 5.3: Recording of mosquito escape kinematics. Examples of two typical mosquito escape manoeuvres while being attacked by either a transparent (*a-d*) or black disk (*g-j*). (a-d) Photo montages. (*a,b*) Instantaneous velocity and acceleration vectors are respectively shown in blue and red. The orange arrows indicate the swatter direction.(*c,d*) Each individual mosquito position is circled by a disk which colour indicates time (see corresponding coloured stripes in panels (*g-j*)). The swatter positions are also indicated using the same colour scheme. (*e*) Airflow velocity field showing a section through the flow field around the position of the mosquito. The airflow induced by the swatter was simulated using CFD (see supplementary Fig. S5.12). (*f*) Schematics explaining how the airflow velocity felt by mosquitoes (e.g. in mosquitoes reference frame) is defined. (*g-j*) Time dynamic of the two mosquito's escape velocity and acceleration as well as the airflow velocity generated by the swatter at mosquito positions and the airflow velocity in mosquitoes reference frame (i.e. airflow velocity felt).

a) top view - transparent disk

b) top view - black disk

swatter

1 m/s
10 m/s²

c) side view - transparent disk

d) side view - black disk

e)

air. vel. (50 cm/s)

f)

air. vel. − mos. vel. = air. vel. felt

g) transparent disk

h) black disk

escape velocity [cm/s]

air. vel.* [cm/s]

i)

j)

escape acceleration [m/s²]

air. vel. felt * [cm/s]

time [s]

time [s]

*along escape direction

(Caption on the previous page.)
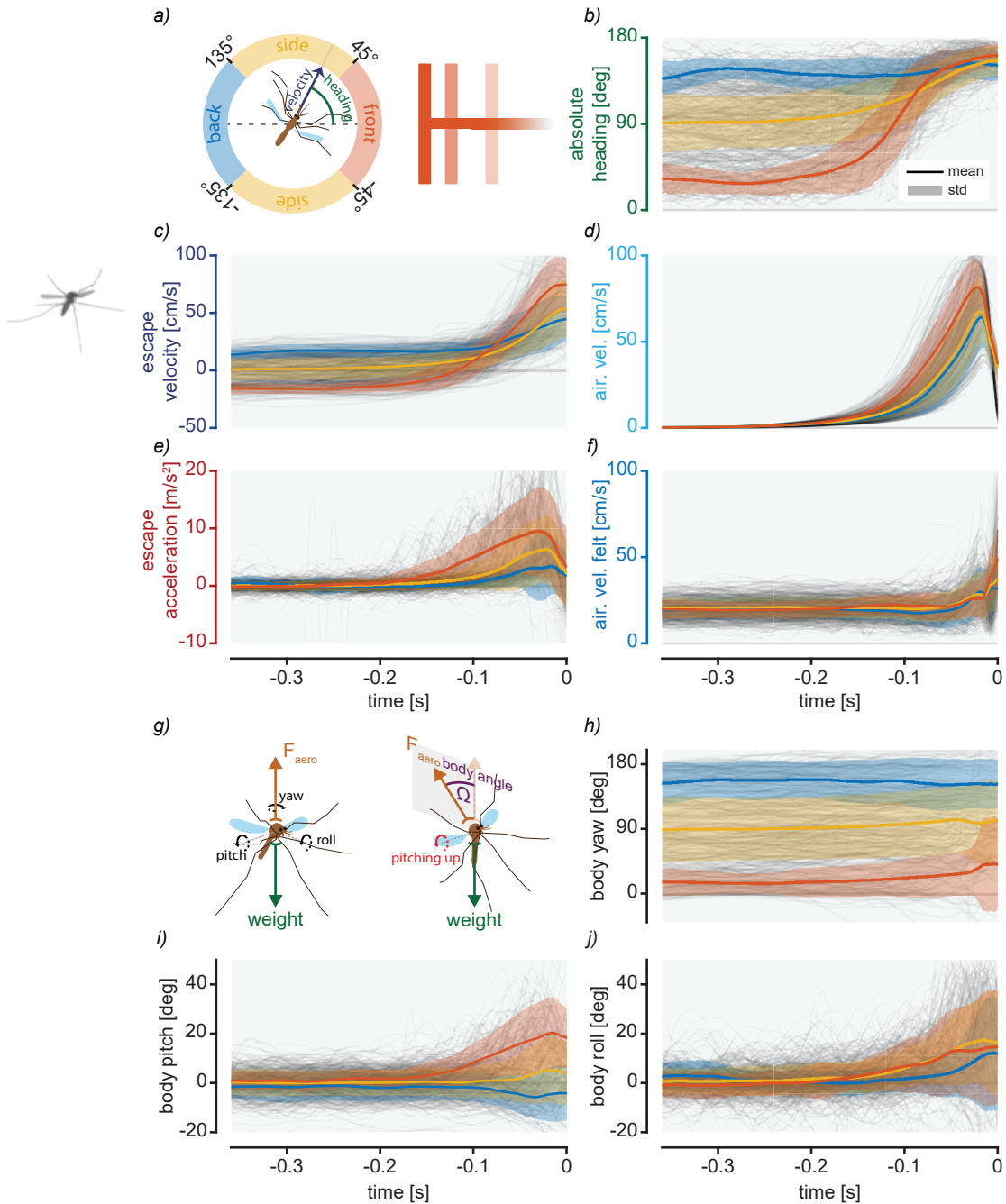
Figure 5.4: Effect of initial heading. (*a*) Mosquito initial heading is defined as the mean angle between mosquito velocity vector and the direction of the swatter between -0.32 and -0.24 seconds before the swatter reaches its most forward position. *Rest of the caption on the next page.*

(*b-f*) Dynamics of various metrics as a function of mosquito initial heading while escaping. (*g*) Schematic showing how the body yaw, pitch and roll are defined (Tait-Bryan convention). As an example, if a mosquito is pitching up, the force generated by its wings will be redirected backward. Mosquito body tilt angle Ω is defined as the angle between the vertical axis and vector normal to the body of the mosquito (i.e. this vector is directed upward when the mosquito is hovering). When hovering, Ω is equal to zero. (*h-j*) Dynamics of mosquitoes' body tilt angles in function of their initial heading. Around half of mosquito manoeuvres have been mirrored in order for their roll to be positive when they rolled away from the swatter (i.e. as if mosquitoes are all flying from the same side). These results confirm that mosquitoes use the so-called 'helicopter model' when escaping, as they re-orient the vector of the aerodynamic force generated by their wing away from the danger. For example, mosquitoes pitched up when facing the swatter and pitched down when being attack in the back. They also exhibit higher escape velocities and accelerations when initially facing the swatter than when initially flying away from it.

To investigate whether mosquitoes use the airflow induced by the attack to escape from it passively, it is interesting to compare the dynamics of mosquitoes to the velocities of the surrounding airflow. Here, we can see that the escape velocity of mosquitoes c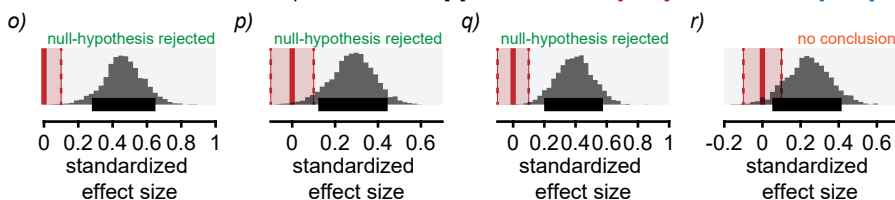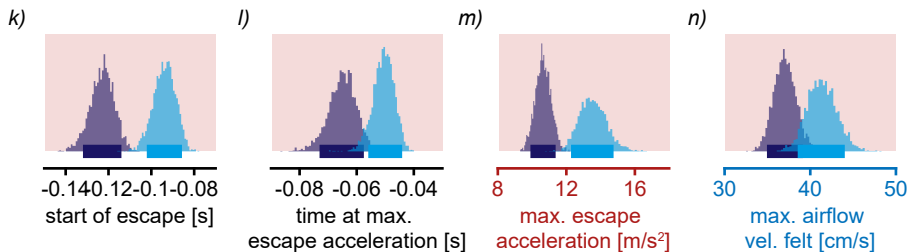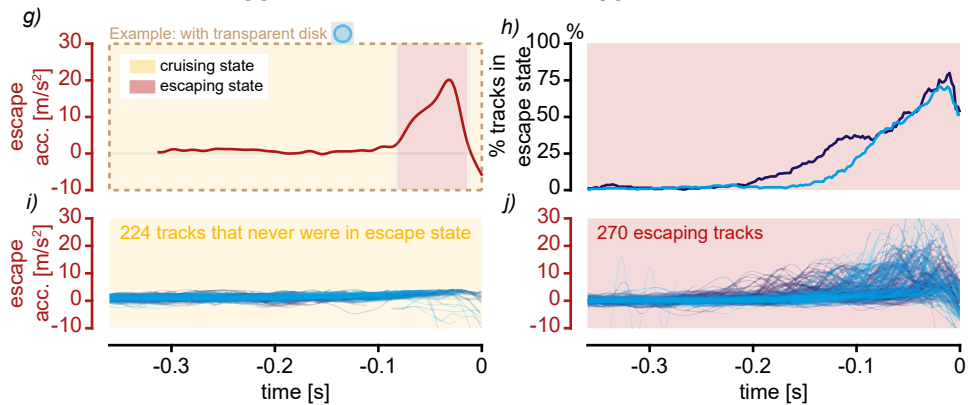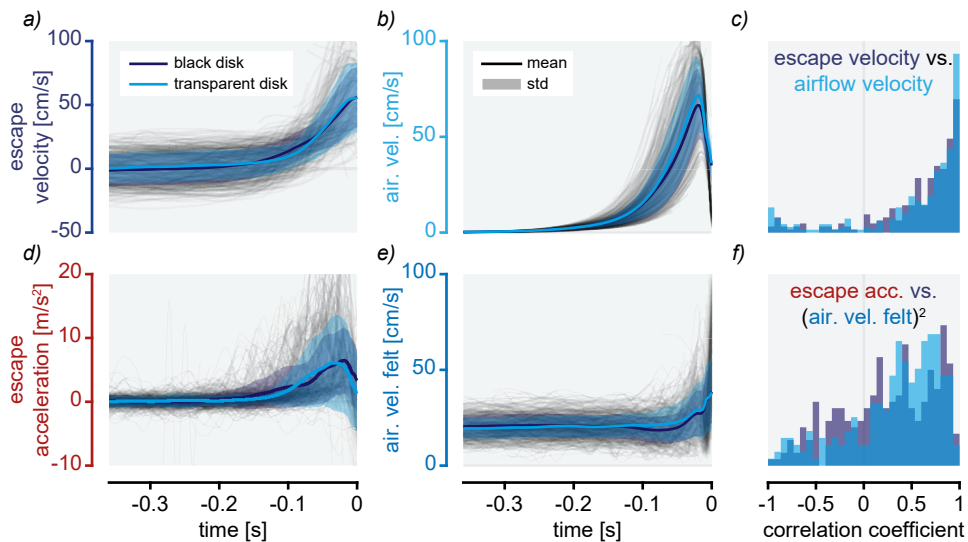orrelates well with the velocity of the airflow surrounding them during much of the manoeuvres (Fig. 5.5*c*), as if mosquitoes were going with the flow. However, the escape acceleration of the mosquitoes did not correlate very well with the relative airflow velocity squared in mosquito's reference frame (Fig. 5.5*f*). This is interesting because, if mosquitoes are only passively being pushed away by the airflow, then we would expect the airflow aerodynamic force applied to the mosquito body to be proportional to the square of the relative airflow velocity in the mosquito's reference frame. Therefore, a low correlation between these two metrics (the escape acceleration and the relative airflow velocity) is a first clue suggesting that the escape manoeuvres of mosquitoes are not fully passive.

5.2.4 Quantifying the effects of visual cues

In our first experiment, only the role of air movements induced by the swatter was investigated. Therefore, for our second experiment, we studied how the visual cues of the swatter impacted the escape performances of mosquitoes. We compared two types of swatters, a transparent and a black one. We found that, at first sight, mosquitoes exhibited similar escape dynamics when attacked by those two swatters in twilight (Fig. 5.5*a,b,d,e*). In both cases, they exhibited high escape velocities that correlated well with the background airflow velocities (Fig. 5.3*g,h* and Fig. 5.5*a-c*). However, we can notice differences concerning when and how much mosquitoes accelerated away from the swatter (Fig. 5.5*d*). To quantify these differences, we used a Hidden Markov Model (HMM) trained on the temporal dynamics of the escape acceleration throughout all flight manoeuvres (Fig. 5.5*d*). This model allowed us to estimate in which of two states (cruising or escaping) a mosquito was during each instant of its manoeuvre (Fig. 5.5*g*). As such, we could divide flight tracks into 224 cruising tracks (that never were in the escaping state) and 270 escaping tracks (Fig. 5.5*i,j*). We also used these results to define several escape performance metrics such as the time at which escaping started (i.e. the first frame at which mosquito entered the escaping state). Finally, using Bayesian statistics, we estimated the distributions of the means of these performance

a) escape velocity [cm/s]
— black disk
— transparent disk

b) air. vel. [cm/s]
— mean
std

c) escape velocity **vs.** airflow velocity

d) escape acceleration [m/s²]

e) air. vel. felt [cm/s]

f) escape acc. vs. (air. vel. felt)²

g) escape acc. [m/s²]
Example: with transparent disk
cruising state
escaping state

h) % tracks in escape state

i) escape acc. [m/s²]
224 tracks that never were in escape state

j) 270 escaping tracks

k) start of escape [s]

l) time at max. escape acceleration [s]

m) max. escape acceleration [m/s²]

n) max. airflow vel. felt [cm/s]

o) null-hypothesis rejected
standardized effect size

p) null-hypothesis rejected
standardized effect size

q) null-hypothesis rejected
standardized effect size

r) no conclusion
standardized effect size

(Caption on the next page.)

Figure 5.5: Escape performances when attacked by a transparent or black disk. (*a-b*, *d-e*) Time dynamic of all mosquitoes' escape velocity and acceleration as well as the airflow velocity generated by the swatter at mosquito positions and the airflow velocity in mosquitoes reference frame (i.e. airflow velocity felt). Only the tracks of mosquitoes that did not collide with the swatter are shown. The mean dynamic of these four metrics are plotted in purple or blue for mosquitoes respectively escaping from the black or transparent disk. (*c,f*) Histograms of the correlation coefficients of all tracks (one value per track): showing the correlation between the escape velocity and the airflow velocity (*c*), and between the escape acceleration and the relative airflow velocity squared (*f*). (*g*) Example of the escape acceleration of a mosquito. Using a Hidden Markov Model (HMM) trained on all tracks (see supplementary Fig. S5.7), we identified when the mosquito was in one of two states, labelled cruising or escaping states. (*h*) Proportion of all tracks that did not collide with the swatter and that were in the escaping state for the black or transparent disk. (*i,j*) Tracks are separated in two groups: (*i*) the cruising tracks that were never in the escaping state, and (*j*) the escaping tracks that were at least once in the escaping state. (*k-n*) Bayesian estimated means of various escape performance metrics of mosquitoes escaping from either the black or transparent disk: (*k*) Time at which mosquitoes entered for the first time in the escape state. (*l*) time at which mosquito reached their maximum escape acceleration. (*m*) maximum escape acceleration. (*n*) maximum airflow velocity from mosquito reference frame. (*o-r*) Standardized effect size of the comparisons between the estimated means of panels (*k-n*). Here the null-hypothesis is rejected for all comparisons except the last, where no conclusion could be made about if the maximum airflow velocity from mosquito reference frame differed between the two disk types.

metrics as well as the standardized effect sizes of the comparison between the two swatters (Fig 5*k-r*). We found that mosquitoes that escaped from the black disk were starting their escape manoeuvres significantly earlier and with lower acceleration peaks than when escaping from the transparent disk. The peak relative airflow velocities at the location and in the reference frame of the mosquito showed a similar trend, but the difference between the two swatters was not found to be significant.

5.2.5 What drives mosquito escapes? Active versus passive effects

To discover whether mosquitoes relied more on passive or active effects to successfully escape from the swatter, we quantitatively estimated the aerodynamic forces involved during the manoeuvres. Using Newton's second law of motion, we can write $\sum \vec{F} = m \cdot \vec{a} = m \cdot \vec{g} + \vec{F}_{aero}$, where the body motion (i.e. mosquito mass m times its acceleration $\vec{a}$) is equal to the sum of the forces applied to the mosquito body: the weight $m \cdot \vec{g}$ and the aerodynamic forces $\vec{F}_{aero} = \vec{F}_{mosquito} + \vec{F}_{airflow}$. With $\vec{F}_{mosquito}$ the aerodynamic force generated by the mosquito with its wings and $\vec{F}_{airflow}$ the aerodynamic force of the relative airflow in the mosquito reference frame (i.e. the drag) on mosquito body (Fig. 5.6*a*). Both $\vec{F}_{mosquito}$ and $\vec{F}_{airflow}$ were initially unknown, although we know that $\vec{F}_{airflow}$ will point in the same direction as the relative airflow velocity in the mosquito's reference frame. Additionally, if the helicopter model apply to escaping mosquitoes, $\vec{F}_{mosquito}$ will be oriented upward to counteract the weight when mosquitoes hover and tilted away from the vertical direction to move the mosquito in the horizontal plane. Finally, we know that $\vec{F}_{airflow}$ is proportional to the square of the relative airflow, and that $\vec{F}_{mosquito}$ is proportional to the product of the wingbeat amplitude and wingbeat frequency.

Our results show that escaping mosquitoes are accelerating away from the swatter, and therefore the aerodynamic forces applied to its body ($\overrightarrow{F}_{mosquito} + \overrightarrow{F}_{airflow}$) are increasing during these manoeuvres (Fig. 5.6c). Such a force increase is correlated with a similar increase in the body tilt angle which quantifies the contribution of a mosquito body pitch and roll to its body rotation (Fig. 5.6d). Assuming that $\overrightarrow{F}_{mosquito}$ is kept normal to the mosquito body during the manoeuvres (helicopter model), the mosquito body tilt angle also quantifies how much $\overrightarrow{F}_{mosquito}$ deviate from pointing upward. Additionally, both the increase of the total aerodynamic force and body tilt angle correlate with increases of the wingbeat amplitudes and frequencies during the manoeuvres (Fig. 5.6e,f). These wingbeat kinematic parameters are unlikely to have been changed by the airflow induced by the attack. Therefore, these results suggest that, during the escapes, mosquitoes are actively increasing the aerodynamic force on their body.

As a last step, we tried to answer to what extent the escape manoeuvres of mosquitoes were passive or active, which amounts to quantitatively estimating how much $\overrightarrow{F}_{airflow}$ or $\overrightarrow{F}_{mosquito}$ contributed to the total aerodynamic forces $\overrightarrow{F}_{aero}$ responsible for their escapes. We did that by estimating those two forces during the escape (i.e. while in the escaping state) using least square solving of the second law of motion (see materials and methods). In this way, we could compare these estimated forces $\overrightarrow{F}_{airflow}$ and $\overrightarrow{F}_{mosquito}$ to $\overrightarrow{F}_{aero}$ (here equal to $m \cdot \overrightarrow{a} - m \cdot \overrightarrow{g}$) and quantify their relative contributions (i.e. proportion) for each swatter type. Thus, the relative contribution of $\overrightarrow{F}_{mosquito}$ to $\overrightarrow{F}_{aero}$ along the escape direction was estimated to be 64% (mode of estimated mean) for the transparent disk and 81.3% for the black disk (Fig. 5.7a,e). Additionally, we estimated that the relative contribution of $\overrightarrow{F}_{airflow}$ to $\overrightarrow{F}_{aero}$ along the escape direction was 41.3% for the transparent swatter and 18.8% for the black swatter (Fig. 5.7b,f). In both cases, these force contributions differed significantly between the two swatters (Fig. 5.7i,j). As expected, the sum of these contributions was close to 100% for both swatters and no significant difference was found between them (Fig. 5.7c,g,k). As a final validation of our method, we found that vertical aerodynamic forces were fully explained by the contribution of $\overrightarrow{F}_{mosquito}$ (Fig. 5.7d) and no significant difference was observed between the swatters in that case (Fig. 5.7h,i).

5.3 Discussion

Here, we studied the escape dynamics of flying nocturnal *Anopheles* mosquitoes by first evaluating their escape performance while attacked by an automatic mechanical swatter in the dark or in twilight. By systematically changing the type of swatter used, we evaluated by how much the escape performance positively correlated with the speed of the airflow produced by the attacker. Secondly, we had a more detailed look at the manoeuvres by recording body and wingbeat kinematics of mosquitoes while using high-speed videography. Using a deep learning network and least square fitting, we achieved three-dimensional track-
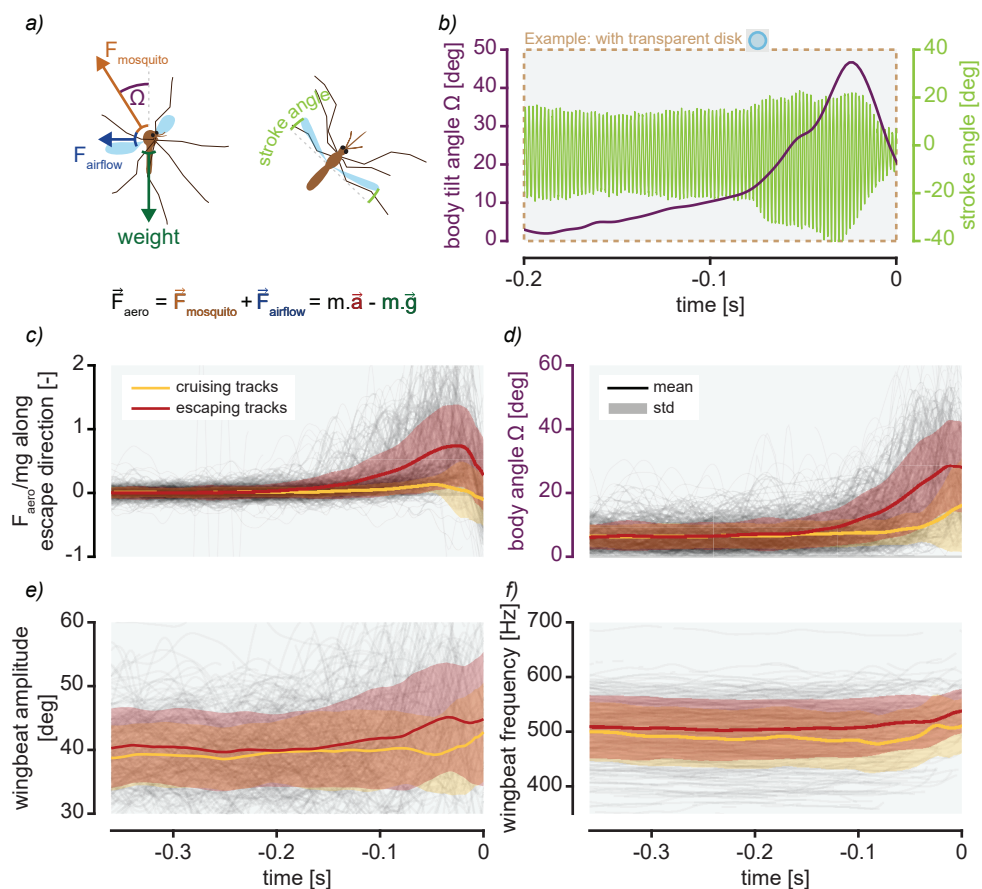
Figure 5.6: Mosquitos actively contribute to their escape manoeuvres. (*a*) Schematics describing the body tilt angle Ω of mosquitoes, the stroke angle as well as the forces acting on its body (free body diagram). (*b*) Typical example of a mosquito body tilt angle and the stroke angle over time during an escape. (*c-f*) The increase in observed escape force is correlated with changes in mosquitoes' body tilt angles as well as with increases of their wingbeat amplitudes and frequencies.

ing of the body and wings of mosquitoes. Coupled with CFD simulations of the airflow induced by the swatter, this allowed us to estimate all aerodynamic forces involved during the escape and their relative contribution to mosquito dynamics.

5.3.1 The more airflow is generated during an attack, the better the mosquito escape

We studied how the air gust produced by an attack influenced the escape performances of mosquitoes by comparing their collision probability while attacked by a solid or perforated swatter. Because they were covered with a clear mesh, the two swatters looked very similar to each other but induced different amounts of air flow while moving. Indeed, the peak

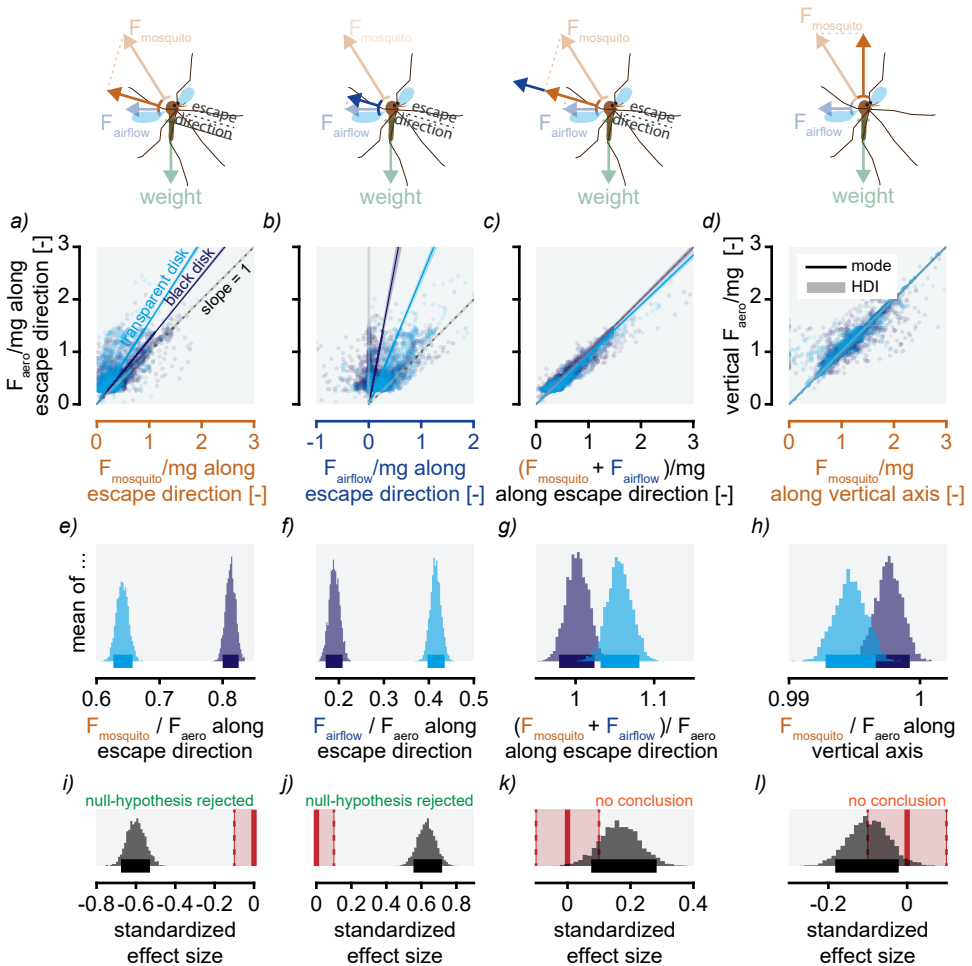**Figure 5.7: Proportion of forces produced during the escapes.** All results presented here have been computed when mosquitoes were in the escaping state (see Fig. 5.5*j*). (*a-d*) $\vec{F}_{aero}$ ($= m \cdot \vec{a} - m \cdot \vec{g}$) as a function of estimated $\vec{F}_{mosquito}$ or $\vec{F}_{airflow}$ for the transparent and black disks. Linear fits have been done using Bayesian estimations of the means of the proportion between $\vec{F}_{aero}$ and the corresponding forces in ordinate. (*e-h*) Distribution of the estimated means of the force proportions (e.g. slopes in panels (*a-c*)). (*i-l*) Effect size of the comparisons between the force proportions for the transparent and black disks. $\vec{F}_{mosquito}$ was found to contribute significantly more to the total $\vec{F}_{aero}$ with the black disk than with the transparent disk.

airspeeds measured in front of them were 26 cm/s for the perforated disk and 56 cm/s for the solid disk. The results from our Bayesian estimations showed that collision probabilities were inversely correlating with the amount of air movement induce by the attack. When attacked by the solid disk, mosquitoes had a probability of getting hit significantly lower than when attacked by the perforated disk (Fig. 5.2*a*). This confirms the intuitive assumption that small flying insects, such as mosquitoes or flies, can use airflow (passively

or actively) to escape successfully from a threat such as a fly swatter. Similar correlations between the velocity of the induced airflow and the degree of reaction have been previously described in cockroaches and crickets (Dangles et al., 2006; Westin et al., 1977). Although, for crickets it was also shown that the probability of escape decreased again at high attack speed (Dangles et al., 2006).

We also compared the escape performance of mosquitoes (the inverse of the probability of being hit) when attacked by the two different swatters to when mosquitoes were not attacked (i.e. collisions with a virtual disk) (Fig. 5.2*a*). In these control experiments, the swatter was turned off and therefore did not induce any sensory cues. Systematically, mosquitoes were significantly hit more often by the virtual swatter than by the two others. This indicates that the perforated disk was still generating enough visual, auditory and/or airflow cues to either be detected by the mosquitoes or passively contribute to their escape movements.

Finally, we found that escape velocities during the manoeuvres correlated well with the airflow velocities at the position of mosquitoes (Fig. 5.5*c*). To our knowledge, this is the first time that flying insects have been shown to go with the flow during an escape. However comparable wind-oriented flight dynamics have been described for the long distance travelling of mosquitoes and other dipteran species (Gao et al., 2020; Huestis et al., 2019; Leitch et al., 2020).

5.3.2 Mosquitoes follow the helicopter model while manoeuvring

In our second experiment, it was demonstrated that mosquitoes systematically pitched and rolled their body away from the swatter during their manoeuvres (Fig. 5.4*i,j*). At the same time, they did not exhibit large changes of their wing kinematics except stroke amplitude and frequency (Fig. 5.6*e,f* and S5.14). This indicates that during fast escape manoeuvres, similarly to fruit flies, moths, cicadas and pigeons (Greeter and Hedrick, 2016; Muijres et al., 2014; Ros et al., 2011; Zeyghami et al., 2016), "helicopter model" applied to mosquitoes when they reorient the vector of the aerodynamic forces generated by their wings away from the attack. This is in line with a previous finding showing that taking off mosquitoes control their body pitch with their legs and only change wing kinematics to modulate force magnitude (Veen and van Veen, 2020). However, when comparing the escape manoeuvres of fruit flies to the ones of mosquitoes, several key differences can be found. If both dipterans are exhibiting similar rolling away from the threat, the dynamics of their body yaw and pitch differ (Fig. 5.4*h-j*). While fruit flies were described partly realigning their yaw angles with their headings and mostly pitch up when manoeuvring (Karasek et al., 2018; Muijres et al., 2014), we found mosquitoes to hardly vary their yaw and to pitch up or down, but always away from the threat. This suggests that mosquitoes might only correct their yaw later, when the danger has already been avoided. It also indicates that the airflow induced by the attack might passively contribute to mosquito body rotations. A passive contribution of the airflow is also suggested by the fact that mosquitoes that were attacked from their

back exhibited pitch down manoeuvres. In this way, they must have redirected their aerodynamic force vectors away from the danger. These pitch down manoeuvres have never been described before.

5.3.3 Escape manoeuvres are mostly active

All previously discussed results could be explained by passive effects of the airflow on mosquito bodies. In that case, mosquito accelerations away from the swatter would be only due to the swatter induced airflow force (i.e. aerodynamic drag). And the observed body rotations of mosquitoes would be the results of aerodynamic torque induced solely by the airflow. The airflow force is proportional to the square of the relative airflow velocity, and thus if mosquito escapes were fully passive, we would expect high correlation between the escape accelerations of mosquitoes and their relative airflow velocities. However, we did not observe such correlation (*Fig. 5f*). Additionally, mosquitoes were found to increase both their wingbeat frequencies and wingbeat amplitudes while escaping (Fig. 5.6*e,f*). This implies that mosquitoes actively increased the forces and torques produced with their wings and thus, this suggests that they controlled, at least partly, their escape accelerations.

Using body and wings kinematics, we estimated the aerodynamic forces involved in escape manoeuvres of mosquitoes (Fig. 5.7). For that, we used our findings that mosquitoes follow the helicopter model and we made the simplifying assumption that the force induced by the airflow could be written as $\overrightarrow{F}_{airflow} = K_{airflow} \cdot \overrightarrow{v}^2_{airflowfelt}$, where the coefficient $K_{airflow}$ would be the same for all directions for an instant in time. This is equivalent to assume that the mosquito body can be approximated by a sphere, and thus that the drag force magnitude on this body will be independent of the wind orientation. Although such assumption may have resulted in estimation errors, we expect these errors to have been maximized along the axis (x and z) where the relative airflow velocities were the smallest. Therefore such errors should not have impacted our conclusions. For both the transparent and the black swatter, we found that the force generated by mosquitoes were contributing more to the escapes than the force induced by the air movements. This indicates that, despite seemingly going with the flow, nocturnal mosquitoes mostly contributed actively to their escape; as if mosquitoes actively steered into the bow wave induced by the attack, and continued to travel with the bow wave as if surfing it.

In addition, our results show that the passive contribution of the airflow is still far from negligible because representing between 18.8% and 41.3% of the forces driving mosquitoes escapes for the black and transparent swatters, respectively. Although passive effects of the air moved during an attack are unlikely to play a role in big or ground-dwelling insects, it is not surprising that the flow does affect small flying insects such as mosquitoes. Indeed, their mass is very low ($\sim$ 1.2 mg (Muijres et al., 2017)), and therefore their inertia is also low. If such passive effects are observed among insects such as mosquitoes, we expect that they might play an even more important role in the escape of smaller insects such as fruit flies, aphids or midges. Many of these small insects are hunted by far larger predators such as bats

or birds. The case of fruit flies is particularly interesting because they already have been the subject of detailed studies on their escape performances (Muijres et al., 2014). Therefore studying how fruit flies escape performance changes when attacked by a threat to generate air movement would certainly yield interesting comparisons. Finally, because passive use of airflow might have been a driver of the evolution of powered controlled flight in insects (Dudley and Yanoviak, 2011), studying how mosquitoes control their partly passive manoeuvres might even help us understand how the control system of flying insects evolved.

5.3.4 How do nocturnal mosquitoes detect an attack?

To investigate the role of visual cues in the escapes of nocturnal mosquitoes, we compared their escape performances while being attacked by a transparent or a black swatter. We found that mosquitoes started their escapes and reached their acceleration peaks earlier when attacked by the black swatter than by the transparent one (Fig. 5.5*k-r*). This suggests that, despite the low light conditions, mosquitoes were able to detect the swatter earlier when it procured contrasting visual cues of the attack. This is in line with anatomical measurements showing that *Anopheles* eyes are well adapted to their diurnal lifestyle (Land et al., 1999). This is in agreement with our previous study which shows that visual information plays an important role in the escape performance of both nocturnal and diurnal mosquitoes (chapter 4). In this study, we can estimate the proportion of the total escape forces associated with visual cues to be around 20% (active contribution for the black disk minus for the transparent disk). Another result in line with our previous study is the fact that mosquitoes were found to reach higher acceleration peaks when flying away from the transparent swatter. We previously observed that mosquitoes were escaping fast more often in low light conditions than in bright light conditions (chapter 4). These results could be explained by the fact that if mosquitoes start their escapes later, they have to accelerate more and fly faster away from the danger in order to be successful. In that context, airflow induced passive effects will be larger (around 20% more for the transparent disk) and then could partly counterbalance the delay in detecting the threat by the mosquitoes.

If *Anopheles* mosquitoes were only using visual information to detect a threat, then they should not be able to detect an attack in the dark or with almost no visual cues of the attack. However, we observed that in dark, twilight and sunrise light condition, mosquitoes exhibited higher escape performances when attacked by a swatter inducing air movements. Additionally, mosquitoes generally exhibited successful escapes when attacked by a transparent swatter. All of this suggest that mosquitoes are actually capable of detecting an attack without using vision. We propose that mosquitoes use information contained in the airflow induced by the attack to detect it. Yet, we did not identify the mechanism allowing mosquitoes to do that and not much is known about their mechanosensory capacities. It has been recently proposed that mosquitoes would use aerodynamic imaging using their Johnston's organ to detect close and invisible obstacles (Nakata et al., 2020). This mechanism describes how mosquitoes would detect the ground or a wall by perceiving their

self-induced airflow patterns as they approach them. This collision-avoidance mechanism would have a detection range limited to one or two mosquito body lengths. Many of the escaping mosquitoes never go that close to the swatter, therefore such mechanism is unlikely to inform a mosquito early enough to trigger an escape while attacked. However, it is possible that in such a case, instead of detecting their self-induced airflow, mosquitoes would simply detect the airflow induced by the attacker. Alternatively, mosquitoes might not detect the airflow directly, but could be informed of the attack by measuring body rotation passively induced by the airflow. Mosquitoes can detect such rotation with short temporal delays using their halteres (i.e. inertial sensors) (Taylor and Krapp, 2007). But more research is needed to test these hypotheses.

5.3.5 Conclusion

In various light conditions, nocturnal malaria mosquitoes exhibited the highest escape performances when the attack induced high air movements. When executing their escape manoeuvres, mosquitoes followed the helicopter model by pitching and rolling their body away from the threat, thus redirecting their aerodynamic force vector away from the attack. They were also seemingly going with the airflow, as their escape velocity correlated well with the velocity of the airflow surrounding them. Nevertheless, mosquitoes mostly actively contributed to their escape by redirecting and increasing the aerodynamic force that they produced as they surfed the bow wave induced by the swatter. Mosquitoes relied partially on visual cues to improve their escape performances, but they still exhibited a majority of successful escapes when almost no visual information about the attack was available. Our results suggest that these nocturnal mosquitoes used the swatter-induced airflow to detect the attack. This highlighted the overlooked role that airflow can play in the escape success of flying insects.

Authors' contributions

AC designed the experiments and build the experimental setup. AC performed the experiments. AC and PG did the airflow measurements. LHC made the numerical simulations. AC analysed the data. FTM provided support for the analysis. AC wrote the first draft of

the manuscript. All authors commented the manuscript. All authors read and approved the final manuscript.

Declaration of Interests

The authors declare no competing or financial interests.

5.4 Material and Methods

5.4.1 Experimental animals

For our experiments, we used non-blood-fed adult *Anopheles coluzzii* females (age = 7.4 ± 1.2 days post emergence (mean ± std)). These mosquitoes came from a colony that originated from Suakoko, Liberia in 1987. This colony was reared in a climate chamber inside the Laboratory of Entomology (Wageningen University & Research, The Netherlands) where the temperature and relative humidity were respectively kept at 27°C and at 70%. The light cycle inside the room consisted of a shifted clock with 12h light and 12h dark periods. Adult mosquitoes were reared in BugDorm cages (30 × 30 × 30 cm, MegaView Science Co. Ltd., Taiwan), where they had constant access to 6% glucose sugar water solution. Mosquitoes were divided in two groups, either to be used for experiments or to be used for rearing. Rearing mosquitoes were blood-fed daily with human blood (Sanquin, Nijmegen, The Netherlands) using a membrane feeding system (Hemotek, Discovery Workshop, UK). These mosquitoes had access to wet filter papers upon which females could lay their eggs. After being collected, these eggs were dried for at least three days and then moved intoplastic larval trays filled with 27°C water containing a few drops of Liquifry No. 1 fish food (Interpet, UK). After emerging, the larvae were fed with TetraMin Baby (Tetra Ltd, UK). To emerge, pupae were moved into new BugDorm cages. Both males and females were kept together.

5.4.2 The flight arena

To understand how mosquitoes escape from being swatted, we filmed them while freely flying in an octagonal flight arena (50x50x48cm (height x width x length)) with transparent Plexiglas walls (Fig. 5.1*a*) (chapter 4). In the front and back of the flight arena, there were two circular holes closed by HFPE insect screening (Howitec, The Netherlands) to allow air circulation and facilitate cleaning (chapter 4). The temperature and relative humidity inside the arena was controlled by the climate control system of the room (Spitzen et al. 2013). To provide visual cues for mosquitoes, visual markers (randomly shaded grey squares printed on paper) were placed on the floor of the flight arena. Also inside, a sensor (AM2302, ASAIR) was recording relative humidity and temperature.

A visible light LED panel was positioned above the arena to change the light condi-

tion from dark (turned off) to twilight or sunrise (Fig. 5.1*a,f*). To mimic twilight condition, multiple polyester neutral density filters of 0.8 ND (LEE filters, Panavision Inc.) were placed in front of the LEDs in order to reduce light intensity. Additionally, the flight arena was surrounded by multiple infrared LED panels. Because mosquitoes cannot see infrared light (Gibson 1995), we could track them in the dark using five infrared enhanced cameras (Basler acA2040-90umNIR) with 12.5 mm lenses (Kowa LM12HC F1.4) and the real-time tracker Flydra (version 0.20.30)(Stowers et al. 2017; Straw et al. 2011). These cameras filmed mosquitoes at 90 frames per second and at a resolution of 680x680px (with a pixel-binning of 3). Lens distortions were corrected by filming a backlighted print of a chequerboard pattern.

We simulated attacks using a mechanical swatter made of a 1 cm diameter black aluminium shaft and a black or transparent plexiglass disk. This disk had a size similar to a human hand with a diameter of 10 cm and a thickness of 1 cm. The swatter was moved along a 50 cm long-toothed belt axes (drylin ZLW-1660-G0BW0-D0A3B-0A0A-500) powered by an AC servo motor (Schneider Electric Lexium BCH2 LD0433CA5C), itself controlled by a programmable motion servo driver (Schneider Electric Lexium LXM28A). The swatter kinematics, similar to a human swatting or a bat attack (Triblehorn and Yager, 2006), was the same as in our previous study (Fig. 5.1*d*)(chapter 4). The swatter was triggered based on real-time prediction of mosquito position 367.5 ms in the future (i.e. when the swatter would be around halfway to its final position, t = -157.5 ms in Fig. 5.1–4.7). These predictions were linear estimations based on mosquito's current three-dimensional position and velocity. Thus, the swatter was triggered if a mosquito was predicted to be in a 10 cm diameter spherical triggering region at the centre of the flight arena (Fig. 5.1*c*). After being triggered, and having waited one second, the swatter was moved slowly back to its initial position. After a delay of ten secondes, another trigger was allowed. Finally, during postprocessing, we filtered out all the triggers for which the mosquitoes were not predicted to be inside the sphere of interest when the swatter would reach its most forward position (t = 0 s).

Two different experiments are presented in this study, the first was carried out to investigate the effect of air gusts on the escape performance of mosquitoes (supplementary *Fig*. S1a and S2). For this, we used two types of transparent disks, a solid and a perforated disk, which generated different amounts of air movement (supplementary Fig. S5.1*b* and Fig. 5.2). In order to control the effect of visual cues, a clear mesh (Ornata plus 95135, howitec.nl) covered both sides.

The main goal of the second experiment was to zoom in on mosquito escapes in order to record in detail their body and wing kinematics during those manoeuvres. For this, three high-speed cameras (FASTCAM SA5, Photron) were added to the setup. These cameras were pointed towards the centre of the flight arena and recorded images at 12500 frames per second and at a resolution of 1024 × 1024 pixels. They filmed a 12x12x12 cm volume around the final position of the swatter, where mosquitoes were initially predicted to fly towards. Several small modifications of the setup were made to allow the addition of the

high-speed cameras. These consisted of the removal of a part of the visible light panel above the arena, the addition of an infrared light panel below the arena, and the decentring a hole in the plexiglass side panel to plug in a mosquito release cage. Finally, to reduce the chance of having individual mosquito out of the focus of the high-speed cameras, the triggering parameters were slightly modified. These involved reducing the size of the triggering region to a 5 cm diameter sphere and in lowering the latency used to compute the predicted positions to 315 ms (t = -0.210 s on Fig. 5.1–4.7).

5.4.3 Experimental procedure

The day before each experimental night, a disk was attached to the swatter rod according to a quasi-randomized planning (see supplementary Fig. S5.1 and Fig. S5.1*a*). The experimenter cleaned the flight arena with paper towels and a 15% ethanol solution. Skin odour contamination was avoided by handling all materials and mosquitoes while wearing nitrile gloves. Then, a calibration of the Basler cameras was done by tracking the position of a manually waved single LED in the arena. The calibration was aligned using an alignment device with eight LEDs at known three-dimensional coordinates. Calibration snapshots were taken with the Photron cameras of a calibration device with 23 3.5 mm beads at various known three-dimensional positions. These snapshots were later used to compute DLT coefficients for each camera. After closing the flight arena, a release cage with 50 female mosquitoes was plugged to its side and mosquitoes were released to fly freely inside. The experimental procedure was then automatically controlled by a Python 2.7 script. This script allowed for the automatic changes of the light condition inside the flight arena, the tracking of mosquitoes and the triggering of the swatter. For the first experiment, trials started the following morning at 2:30 a.m., two hours after the start of mosquitoes normal dark phase. Three different light conditions were tested consecutively per night, each for 160 minutes. The order of these light conditions was changed following the previously mentioned quasi-randomized planning (Fig. S5.1*a*). For the second experiment, only the twilight condition was tested, and the experiment lasted through the entire dark phase of mosquitoes (0:30 a.m. to 0:30 p.m.) (Fig. S5.1*b*). In the afternoon, mosquitoes were removed from the arena using a vacuum cleaner, and left inside its bag to desiccate.

5.4.4 Analysis of three-dimensional flight tracks

We did the pre-processing of the first experiment dataset using Python 2.7. First, collisions were identified by looking at the two-dimensional tracking results of the Basler cameras positioned at the side of the flight arena. Then, the two-dimensional points corresponding to the swatter were filtered, and three-dimensional tracks were reconstructed again. To be able to compare the chance of being hit by the swatter with or without a disk, collisions with a virtual swatter were determined. These virtual collisions were estimated by computing if and when mosquito flight tracks would have crossed the path of a virtual disk. Then the

data was analysed using Matlab R2019b (as in chapter 4). Outliers of computed three-dimensional points were filtered out using the covariance matrices estimated by the Flydra tracker extended Kalman filter. Segments that were shorter than 4 points (at 90 fps) long were filtered out and segments that were separated by more than 15 points were divided into separated tracks. Then, missing values were interpolated (makima, Matlab) and smoothed using a Savitzky-Golay filter with a moving window of five frames. Finally, for the rest of the analysis, we only kept the tracks that started at least 60 frames before and 30 frames after the time at which the swatter reached its most forward position (t = 0s on all the figures).

The second dataset (using the high-speed cameras as shown in Fig. 5.1) was also analysed using Matlab R2019b. Only the tracks that did not end up in a collision (if mosquitoes touched the disk with any body part) were kept for further analysis. Three-dimensional track segments that were shorter than 50 frames (at 12500 fps) were filtered out. Similarly, segments that were separated by more than 20 frames from the main track were also filtered out. Instantaneous wingbeat amplitudes and frequencies were estimated using a Hilbert transform on the wings' stroke angles. Then body and wings parameters were smoothed using a Savitzky-Golay filter with a moving window of 251 frames. After that, framerate was lowered to 500 fps (linear resampling) for the rest of the analysis.

For both datasets, flight velocities and accelerations over time were computed using central finite difference schemes (with an accuracy of 6). Initial and final values were estimated respectively using forward and backward finite difference schemes. Then, the escape velocity and escape acceleration were defined and computed by projecting mosquito velocity or acceleration over time on the moving line between the nearest point on the swatter and mosquito three-dimensional position (see Fig. 5.2c).

5.4.5 Estimating body and wing motion

To investigate mosquitoes' reaction to the swatter attack, it was necessary to accurately estimate their position as well as their body and wing angles throughout the manoeuvres. Tracking the body parts of mosquitoes from our dataset was challenging. Indeed, due to the relatively large three-dimensional volume filmed and to experimental lighting limitations, body resolution was low and contrast was restricted. This meant that classical automatic tracking methods would most likely yield poor results. Manually tracking body parts was also not an option because our dataset comprised of several hundreds of thousands of images. Thus tracking needed to be automated with an accuracy close to human tracking. To accomplish this goal, we developed a new flying insect tracker written in Python 3.6 and based on the deep neural network package DeepLabCut (Mathis et al., 2018). This open-source package uses transfer learning to do markerless pose estimation using relatively low numbers of labelled images.

The tracking process is described in detail in the supplementary Fig. S5.8. It starts with preparing low-resolution videos to be used by DeepLabCut. First, mosquitoes are

tracked in two-dimension on each of the three different camera views using the opencv2 blob detection algorithm. Then, in order to filter out noise, three-dimensional tracks are reconstructed using previously computed DLT coefficients and the tracks are re-projected in each camera two-dimensional views. From these two-dimensional coordinates, the original images are cropped around mosquitoes' positions over time. These cropped images are stitched together and converted into a single .avi video per manoeuvre. Such video presents several advantages when compared to the original recordings in order to be used by DeepLabCut, namely of having a greatly reduced resolution, thus increasing the tracking speed. And it gathered all camera views together, thus allowing the network to learn positional correlation between the views. Using the DeepLabCut GUI, we trained a deep neural network based on the pre-trained network resnet50 and 230 manually labelled images of escaping mosquitoes. For each camera views, we labelled 40 points over the mosquito body and wings, thus resulting in a total of 120 points per image (Supplementary Fig. S5.9). The deep neural network was then used to automatically estimate positions of these points on all recorded images.

Next, from the two-dimensional results of DeepLabCut we estimated body parameters (i.e. position, lengths and angles of body parts and wings) over time using a custom-made Python 3.6 package. The first steps were to remove outliers with likelihood (provided by DeepLabCut) lower than 0.85 and to reconstruct three-dimensional coordinates of each body part. Then, initial estimation of body parameters were obtained using simple calculus. Because initial estimation of body and wings angles were found to be noisy, updated estimation of these parameters were then obtained by minimizing the sum of squares (scipy.optimize.leastsq) of the root-mean-square deviation between the coordinate of the skeletons joints and the three-dimensional points. Estimated body or wing parameters were filtered out if the root-mean-square deviation was superior to 0.1 mm and if the number of points per wing or body used to do the 3d fitting was lower than 4. Finally, body parameters (but not the wing parameters) were smoothed over time with a low pass Butterworth filter using a cut-off frequency of 100 Hz.

5.4.6 Classifying tracks as cruising or escaping

To classify flight tracks as either "cruising" (i.e. missing the swatter by chance) or "escaping", we used a Hidden Markov model (HMM) (Matlab toolbox by Kevin Murphy (Murphy, 1998)). In such a model, the studied system is assumed to be a Markov process with hidden states (here cruising or escaping), where the current probability of the system to be in a particular state is only dependent on the previous state. Our HMM was trained on all escape accelerations over time of all tracks that didn't end up in a collision. We estimated the initial parameter of the model by fitting a mixture of two Gaussians (fitgmdist, Matlab) to the distribution of all instantaneous escape accelerations (see supplementary Fig. S5.7c). Then the remaining unknown parameters of the HMM were estimated using a Baum–Welch algorithm, with fixed means and standard deviations (see supplementary

Fig. S5.7a,b). The state with the highest mean acceleration was labelled as the "escaping" state while the second was labelled as the "cruising" state. We used the Viterbi algorithm to compute the most-likely corresponding sequence of states for each track (see examples on Fig. 5.5g). Then we computed the overall proportion of tracks that were in either of the two states for each point in time (Fig. 5.5h). Finally, we labelled all the tracks as escaping if they were found to be at least once in the "escaping" state. The remaining tracks were labelled as cruising (Fig. 5.5i,j) .

5.4.7 Simulating the airflow conditions

To investigate the role of the airflow generated by the swatter, we simulated this airflow using Computational Fluid Dynamics (CFD) simulation. The simulation of the swatter was performed with the aid of the dynamic mesh PIMPLE solver available in OpenFOAM (version 19.12 (Weller et al., 1998)), namely overPimpleDyMFoam. The simulations were configured to run with a second order accurate backwards time scheme. The domain consisted of a cylinder (radius = 250 mm and length = 580 mm) with a disk moving in it. An overset (chimera) mesh was employed to enable the movement of the disk, with predetermined kinematics, inside the cylindrical computational domain . This approach combined two distinct unstructured cartesian grids constructed with the aid of CFMesh. A grid was constructed around the disk, and another filled the cylinder domain acting as background grid. Both were predominantly composed of hexahedral cells of 2 mm and 4 mm respectively. No-slip and inletOutlet velocity boundary conditions were imposed at the disk and outer boundaries respectively. Additionally, the simulation used a U-RANS model to account for turbulence effect, more specifically has accomplished that with the aid of a Spalart-Allmaras turbulence model.

The CFD results were validated by comparing them with experiment measurements obtained with a hotwire anemometer (tetso 405i) (see supplementary Fig. S5.10). Two sets of parametric studies were conducted varying the cell sizes and the Courant–Friedrichs–Lewy (CFL) number (Fig. S5.10 and Fig. S5.11). The cell sizes of the meshes were selected after comparing multiple mesh sizes to be at the maximum 4 mm for the background mesh and 2 mm for the overset mesh 2 mm. Similarly, various Courant–Friedrichs–Lewy (CFL) number were compared and we selected a final CFL number of 0.4. Because of the chaotic nature of airflow turbulence generated during the movement of the swatter, we could not predict the exact conditions that each individual mosquito experienced. Thus all of the CFD results presented in this study have been averaged around the axis of the swatter movement (i.e. the three-dimensional axis of symmetry of the swatter) into two-dimensional planes for each millisecond (see supplementary Fig. S5.12). Airflow velocities at each instantaneous mosquito three-dimensional positions have been interpolated from these two-dimensional planes using modified Akima piecewise cubic Hermite interpolation (makima, Matlab).

5.4.8 Estimating aerodynamic forces

To disentangle mosquito active contribution to their escape from the passive effect of them being pushed away by the air movement, we estimated the contribution of involved aerodynamic forces (see free body diagram Fig. 5.6a). Using Newton's second law of motion we can write $\sum \overrightarrow{F} = m \cdot \overrightarrow{a} = \overrightarrow{F}_{aero} + m \cdot \overrightarrow{g}$, with m being mosquito mass and $\overrightarrow{a}$ its body acceleration vector. Additionally we can define $\overrightarrow{F}_{aero} = \overrightarrow{F}_{mosquito} + \overrightarrow{F}_{airflow}$ with $\overrightarrow{F}_{mosquito}$ being the aerodynamic force generated by the mosquito with its wings. And $\overrightarrow{F}_{airflow}$ the force of the moving airflow on mosquito's body (e.g. due to mosquitoes motion in reference to the surrounding air mass). By assuming a quasi-steady hypothesis, both of these forces can be written in the form $\overrightarrow{F} = \frac{1}{2} \cdot \rho \cdot S \cdot \overrightarrow{v}^2 \cdot C$ with ρ the air density, S the cross-sectional area of mosquito body, $\overrightarrow{v}$ the air velocity and C an unknown coefficient. In the case of $\overrightarrow{F}_{mosquito}$, $\overrightarrow{v}^2$ can be replaced by $v_{wb}^2 \cdot \overrightarrow{l}$ with the average wingbeat velocity v_{wb} and the unit total aerodynamic force vector $\overrightarrow{l}$. This vector is normal to mosquito body and directed upward when the mosquito is hovering. Because the velocity of mosquito body in the surrounding air mass is negligible when compared to the velocity of the wings in reference to its body, we can define the average wingbeat velocity as $v_{wb} = f_{wb}.A_{wb}.\frac{span}{2}$. With mosquito mean wingbeat frequency f_{wb} and mean stroke amplitude A_{wb}. We can simplify the two aerodynamic forces to:

$$\overrightarrow{F}_{mosquito} = K_{mosquito} \cdot v_{wb}^2 \cdot \overrightarrow{l} \tag{5.1}$$

$$\overrightarrow{F}_{airflow} = K_{airflow} \cdot \overrightarrow{v}^2_{airflowfelt} \tag{5.2}$$

and rewrite the second law of Newton too:

$$m \cdot \overrightarrow{a} - m \cdot \overrightarrow{g} == K_{mosquito} \cdot v_{wb}^2 \cdot \overrightarrow{l} + K_{airflow} \cdot \overrightarrow{v}^2_{airflowfelt} \tag{5.3}$$

By normalizing this equation by mosquito weight ($m.g$), we get:

$$\frac{\overrightarrow{a} - \overrightarrow{g}}{g} = \frac{K_{mosquito}}{m \cdot g} \cdot v_{wb}^2 \cdot \overrightarrow{l} + \frac{K_{airflow}}{m \cdot g} \cdot \overrightarrow{v}^2_{airflowfelt} \tag{5.4}$$

with the two unknown coefficients $\frac{K_{mosquito}}{m \cdot g}$ and $\frac{K_{airflow}}{m \cdot g}$. Then we estimated these two coefficients for each point in time (i.e. frame) by solving the equation 5.4 using a linear least square solver (lsqlin, Matlab) and constraining the coefficients to be positive. Then, we filtered out estimations with normed residuals superior to 5% of the normalized weight $\frac{\overrightarrow{g}}{g}$ (=1). Finally, we computed $\overrightarrow{F}_{mosquito}$ and $\overrightarrow{F}_{airflow}$ using the estimated coefficients, and

compared these forces during escapes (i.e. while being in the "escaping" state) to $\frac{\vec{d}-\vec{g}}{g}$ (Fig. 5.7 and supplementary Fig. S5.13).

5.4.9 Statistical analysis

In this study, instead of usual frequentist statistics, we used Bayesian statistics because we think it is conceptually clearer and because it offers richer results by providing estimations of the full-probability distribution of the parameters of interest. We estimated means of mosquitoes' probability of being hit (Fig. 5.2*a*) for each combination of light condition and swatter type using MATJAGS, a Matlab interface for JAGS (Steyvers and Kalish, 2014), and the Matlab Toolbox for Bayesian Estimation (MBE) (Winter, 2016), a Matlab implementation of Kruschke's R code (Kruschke, 2013). To model the probability of being hit we used a Bernoulli distribution and a logistic link function. Additionally, to compare the escape performance of mosquitoes when attacked by the black or the transparent disk, we estimated means of various performance metrics (Fig. 5.5*k-n*) and means of the proportion of forces applied to the body of mosquitoes (Fig. 5.7*e-h*) using Bayesian estimation (Kruschke, 2013). We used a normal distribution to model the performance metrics and student t distributions to model the force proportions. Then, we defined standardized effect sizes of the comparison between the two disk types (black and transparent) as the difference of their estimated means divided by the norm of their estimated standard deviations.

Finally, we tested for the null hypothesis using the "HDI+ROPE decision rule" (Kruschke and Liddell, 2018). For this, we first define the 89% HDI (Highest Density Interval) as the 89% interval in which all the points have a higher probability density than points outside. And the ROPE (Region of Practical Equivalence) is defined as the range around zero (i.e. the null hypothesis) where a parameter would be found to have "practically no effect". Therefore, the "HDI+ROPE decision rule" says that the null hypothesis is rejected if the 89% HDI of the standardized parameter (e.g. slopes) completely fall outside the ROPE =[-0.1, 0.1].

References

Benelli, G., Jeffries, C. L. and Walker, T. (2016). Biological control of mosquito vectors: Past, present, and future. *Insects* **7**.

Bomphrey, R. J., Nakata, T., Phillips, N. and Walker, S. M. (2017). Smart wing rotation and trailing-edge vortices enable high frequency mosquito flight. *Nature* **544**, 92–95.

Cardé, R. T. (2015). Multi-cue integration: How female mosquitoes locate a human host. *Curr. Biol.* **25**, R793–r795.

Cator, L. J., Arthur, B. J., Harrington, L. C. and Hoy, R. R. (2009). Harmonic convergence in the love songs of the dengue vector mosquito. *Science (80-.).* **323**, 1077–1079.

Chapman, T. and Webb, B. (1999). A neuromorphic hair sensor model of wind-mediated escape in the cricket. *Int. J. Neural Syst.* **9**, 397–403.

Cheng, B., Tobalske, B. W., Powers, D. R., Hedrick, T. L., Wethington, S. M., Chiu, G. T. C. and Deng, X. (2016). Flight mechanics and control of escape manoeuvres in hummingbirds. I. Flight kinematics. *J. Exp. Biol.* **219**, 3518–3531.

Clements, A. N. (1999). *The biology of mosquitoes. Volume 2: sensory reception and behaviour*, volume 2. CABI Publishing, 752 pp.

Corcoran, A. J. and Conner, W. E. (2016). How moths escape bats: predicting outcomes of predator-prey interactions. *J. Exp. Biol.* **219**, 2704–2715.

Dangles, O., Ory, N., Steinmann, T., Christides, J. P. and Casas, J. (2006). Spider's attack versus cricket's escape: velocity modes determine success. *Anim. Behav.* **72**, 603–610.

Darbro, J. M. and Harrington, L. C. (2007). Avian defensive behavior and blood-feeding success of the West Nile vector mosquito, Culex pipiens. *Behav. Ecol.* **18**, 750–757.

Dekker, T., Geier, M. and Cardé, R. T. (2005). Carbon dioxide instantly sensitizes female yellow fever mosquitoes to human skin odours. *J. Exp. Biol.* **208**, 2963–2972.

Dickinson, M. H. and Muijres, F. T. (2016). The aerodynamics and control of free flight Manoeuvres in Drosophila. *Philos. Trans. R. Soc. B Biol. Sci.* **371**, 20150388.

Dudley, R. and Yanoviak, S. P. (2011). Animal aloft: The origins of aerial behavior and flight. In *Integr. Comp. Biol.*, volume 51, pp. 926–936. Oxford Academic.

Dupuy, F., Steinmann, T., Pierre, D., Christidés, J. P., Cummins, G., Lazzari, C., Miller, J. and Casas, J. (2012). Responses of cricket cercal interneurons to realistic naturalistic stimuli in the field. *J. Exp. Biol.* **215**, 2382–2389.

Edman, J. D., Day, J. F. and Walker, E. D. (1984). Field confirmation of laboratory observations on the differential antimosquito behavior of herons. *Condor* **86**, 91.

Edman, J. D. and Scott, T. W. (1987). Host defensive behaviour and the feeding success of mosquitoes. *Int. J. Trop. Insect Sci.* **8**, 617–622.

Fournier, J. P., Dawson, J. W., Mikhail, A. and Yack, J. E. (2013). If a bird flies in the

forest, does an insect hear it? *Biol. Lett.* **9**, 20130319.

Fuller, S. B., Straw, A. D., Peek, M. Y., Murray, R. M. and Dickinson, M. H. (2014). Flying Drosophila stabilize their vision-based velocity controller by sensing wind with their antennae. *Proc. Natl. Acad. Sci. U. S. A.* **111**, E1182–e1191.

Ganihar, D., Libersat, F., Wendler, G. and Camhi, J. M. (1994). Wind-evoked evasive responses in flying cockroaches. *J. Comp. Physiol. A Neuroethol. Sensory, Neural, Behav. Physiol.* **175**, 49–65.

Gao, B., Wotton, K. R., Hawkes, W. L. S., Menz, M. H. M., Reynolds, D. R., Zhai, B.-P., Hu, G. and Chapman, J. W. (2020). Adaptive strategies of high-flying migratory hoverflies in response to wind currents. *Proc. R. Soc. B Biol. Sci.* **287**, 20200406.

Greeter, J. S. and Hedrick, T. L. (2016). Direct lateral maneuvers in hawkmoths. *Biol. Open* **5**, 72–82.

Hiscox, A., Otieno, B., Kibet, A., Mweresa, C. K., Omusula, P., Geier, M., Rose, A., Mukabana, W. R. and Takken, W. (2014). Development and optimization of the Suna trap as a tool for mosquito monitoring and control. *Malar. J.* **13**, 257.

Hoy, R., Nolen, T. and Brodfuehrer, P. (1989). The neuroethology of acoustic startle and escape in flying insects. *J. Exp. Biol.* **146**, 287–306.

Huestis, D. L., Dao, A., Diallo, M., Sanogo, Z. L., Samake, D., Yaro, A. S., Ousman, Y., Linton, Y. M., Krishna, A., Veru, L. et al. (2019). Windborne long-distance migration of malaria mosquitoes in the Sahel. *Nature* **574**, 404–408.

Karasek, M., Muijres, F. T., Wagter, C. D., Remes, B. D. and De Croon, G. C. (2018). A tailless aerial robotic flapper reveals that flies use torque coupling in rapid banked turns. *Science (80-.).* **361**, 1089–1094.

Kim, D., DeBriere, T. J., Cherukumalli, S., White, G. S. and Burkett-Cadena, N. D. (2021). Infrared light sensors permit rapid recording of wingbeat frequency and bioacoustic species identification of mosquitoes. *Sci. Rep.* **11**, 10042.

Kruschke, J. K. (2013). Bayesian estimation supersedes the t test. *J. Exp. Psychol. Gen.* **142**, 573–603.

Kruschke, J. K. and Liddell, T. M. (2018). The Bayesian New Statistics: Hypothesis testing, estimation, meta-analysis, and power analysis from a Bayesian perspective. *Psychon. Bull. Rev.* **25**, 178–206.

Land, M. F., Gibson, G., Horwood, J. and Zeil, J. (1999). Fundamental differences in the optical structure of the eyes of nocturnal and diurnal mosquitoes. *J. Comp. Physiol. - A Sensory, Neural, Behav. Physiol.* **185**, 91–103.

Leitch, K., Ponce, F., van Breugel, F. and Dickinson, M. (2020). The long-distance flight behavior of Drosophila suggests a general model for wind-assisted dispersal in insects. *bioRxiv* p. 2020.06.10.145169.

Matherne, M. E., Cockerill, K., Zhou, Y., Bellamkonda, M. and Hu, D. L. (2018).

Mammals repel mosquitoes with their tails. *J. Exp. Biol.* **221**, jeb178905.

Mathis, A., Mamidanna, P., Cury, K. M., Abe, T., Murthy, V. N., Mathis, M. W. and Bethge, M. (2018). DeepLabCut: markerless pose estimation of user-defined body parts with deep learning. *Nat. Neurosci.* **21**, 1281–1289.

McMeniman, C. J., Corfas, R. A., Matthews, B. J., Ritchie, S. A. and Vosshall, L. B. (2014). Multimodal integration of carbon dioxide and other sensory cues drives mosquito attraction to humans. *Cell* **156**, 1060–1071.

Menda, G., Nitzany, E. I., Shamble, P. S., Wells, A., Harrington, L. C., Miles, R. N. and Hoy, R. R. (2019). The long and short of hearing in the mosquito Aedes aegypti. *Curr. Biol.* **29**, 709–714.e4.

Muijres, F. T., Chang, S. W., van Veen, W. G., Spitzen, J., Biemans, B. T. T., Koehl, M. A. R. and Dudley, R. (2017). Escaping blood-fed malaria mosquitoes minimize tactile detection without compromising on take-off speed. *J. Exp. Biol.* **220**, 3751–3762.

Muijres, F. T., Elzinga, M. J., Melis, J. M., Dickinson, M. H., Florian T. Muijres, 1 Michael J. Elzinga, 1 Johan M. Melis, 1, . M. H. D. and Avoiding (2014). Flies evade looming targets by executing rapid visually directed banked turns. *Science (80-.).* **344**, 172–7.

Murphy, K. Hidden Markov Model (HMM) Toolbox for Matlab.

Nakata, T., Phillips, N., Simões, P., Russell, I. J., Cheney, J. A., Walker, S. M. and Bomphrey, R. J. (2020). Aerodynamic imaging by mosquitoes inspires a surface detector for autonomous flying vehicles. *Science* **368**, 634–637.

Reid, J. N., Hoffmeister, T. S., Hoi, A. G. and Roitberg, B. D. (2014). Bite or flight: The response of mosquitoes to disturbance while feeding on a defensive host. *Entomol. Exp. Appl.* **153**, 240–245.

Ritzmann, R. E. (1984). The Cockroach Escape Response. In *Neural Mech. Startle Behav.*, pp. 93–131. Springer US.

Ros, I. G., Bassman, L. C., Badger, M. A., Pierson, A. N. and Biewener, A. A. (2011). Pigeons steer like helicopters and generate down-and upstroke lift during low speed turns. *Proc. Natl. Acad. Sci. U. S. A.* **108**, 19990–19995.

Sane, S. P. (2003). The aerodynamics of insect flight. *J. Exp. Biol.* **206**, 4191–4208.

Santer, R. D., Rind, F. C. and Simmons, P. J. (2012). Predator versus prey: locust looming-detector neuron and behavioural responses to stimuli representing attacking bird predators. *PLoS One* **7**, e50146.

Steyvers, M. and Kalish, M. MATJAGS, a Matlab interface for JAGS.

Tauber, E. and Camhi, J. M. (1995). The wind-evoked escape behavior of the cricket Gryllus bimaculatus: Integration of behavioral elements. *J. Exp. Biol.* **198**, 1895–1907.

Taylor, G. K. and Krapp, H. G. (2007). Sensory systems and flight stability: what do insects measure and why? *Adv. In Insect Phys.* **34**, 231–316.

Ter Hofstede, H. M. and Ratcliffe, J. M. (2016). Evolutionary escalation: The bat-moth arms race. *J. Exp. Biol.* **219**, 1589–1602.

Triblehorn, J. D., Ghose, K., Bonn, K., Moss, C. F. and Yager, D. D. (2008). Free-flight encounters between praying mantids (Parasphendale agrionina) and bats (Eptesicus fuscus). *J. Exp. Biol.* **211**, 555–562.

Triblehorn, J. D. and Yager, D. D. (2006). Wind generated by an attacking bat: Anemometric measurements and detection by the praying mantis cercal system. *J. Exp. Biol.* **209**, 1430–1440.

van Breugel, F., Riffell, J., Fairhall, A. and Dickinson, M. H. (2015). Mosquitoes use vision to associate odor plumes with thermal targets. *Curr. Biol.* **25**, 2123–2129.

Veen, W. G. V. and van Veen, W. G. (2020). *Aerodynamics of insect flight*. Ph.D. thesis, University of Wageningen.

Walker, E. D. and Edman, J. D. (1985). The influence of host defensive behavior on mosquito (diptera: culicidae) biting persistence. *J. Med. Entomol.* **22**, 370–372.

Weller, H. G., Tabor, G., Jasak, H. and Fureby, C. (1998). A tensorial approach to computational continuum mechanics using object-oriented techniques. *Comput. Phys.* **12**, 620.

Westin, J., Langberg, J. J. and Camhi, J. M. (1977). Responses of giant interneurons of the cockroach Periplaneta americana to wind puffs of different directions and velocities. *J. Comp. Physiol. A Neuroethol. Sensory, Neural, Behav. Physiol.* **121**, 307–324.

Who (2020). *World Malaria Report 2020*, volume 73. WHO Press, Geneva, 1–4 pp.

Winter, N. GitHub - NilsWinter/matlab-bayesian-estimation: Matlab Toolbox for Bayesian Estimation.

Zeyghami, S., Babu, N. and Dong, H. (2016). Cicada (Tibicen linnei) steers by force vectoring. *Theor. Appl. Mech. Lett.* **6**, 107–111.

Supplementary materials ──────────────────────────────

Mosquitoes escape from being swatted by actively surfing the swatter-induced bow wave

Antoine Cribellier[1], Leonardo Honfi Camilo[1], Pulkit Goyal[1], Florian T. Muijres[1]

[1] Experimental Zoology Group, Wageningen University & Research, Wageningen, The Netherlands

Consisting of:

- Supplementary figures S5.1–S5.14
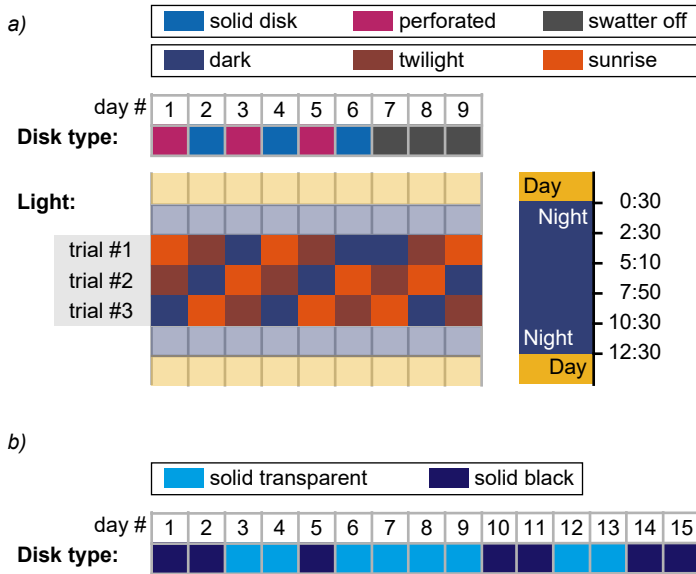
Figure S5.1: Experimental conditions. (*a*) Experimental planning and conditions for the experiment #1 (results presented in Fig. 5.2, setup Fig. S5.2). (*b*) Experimental planning and conditions for the experiment #2 (results presented in Fig. 5.3–5.7).
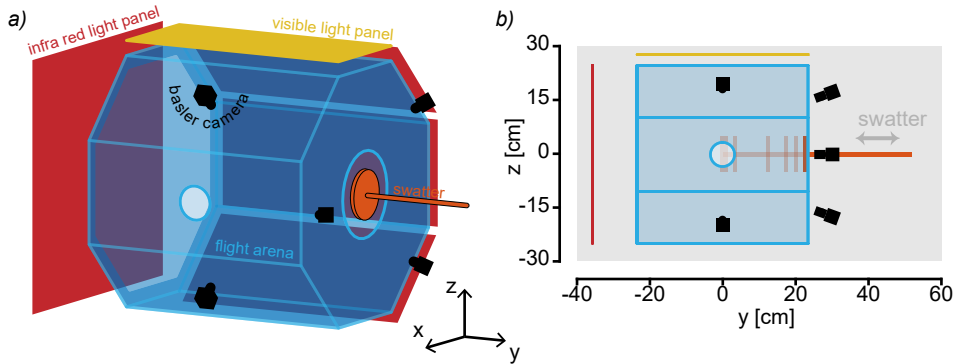
Figure S5.2: Experimental setup to record mosquito flight kinematics. (*a-b*) The experimental setup used for the first experiment. In the second experiment, the light panels were modified and the hole to plug a release cage was moved towards the swatter side (see Fig. 5.1).

Bayesian estimation (null-hypothesis testing) the "HDI+ROPE decision rule"

> the null-hypothesis is rejected if the 89% Highest Density Interval (HDI: ▬) of the standardized parameter is outside the Region of Practical Equivalence (ROPE: ▯)

0% in ROPE VS. 100% in ROPE

β (standardized slope)   β (standardized slope)
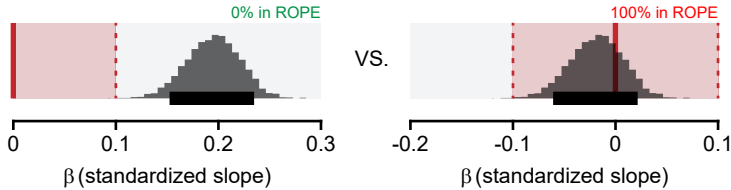
> the null-hypothesis is accepted if the HDI is fully inside the ROPE
> otherwise (e.g. 32% of the HDI is inside the ROPE), no conclusion is made

Figure S5.3: Null hypothesis testing with Bayesian estimation. Examples of two distributions of the estimated mean of a standardized parameter β in black. The null hypothesis is rejected (left) if the Highest Density Interval (HDI) is outside the Region Of Practical Equivalence (ROPE). The null-hypothesis is accepted (right) if the full HDI is inside the ROPE.

solid disk ● with clear mesh

perforated disk ⊕ with clear mesh

solid transparent disk ○
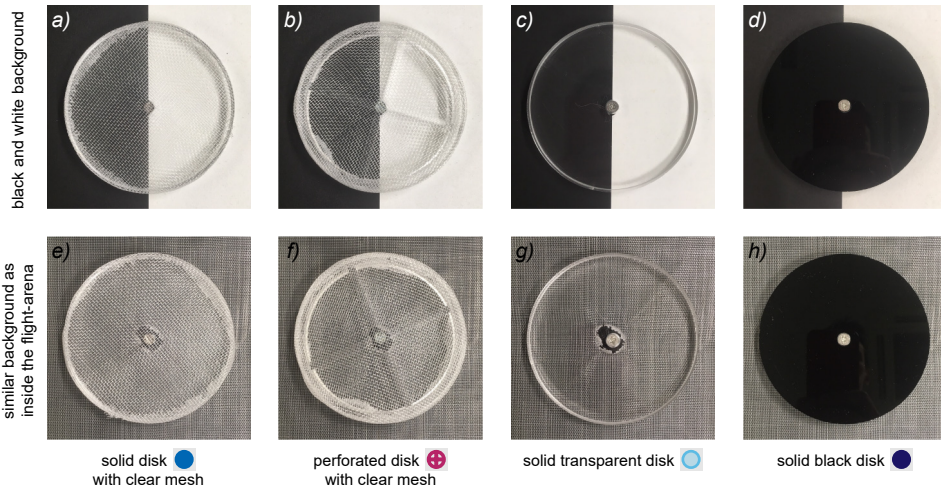
solid black disk ●

Figure S5.4: Disk with black and clear meshes. (*a,b,e,f*) Pictures of the solid and perforated disks with a clear mesh that were used in the experiment #2. (*c,d,g,h*) Picture of the transparent and black disks that were used in the experiment presented in the Fig. 5.3–5.7.
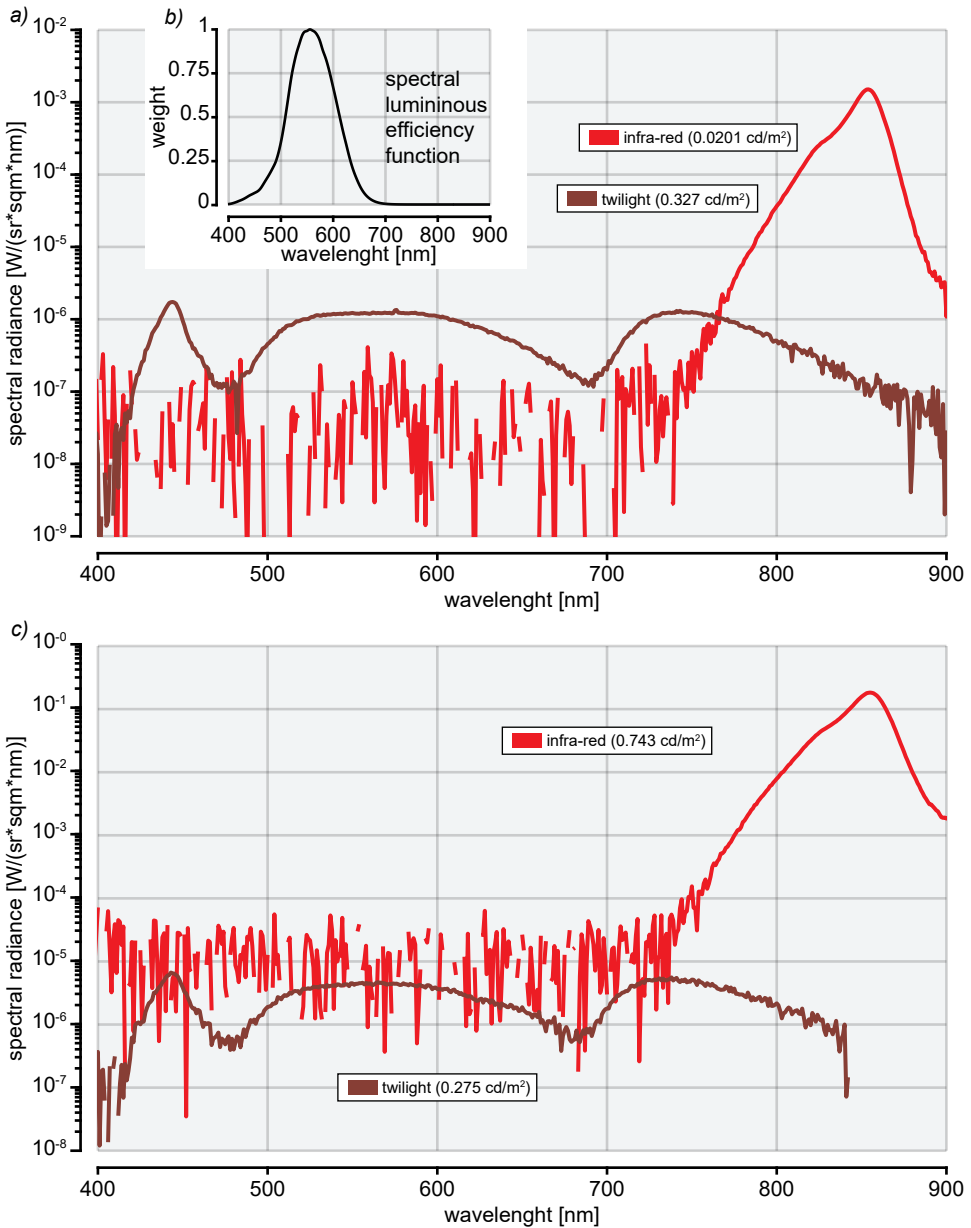
Figure S5.5: Spectrum of the various light conditions. (*a*) Spectral radiance in log scale of the twilight condition and of the infrared light measured in the middle of flight arena (as presented in Fig. S5.2) with a spectrometer (specbos 1211, JETI) and using a diffuse reflector (USRS-99-010-EPV, Labsphere). The low radiance parts of the spectrums appear noisy due to limitation in the range of the radiance that can be measured at the same time. (*b*) Spectral luminous function of humans (Sharpe et al., 2005) used to compute the luminance of each light condition. (*c*) Spectral radiance of the light conditions in the experimental setup presented in the supplementary Fig. 5.1.
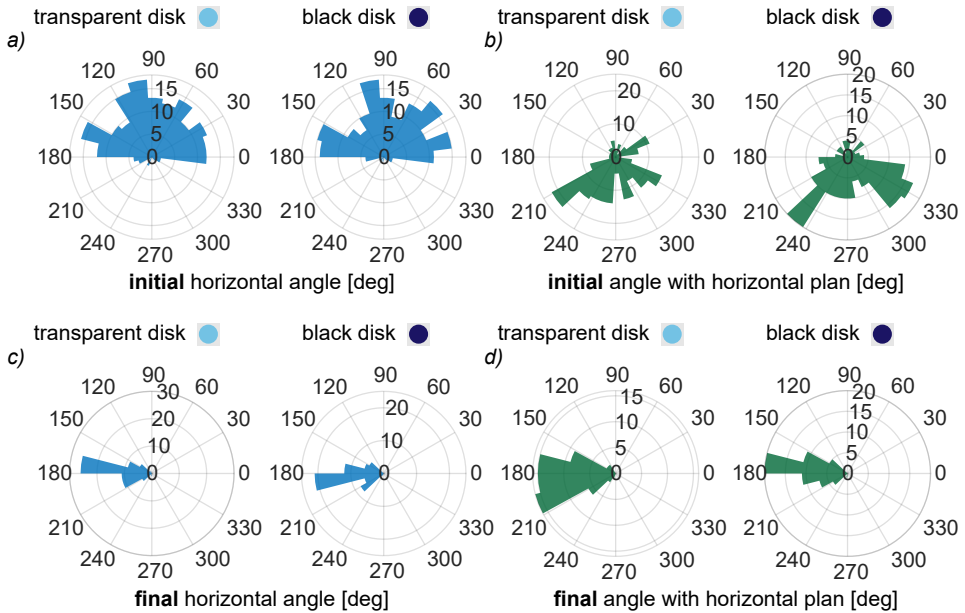
Figure S5.6: Initial and final flight angles. (*a,c*) Rose plots of mosquito flight angle in the horizontal plan at trigger time ((*a*) - initial) and when the swatter reach its most forward position ((*c*) - final). The large majority of tracks are showed to be initially coming from one side because the tracks that had negative initial heading (see Fig. 5.4) were mirrored. (*b,d*) Rose plots of the initial and final mosquito flight angle with horizontal plan. The swatter is coming from the right (0° angle). Radial scale showing the number of tracks in each bar.

Figure S5.7: Hidden Markov Model parameters. (*a*) Transition matrix. Each number is the probability of transition from the current state (on the abscise) to a new state (on the ordinate). (*b*) Prior probability to be on each one of the two states. (*c*)) Distribution of all escape accelerations of the mosquitoes with the Gaussian distribution of the two states used in the HMM.
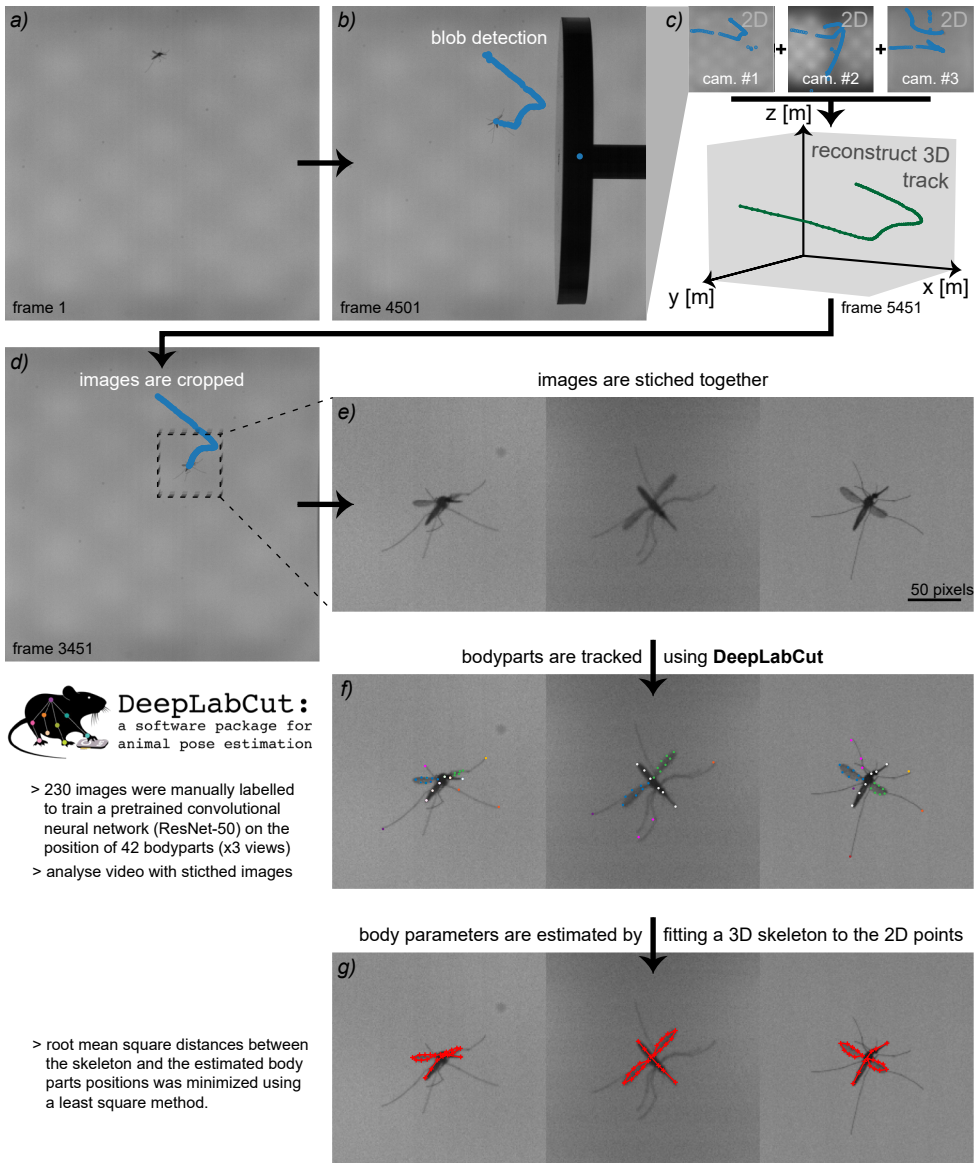
Figure S5.8: Mosquito tracking process. (*a*) An example of a frame recorded by the side camera while a mosquito was attacked by the mechanical swatter. (*b*) Blobs are detec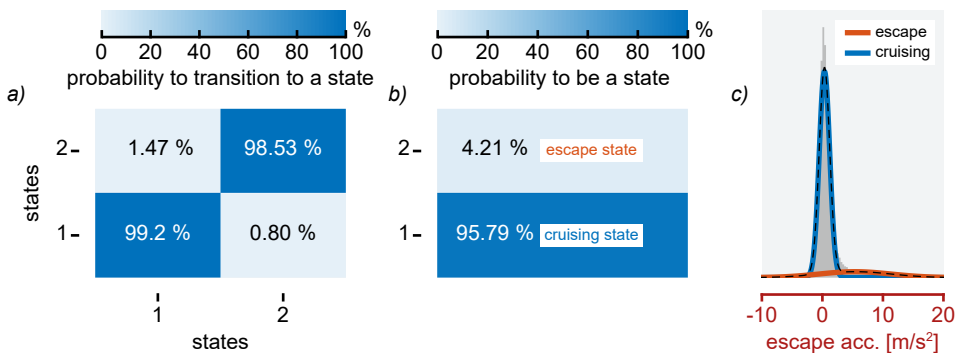ted for all frames of the recording using background subtraction. (*c*) The 2d coordinates resulting from the blob detection on all three camera views are used to reconstruct the 3d tracks of the mosquito. (*d*) The 3d coordinates are then re-projected into each camera view, and the images are cropped around the mosquito positions using a 200 x 200 pixels window. (*e*) The cropped images of the three views are stitched together and converted into a single .avi video. (*f*) The video is analysed using a deep learning network trained with 230 manually labelled images (Mathis et al., 2018). (*g*) For each frame, a 3d skeleton of a mosquito with variable parameters (e.g. body lengths, span, body and wings angles) is fitted to the reconstructed 3d coordinated of mosquitoes various body parts.
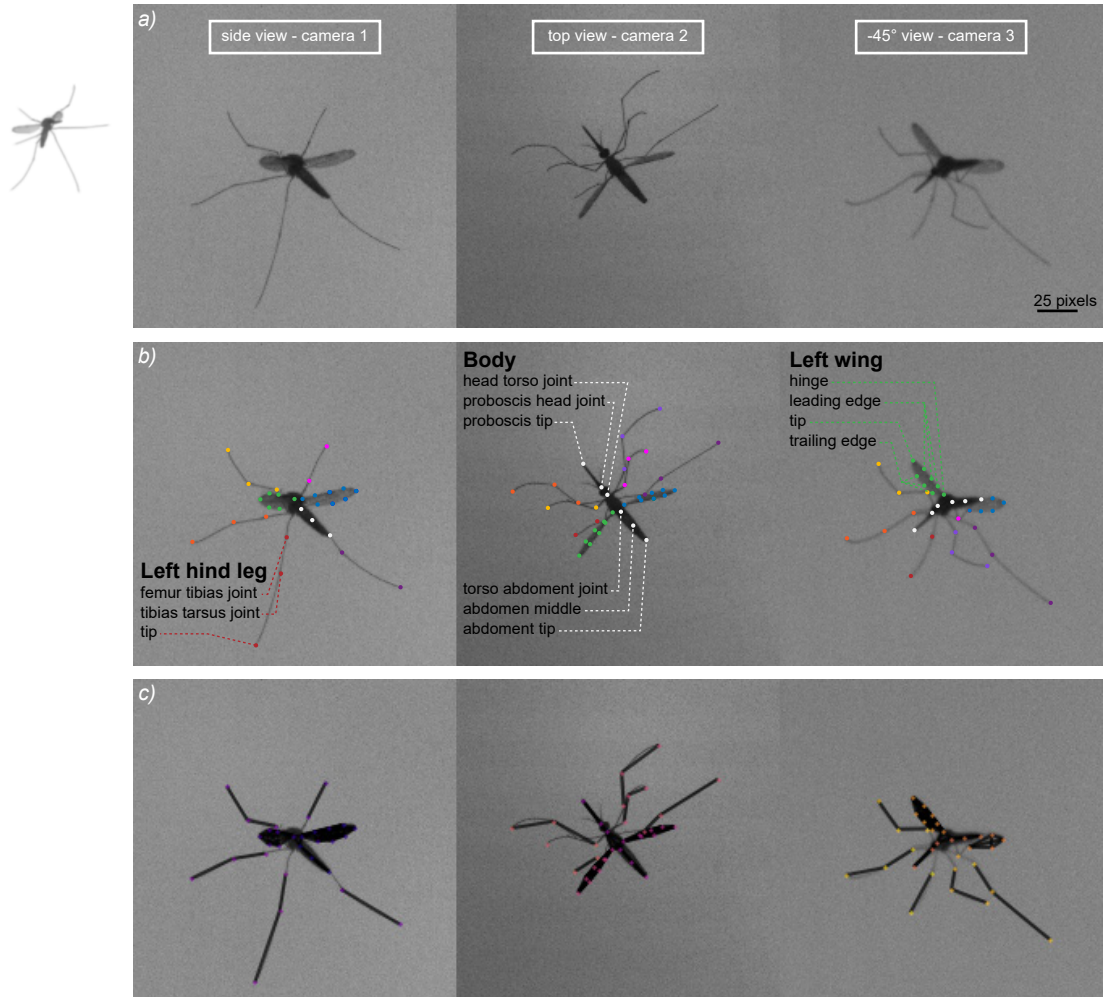
Figure S5.9: DeepLabCut: Body part labels and skeleton. (*a*) Example of a video frame used in DeepLabCut for the pose estimation of body parts. (*b*) 42 body parts are labelled on each view (x3). (*c*) A skeleton linking the various body parts is defined in DeepLabCut to improve tracking accuracy.
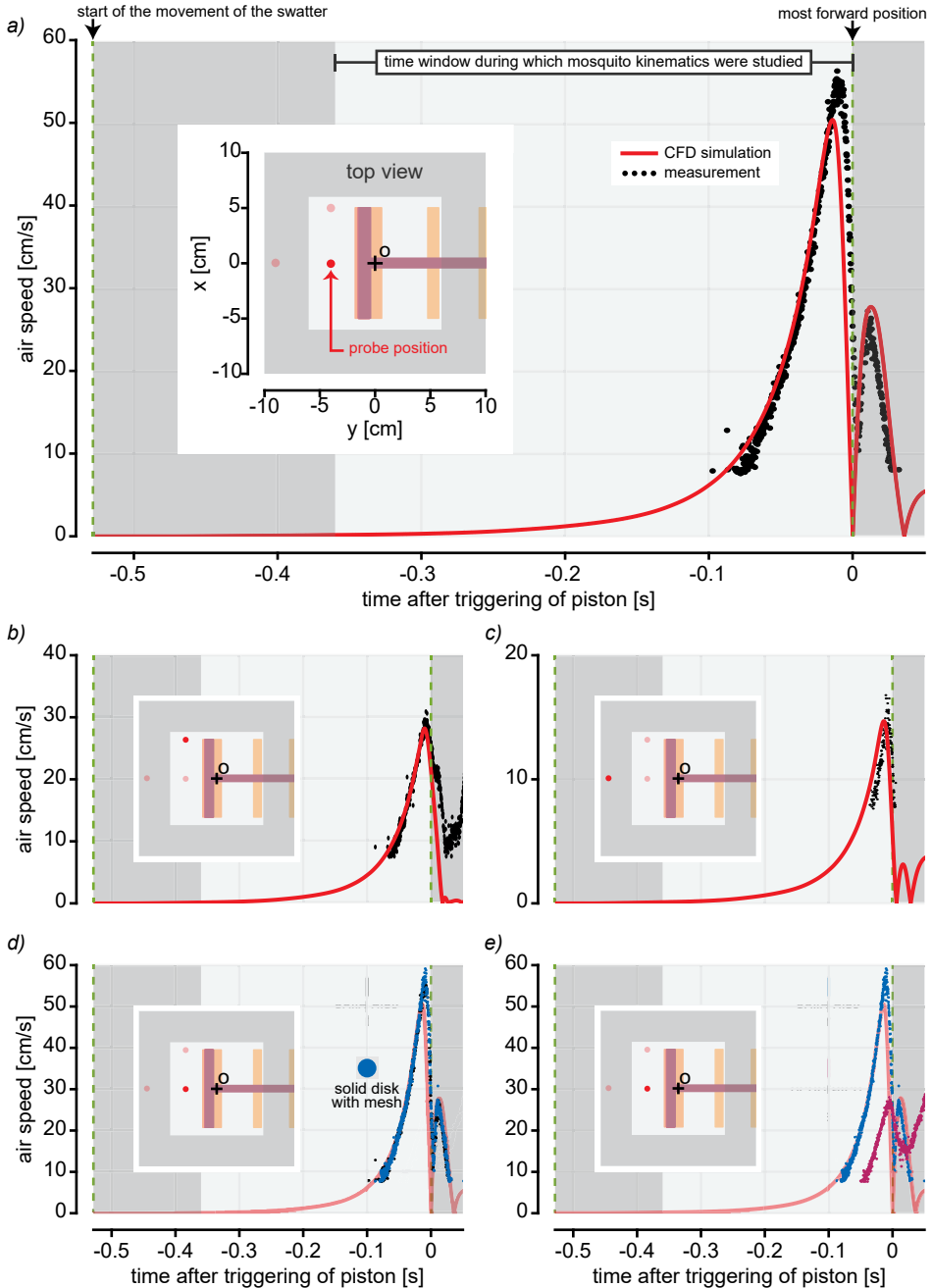
Figure S5.10: CFD simulation validation. (*a-c*) Comparison between the Computer Fluid Dynamic (CFD) simulation results and the hotwire measurements at three different probe position in from of the swatter with the full disk with mesh. (*d,e*) Comparison between hotwire measurements with the three different disk type: the solid disk with or without a mesh, and the perforated disk with a mesh (as showed Fig. S5.4).
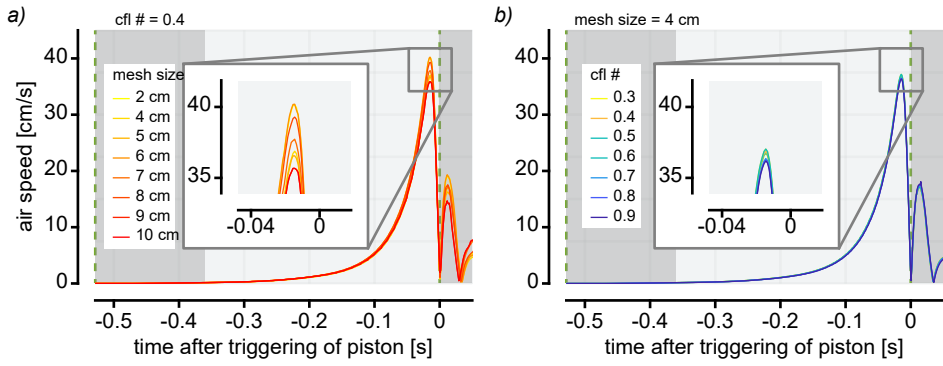
Figure S5.11: Mesh and CFL study. (*a,b*) Comparison between airflow speed from CFD simulation with various mesh sizes or various cfl (Courant–Friedrichs–Lewy) numbers at the same probe position as in supplementary Fig. S5.10*a*).
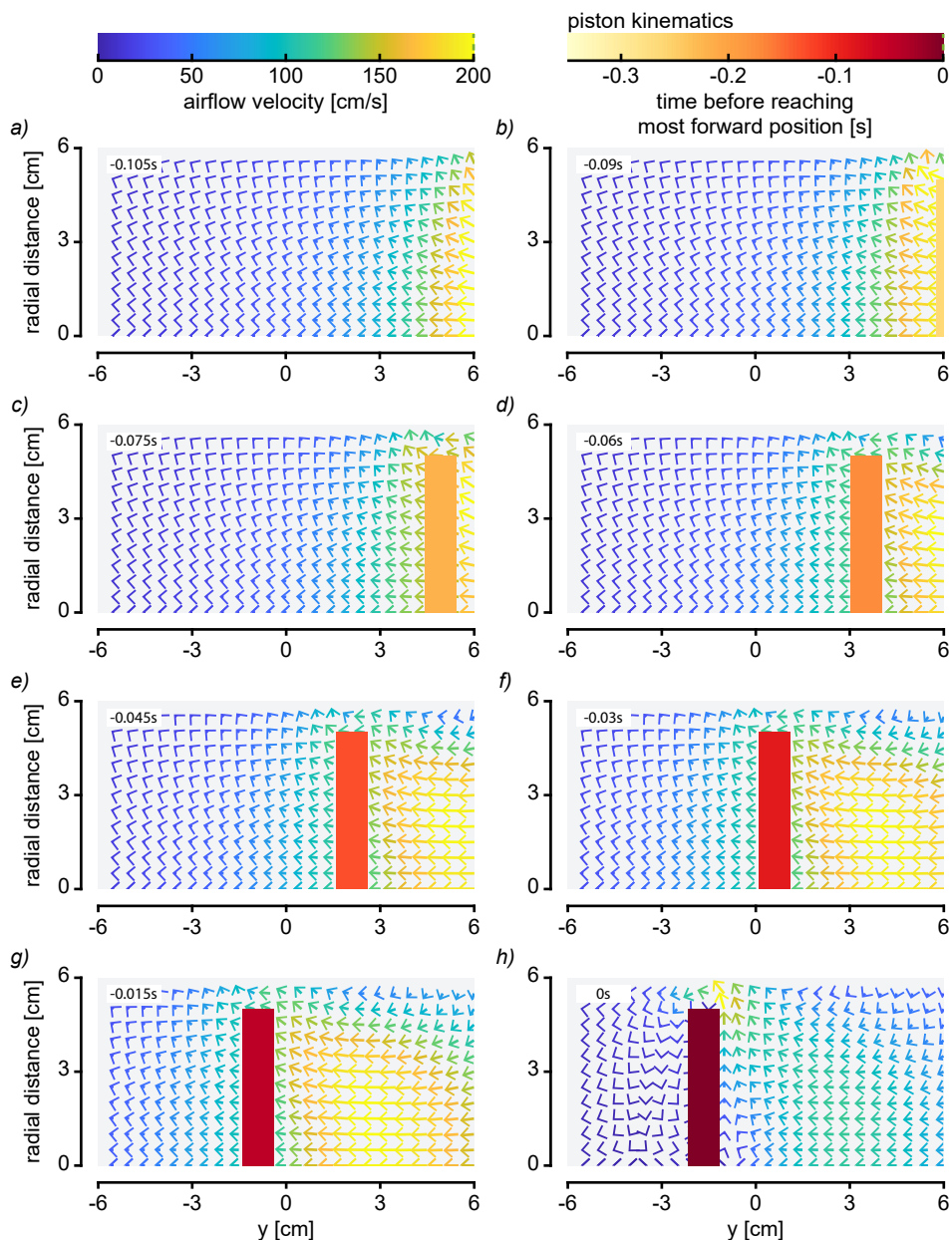
Figure S5.12: Simulated airflow velocity field. (*a-h*) Airflow velocity field from the CFD simulation used in the study. Because the results are following the axial symmetry of the swatter (around *y* axis), the three-dimensional airflow can be projected into two-dimensional planes. The air is both pushed and pulled by the swatter towards the left, where a mosquito was predicted to be.
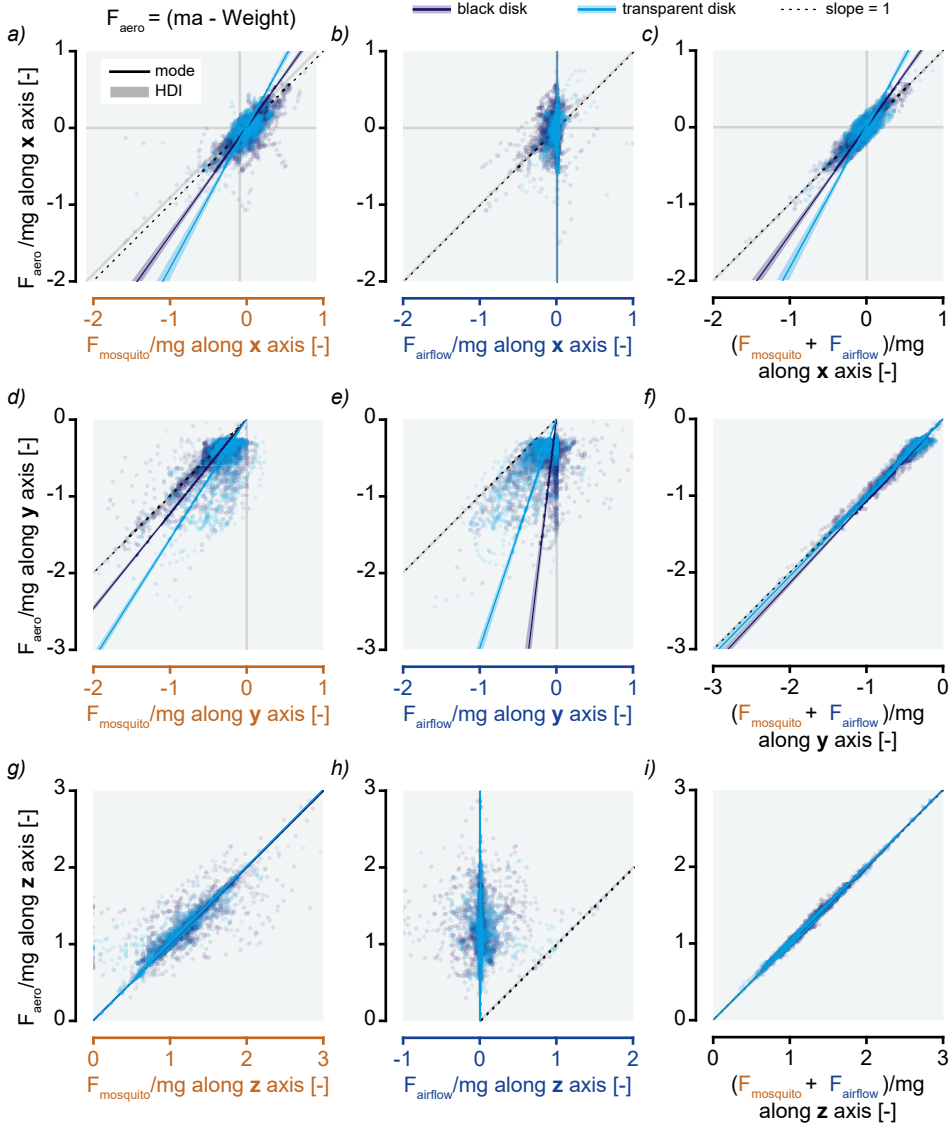
Figure S5.13: Proportion of $\vec{F}_{aero}$ explained by $\vec{F}_{mosquito}$ or $\vec{F}_{airflow}$. $(a\text{-}i)$ $\vec{F}_{aero}$ $(= m \cdot \vec{a} - m \cdot \vec{g})$ in function of estimated $\vec{F}_{mosquito}$ or $\vec{F}_{airflow}$ for the transparent and black disks. Linear fits have been estimated using Bayesian estimations of the means of the proportion between $\vec{F}_{aero}$ and the corresponding forces in ordinate.
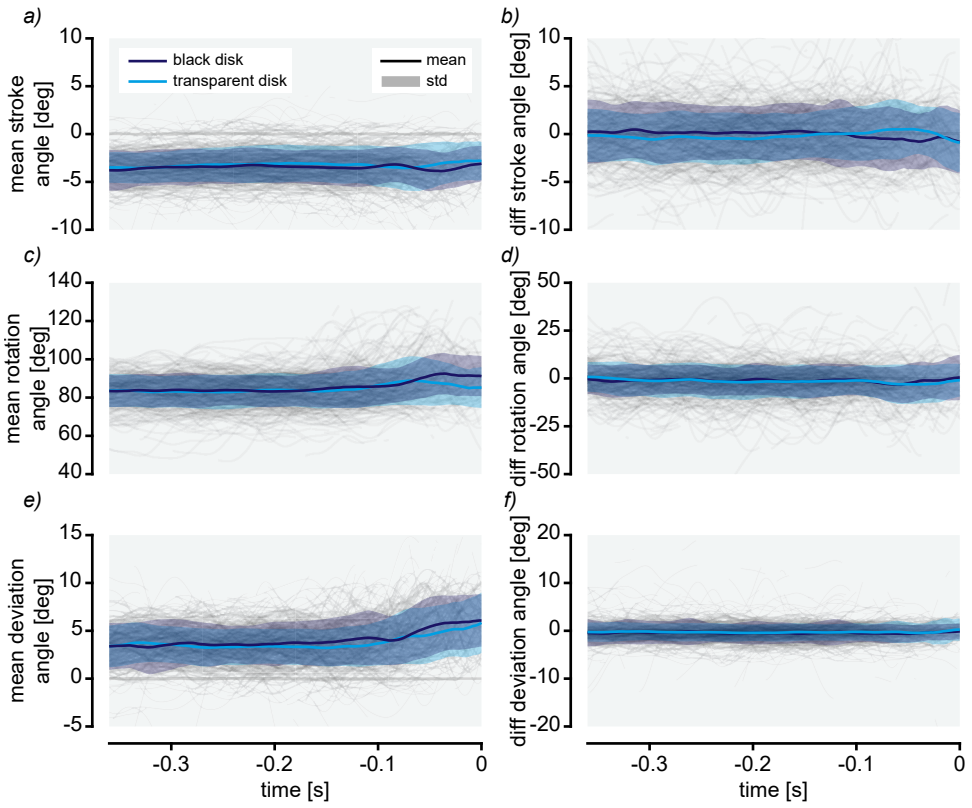
Figure S5.14: Wing angles. (*a,c,e*) wingbeat average of the mean both wings of the three wing angles during all the manoeuvres: stroke angle, rotation angle and deviation angle. (*b,d,f*) wingbeat average of the difference between the right and the left wings of the three wing angles during all the manoeuvres.

References

Mathis, A., Mamidanna, P., Cury, K. M., Abe, T., Murthy, V. N., Mathis, M. W. and Bethge, M. (2018). DeepLabCut: markerless pose estimation of user-defined body parts with deep learning. *Nat. Neurosci.* **21**, 1281–1289.

Sharpe, L. T., Stockman, A., Jagla, W. and Jaägle, H. (2005). A luminous efficiency function, V*(λ), for daylight adaptation. *J. Vis.* **5**, 948–968.

Chapter 6
General discussion

In this thesis, I aimed to contribute to our understanding of how flying insects behave in the vicinity of vertebrates, and in particular how haematophagous mosquitoes interact with their blood hosts. I did this by investigating two behaviours that are crucial for reproduction and the spreading of diseases: how mosquitoes host seek, detect, and react to short-range cues indicating human presence and how mosquitoes escape from a looming threat.

In chapter 2, I visualized the flight behaviours of mosquitoes in the close vicinity of an odour-baited trap. I compared the average flight dynamics of flying mosquitoes around a trap in a hanging or standing orientation to represent two widely used traps. I elucidated how mosquitoes reacted to these traps and how that affected their approach or capture. We found that mosquitoes approached the traps by flying downward and exhibited upward acceleration when close to the capture zone of each trap.

Based on these results and on literature, we developed a new trap that implements additional short-range cues, the M-Tego. As described in chapter 3, we tested this trap in the laboratory and in semi-field conditions as well as with- or without these short-range cues. By systematically comparing the M-Tego capture performances and visualizing mosquito flight behaviours around it, I could show why mosquitoes were much more likely to be captured by this new trap when it produced heat and humidity in addition to the odour bait.

Although we did observe evasive manoeuvres above the trap inlet in chapter 2, escape manoeuvres of flying mosquitoes had never been the subject of a dedicated study. Therefore, in the second part of this thesis, I investigated these escape manoeuvres. In chapter 3, I investigated whether diurnal and nocturnal mosquitoes had different escape strategies and whether those changed with the light conditions they flew in. We found that both day- and night-active mosquitoes were performing best at their respective natural light condition (i.e. when active). Interestingly, they did so by using opposite strategies: with night-active *Anopheles* mosquitoes relied most on their hard-to-predict flight path in the dark; whereas day-active *Aedes* mosquitoes relied more on their escape performances in overcast light conditions.

Finally, in chapter 5,, I studied in detail the flight kinematics of night-active mosquitoes while they performed escape manoeuvres. I estimated the aerodynamic force generated by mosquitoes as well as those induced by a mechanical swatter. By comparing these, I could show that mosquitoes are mostly contributing actively to their escapes, but also that the passive effect of the swatter-induced airflow cannot be neglected.

In this general discussion, I first place these results into a broader context of mosquito interactions with vertebrates. Because the research chapters of this thesis focused on anthropophilic mosquitoes, I will mostly discuss mosquitoes' interactions with humans. First, I summarize some of our findings on mosquito flight behaviour and I address how these findings inform us about the attractive and disruptive cues that flying mosquitoes use to navigate and to control their flight. Additionally, I discuss how the knowledge we

gained on the escape manoeuvres of mosquitoes inform us about insect flight. I address the technical aspect of our work by discussing the strengths and limits of the methods I used, as well as the chosen general approach for the analysis of our data. Then, I highlight what are, in my opinion, the next research questions to tackle on these topics. I address how other flight behaviours of mosquitoes could benefit from studies like the one presented in this thesis. I propose new directions concerning analysis methods that could be used for future research on insect flight. Finally, I discuss the difficulties and advantages of laboratory experiments and how well these results can translate to the field. Also, I propose a few ideas on how our findings could be used for the improvement of vector control tools.

6.1 The interaction of mosquitoes with vertebrates

Most female mosquitoes need a blood meal to be able to develop their eggs, and consequently must seek a vertebrate host. For this, mosquitoes need to detect CO_2 and volatiles that signal the presence of a nearby host upwind (Cardé, 2015; Cardé et al., 2010). Then, a flying mosquito will rely on its cast and surge behaviour, as well as on visual cues to find the source of the odour plume (van Breugel et al., 2015; Vinauger et al., 2019). Up until this point, the host-seeking flight behaviour of mosquitoes has been studied extensively, most often in wind-tunnel experiments (van Breugel et al., 2015; Cooperband and Cardé, 2006b; Hawkes and Gibson, 2016; Kennedy, 1940; Spitzen et al., 2013). Then, the mosquito will use additional cues, so-called short-range cues such as heat and humidity, to decide whether and where it will land (Beeuwkes et al., 2008; Hawkes and Gibson, 2016; Howlett, 1910). The importance of these cues is also well established but the flight dynamics of mosquitoes and the role of airflow – another important cue used by mosquitoes – in close vicinity of their hosts is still relatively poorly understood.

6.1.1 Odour-baited counter-flow traps as human mimics

In this thesis, I studied the flight behaviour of mosquitoes around odour-baited counter-flow traps that imitate humans. These traps generate most of the cues that attract mosquitoes to humans, namely CO_2 (Dekker et al., 2005; Gillies, 1980; McMeniman et al., 2014), odours (Cardé, 2015; Dekker et al., 2005; van Loon et al., 2015; Verhulst et al., 2009), visual cues (van Breugel et al., 2015; Hawkes and Gibson, 2016; Vinauger et al., 2019), heat and humidity (Beeuwkes et al., 2008; Hawkes and Gibson, 2016; Howlett, 1910). Each one of these human cues has been shown to play an important role in mosquito host seeking behaviour. Mosquitoes use all of these cues at various distances from the source, and integrate them together when host seeking (van Breugel et al., 2015; Cardé, 2015; McMeniman et al., 2014). In that way, odour-baited traps can trick mosquitoes into believing that they are flying towards blood host, and this up until the point they get captured.

Nevertheless, traps are still not as attractive as humans (Batista et al., 2018; Kenea et al., 2017; Tambwe et al., 2021; Tangena et al., 2015). Probably, multiple factors contribute to

this difference. First, the odour blends used in traps are usually a mix of no more than six compounds (Kröckel et al., 2006; van Loon et al., 2015), whereas more than 10 microbial volatile attractants have been identified (Verhulst et al., 2009). In addition, the fact that odour attractiveness can vary significantly between individuals (Qiu et al., 2006), indicates that much still has to be discovered about what makes an odour attractive to mosquitoes. One other aspect in which traps clearly differ from humans is in the visual cues they produce. Because both diurnal and nocturnal mosquitoes have been shown to use visual cues during host seeking (van Breugel et al., 2015; Hawkes and Gibson, 2016), it is also possible that mosquitoes find human visual cues more attractive than the ones of traps. All of this is in line with the fact that some mosquito preferences for odour-baited traps vary between species (Englbrecht et al., 2015; Gama et al., 2013; Lühken et al., 2014), with for example, some traps seemingly being more efficient against nocturnal mosquitoes (Batista et al., 2017; Gama et al., 2013).

Despite the difference between odour-baited traps and humans, these traps can be ideal tools to study mosquito short-range host seeking behaviour. As discussed in the general introduction, these traps can be used in highly reproducible experiments and provide a means of controlling experimental condition (by adding or removing host cues). These things are very difficult to achieve with human volunteers. One consequence of this is that recording large dataset of flight tracks is made possible using odour-baited trap in videography experiments. This was found to be particularly important in this thesis.

6.1.2 Simulating host defensive behaviour

Mosquito hosts such as birds (Darbro and Harrington, 2007; Edman et al., 1984), frogs (de Silva et al., 2020), humans (Reid et al., 2014; Walker and Edman, 1985) and other mammals (Edman and Scott, 1987; Matherne et al., 2018), exhibit various defensive behaviours to protect themselves against the biting. These defensive behaviours are very successful in reducing the persistence of mosquitoes trying to feed on a host (Walker and Edman, 1985). Additionally, these behaviours can vary significantly between species, individuals and with factors such as mosquitoes density (Darbro and Harrington, 2007; Edman and Scott, 1987). Some hosts use foot stomps, body shakes, tail swinging or even grooming to get rid of harassing mosquitoes (Darbro and Harrington, 2007; Matherne et al., 2018; Waage and Nondo, 1982). Others such as birds and frogs can also directly predate on these mosquitoes (Darbro and Harrington, 2007; Raghavendra et al., 2008). To my knowledge, there is no study that described in detail how human swat mosquitoes. Therefore, it is complicated to compare the kinematics of our mechanical swatter to such attack.

Before doing the experiments of chapter 4, we ran a preliminary experiment involving human volunteers that slapped a hanging ping-pong ball. Results from this experiment showed that the attacks speed range from around one to more than five metres per second. These attack speeds are in line with the speeds at which mammals are swinging their tail to defend themselves and of attacks from dragonflies (Lin and Leonardo, 2017; Matherne

et al., 2018). Our swatter maximum speed was around one metre per second, and therefore it simulated relatively slow attacks. Consequently, it is possible that, when attacked by faster threats, mosquitoes would exhibit different escape performances from the one we observed in this thesis. Intuitively, we could guess that mosquitoes would be hit more often in that case. However, it is possible that the passive contribution of the airflow would counterbalance the higher risk associated with such faster attacks. In addition, because the attacks induced by the swatter were unidirectional, they probably also differed significantly from more natural attacks. Nevertheless, our mechanical swatter was a suitable mimic because it induced what are probably the most important cues of an attack: airflow and visual cues.

6.1.3 What we learned about mosquito flight behaviour

Before us, the flight behaviour of mosquitoes around odour-baited traps had been studied only once by Cooperband and Carde (Cooperband and Cardé, 2006a). They showed that *Culex* mosquitoes that approached the trap exhibited low flight speeds and higher flight tortuosity, which have been associated with host-seeking behaviours (Hawkes and Gibson, 2016; Spitzen et al., 2013). In addition, they could demonstrate that odour-baited traps usually have relatively low capture efficiency (i.e. ratio between captures over approaches). In chapters 2 and 3, I confirmed these findings for *Anopheles* mosquitoes flying around the Suna or the M-Tego. Recent studies also showed similar finding for *Aedes* and *Anopheles* mosquitoes respectively flying around the BG-Sentinel and BG-Malaria (Amos et al., 2020; Batista et al., 2019). From this, one can ask the question: if traps are attractive and trigger the host-seeking of mosquitoes, why do they have low capture efficiency? A beginning of the answer was already given by Cooperband and Carde as they observed that mosquitoes were flying for a longer time around the trap with the lowest capture efficiency (Cooperband and Cardé, 2006a). They also speculated that the low capture efficiency might be the result of a lack of some host cues, or due to poor capture mechanisms of the traps. In chapters 2 and 3, we show that these hypotheses are most likely correct. By visualizing mosquito flight behaviour around traps in detail, I demonstrated that despite having good attractiveness, odour-baited traps were not always good at capturing mosquitoes. This seemed to be either caused by a lack of short-range host cues (as shown in chapter 3) or because the capture mechanism of the trap triggered upward escape manoeuvres (as suggested in chapter 2). *Anopheles* mosquitoes approached the traps by flying downward and were especially attracted to a region above and around the inlet and outlet of the traps. They also exhibited higher attractivity towards and longer flight in this region when short-range cues were present. Then, above the standing Suna trap, mosquitoes were observed to be able to escape capture by exhibiting upward acceleration. The observed fast upward manoeuvres are also in line with the manoeuvres exhibited by horse and deer flies after they encounter host cues (Thorsteinson et al., 1965; Townes, 1962). Furthermore, this is in line with our results showing that mosquitoes had the tendency of flying upward after escaping from the

swatter (see supplementary material of chapter 4). As we already discussed in chapter 2, these upward-direct manoeuvres could be a way for mosquitoes to find refuges away from terrestrial hosts such as humans.

In this thesis, I present the first studies on the escape manoeuvres of flying mosquitoes. In chapters 4 and 5, we found that mosquitoes escaped from being swatted by accelerating quickly away from the attacker. This is in line with the escape strategies of fruit flies (Muijres et al., 2014). Mosquitoes were also found to escape slightly upward, but otherwise they did not exhibit any particular escape dynamics contrary to some insects such as moths that have been shown to exhibit stereotypical escape responses such as diving (Rodríguez and Greenfield, 2004; Spangler and Hayden, 1984) or manoeuvres directed towards safety zones at the flank of the attacker (Corcoran and Conner, 2016). Additionally, mosquitoes exhibited a relatively high randomness in their directions of escape. This is also consistent with existing literature on the escape behaviour of other flying animals, because many were shown to adopt middle ground strategies between random trajectories (to maximize unpredictability (Moore et al., 2017) and escapes that are directed straight away from the threat (Domenici et al., 2011, 2008). Our findings on the escape strategies of mosquitoes are novel in another aspect. In chapter 4, we describe how the diurnal *Aedes* and nocturnal *Anopheles* mosquitoes rely on different strategies to successfully escape from a threat at their respective natural light condition. In the dark, *Anopheles* mosquitoes were shown to rely mostly on the natural unpredictability of the flight paths to escape successfully, whereas *Aedes* mosquitoes relied more on escape manoeuvrability in overcast daylight. Finally, we found that these strategies changed in function of the light condition, with for example, *Anopheles* mosquitoes relying less on their natural unpredictability and more on their escape manoeuvrability in brighter light conditions (chapter 4). These results suggest that these two mosquito species exhibit strategies that are optimized for their activity time, whereby *Aedes* relies on its detection and manoeuvre performance in the day, and *Anopheles* mosquitoes enhance their unpredictability in the night because it may be more difficult to detect a threat in the dark.

6.1.4 How attractive host-cues influence the behaviour of mosquitoes

Here, I will discuss how our findings inform us about the host-seeking behaviour of mosquitoes when flying in the presence of attractive host cues. First, by visualizing mosquito flight behaviour in a three-dimensional space (chapters 2 and 3), we confirm that mosquitoes showed a high attractiveness to synthetic blend based on human odours. In our studies, *Anopheles* mosquitoes were consistently attracted to the region near the traps where the odour concentration is expected to be highest and exhibited higher attractivity towards the traps that generated heat and/or humidity, which is also in line with previous findings (Hawkes et al., 2017; Howlett, 1910; Spitzen et al., 2013). Furthermore, our results suggest that despite the significant role played by CO_2 to trigger host seeking behaviour, mosquitoes were not particularly interested in the region where CO_2 concentrations are expected

to be the highest (e.g. near the CO_2 release point). Actually, it even seemed like mosquitoes were avoiding these regions in our experiments (as in (Spitzen et al., 2008)), maybe because such places are analogous to the human face, and therefore intrinsically more dangerous (e.g. higher chance of detection).

The role of CO_2, odours, heat and humidity on the behaviour of mosquitoes have been well studied (van Breugel et al., 2015; Cardé, 2015; McMeniman et al., 2014; Spitzen et al., 2013). However, the role of air movements on the flight behaviour of mosquitoes is less well known. Mosquitoes, like many other insects, can find the source of an odour plume by flying upwind and exhibiting cast- and surge behaviour (Cardé and Willis, 2008; Dekker and Cardé, 2011; Kennedy, 1940). This behaviour has been studied primarily in wind-tunnel experiments, where the airflow is mostly unidirectional and horizontal (van Breugel and Dickinson, 2014; van Breugel et al., 2015; Spitzen et al., 2013). These stable conditions can be quite different from natural conditions close to a host, where the airflow will be deviated by the host, and be redirected upward thanks to heat convection from the host's body. When this close to a host, a mosquito may not need the airflow anymore to find the source of the odour. However, it might still use the air movement to select a biting place, or even to detect defensive behaviour from the host (Cardé et al., 2010; McMeniman et al., 2014; Spitzen et al., 2013).

To some extent, counter-flow traps reproduce the local airflow conditions near a host (Hiscox et al., 2014), by generating an outward upward flow (in the case of upward directed traps), they simulate the heat convection currents generated by hosts (supplementary Fig. S2.7 and (Li et al., 2018)). Having said this, it is not surprising that we observed that mosquitoes approached the traps by flying downward (chapters 2 and 3), as they may have done to go "upwind" of thermal currents (Daykin, 1967). Nevertheless, we still know very little about this behaviour and about the typical airflow conditions near the hosts (Dekker et al., 1998). In particular, it is still unclear whether and how mosquitoes use thermal currents or gradients to select a landing spot. In our experiments, we did not observe any clear differences in average flight paths with or without adding heat despite the higher catching efficacy when heat was added. It is probable that the placement of the heat source combined with the complexity of the airflow generated by the M-Tego trap prevented us from detecting any such effect (chapter 3).

6.1.5   How airflow and visual cues inform mosquitoes about a threat

Counter-flow traps use rapid airflow to capture mosquitoes, and thus they generate potentially disruptive cues that seem to elicit avoidance behaviours (see chapter 2, (Amos et al., 2020; Batista et al., 2019)). The high airflow velocity regions near the Suna trap inlet, possibly combined with a lack of short-range cues, probably induced upward acceleration of flying *Anopheles* mosquitoes after approaching the traps downward. Such manoeuvres are similar to the way horse- and deer flies fly upward after inspecting visually interesting objects (Thorsteinson et al., 1965; Townes, 1962), and could be a specific behaviour of host

seeking insects that want to reduce the risk of interacting with vertebrates. Interestingly, female mosquitoes that escaped successfully from the mechanical swatter (supplementary Fig. S4.6), were also observed to flight slightly upward despite the absence of host cues. For this reason, and because mosquitoes have been shown to be able to aversively learn specific host odours (Vinauger et al., 2018), it would be particularly interesting to test whether mosquitoes exhibit higher escape performances (e.g. smaller delays and stronger accelerations) when attacked after having detected host cues (e.g. CO_2 and odours). Knowing the importance of protean behaviour in mosquitoes escaping success (chapter 4), I would be curious to see whether mosquitoes decrease their flight-path predictability in the presence of host cues.

From investigating how mosquitoes escaped from being swatted, it became clear that visual information plays an important role in this behaviour for both diurnal and nocturnal mosquitoes. First, both *Aedes* and *Anopheles* were found to exhibit higher escape accelerations when attacked in brighter light conditions (chapter 4). And secondly, the nocturnal *Anopheles* mosquitoes reacted faster when attacked by the black swatter instead of the transparent one (chapter 5). This indicates that mosquitoes rely strongly on visual information about the attack to trigger their reaction and modulate its strength even in low-light conditions. This is not entirely surprising when we consider that both species have been shown to use visual cues when host seeking (van Breugel et al., 2015; Hawkes and Gibson, 2016), and that insects can integrate visual and airflow information before exhibiting such flight behaviour (Fuller et al., 2014). Nevertheless, we found that in the dark, mosquitoes were able to successfully escape from a threat. This suggests that visual information is not always necessary in the mosquito decision-making process. In that case, it seems that only airflow cues were used to trigger an escape manoeuvre. This is particularly relevant for species such as *Anopheles coluzzii* that prefer feeding on sleeping humans.

6.1.6 *Mosquito-vertebrate interaction – Some additional perspectives*

Our findings seem to indicate that when mosquitoes interact with vertebrates, airflow can significantly affect the behaviour they will exhibit (i.e. attraction or avoidance). There is still much we do not know about how mosquitoes perceive airflow and how they react to them. Specifically, we lack information about whether and how mosquito behaviours are triggered by specific airflow characteristics such as flow directionality or speed. Therefore, fundamental studies are needed that look at these aspects; for example, to characterize the performances of mosquitoes at detecting upward or downward directed airflow, and how they react to these. Additionally, the effect of airflow turbulence (both the level and eddy sizes) on mosquito flight behaviour would also benefit from more research. Despite that this aspect of mosquito flight has probably a large impact on the behaviours of mosquitoes (Combes and Dudley, 2009; Jatta et al., 2021), our understanding about it is still very limited.

Improving our understanding of what are the specific airflow characteristics that mos-
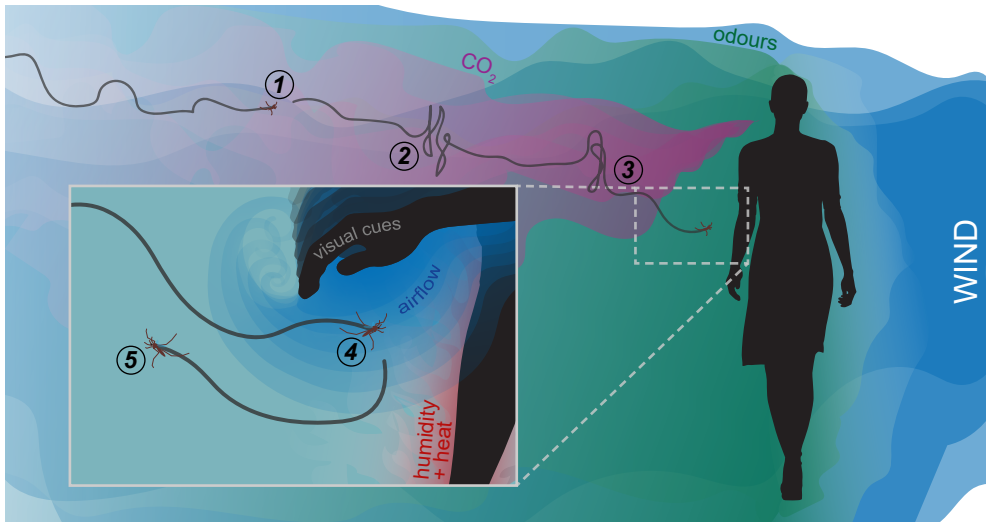
Figure 6.1: Infographic on the role of attractive and disruptive cues. Using our findings, we can update the infographic about host seeking of mosquitoes (see general introduction).**(1)** A flying female mosquito encounter CO_2 and odour plumes. **(2)** The mosquito will surge upwind and cast crosswinds to find the source. **(3)** The mosquito will inspect visually interesting objects. **(4)** If the mosquito is detected, it may be attacked. In that case, it will rely on the airflow and visual cues to detect the attack. To escape, the mosquito will actively surf the airflow, and then fly away **(5)**, and probably upwards.

quitoes used to discriminate between attractive and disruptive cues would be particularly useful for the development of vector control tools. Coupled with simulations of airflow and host cues, this information could allow us to simulate the flight behaviours of mosquitoes (e.g. using agent-based modelling (de Almeida et al., 2010; Maneerat and Daudé, 2016; Shcherbacheva et al., 2018)) in the vicinity of odour-baited traps. For this, our datasets, could prove particularly useful, as it would procure a very rich means of validating such simulations. In this way, we could test whether simulating the behaviours of mosquitoes using simple behavioural rules about mosquito attractiveness and avoidance towards cues would result in similar flight paths and activity as the ones we observed around the traps. If this was confirmed, it might even be possible to test and optimize trap designs numerically, to maximize attractiveness and use it to steer mosquitoes towards capture zones with minimum disruptive cues. Finally, trap prototypes could be built and tested in laboratory or field experiments.

6.2 Studying the capture and escape responses of mosquitoes

In this section, I will describe and discuss the research approach used in this thesis for the study of insect flight behaviour. This approach starts with the identification of insect species of which the ecology is particularly interesting. In the general introduction, I explained why haematophagous insects are a good example of an ecologically interesting group of

animals because they have to interact while flying near vertebrate hosts. To be successful in this interaction, flying insects need to detect their hosts, navigate towards them, land on them, get their blood meal and take off quickly and stealthily (Allan et al., 1987; Cardé et al., 2010; Jones and Pilitt, 1973; Lazzari, 2009; Muijres et al., 2017). This requires the capacity to detect host cues, and to integrate this information with other sensory inputs such as vision. But also, in this interaction it is possible that these blood-seeking insects will have to escape from attacks from their hosts. When exhibiting other flight behaviours such as foraging or migrating, insects will try to maximize energy efficiency. In contrast, when exhibiting escapes, flying insects will need to maximize their chance of success because the situation is a matter of life and death for them. Therefore, we can expect that the performances exhibited by insects during their escapes can inform us about the near-maximum performance of their sensory-motor flight control systems. This explains why such insect-vertebrate interactions are particularly interesting for understanding insect flight.

In this section, I will describe how I studied escape dynamics of flying mosquitoes and how escape strategies might be influenced by environmental conditions such as light intensity or by the airflow generated by an attack. For this goal, a new experimental setup had to be built. This setup had to allow the automatic triggering of an attack (by our mechanical swatter), and the automatic control of light intensity. Then, to describe the escape dynamics of mosquitoes, thousands of tracks had to be analysed using various data visualization techniques. To learn about the role of airflow and visual cues in mosquito escapes, relevant performance metrics needed to be identified and compared between experimental conditions. Finally, to learn if mosquitoes relied on the airflow to successfully escape, the aerodynamic forces involved in their manoeuvres had to be estimated.

6.2.1 The right setup to answer our questions

The second and main step of this thesis approach consist of the study of the previously selected flight behaviour, here the interaction of flying mosquitoes with vertebrates. In this step, the chosen behaviour will be quantitatively described in detail. This has to be done by recording the insect behaviour in controlled conditions and in an environment as natural as possible. For instance, this means controlling the climate condition (e.g. temperature and humidity). Often, these two goals are conflicting and therefore compromises have to be made. For example, the size of our flight arena could not be as large as an average bedroom because it would have resulted in a low number of events that could trigger an attack of the swatter (chapters 4 and 5). Dedicated experimental setups often have to be built to achieve these goals. Such setups usually incorporate many high-speed video cameras and apparatus, such as our swatter, that will lead the animal to exhibit the studied behaviour (Muijres et al., 2014; Voesenek et al., 2016). For this thesis, I build a new octagonal flight arena (chapter 4), where female mosquitoes could fly freely while being tracked in real time using five cameras. This was made possible by the low-latency tracking software (flydra) that we used to compute in real time the three-dimensional positions and velocit-

ies of mosquitoes (Straw et al., 2011). Such information was crucial to allow the automatic triggering of the mechanical swatter and could be used in many different experiments that would aim at simulating dynamic stimulus regimes. Such tracking software could also be used in combination with a virtual reality display system, which opens many possibilities for further research (Stowers et al., 2017). In our case, this system allowed experiments to be run automatically and necessitate less than an hour of human work per day. As a consequence, thousands of triggering events could be recorded in our experiments, whereas it remains relatively rare that more than a hundred of events are recorded in similar studies (Dawson et al., 2004; Muijres et al., 2014; Voesenek et al., 2016).

6.2.2 Analysing thousands of flight tracks

After running experiments, one can visualize the flight dynamics of the insects when exhibiting the behaviour of interest. That was done in this thesis by computing the average flight position, speed and acceleration of mosquitoes over time. The large amount of recorded flight tracks was key for describing in detail the average flight behaviour of mosquitoes. For example, visualizing their average flight dynamics using two-dimensional heat-maps or vector fields (chapters 2 and 3), requires to reach a minimum density of tracks in all regions of interest. Achieving this can be particularly challenging because mosquitoes do not have a uniform positional likelihood. When visualizing the average flight behaviour of mosquitoes, I partially ignored the fact that individual mosquitoes will only rarely follow closely their average flight paths. This kind of behavioural stochasticity is to be expected in animal experiments, but it should be addressed; for example, by visualizing the mean standard deviations of the metrics of interests (as in chapter 2, Supplementary Material). In chapter 4, we showed that such behavioural stochasticity or unpredictability was explaining the great majority of the escapes of mosquitoes. In addition to dynamic quantities such as flight speed, I used several other metrics to describe the average flight behaviour of mosquitoes such as the positional likelihood, capture probability and mean time spent in a region. When united with three-dimensional information about available cues (e.g. heat and airflow), all of these quantities could lead to a deeper understanding about how mosquitoes behave near vertebrates and why.

To a certain extent, recording thousands of mosquito flight tracks also allowed to use advanced statistical modelling. In chapters 4 and 5, I used Hidden Markov models to estimate in which of several states, such as cruising or escaping, mosquitoes were in at each instant in time. These models are particularly powerful for analysing dynamic processes as they can inform us about unobservable states only via the observation of one or more state variables. Except from the number of states, all the model parameters can be learned from the available set of sequences using maximum-likelihood estimation (e.g. Baum-Welch algorithm). Hidden Markov models could also be used to estimate whether and when mosquitoes are host-seeking only by looking at their linear and angular flight speeds. Thus, it could be an additional tool to understand when (and therefore why) mosquitoes are attrac-

ted or repulsed by the sensory information induced by traps. In chapters 4 and 5, Bayesian statistics were used instead of the more common frequentist statistics. I detailed this choice in the materials and methods of chapter 4, but here I would like to emphasize two important aspects of the way I used Bayesian statistics. First, because Bayesian statistics is about estimating the distribution of the variable of interest (Efron, 2013), using Bayesian statistics permitted the creation of information-rich figures. This is important as it allows readers to easily visualize and therefore apprehend results (Tufte, 1988). Secondly, Bayesian statistics offer at least one intuitive way of testing hypotheses with good confidence. When analysing large datasets, it becomes more and more likely to find significant results with low effect size. As a consequence, we also have to estimate such effect size before making any conclusion about the importance of any statistical result. In Bayesian statistics we can simply use the "HDI+ROPE decision rule" to both test significance and check whether the parameters have a high enough effect size to be taken into consideration (Kruschke and Liddell, 2018). By using standardized effect sizes, this decision rule also allows clear comparisons between the effect of the various estimated parameters.

6.2.3 From body motion to forces

In biomechanics studies, inverse dynamics is very often used (Bode-Oke et al., 2018; Fry et al., 2005; Liu and Sun, 2008; Muijres et al., 2017, 2014; Voesenek et al., 2019; Zeyghami et al., 2016), to derives the forces and torques applied to a body from measured body kinematics. For flying insects, this technique most often comes down first to measure body positions to compute the acceleration $\overrightarrow{a}$ of the insect, and therefore to estimate its inertia ($= mass \cdot \overrightarrow{a}$). And second, to estimate the aerodynamic force generated by the wings of the insect ($= \overrightarrow{F}_{wings}$). The simplest case is when no other sources of external force are present (e.g. the insect is hovering in still air), and thus when the inertia equals the gravity plus the aerodynamic force generated by the insect ($\overrightarrow{F}_{wings} = m \cdot \overrightarrow{a} - m \cdot \overrightarrow{g}$). In that case, the wing force can be simply estimated from the computed inertia and the know gravity force $\overrightarrow{g}$. However, in many cases there is at least one additional force that has to be taken into account. In the case of mosquitoes taking-off, it is the force produced by their legs ($\overrightarrow{F}_{wings} + \overrightarrow{F}_{legs} = m \cdot \overrightarrow{a} - m \cdot \overrightarrow{g}$) (Muijres et al., 2017). And in the case of mosquito escape responses to our mechanical swatter, this additional force is the aerodynamic force induced by the airflow on the body of mosquitoes ($\overrightarrow{F}_{wings} + \overrightarrow{F}_{airflow} = m \cdot \overrightarrow{a} - m \cdot \overrightarrow{g}$ in chapter 5). In those cases, the unknown forces can usually be estimated using airflow simulations (Bode-Oke et al., 2018; Liu and Sun, 2008; Veen and van Veen, 2020) or using models (Muijres et al., 2017; Zeyghami et al., 2016).

Estimating aerodynamic forces using simulations or models most often require to measure the kinematics of the body and wings of the flying insect (Fry et al., 2005; Liu and Sun, 2008; Muijres et al., 2017). For that, one can use manual tracking, but insects flap their wings at high wingbeat frequencies and therefore tracking the position of their wings can

become very cumbersome. An alternative is to use automatic tracking software such as the one developed by Fontaine et al. which was used to track escaping fruit flies and mosquitoes taking off (Fontaine et al., 2009; Muijres et al., 2017, 2014). However, to give good tracking accuracy such software most often relies on a homogeneous background and on high-resolution images (Fontaine et al., 2009; Ristroph et al., 2009). These prerequisites were particularly difficult to meet when recording the escapes of mosquitoes (chapter 5). This is because we had to film a relatively large volume (approximately 12x12x12 cm) in order to capture entire escape manoeuvres, and because recording at 12500 fps meant that it was challenging to illuminate the manoeuvres with enough infrared light for the image quality to be high. As such, I decided to develop my own mosquito posture tracker based on Deeplabcut, a markerless pose estimation software using deep neural networks and capable of reaching human tracking accuracy (Mathis et al., 2018). This software was the first to allow the training of a deep neural network for specific animal tracking tasks (e.g. tracking the body part of a flying mosquito) and using a relatively low number of labelled images. This is made possible by the fact that Deeplabcut is using transfer learning, where a network previously trained with many thousands of labelled images can be retrained with a much smaller set of newly labelled images. Additionally, such deep neural networks can deal very well with low-resolution images and complex backgrounds (Mathis et al., 2018). In this way, I needed only 230 manually labelled images to train a network capable of automatically tracking the two-dimensional positions of the body and wings of mosquitoes in almost 800 manoeuvres each comprising of around 5000 images. The final step consisted in fitting a three-dimensional model of a flying mosquito to the two-dimensional coordinates from Deeplabcut. This step was performed by my tracker and allowed the estimation of the body and wing angles during the manoeuvres. Such tracking system could be used in many diverse situations such as in field experiments where other trackers are limited. And also when multiple animals are filmed together, or even potentially to estimate body kinematics in real time (Mathis et al., 2018).

After estimating the body and wing kinematics of mosquitoes, we can compute the aerodynamic forces involved in the manoeuvres. For that, one can use CFD simulations where the airflow around the flying insect is entirely simulated. If previously validated, such simulations are a very powerful means of studying flight manoeuvres. They provide detailed information about the flow, and consequently, they can be used to compute precisely the aerodynamic forces and torques applied to the insect body. However, in chapter 5, I deem such simulations to be too expensive and time consuming to be used on the almost 100,000 wingbeats recorded, which is more than 2 orders of magnitude the number of wingbeats simulated in recent studies on mosquitoes (Bomphrey et al., 2017; Veen and van Veen, 2020). One solution to that problem would have been to manually select a subset of typical manoeuvres to be simulated. However this might have introduced a selection bias in our analysis. Another solution would have been to use Fourier series to parameterize each wingbeat and then to generate one or a few average manoeuvres (Muijres et al., 2014). This solution would also have the advantage to greatly reduce the number of man-

oeuvres to simulate, but here at the cost of losing the diversity of the manoeuvres exhibited by mosquitoes. Another possible way to compute the aerodynamic force generated by the mosquitoes would have been to use a quasi-steady model. This kind of model is based on the partially false assumption that the flow around the wings is not affected by its history. Such model has been used both for reaching a better understanding of the aerodynamic mechanisms involved in force production by flapping wings and for prediction purposes (Muijres et al., 2017; Sane, 2003; Veen and van Veen, 2020). However, their predicting capacities have often been criticized, especially when they are used outside of the parametric space in which they have been conceived (Ellington, 1984; Veen and van Veen, 2020). These models are often based on the wing kinematics of hovering insects, and therefore it is likely that these models will yield deficient results when applied to the kinematics of quickly manoeuvring insects.

In chapter 5, I estimated the two aerodynamic forces involved in mosquito escapes using a novel approach. This approach assumes that we can predict the direction of these aerodynamic forces from the body orientation of the mosquitoes and from a computational fluid dynamic (CFD) simulation of the airflow (see chapter 5 for a detailed discussion about the assumption). This was made possible by the finding that the helicopter model can be applied to escaping mosquitoes, meaning that they mostly keep their aerodynamic force vector fixed in their body reference frame. Thus, *Anopheles* mosquitoes were both pitching and rolling their body away from the swatter during the attacks while keeping their wing kinematics relatively constant through the manoeuvres. In this way, the directions of the two aerodynamic force vectors ($\overrightarrow{F}_{wings} + \overrightarrow{F}_{airflow}$) were known, and therefore we could estimate the magnitude of these forces using a least-square optimization algorithm. This led to the discovery that these nocturnal mosquitoes were using the airflow passively and actively to successfully escape. Finally, this also permitted to quantify how much these mosquitoes were relying on visual cues during these escape manoeuvres.

6.2.4 Quantifying flight performance to understand perception

The final step of this thesis approach for the study of the flight of mosquitoes consisted of the quantification of their performances, and then of the comparison of these performances between distinct experimental conditions. in chapters 2 and 3, I did this by comparing the performances of traps in a hanging or standing orientation, as well as with or without host cues. Performance of the traps were then quantified using metrics such as the capture rate or the time spend and positional likelihood of mosquitoes. in chapters 4 and 5, I compared the escape performances of mosquitoes when attacked in various light conditions or by different types of swatter to vary the induced cues. For this, I compared mosquitoes' collision probabilities, unpredictability or initial dynamics. By making such comparisons of the performances of mosquitoes in free flight and with varying sensory cues, we could learn about how mosquitoes rely on those cues for flight control and navigation. For instance, the differences that we observed in the escape strategies of diurnal and nocturnal

mosquitoes may teach us about the performance of the neuro-sensory system and muscular system of these animals (Card, 2012; Dakin et al., 2018). Our results indicate that diurnal *Aedes* mosquitoes are better at detecting and reacting to visual cues than *Anopheles* mosquitoes. But also, that *Anopheles* mosquitoes must rely on a protean strategy that is probably energetically costlier than the strategy of *Aedes* mosquitoes. One important way of quantifying the performances of the neuro-sensory system of escaping animals is to compute their neural and biomechanical delays (Liu and Cheng, 2017; Muijres et al., 2014). Sadly, this was not possible in chapters 4 and 5, because we did not know exactly when the sensory information was detected, and when active manoeuvres were started. Therefore, further research would need to be done, maybe using tethered animals, to complete our free-flight measurements. Finally, much could still be learned by doing similar studies on other insect species, and specifically on dipterans to compare the performance of closely related species. As for hummingbirds (Dakin et al., 2018), such comparison would probably yield interesting insight in the evolution of specific morphological traits and their link to ecology of these species.

6.2.5 Flight dynamics of mosquitoes – additional perspectives

Here I will discuss the perspectives that I am the most excited about for the research on the flight dynamics of mosquitoes. Recently, several studies addressed the flight behaviour of mosquitoes around traps (chapters 2 and 3, (Amos et al., 2020; Batista et al., 2019)). I hope this trend will continue in the following years, as I believe such studies can accelerate the development of such tools (more about that in section 3.). I also hope that similar studies will become more common for deepening our understanding of mosquito flight behaviours around other vector tools such as bed nets or "improved" houses. These subjects have been already investigated in the past (Jones et al., 2021; Parker et al., 2015; Spitzen et al., 2016; Sutcliffe and Colborn, 2015; Sutcliffe and Yin, 2014). However, the three-dimensional aspect of their flight behaviour has often been ignored. And important metrics such as positional likelihood and time spent were rarely computed and visualized over the studied space. In addition, some of the already identified behaviours should be further studied. For instance, mosquitoes were observed to "dip" or "bounce" when flying near to bed nets or other surfaces in the presence of host cues (Hawkes and Gibson, 2016; Parker et al., 2015). This behaviour might be used to probe cues such as heat and humidity when mosquitoes are close to surfaces and then to "taste" the surface using their legs before landing (Bougatsia, 2021; Dennis et al., 2019). Consequently I would be particularly interested in learning more about this particular behaviour, and to see whether some characteristics of these cues trigger the landing or the flying away of mosquitoes (Fig. 6.2*a*).

There is still much we don't know about the escape behaviour of mosquitoes and there are many ways it could be investigated further. For example, one possible approach would be to map the behaviours of mosquitoes when manoeuvring using t-distributed stochastic neighbour embedding (t-SNE) (Berman et al., 2014; van Der Maaten and Hinton, 2008).

Such method models high-dimensionality problems by a two- or three-dimensional map and then use clustering to identify stereotypical behaviours. For that, one needs a large data dataset with high dimensionality such as ours describing in detail the kinematics of manoeuvring mosquitoes (in chapter 5). Our understanding of mosquito escapes would also greatly benefit from more research on the passive effects of the airflow on the body rotation of mosquitoes during escapes. To study this, one would need to correlate the wing kinematics of mosquitoes and the airflow induced by the attacker to the rotations of their body (Muijres et al., 2014). This could be done using CFD simulations to compute aerodynamic torques involved in the manoeuvres. In addition, tethered experiments with mosquitoes could be done to further investigate the role of disruptive cues on the escape of mosquitoes and how mosquitoes use their neuromuscular system to control their manoeuvres (Mamiya and Dickinson, 2015; Robie et al., 2017; Tammero and Dickinson, 2002). Ultimately, one could use control theory and system identification techniques to model mosquito dynamic systems (Dickinson and Muijres, 2016; Rohrseitz and Fry, 2011; Taylor et al., 2008). This could allow one to learn about how mosquitoes control their manoeuvres, and would probably yield interesting comparison with other insects species such as fruit flies.

Finally, the research approach of this thesis could be applied to the study of many mosquito flight behaviours throughout their life cycle that are still poorly understood such as landing (Fig. 6.2*a* (Smith et al., 2020)). Such approach would fit particularly the study of behaviours when mosquitoes have to exhibit high performances such as when they get hit by a threat or (Fig. 6.2*b*) when they mate in-flight (Fig. 6.2*c*).
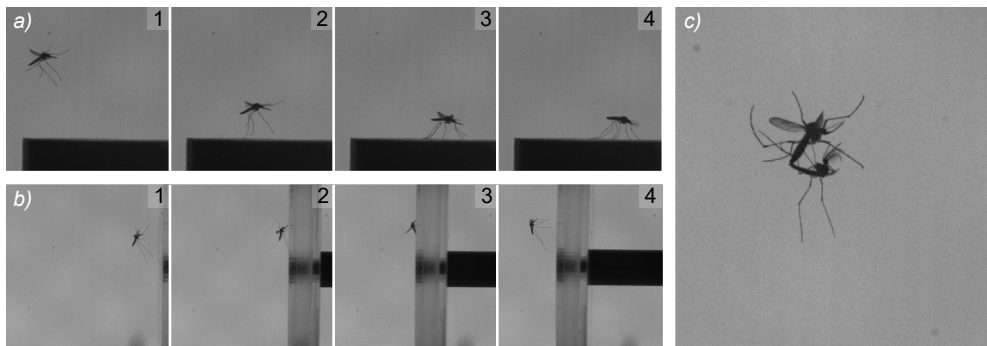
Figure 6.2: Examples of interesting flight behaviour that remains to be studied. (*a*) Images showing the landing of a host-seeking mosquito. (*b*) Images showing a collision between a flying mosquito and our mechanical swatter, the mosquito seems to mitigate the collision using her legs (Smith et al., 2020). (*c*) A female (top) and a male mosquito (bottom with hairy antennae) mating while flying. Unpublished data that was collected using the same or a very similar experiment setup as in chapters 4 and 5.

6.3 From fundamental research towards application

6.3.1 Developing an improved mosquito trap

Odour-baited traps are highly attractive to host-seeking mosquitoes. However, they have a relatively low capture efficiency (chapter 2 and (Cooperband and Cardé, 2006a)). From this observation, I decided to investigate how these traps, in particular counter-flow traps, could be improved. Thanks to our findings in chapter 2, I identified three important aspects which govern overall efficacy of traps:

1. The attraction efficacy of the trap, expressed by the ratio between the number of mosquitoes that approach the trap over the number of mosquitoes in the population (e.g. released).

2. The residence time of mosquitoes around the trap, as longer residence time can lead to a larger chance of being captured.

3. The capture efficiency defined as the proportion of approaching mosquitoes that get caught.

To improve an odour-baited trap, the redesign should aim to optimize all these aspects. How well a trap will perform at each one of these aspects is somewhat dependent on experimental conditions, namely the size of the volume-of-interest around the trap and the accuracy of the videography system used. This is because it is usually impossible to keep track of individuals – they can be counted multiple times. Thus, to quantitatively compare these aspects, it is best to use very similar experimental setups. In addition, identifying which of these aspects might explain the overall efficacy can be difficult without estimating all of them. This is because traps that have similar overall trapping efficacy may perform very differently at each one of these aspects. As an example, in chapter 2 I found that the standing trap was exhibiting higher attractiveness but lower capture efficiency than the hanging trap. Therefore, improving the design of odour-baited trap requires testing novel trap designs in lab conditions:

- Systematically, to make sure that we can compare trap capture performances.

- Iteratively, by testing one single design idea at a time, to identify what works and what does not.

In chapter 2, the standing Suna trap captured more *Anopheles coluzzii* mosquitoes when standing than when hanging (i.e. it's default orientation), and therefore we choose to use the standing trap as our baseline for the design of an improved trap. Also in chapter 2, mosquitoes were found to exhibit looping behaviour above the trap, which resulted in

them staying longer there. Because of this, we decided to focus on improving the two other aspects which govern overall efficacy of traps: the capture mechanism and the attractiveness of the trap. To improve the capture efficiency of the trap, we thought of modifying its design (e.g. shape and size) either by constraining the escape routes of mosquitoes (chapter 2 and (Bracken and Thorsteinson, 1965)), or by altering the airflow generated by the trap and reduce disruptive cues. And, to increase trap attractiveness and convince mosquitoes to fly closer to the trap inlet, we thought of adding short-range cues (heat and humidity) (Hawkes et al., 2017; Kline and Lemire, 1995; McMeniman et al., 2014; Spitzen et al., 2013). All other characteristics of the trap (e.g. the fan and odour blend) were conserved at this point. Prototypes were then built and tested against the standing Suna trap in dual choice experiments (Fig. 6.3*b,c*). Results from these experiments were not very conclusive concerning the various shape modifications that we tested. However, the addition of short-range cues was quickly identified as being promising. From this, a new trap prototype was designed, the first M-Tego (Fig. 6.3*d*). In addition to the fact that the M-Tego prototype was able to generate heat and humidity, it was foldable and smaller than the Suna trap. It also had an inlet module with an improved catch bag (supplementary Fig. S3.1, (Fairbairn, 2018)). All these design characteristics have little to no impact on capture efficacy of the trap, but can significantly improve the ease-of-use of the trap in the field.

Then, we tested how this new trap, the M-Tego prototype, was performing against the Suna trap (chapter 3). We found that the capture performance of the trap increased significantly when it generated heat or humidity. But also, the M-Tego prototype without additional cues was found to capture more than twice as many mosquitoes than the standing Suna trap. The data suggests that this is because mosquitoes are not exhibiting upward escape manoeuvres above the M-Tego, probably because of altered airflow conditions. This finding highlights the importance of studying the flight behaviours of mosquitoes around traps to improve their design. In the past, new odour-baited traps have been mostly developed using an iterative process where new traps are tested (e.g. in dual-choice experiments) against older traps (Gama et al., 2013; Hiscox et al., 2014; Verhulst et al., 2015). However, without recording the flight of mosquitoes around the trap, it would have been difficult to make a hypothesis concerning why the M-Tego captured much more mosquitoes than the Suna trap even without additional host cues. Consequently, trap development can be significantly accelerated by such detailed behavioural study. And therefore, it is encouraging that more and more studies looking at mosquito flight behaviours around traps are being published (Amos et al., 2020; Batista et al., 2019).
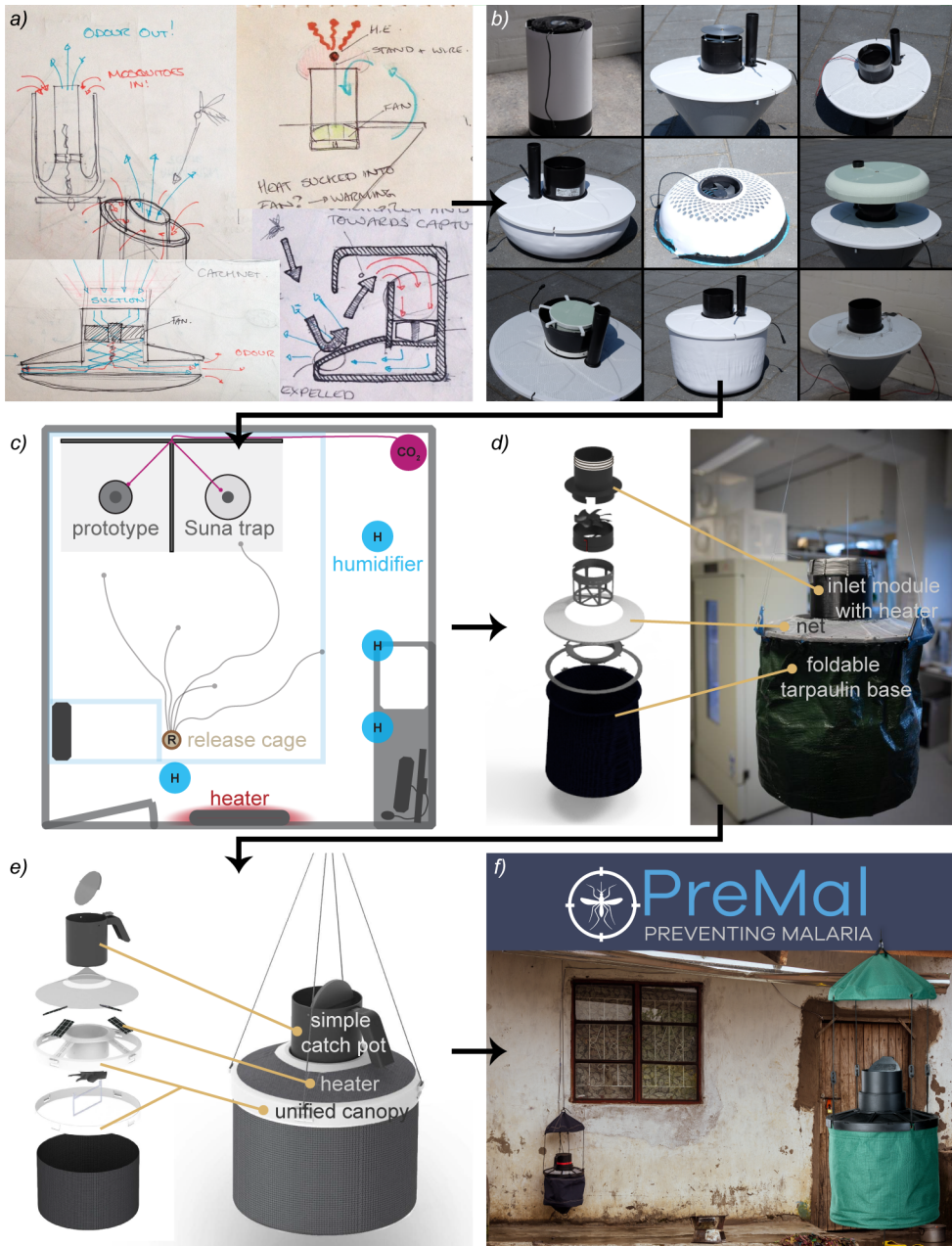
Figure 6.3: The development of the M-Tego. After discovering that counter-flow traps had low capture efficiency, the M-Tego trap was developed. (*a*) Many design ideas were put on paper. (*b*) Nine prototypes were built in order to test the most promising ideas. (*c*) The prototypes were tested against the standing Suna trap in dual-choice experiments. (*d*) A new trap, the M-Tego, was designed and a first prototype was built. This is the prototype that was tested in chapter 3 (Fairbairn, 2018). (*e*) A second version of the M-Tego was designed to make it easier to use and cheaper to build (van de Geer, 2019). (*f*) The final M-Tego was designed. It is now produced and distributed around the world by PreMal.

Now that odour-baited traps can be considered as vector control tools (Homan et al., 2016), one important aspect of trap development is to make the trap design appropriate for this goal. Most of the available odour-baited traps have been developed to be used by researchers or experts for monitoring populations of mosquitoes (Bhalala and Arias, 2009; Gama et al., 2013; Kröckel et al., 2006; Verhulst et al., 2015). However, if odour-baited traps are to be used for vector control, many aspects of their design need to be revised. For instance, odour-baited traps are often bulky (difficult to transport), not user-friendly and expensive (Fairbairn, 2018; van de Geer, 2019). For a trap to be context appropriate for vector control, it would need to be easy to set up and to maintain, cheap, durable and probably visually appealing (Fairbairn, 2018; van de Geer, 2019). One important step to achieve that is to test the trap in field conditions (van de Geer, 2019). These kinds of tests are useful both for validating results from the lab, and because it provides information about whether the trap is context appropriate. For example, after testing the M-Tego prototype in Ifakara Health Institutes (Tanzania), it was clear to us that the use of CO_2 in the field was a major constraint. This is because CO_2 cans are expensive, bulky and need to be refilled regularly. This constrains explains why there have been many studies that aimed at finding alternative ways of getting CO_2 or even a good CO_2 mimic (Kessy et al., 2020; Mboera et al., 2000; Mburu et al., 2017; Mweresa et al., 2014; Saitoh et al., 2004; Turner et al., 2011). In Tanzania, we could also identify several other aspects of the trap design that needed to be improved such as the type of material the trap was made of, or the design of the capture pot (Fig. 6.3e, (van de Geer, 2019)). These findings lead to the further design and development of the M-Tego mosquito trap (Fig. 6.3f). PreMal BV, a start-up and spin-off from Wageningen University, was co-founded by Henry Fairbairn with whom I initially developed the trap. The M-Tego is now available in several regions around the world, specifically in regions most affected by vector-borne diseases.

6.3.2 Some perspectives for the development of vector control tools

Odour-baited traps are pesticide-free tools that have great potential for vector control (Homan et al., 2016). However, there are still several important steps to take before these traps are used widely for this purpose. To maximize the trapping efficiency for reducing the incidence of mosquito-borne disease, odour-baited traps have to be integrated into the already existing prevention strategies (e.g. next to bed nets) control (Homan et al., 2016). One crucial step to make this possible at the scale of countries would be that the World Health Organisation (WHO) approved traps as being safe and effective. One key condition for such a recommendation would be to successfully show the efficiency of these traps in a second large epidemiological trial (Who, 2019). Another step towards the wide use of traps for disease prevention is to achieve production of cheap effective traps. This can be done partly through economies of scale and the redesign of trap parts. Cheap traps are necessary because countries that are the most vulnerable to mosquito-borne disease such as malaria are often amongst the poorest countries in the world. As such, governments and

households of these countries cannot afford to pay any of the traps currently on the market (van de Geer, 2019; Onwujekwe et al., 2001). I also expect that NGOs would not heavily invest in traps if their prices did not decrease significantly. Finally, counter-flow odour-baited traps need electricity to operate. However many households in rural sub-Saharan Africa are still lacking access to electricity (Blimpo and Cosgrove-Davies, 2019). Nevertheless, solar panels are becoming increasingly widespread (Gogla, 2020), and therefore this might not be a major problem in the future. In addition, distribution and maintenance of traps could even be done by the large companies that currently distribute and maintain solar panels in Africa as these two tasks requires similar competences (van de Geer, 2019).

Our findings highlight the importance of airflow as disruptive cues for mosquitoes (chapters 2, 4 and 5). Consequently, I think that the next step for improving counter-flow traps would be to optimize how mosquitoes are captured by the trap. For this goal, I would recommend simulating the airflow around the M-Tego and the Suna trap to compare it to the already known mosquito flight dynamics. Then, to rapidly test ideas, modification of the trap could be simulated in order to generate particular airflow conditions. The most interesting concept would then be built and tested in similar experiments as in chapters 2 and 3. For instance, I would be particularly interested in investigating whether it is possible to purposely trigger mosquito escape manoeuvres to make them fly towards another capture region (e.g. above the trap). I would also like to see whether the placement of the heat source can be optimized to attract mosquitoes closer to the capture region of the traps. Finally, I am very interested in testing whether changing the turbulence level and eddy sizes of the airflow generated by the trap would lead to changes in mosquito flight behaviour, and whether this could be used to improve overall capture efficacy. Other vector control tools could also benefit from our findings. For example, the fact that mosquitoes seem to escape by flying up, similarly to horse flies, might lead to the development of bed-net traps somewhat like the human-baited double net (Gao et al., 2018; Tangena et al., 2015). Such improved bed nets would use the human it protects to attract mosquitoes, and use its shape and structure to direct mosquitoes inside trapping zones in a similar way as fish traps or horse fly traps (Thorsteinson et al., 1964).

To this day, the most effective approach against mosquito-borne diseases such as malaria is to control the vector (Who, 2020). Currently, insecticide-treated bed nets and residual spraying are the most used vector control strategies globally. However, mosquitoes are becoming increasingly resistant to insecticides, and damage to the wildlife can no longer be ignored (Rehman et al., 2014; Who, 2020). Therefore, there is an increased need for new or improved vector control tools such as odour-baited traps. In this thesis, I show that studying in detail the flight behaviour of mosquitoes when interacting with host cues can lead to the improvement of such tools. I also highlight a research approach that could be used for further similar research on insect flight behaviours. When comparing new vector control tools to other non-vector-related solutions such as vaccines, one may think they have less potential for eradicating mosquito-borne pathogens. However, this ignores the

fact that most progress in the fight against these pathogens has been made using vector control, and that defeating these pathogens will require complementary strategies (Who, 2020). Additionally, the comparatively low amount of investment currently devoted to vector-control means that any small increase of investment for the understanding and development of vector-control tools has a high probability to significantly impact the fight against mosquito-borne diseases.

References

Allan, S. A., Day, J. F. and Edman, J. D. (1987). Visual ecology of biting flies. *Annu. Rev. Entomol.* **32**, 297–316.

Amos, B. A., Staunton, K. M., Ritchie, S. A. and Cardé, R. T. (2020). Attraction versus capture: Efficiency of BG-Sentinel trap under semi-field conditions and characterizing response behaviors for female Aedes aegypti (Diptera: Culicidae). *J. Med. Entomol.* .

Batista, E. P., Ngowo, H., Opiyo, M., Shubis, G. K., Meza, F. C., Siria, D. J., Eiras, A. E. and Okumu, F. O. (2018). Field evaluation of the BG-Malaria trap for monitoring malaria vectors in rural Tanzanian villages. *PLoS One* **13**, e0205358.

Batista, E. P. A., Mapua, S. A., Ngowo, H., Matowo, N. S., Melo, E. F., Paixão, K. S., Eiras, A. E. and Okumu, F. O. (2019). Videographic analysis of flight behaviours of host-seeking Anopheles arabiensis towards BG-Malaria trap. *PLoS One* **14**, e0220563.

Batista, E. P. A., Ngowo, H. S., Opiyo, M., Shubis, G. K., Meza, F. C., Okumu, F. O. and Eiras, A. E. (2017). Semi-field assessment of the BG-Malaria trap for monitoring the African malaria vector, Anopheles arabiensis. *PLoS One* **5**, 1–17.

Beeuwkes, J., Spitzen, J., Spoor, C. W., van Leeuwen, J. L. and Takken, W. (2008). 3-D flight behaviour of the malaria mosquito Anopheles gambiae s . s . inside an odour plume. *Proc. Netherlands Entomol. Soc. Meet.* **19**, 137–146.

Berman, G. J., Choi, D. M., Bialek, W. and Shaevitz, J. W. (2014). Mapping the stereotyped behaviour of freely moving fruit flies. *J. R. Soc. Interface* **11**, 20140672.

Bhalala, H. and Arias, J. R. (2009). The Zumba mosquito trap and BG-Sentinel trap: Novel surveillance tools for host-seeking mosquitoes. *J. Am. Mosq. Control Assoc.* **25**, 134–139.

Blimpo, M. P. and Cosgrove-Davies, M. (2019). *Electricity access in sub-saharan Africa: pptake, reliability, and complementary factors for economic impact*. Washington, DC: World Bank.

Bode-Oke, A. T., Zeyghami, S. and Dong, H. (2018). Flying in reverse: Kinematics and aerodynamics of a dragonfly in backward free flight. *J. R. Soc. Interface* **15**.

Bomphrey, R. J., Nakata, T., Phillips, N. and Walker, S. M. (2017). Smart wing rotation and trailing-edge vortices enable high frequency mosquito flight. *Nature* **544**, 92–95.

Bougatsia, A. (2021). *Landing approach of the mosquito Anopheles coluzzii under the presence of host cues*. Ph.D. thesis, Wageningen University.

Bracken, G. K. and Thorsteinson, A. J. (1965). The orientation of horse flies and deer flies (Tabanidae, Diptera): IV. The influence of some physical modification of visual decoys on orientation of horse flies. *Can. J. Zool.* **8**, 314–318.

Card, G. M. (2012). Escape behaviors in insects. *Curr. Opin. Neurobiol.* **22**, 180–186.

Cardé, R. T. (2015). Multi-cue integration: How female mosquitoes locate a human host.

Curr. Biol. **25**, R793–1795.

Cardé, R. T., Gibson, G., Cardé, T. R. and Gibson, G. (2010). Host finding by female mosquitoes : mechanisms of orientation to host odours and other cues. In *Olfaction Vector-Host Interact.*, volume 2, pp. 115–136. Wageningen Academic Publishers.

Cardé, R. T. and Willis, M. A. (2008). Navigational strategies used by insects to find distant, wind-borne sources of odor. *J. Chem. Ecol.* **34**, 854–866.

Combes, S. A. and Dudley, R. (2009). Turbulence-driven instabilities limit insect flight performance. *Proc. Natl. Acad. Sci.* **106**, 9105–9108.

Cooperband, M. F. and Cardé, R. T. (2006a). Comparison of plume structures of carbon dioxide emitted from different mosquito traps. *Med. Vet. Entomol.* **20**, 1–10.

Cooperband, M. F. and Cardé, R. T. (2006b). Orientation of Culex mosquitoes to carbon dioxide-baited traps: Flight manoeuvres and trapping efficiency. *Med. Vet. Entomol.* **20**, 11–26.

Corcoran, A. J. and Conner, W. E. (2016). How moths escape bats: predicting outcomes of predator-prey interactions. *J. Exp. Biol.* **219**, 2704–2715.

Dakin, R., Segre, P. S., Straw, A. D. and Altshuler, D. L. (2018). Morphology, muscle capacity, skill, and maneuvering ability in hummingbirds. *Science (80-.).* **359**, 653–657.

Darbro, J. M. and Harrington, L. C. (2007). Avian defensive behavior and blood-feeding success of the West Nile vector mosquito, Culex pipiens. *Behav. Ecol.* **18**, 750–757.

Dawson, J. W., Kutsch, W. and Robertson, R. M. (2004). Auditory-evoked evasive manoeuvres in free-flying locusts and moths. *J. Comp. Physiol. A Neuroethol. Sensory, Neural, Behav. Physiol.* **190**, 69–84.

Daykin, P. N. (1967). Orientation of aedes aegypti in vertical air currents. *Can. Entomol.* **99**, 303–308.

de Almeida, S. J., Martins Ferreira, R. P., Eiras, Á. E., Obermayr, R. P. and Geier, M. (2010). Multi-agent modeling and simulation of an Aedes aegypti mosquito population. *Environ. Model. Softw.* **25**, 1490–1507.

de Silva, W. A. P., Bernal, X. E., Chathuranga, W. G., Herath, B. P., Ekanayake, C., Abeysundara, H. T. and Karunaratne, S. H. (2020). Feeding patterns revealed host partitioning in a community of frog-biting mosquitoes. *Ecol. Entomol.* **45**, 988–996.

Dekker, T. and Cardé, R. T. (2011). Moment-to-moment flight manoeuvres of the female yellow fever mosquito (Aedes aegypti L.) in response to plumes of carbon dioxide and human skin odour. *J. Exp. Biol.* **214**, 3480–3494.

Dekker, T., Geier, M. and Cardé, R. T. (2005). Carbon dioxide instantly sensitizes female yellow fever mosquitoes to human skin odours. *J. Exp. Biol.* **208**, 2963–2972.

Dekker, T., Takken, W., Knols, B. G. J., Bouman, E., Van de Laak, S., de Bever, A. and Huisman, P. W. T. (1998). Selection of biting sites on a human host by Anopheles gambiae s.s., An. arabiensis and An. quadriannulatus. *Entomol. Exp. Appl.* **87**, 295–300.

Dennis, E. J., Goldman, O. V. and Vosshall Correspondence, L. B. (2019). Aedes aegypti mosquitoes use their legs to sense DEET on contact. *Curr. Biol.* .

Dickinson, M. H. and Muijres, F. T. (2016). The aerodynamics and control of free flight Manoeuvres in Drosophila. *Philos. Trans. R. Soc. B Biol. Sci.* **371**, 20150388.

Domenici, P., Blagburn, J. M. and Bacon, J. P. Animal escapology I: Theoretical issues and emerging trends in escape trajectories.

Domenici, P., Booth, D., Blagburn, J. M. and Bacon, J. P. (2008). Cockroaches keep predators guessing by using preferred escape trajectories. *Curr. Biol.* **18**, 1792–1796.

Edman, J. D., Day, J. F. and Walker, E. D. (1984). Field confirmation of laboratory observations on the differential antimosquito behavior of herons. *Condor* **86**, 91.

Edman, J. D. and Scott, T. W. (1987). Host defensive behaviour and the feeding success of mosquitoes. *Int. J. Trop. Insect Sci.* **8**, 617–622.

Efron, B. (2013). Bayes' theorem in the 21st century. *Science (80-.).* **340**, 1177–1178.

Ellington, C. P. (1984). The aerodynamics of hovering insect flight. III. Kinematics. *Philos. Trans. R. Soc. London. B, Biol. Sci.* **305**, 41–78.

Englbrecht, C., Gordon, S., Venturelli, C., Rose, A. and Geier, M. (2015). Evaluation of BG-sentinel trap as a management tool to reduce aedes albopictus nuisance in an urban environment in Italy. *J. Am. Mosq. Control Assoc.* **31**, 16–25.

Fairbairn, H. (2018). *Design of an Odour Baited Mosquito Trap for Malaria Prevention in Africa*. Ph.D. thesis, University of Wageningen.

Fontaine, E. I., Zabala, F., Dickinson, M. H. and Burdick, J. W. (2009). Wing and body motion during flight initiation in Drosophila revealed by automated visual tracking. *J. Exp. Biol.* **212**, 1307–1323.

Fry, S. N., Sayaman, R. and Dickinson, M. H. (2005). The aerodynamics of hovering flight in Drosophila. *J. Exp. Biol.* **208**, 2303–2318.

Fuller, S. B., Straw, A. D., Peek, M. Y., Murray, R. M. and Dickinson, M. H. (2014). Flying Drosophila stabilize their vision-based velocity controller by sensing wind with their antennae. *Proc. Natl. Acad. Sci. U. S. A.* **111**, E1182–e1191.

Gama, R. A., da Silva, I. M., Geier, M. and Eiras, Á. E. (2013). Development of the BG-Malaria trap as an alternative to human-landing catches for the capture of Anopheles darlingi. *Mem. Inst. Oswaldo Cruz* **108**, 63–771.

Gao, Q., Wang, F., Lv, X., Cao, H., Zhou, J., Su, F., Xiong, C. and Leng, P. (2018). Comparison of the human-baited double net trap with the human landing catch for Aedes albopictus monitoring in Shanghai, China. *Parasites and Vectors* **11**, 1–12.

Gillies, M. T. (1980). The role of carbon dioxide in host-finding by mosquitoes (Diptera: Culicidae): A review. *Bull. Entomol. Res.* **70**, 525–532.

Gogla. Global Off-Grid Solar Market Report | GOGLA.

6

Hawkes, F. and Gibson, G. (2016). Seeing is believing: the nocturnal malarial mosquito Anopheles coluzzii responds to visual host-cues when odour indicates a host is nearby. *Parasites and Vectors* **9**, 320.

Hawkes, F. M., Dabiré, R. K., Sawadogo, S. P., Torr, S. J. and Gibson, G. (2017). Exploiting Anopheles responses to thermal, odour and visual stimuli to improve surveillance and control of malaria. *Sci. Rep.* **7**, 17283.

Hiscox, A., Otieno, B., Kibet, A., Mweresa, C. K., Omusula, P., Geier, M., Rose, A., Mukabana, W. R. and Takken, W. (2014). Development and optimization of the Suna trap as a tool for mosquito monitoring and control. *Malar. J.* **13**, 257.

Homan, T., Hiscox, A., Mweresa, C. K., Masiga, D., Mukabana, W. R., Oria, P., Maire, N., Pasquale, A. D., Silkey, M., Alaii, J. et al. (2016). The effect of mass mosquito trapping on malaria transmission and disease burden (SolarMal): a stepped-wedge cluster-randomised trial. *Lancet* **388**, 1193–1201.

Howlett, F. M. (1910). The influence of temperature upon the biting of mosquitoes. *Parasitology* **3**, 479–484.

Jatta, E., Carrasco-Tenezaca, M., Jawara, M., Bradley, J., Ceesay, S., D'Alessandro, U., Jeffries, D., Kandeh, B., Lee, D. S. H., Pinder, M. et al. (2021). Impact of increased ventilation on indoor temperature and malaria mosquito density: An experimental study in the Gambia. *J. R. Soc. Interface* **18**.

Jones, J., Murray, G. P. and McCall, P. J. (2021). A minimal 3D model of mosquito flight behaviour around the human baited bed net. *Malar. J.* **20**, 24.

Jones, J. C. and Pilitt, D. R. (1973). Blood-feeding behavior or adult Aedes aegypti mosquitoes. *Biol. Bull.* **145**, 127–139.

Kenea, O., Balkew, M., Tekie, H., Gebre-Michael, T., Deressa, W., Loha, E., Lindtjørn, B. and Overgaard, H. J. (2017). Comparison of two adult mosquito sampling methods with human landing catches in south-central Ethiopia. *Malar. J.* **16**, 1–15.

Kennedy, J. S. (1940). The visual Responses of flying mosquitoes. *Proc. Zool. Soc. London* **109 A**, 221–242.

Kessy, S. T., Nyundo, B. A., Mnyone, L. L. and Lyimo, I. N. (2020). The use of granular cyclopentanone as alternative to artificial Source of carbon dioxide in improved Passive Outdoor Host Seeking Device (POHD). *Sci. World J.* **2020**.

Kline, D. L. and Lemire, G. F. (1995). Field evaluation of heat as an added attractant to traps baited with carbon dioxide and octenol for Aedes taeniorhynchus. *J. Am. Mosq. Control Assoc.* **11**, 454–456.

Kröckel, U., Rose, A., Eiras, Á. E. and Geier, M. (2006). New tools for surveillance of adult yellow fever mosquitoes: Comparison of trap catches with human landing rates in an urban environment. *J. Am. Mosq. Control Assoc.* **22**, 229–238.

Kruschke, J. K. and Liddell, T. M. (2018). The Bayesian New Statistics: Hypothesis test-

ing, estimation, meta-analysis, and power analysis from a Bayesian perspective. *Psychon. Bull. Rev.* **25**, 178–206.

Lazzari, C. R. (2009). Chapter 1 Orientation towards hosts in haematophagous insects: An integrative perspective. In *Adv. In Insect Phys.*, volume 37, pp. 1–58. Elsevier Ltd.

Li, J., Cao, X., Liu, J., Mohanarangam, K. and Yang, W. (2018). PIV measurement of human thermal convection flow in a simplified vehicle cabin. *Build. Environ.* **144**, 305–315.

Lin, H. T. and Leonardo, A. (2017). Heuristic rules underlying dragonfly prey selection and interception. *Curr. Biol.* **27**, 1124–1137.

Liu, P. and Cheng, B. (2017). Limitations of rotational manoeuvrability in insects and hummingbirds: Evaluating the effects of neuro-biomechanical delays and muscle mechanical power. *J. R. Soc. Interface* **14**.

Liu, Y. and Sun, M. (2008). Wing kinematics measurement and aerodynamics of hovering droneflies. *J. Exp. Biol.* **211**, 2014–2025.

Lühken, R., Pfitzner, W. P., Börstler, J., Garms, R., Huber, K., Schork, N., Steinke, S., Kiel, E., Becker, N., Tannich, E. et al. (2014). Field evaluation of four widely used mosquito traps in Central Europe. *Parasites and Vectors* **7**, 1–11.

Mamiya, A. and Dickinson, M. H. (2015). Antennal mechanosensory neurons mediate wing Motor reflexes in flying drosophila. *J. Neurosci.* **35**, 7977–7991.

Maneerat, S. and Daudé, E. (2016). A spatial agent-based simulation model of the dengue vector Aedes aegypti to explore its population dynamics in urban areas. *Ecol. Modell.* **333**, 66–78.

Matherne, M. E., Cockerill, K., Zhou, Y., Bellamkonda, M. and Hu, D. L. (2018). Mammals repel mosquitoes with their tails. *J. Exp. Biol.* **221**, jeb178905.

Mathis, A., Mamidanna, P., Cury, K. M., Abe, T., Murthy, V. N., Mathis, M. W. and Bethge, M. (2018). DeepLabCut: markerless pose estimation of user-defined body parts with deep learning. *Nat. Neurosci.* **21**, 1281–1289.

Mboera, L. E., Takken, W. and Sambu, E. Z. (2000). The response of Culex quinquefasciatus (Diptera: Culicidae) to traps baited with carbon dioxide, 1-octen-3-ol, acetone, butyric acid and human foot odour in Tanzania. *Bull. Entomol. Res.* **90**, 155–159.

Mburu, M. M., Mweresa, C. K., Omusula, P., Hiscox, A., Takken, W. and Mukabana, W. R. (2017). 2-Butanone as a carbon dioxide mimic in attractant blends for the Afrotropical malaria mosquitoes Anopheles gambiae and Anopheles funestus. *Malar. J.* .

McMeniman, C. J., Corfas, R. A., Matthews, B. J., Ritchie, S. A. and Vosshall, L. B. (2014). Multimodal integration of carbon dioxide and other sensory cues drives mosquito attraction to humans. *Cell* **156**, 1060–1071.

Moore, T. Y., Cooper, K. L., Biewener, A. A. and Vasudevan, R. (2017). Unpredictability of escape trajectory explains predator evasion ability and microhabitat preference of

6

desert rodents. *Nat. Commun.* **8**, 1–9.

Muijres, F. T., Chang, S. W., van Veen, W. G., Spitzen, J., Biemans, B. T. T., Koehl, M. A. R. and Dudley, R. (2017). Escaping blood-fed malaria mosquitoes minimize tactile detection without compromising on take-off speed. *J. Exp. Biol.* **220**, 3751–3762.

Muijres, F. T., Elzinga, M. J., Melis, J. M., Dickinson, M. H., Florian T. Muijres, 1 Michael J. Elzinga, 1 Johan M. Melis, 1, . M. H. D. and Avoiding (2014). Flies evade looming targets by executing rapid visually directed banked turns. *Science (80-.).* **344**, 172–7.

Mweresa, C. K., Omusula, P., Otieno, B., van Loon, J. J., Takken, W. and Mukabana, W. R. (2014). Molasses as a source of carbon dioxide for attracting the malaria mosquitoes Anopheles gambiae and Anopheles funestus. *Malar. J.* **13**, 1–13.

Onwujekwe, O., Chima, R., Shu, E., Nwagbo, D. and Okonkwo, P. (2001). Hypothetical and actual willingness to pay for insecticide-treated nets in five Nigerian communities. *Trop. Med. Int. Heal.* **6**, 545–553.

Parker, J. E., Angarita-Jaimes, N., Abe, M., Towers, C. E., Towers, D. and McCall, P. J. (2015). Infrared video tracking of Anopheles gambiae at insecticide-treated bed nets reveals rapid decisive impact after brief localised net contact. *Sci. Rep.* **5**, 13392.

Qiu, Y. T., Smallegange, R. C., van Loon, J. J., Ter Braak, C. J. and Takken, W. (2006). Interindividual variation in the attractiveness of human odours to the malaria mosquito Anopheles gambiae s. s. *Med. Vet. Entomol.* **20**, 280–287.

Raghavendra, K., Sharma, P. and Dash, A. P. (2008). Biological control of mosquito populations through frogs: Opportunities & constrains. *Indian J. Med. Res.* **128**, 22–25.

Rehman, H., Aziz, A. T., Saggu, S., Abbas, Z. K., Mohan, A. and Ansari, A. A. (2014). Systematic review on pyrethroid toxicity with special reference to deltamethrin. *J. Entomol. Zool. Stud. JEZS* **2**, 60–70.

Reid, J. N., Hoffmeister, T. S., Hoi, A. G. and Roitberg, B. D. (2014). Bite or flight: The response of mosquitoes to disturbance while feeding on a defensive host. *Entomol. Exp. Appl.* **153**, 240–245.

Ristroph, L., Berman, G. J., Bergou, A. J., Wang, Z. J. and Cohen, I. (2009). Automated hull reconstruction motion tracking (HRMT) applied to sideways maneuvers of free-flying insects. *J. Exp. Biol.* **212**, 1324–1335.

Robie, A. A., Hirokawa, J., Edwards, A. W., Umayam, L. A., Lee, A., Phillips, M. L., Card, G. M., Korff, W., Rubin, G. M., Simpson, J. H. et al. (2017). Mapping the Neural Substrates of Behavior. *Cell* **170**, 393–406.e28.

Rodríguez, R. L. and Greenfield, M. D. (2004). Behavioural context regulates dual function of ultrasonic hearing in lesser waxmoths: Bat avoidance and pair formation. *Physiol. Entomol.* **29**, 159–168.

Rohrseitz, N. and Fry, S. N. (2011). Behavioural system identification of visual flight

speed control in Drosophila melanogaster. *J. R. Soc. Interface* **8**, 171–185.

Saitoh, Y., Hattori, J., Chinone, S., Nihei, N., Tsuda, Y., Kurahashi, H. and Kobayashi, M. (2004). Yeast-generated CO2 as a convenient source of carbon dioxide for adult mosquito sampling. *J. Am. Mosq. Control Assoc.* **20**, 261–264.

Sane, S. P. (2003). The aerodynamics of insect flight. *J. Exp. Biol.* **206**, 4191–4208.

Shcherbacheva, A., Haario, H. and Killeen, G. F. (2018). Modeling host-seeking behavior of African malaria vector mosquitoes in the presence of long-lasting insecticidal nets. *Math. Biosci.* **295**, 36–47.

Smith, N. M., Balsalobre, J. B., Doshi, M., Willenberg, B. J. and Dickerson, A. K. (2020). Landing mosquitoes bounce when engaging a substrate. *Sci. Rep.* **10**, 1–10.

Spangler, H. G. and Hayden, C. (1984). Responses of the greater wax moth, galleria mellonella L. (Lepidoptera: Pyralidae) to continuous high-frequency sound. *J. Kansas Entomol. Soc.* **57**, 44–49.

Spitzen, J., Koelewijn, T., Mukabana, W. R. and Takken, W. (2016). Visualization of house-entry behaviour of malaria mosquitoes. *Malar. J.* **15**, 233.

Spitzen, J., Smallegange, R. C. and Takken, W. (2008). Effect of human odours and positioning of CO2 release point on trap catches of the malaria mosquito Anopheles gambiae sensu stricto in an olfactometer. *Physiol. Entomol.* **33**, 116–122.

Spitzen, J., Spoor, C. W., Grieco, F., ter Braak, C., Beeuwkes, J., Van Brugge, S. P., Kranenbarg, S., Noldus, L. P. J. J., van Leeuwen, J. L. and Takken, W. (2013). A 3D analysis of flight behavior of Anopheles gambiae sensu stricto malaria mosquitoes in response to human odor and heat. *PLoS One* **8**, 1–12.

Stowers, J. R., Hofbauer, M., Bastien, R., Griessner, J., Higgins, P., Farooqui, S., Fischer, R. M., Nowikovsky, K., Haubensak, W., Couzin, I. D. et al. (2017). Virtual reality for freely moving animals. *Nat. Methods* **14**, 995–1002.

Straw, A. D., Branson, K., Neumann, T. R. and Dickinson, M. H. (2011). Multi-camera real-time three-dimensional tracking of multiple flying animals. *J. R. Soc. Interface* **8**, 395–409.

Sutcliffe, J. and Colborn, K. L. (2015). Video studies of passage by Anopheles gambiae mosquitoes through holes in a simulated bed net: effects of hole size, hole orientation and net environment. *Malar. J.* **14**, 1–13.

Sutcliffe, J. F. and Yin, S. (2014). Behavioural responses of females of two anopheline mosquito species to human-occupied, insecticide-treated and untreated bed nets. *Malar. J.* **13**, 294.

Tambwe, M. M., Saddler, A., Kibondo, U. A., Mashauri, R., Kreppel, K. S., Govella, N. J. and Moore, S. J. (2021). Semi-field evaluation of the exposure-free mosquito electrocuting trap and BG-Sentinel trap as an alternative to the human landing catch for measuring the efficacy of transfluthrin emanators against Aedes aegypti. *Parasites*

6

and Vectors **14**, 265.

Tammero, L. F. and Dickinson, M. H. (2002). Collision-avoidance and landing responses are mediated by separate pathways in the fruit fly, Drosophila melanogaster. *J. Exp. Biol.* **205**, 2785–2798.

Tangena, J. A. A., Thammavong, P., Hiscox, A., Lindsay, S. W. and Brey, P. T. (2015). The human-baited double net trap: An alternative to human landing catches for collecting outdoor biting mosquitoes in Lao PDR. *PLoS One* **10**, e0138735.

Taylor, G. K., Bacic, M., Bomphrey, R. J., Carruthers, A. C., Gillies, J., Walker, S. M. and Thomas, A. L. (2008). New experimental approaches to the biology of flight control systems. In *J. Exp. Biol.*, volume 211, pp. 258–266.

Thorsteinson, A. J., Bracken, G. K. and Hanec, W. (1964). The Manitoba Horse Fly Trap. *Can. Entomol.* **96**, 166.

Thorsteinson, A. J., Bracken, G. K. and Hanec, W. (1965). The orientation of horse flies and deer flies (Tabanidae, Diptera): III. the use of traps in the study of orientation of Tabanids in the field. *Entomolia Exp. Appl.* **8**, 189–192.

Townes, H. (1962). Design For A Malaise Trap. *Proc. Entomol. Soc. Washingt.* **64**, 253 – 262.

Tufte, E. R. (1988). *The visual display of quantitative information*, volume 8. Cambridge University Press, 20 pp.

Turner, S. L., Li, N., Guda, T., Githure, J., Cardé, R. T. and Ray, A. (2011). Ultra-prolonged activation of CO_2-sensing neurons disorients mosquitoes. *Nature* **474**, 87–91.

van Breugel, F. and Dickinson, M. H. (2014). Plume-tracking behavior of flying drosophila emerges from a set of distinct sensory-motor reflexes. *Curr. Biol.* **24**, 274–286.

van Breugel, F., Riffell, J., Fairhall, A. and Dickinson, M. H. (2015). Mosquitoes use vision to associate odor plumes with thermal targets. *Curr. Biol.* **25**, 2123–2129.

van de Geer, C. (2019). *Adapting a mosquito trap for future deployment in African communities*. Ph.D. thesis, University of Wageningen.

van Der Maaten, L. and Hinton, G. (2008). Visualizing Data using t-SNE. *J. Mach. Learn. Res.* **9**, 2579–2605.

van Loon, J. J. J. A., Smallegange, R. C., Bukovinszkiné-Kiss, G., Jacobs, F., De Rijk, M., Mukabana, W. R., Verhulst, N. O., Menger, D. J. and Takken, W. (2015). Mosquito attraction: crucial role of carbon dioxide in formulation of a five-component blend of human-derived volatiles. *J. Chem. Ecol.* **41**, 567–73.

Veen, W. G. V. and van Veen, W. G. (2020). *Aerodynamics of insect flight*. Ph.D. thesis, University of Wageningen.

Verhulst, N. O., Beijleveld, H., Knols, B. G., Takken, W., Schraa, G., Bouwmeester, H. J. and Smallegange, R. C. (2009). Cultured skin microbiota attracts malaria mos-

quitoes. *Malar. J.* **8**, 1–12.

Verhulst, N. O. N. N. O., Bakker, J. W. J. and Hiscox, A. (2015). Modification of the Suna Trap for Improved Survival and Quality of Mosquitoes in Support of Epidemiological Studies. *J. Am. Mosq. Control Assoc.* **31**, 223–232.

Vinauger, C., Lahondère, C., Wolff, G. H., Locke, L. T., Liaw, J. E., Parrish, J. Z., Akbari, O. S., Dickinson, M. H. and Riffell, J. A. (2018). Modulation of host learning in Aedes aegypti mosquitoes. *Curr. Biol.* **28**, 333–344.e8.

Vinauger, C., van Breugel, F., Locke, L. T., Tobin, K. K., Dickinson, M. H., Fairhall, A. L., Akbari, O. S. and Riffell, J. A. (2019). Visual-olfactory integration in the human disease vector mosquito Aedes aegypti. *Curr. Biol.* **29**, 2509–2516.e5.

Voesenek, C. J., Pieters, R. P., Muijres, F. T. and van Leeuwen, J. L. (2019). Reorientation and propulsion in fast-starting zebrafish larvae: An inverse dynamics analysis. *J. Exp. Biol.* **222**.

Voesenek, C. J., Pieters, R. P. and Van Leeuwen, J. L. (2016). Automated reconstruction of three-dimensional fish motion, forces, and torques. *PLoS One* **11**, e0146682.

Waage, J. K. and Nondo, J. (1982). Host behaviour and mosquito feeding success: an experimental study. *Trans. R. Soc. Trop. Med. Hyg.* **76**, 119–122.

Walker, E. D. and Edman, J. D. (1985). The influence of host defensive behavior on mosquito (diptera: culicidae) biting persistence. *J. Med. Entomol.* **22**, 370–372.

Who (2019). Guidelines for malaria vector control. Technical report, Who.

Who (2020). *World Malaria Report 2020*, volume 73. WHO Press, Geneva, 1–4 pp.

Zeyghami, S., Babu, N. and Dong, H. (2016). Cicada (Tibicen linnei) steers by force vectoring. *Theor. Appl. Mech. Lett.* **6**, 107–111.

6

Summary

Hematophagous female mosquitoes have to get a blood meal to obtain the proteins necessary for egg production. To get this blood meal, mosquitoes need to detect a vertebrate host such as a bird or a mammal, fly towards this host and land on it. When interacting with their hosts, flying mosquitoes have to be quick and stealthy to avoid being detected. If they are detected, mosquitoes can be attacked by their host and then they may end up being swatted. However, if they are not detected, they will be able to get their blood meal and successfully continue their life cycle. Many dangerous pathogens such as the malaria parasite and the dengue virus take advantage of this mosquito–vertebrate interaction to spread themselves. This is what made arguably the most annoying animal in the world, certainly the most dangerous animal in the world. Malaria alone kills more than 400,000 people – mostly young children – every year, and killed many more in the past.

In this thesis, I aim to better understand how mosquitoes interact with their hosts and, in doing so, to learn more about the sensory cues that they use to control their flight (as discussed in the **chapter 1**).. For that, first we simulated human presence using counter-flow odour-baited traps. These traps aim to mimic humans using host cues such as CO_2, odours and visual cues to attract host-seeking mosquitoes. In addition to these host cues, these traps generate a circulating airflow using a fan to spread the CO_2 and odours away from itself and to capture mosquitoes that get too close. Second, we simulated attacks using a mechanical swatter to study the escape manoeuvres of mosquitoes as well as to learn whether mosquitoes are using airflow and visual cues to detect the attacks.

In **chapter 2**, we studied how mosquitoes behave around counter-flow odour-baited traps. We recorded thousands of three-dimensional flight tracks of female malaria mosquitoes (Anopheles coluzzii) around a well-known trap, the BG-Suna, in opposite orientations to represent two widely used traps. We visualized the average behaviour of mosquitoes and flight dynamics around the traps on two-dimensional heat maps. This allowed us to identify that mosquitoes were following stereotypical behaviours: when approaching the traps, by flying downward, and when close to the inlet of the traps, by accelerating upward. These behaviours led to very different capture dynamics of mosquitoes, and consequently to contrasting short-range attractiveness and capture mechanisms of the two traps. For example, the standing BG-Suna was more attractive than the hanging BG-Suna, while being also the only trap that triggered escape-like responses of mosquitoes.

Based on our findings from chapter 2, integrated with the literature, we developed a new counter-flow odour-baited trap: the M-Tego. One specificity of this trap is that it can generate two additional host cues that have been found to attract mosquitoes at short range, namely heat and humidity. As described in **chapter 3**, we tested this new trap against the BG-Suna in laboratory and semi-field conditions. In both conditions, the M-Tego

S

without additional short-range cues was found to capture more than twice as many An. coluzzii than the standing BG-Suna. And when the M-Tego generated heat and humidity, it captured around 4.5 times as many mosquitoes as the BG-Suna. To understand why the M-Tego exhibited such improved capture rates, we recorded the flight tracks of mosquitoes around this new trap with or without additional short-range cues. Using similar analysis tools as in chapter 2, we showed that mosquitoes are more attracted to the M-Tego and spent more time close to it when the trap generates heat and/or humidity. Additionally, we did not observe escape-like responses of mosquitoes near the M-Tego, which explains why the M-Tego captures more mosquitoes than the standing BG-Suna even when they produce the same host cues.

In **chapter 4**, we focused on the escape manoeuvres of flying mosquitoes. To study those, we built a new experimental setup where mosquitoes were tracked in three dimensions and in real time. Based on the real-time position of a mosquito, a mechanical swatter was then automatically triggered to simulate an attack towards it. This allowed us to study the escape performance of day-active and night-active mosquitoes (Aedes aegypti and An. coluzzii, respectively). For that, we recorded the flight behaviour of these two species when attacked by the swatter in four light intensities ranging from dark to overcast daylight conditions. Using Bayesian generalized linear models (B-GLM), we discovered that these mosquitoes exhibited enhanced escape performances in their respective natural light conditions (overcast for Aedes and dark for Anopheles). Furthermore, the high escape performance of Anopheles in the dark was mostly explained by its increased flight unpredictability in this light condition, whereas the higher escape performance of Aedes in overcast daylight compared with sunrise was due to its fast visually induced escapes.

In **chapter 5**, we zoomed in on the escape manoeuvres of An. coluzzii mosquitoes with the aim to understand whether they rely on the airflow induced by the attacker to escape successfully. First, we compared the escape performance of mosquitoes when attacked by either a solid or a perforated swatter, in both dark and low-light conditions. We showed that the faster the air movements induced by the attack, the fewer mosquitoes that were hit by the swatter. This demonstrates that airflow plays an important role in the escapes of these mosquitoes. However, at this point, it was still unknown whether mosquitoes are using the airflow passively or actively. Then, using high-speed video cameras (12500 fps) and a newly developed neural-network-based tracker, we recorded the kinematics of the body and wings of flying mosquitoes when escaping. By combining this with results from a CFD simulation of the airflow induced by the attack, we estimated the aerodynamic forces involved during mosquito manoeuvres. We discovered that, although seemingly moving passively with the airflow, these mosquitoes were actively surfing the bow wave induced by the swatter. Moreover, we found that, despite that mosquitoes contributed actively to most of their escape acceleration, the passive effect of the airflow also significantly contributed to their success.

Finally, in the **general discussion**, I put the findings of this thesis in a wider scientific context. I summarize what we learned about attractive and disruptive cues and how mos-

quitoes react to these cues. I highlight that visual cues and airflow are important disruptive cues for mosquitoes, notably because mosquitoes were found to escape fast more often the brighter the light condition, and because they actively use airflow to enhance their escape performance. However, our knowledge on how airflow characteristics influence mosquito flight behaviours is still limited, and consequently there is a need for further research on this topic. Then, I describe my approach for the study of mosquito capture and escape response. Two important aspects of this approach are: (1) the visualization of mosquitoes' flight behaviour using various data visualization techniques and (2) the quantification of flight performances using advanced statistics. Then, I discuss how this approach could also be used to better understand other flight behaviours of mosquitoes, such as landing. To conclude, I highlight three important aspects that govern trap efficacy: the attractiveness of the trap, the residence time of mosquitoes near a trap and the capture efficiency of the trap. I explain how we developed the M-Tego trap while trying to optimize these aspects by systematically testing prototypes and making design iterations. Based on this experience, I provide suggestions about how our findings could be used for the further development of tools to control mosquitoes, and therefore to reduce the spread of mosquito-borne diseases.

S

Résumé

Les moustiques femelles hématophages doivent se nourrir de sang pour obtenir les protéines nécessaires à la production d'œufs. Pour obtenir ce sang, les moustiques doivent détecter un hôte comme un oiseau ou un mammifère, voler vers cet hôte et se poser dessus. Lorsqu'ils interagissent avec leurs hôtes, les moustiques volants doivent être rapides et furtifs pour éviter d'être détectés. S'ils sont détectés, les moustiques peuvent être attaqués par leur hôte et être écrasés. S'ils ne sont pas détectés, ils pourront obtenir leur repas de sang et poursuivre avec succès leur cycle de vie. De nombreux pathogènes dangereux tels que le parasite du paludisme et le virus de la dengue profitent de cette interaction moustique-vertébré pour se propager. Cela fait de ce qui est peut-être l'animal le plus agaçant du monde, aussi l'animal le plus dangereux du monde. Le paludisme à lui seul tue chaque année plus de 400 000 personnes – pour la plupart de jeunes enfants.

Dans cette thèse, je vise à mieux comprendre comment les moustiques interagissent avec leurs hôtes et, ce faisant, à en apprendre davantage sur les signaux sensoriels qu'ils utilisent pour contrôler leur vol (comme discuté dans le **chapitre 1**). Pour cela, nous avons d'abord simulé la présence humaine à l'aide de pièges odorants à flux d'air circulant. Ces pièges visent à imiter les humains en utilisant des signaux indiquant la présence d'un hôte tels que le CO_2, des odeurs et des signaux visuels pour attirer les moustiques à la recherche d'hôtes. En plus de ces signaux, ces pièges génèrent un flux d'air circulant à l'aide d'un ventilateur pour disperser le CO_2 et les odeurs, et pour capturer les moustiques qui s'approchent trop près. Ensuite, nous avons simulé des attaques à l'aide d'une tapette mécanique pour étudier les manœuvres de fuite des moustiques ainsi que pour savoir si les moustiques utilisent le flux d'air et des repères visuels pour détecter les attaques.

Dans le **chapitre 2**, nous avons étudié le comportement des moustiques autour de pièges odorants à flux d'air circulant. Nous avons enregistré des milliers de trajectoires de vol de moustiques femelles vecteur du paludisme (Anopheles coluzzii) autour d'un piège bien connu, le BG-Suna, et dans des orientations opposées pour représenter deux pièges largement utilisés (suspendu ou debout). Nous avons visualisé le comportement moyen des moustiques et leur dynamique de vol autour des pièges sur des cartes thermiques bidimensionnelles. Cela nous a permis d'identifier que les moustiques suivaient des comportements stéréotypés : ils approchent ces pièges en volant vers le bas, et accélèrent vers le haut après être arrivés à proximité de l'entrée des pièges. Ces comportements conduisent à des dynamiques de capture des moustiques très différentes, et par conséquent à des mécanismes contrastés d'attractivité et de capture à courte portée des deux pièges. Par exemple, le BG-Suna debout était plus attrayant que le BG-Suna suspendu, tout en étant également le seul piège qui déclenchait des réactions de fuite des moustiques.

Sur la base de nos résultats du chapitre 2 intégrés à la littérature, nous avons développé

un nouveau piège odorant à flux d'air circulant : le M-Tego. Une spécificité de ce piège est qu'il peut générer deux signaux d'hôte supplémentaires qui attirent les moustiques à courte distance, à savoir la chaleur et l'humidité. Dans le **chapitre 3**, nous avons comparé ce nouveau piège au BG-Suna en laboratoire et sur le terrain. Dans les deux conditions, le M-Tego sans signaux supplémentaires à courte portée s'est avéré capturer plus de deux fois plus d'An. coluzzii que le BG-Suna debout. Et lorsque le M-Tego a généré de la chaleur et de l'humidité, il a capturé environ 4,5 fois plus de moustiques que le BG-Suna. Pour comprendre pourquoi le M-Tego présentait des taux de capture si importants, nous avons enregistré les trajectoires de vol des moustiques autour de ce nouveau piège avec ou sans signaux supplémentaires à courte portée. En utilisant des outils d'analyse similaires à ceux présenté dans le chapitre 2, nous avons montré que les moustiques sont plus attirés par le M-Tego et passent plus de temps à proximité lorsque le piège génère de la chaleur et/ou de l'humidité. En outre, nous n'avons pas observé de réaction de fuite des moustiques près du M-Tego, ce qui pourrait expliquer pourquoi le M-Tego capture plus de moustiques que le BG-Suna debout y compris lorsqu'il produit les mêmes signaux d'hôte.

Dans le **chapitre 4**, nous nous sommes concentrés sur les manœuvres de fuite des moustiques volants. Pour les étudier, nous avons construit un nouveau système expérimental où les moustiques ont été suivis en trois dimensions et en temps réel. Sur la base de la position en temps réel d'un moustique, une tapette mécanique a ensuite été automatiquement déclenchée pour simuler une attaque contre lui. Cela nous a permis d'étudier les performances d'évasion des moustiques diurnes et nocturnes (Aedes aegypti et An. coluzzii, respectivement). A cette fin, nous avons enregistré le comportement de vol de ces deux espèces lorsqu'elles sont attaquées par la tapette selon quatre intensités lumineuses allant de l'obscurité à la lumière du jour par temps couvert. En utilisant des modèles linéaires généralisés Bayésiens (B-GLM), nous avons découvert que ces moustiques présentaient des performances d'évasion améliorées dans leurs conditions de lumière naturelle respectives (jour par temps couvert pour Aedes et sombre pour Anopheles). De plus, la performance d'évasion élevée d'Anopheles dans l'obscurité s'expliquait principalement par son imprévisibilité accrue dans ces conditions de lumière, tandis que la performance d'évasion plus élevée d'Aedes par temps couvert par rapport au lever du soleil était due à ses évasions rapides induites visuellement.

Dans le **chapitre 5**, nous avons zoomé sur les manœuvres d'évasion d'An. coluzzii dans le but de comprendre si ils utilisent le flux d'air induit par l'agresseur pour réussir à s'échapper. Tout d'abord, nous avons comparé les performances d'évasion des moustiques lorsqu'ils sont attaqués par une tapette pleine ou perforée, dans des conditions d'obscurité et de faible luminosité. Nous avons montré que plus les mouvements d'air induits par l'attaque sont rapides, moins les moustiques sont touchés par la tapette. Cela démontre que le flux d'air joue un rôle important dans les fuites de ces moustiques. Cependant, à ce stade, on ne savait toujours pas si les moustiques utilisaient le flux d'air de manière passive ou active. Ensuite, à l'aide de caméras vidéo haute vitesse (12 500 images per secondes) et d'un nouveau logiciel de suivi basé sur un réseau de neurones profond, nous avons enregistré la

cinématique du corps et des ailes des moustiques volants lorsqu'ils s'échappaient. En combinant cela avec les résultats d'une simulation numérique (CFD) du flux d'air induit par l'attaque, nous avons estimé les forces aérodynamiques impliquées lors des manœuvres des moustiques. Nous avons découvert que, bien qu'apparemment se déplaçant passivement avec le flux d'air, ces moustiques surfaient activement sur la vague d'étrave induite par la tapette. De plus, nous avons constaté que, bien que les moustiques aient contribué activement à la majeure partie de leur accélération de fuite, l'effet passif du flux d'air contribuait également de manière significative à leur succès.

Enfin, dans la **discussion générale**, j'ai replacé les résultats de ces recherches dans un contexte scientifique plus large. Je résume ce que nous avons appris sur les signaux attrayants et perturbateurs pour les moustiques et sur la façon dont ils réagissent à ces signaux. Je souligne que les repères visuels et le flux d'air sont d'importants signaux perturbateurs pour les moustiques, notamment parce que les moustiques s'échappent plus souvent lorsque l'intensité lumineuse est importante, et parce qu'ils utilisent activement le flux d'air pour améliorer leurs performances d'évasion. Cependant, nos connaissances sur la façon dont les caractéristiques du flux d'air influencent les comportements de vol des moustiques sont encore limitées et, par conséquent, il est nécessaire de poursuivre les recherches sur ce sujet. Ensuite, je décris mon approche pour l'étude de la capture des moustiques et de leur réponse d'évasion. Deux aspects importants de cette approche sont : (1) la visualisation du comportement de vol des moustiques à l'aide de diverses techniques de visualisation de données et (2) la quantification des performances de vol à l'aide de statistiques avancées. Ensuite, j'explique comment cette approche pourrait également être utilisée pour mieux comprendre d'autres comportements de vol des moustiques, comme l'atterrissage. Pour conclure, je mets en évidence trois aspects importants qui régissent l'efficacité du piège : l'attractivité du piège, le temps de résidence des moustiques à proximité d'un piège et l'efficacité de capture du piège. J'explique comment nous avons développé le piège M-Tego en essayant d'optimiser ces aspects en testant systématiquement des prototypes et en faisant des itérations de conception. Sur la base de cette expérience, je fais des suggestions sur la façon dont nos résultats pourraient être utilisés pour le développement ultérieur d'outils de lutte contre les moustiques, et donc pour réduire la propagation des maladies transmises par les moustiques.

Acknowledgements

Although I am passionate about flying things, for as long as I can remember, I felt like **mosquitoes** have a personal vendetta against me, and consequently I always considered them as my nemesis. Despite that, when I was first contacted by Florian to discuss a project to study the flight of mosquitoes, I was hooked right away. I believe that this topic was perfect for me. It allowed me to learn more about insect flight, to make new fundamental discoveries and to contribute to the fight against mosquito-borne diseases. Doing all these things required me to learn much about insect biology, build and use complex experimental setups and to do advanced data analysis, all of which I enjoyed very much.

For this I am very grateful to **Florian**, who gave me the opportunity to work on this project and with whom I wrote my PhD proposal. Your coaching (together with Johan and others at EZO) before presenting my project to the WIAS jury will always remain in my mind as the most intense and instructive three days of my life. I am even more grateful to Florian for his supervision and support during my PhD project. I could not have wished for a better supervisor. Your expertise, enthusiasm, and patience (sorry for being so stubborn) during our numerous exciting discussions were very precious to me. You gave me the freedom to be creative and even to make my own mistakes sometimes. I learned so much also because of this. Finally, I really enjoyed our various debates and going to conferences with you (especially if it was to eat some delicious salmon in the countryside of Sweden or to hike in the French Alps).

Then I want to express my sincere gratitude to **Johan**, first for welcoming me in EZO (you have built a great team there) and secondly for his supervision. I heard before coming to Wageningen that you really cared about students, and I quickly realized that this is true. I believe that you genuinely enjoy sharing your experience and passion for science, which might explain why you always manage to find time for the PhD candidates in EZO. In addition to those things, your abilities to pinpoint weaknesses in an analysis or a story, and to get people to do their best were also very valuable to me during this project.

Jeroen, I am glad your role in the supervision team grew over the years, especially when at the same time I went more and more into fundamental science. You brought balance to the team by reminding us of the applied goals and that mosquitoes do not usually live inside ultra-controlled experimental setups. Your many technical advice and great knowledge of the literature were also really helpful. In addition, your optimism was very important to me, especially in stressful times. Finally, thanks for showing me your little personal heaven, this reminded me that there are more important things in life than work.

I am also grateful to **Andrew**, who got me to learn Python and showed me for the first time how deep neural networks could be used for animal tracking. Thank you very much

A

for your patient help and for inviting me to visit your nice team in Freiburg. Many technical aspects of my thesis have been influenced by our collaboration, and I hope my future work will be too. **Martin**, I really enjoyed discussing with you, although these talks are often quite long, they are always really interesting. I also valued very much your numerous pertinent questions during lunch meetings.

The secret weapon of EZO is its team of technicians. Very skilled and always willing to help PhD candidates with their thousands of problems. Thank you all!! **Remco** ('the setup architect'), despite being overworked you always come up with cool and practical solutions. I really enjoyed designing experimental setups with you. **Henk**, thanks for your patience and good mood. Sorry for always bothering you with uninteresting computer issues, I promise sometimes I will come up with a nice histology problem. **Leo**, thanks for all the energy that you invested in simulating the mechanical swatter. **Annemarie** ('EZO's mum'), you are the corner stone of EZO, without you, everything would probably fall down. Thanks for your constant helpfulness.

During my years as a PhD candidate, I had the joy of working with a few students. **Ton**, **Henry**, **Cedric** and **Antigoni**, it was a pleasure supervising you, I have learned much through this. **Henry** I am super proud of what we (mostly you) achieved. Working with you was always eventful and exciting. Sadly, I never managed to convince you that insects were mostly our friends. **Cedric**, thanks for having the courage to face malaria mosquitoes in their natural habitat and for the very nice design inputs (the handle!). **Antigoni**, I really enjoyed our discussions and your enthusiasm. I promise I will have time to dive into your great dataset at some point.

Going to a new country to do a PhD can be quite a stressful experience. Luckily, I felt welcomed right away and I could build a comfortable little nest in the e-wing of the Zodiac building. This is mostly due to the great people of the Experimental Zoology group (**EZO**) and of the Cell Biology and Immunology group (**CBI**). In particular, I want to thank all my fellow (sometimes former) PhD candidates in EZO and CBI: **Adrià**, **Andres** ('the wizard of statistics'), **Annelieke**, **Carmen**, **Cees**, **Esther**, **Gauthier**, **Henri**, **Jules**, **Julia**, **Julian**, **Lana**, **Mark**, **Marloes**, **Mike**, **Mirelle**, **Mojtaba**, **Myrthe** ('the lady with the fancy drink'), **Noraly**, **Olaf**, **Paulina** ('the smuggler'), **Pim** ('the electrician'), **Pulkit**, **Sem**, **Tiffany**, **Uroš** and **Wouter**. Thanks for the amazing PhD weekends, the PhD movies, the Rhine barbecues and all the movie nights (#IwillmakeyouloveMiyazaki)! And also, thanks to all of you and to **Annemarie**, **Ellen**, **Florian**, **Guillermo**, **Henk**, **Johan**, **Karen**, **Leo**, **Martin**, **Remco**, **Sander**, **Sander**, and **Steffen**, for the many great moments during lunch and coffee breaks, Labuitje (#Ceesbellydancing) and evening drinks. Finally, thanks to everyone in EZO for all your nice input during our weekly lunch meetings.

In EZO, I shared an office with **Cees**, **Pulkit** and **Wouter**. Thanks to you three for making my time there fun and comfortable. Because of you I discovered new music (#taytayforewer), had nice discussions and had plenty of occasions to complain about anything that didn't work in my project. Shout out to **Carmen** and **Annelieke** for their amazing office

makeovers! I will always remember the large number of items that you handpicked for us (and the human-sized Eiffel Tower!). **Cees** and **Pulkit**, thanks for being my paranymphs! If everything goes well, you will walk with me to the aisle of science. That means a lot to me.

I am also very grateful to **Willem** and then **Sander** for welcoming me in the One Health Entomology group! And, thanks to the entire group and especially to **Helen**, **Jeannine**, **Jeroen**, **Julian**, **Marieke**, **Marilyn**, **Pieter**, **Tessa** ('the tiger tamer') and **Tim**. Your hospitality and knowledge were crucial for my project. I always enjoyed our weekly meetings during which I learned so much about vector control.

Doing a PhD can be a rather demanding activity, luckily, I did plenty of other things that allowed me to think about something else. Many thanks to all my climbing buddies from the #PowerPof group: **Annelieke**, **Carmen**, **Cees** ('the clamp'), **Florian**, **Mike** ('the nomenclator), **Sander** and **Uroš** ('the cleaner'). It was a real pleasure to learn how to crawl over rocks with you. **Mirelle**, thanks for all the nice hikes! I really enjoyed hunting mushrooms, boars and even owls with you. **Carmen**, **Cees**, **Marloes**, **Mike** and **Pimie**, thanks for the great times at Rock Werchter! I never felt as tired of standing than after those weekends, but it was definitely worth it. I would also like to thank **Annelieke**, **Pulkit**, **Lisa** (fish), **Noraly**, **Lisa** (frog) and **Cas** for taking (good?) care of our vegetable garden with me. Having this project next to my PhD was super important for my mental health. Surprisingly, we always managed to have some vegetables (OK mostly it was zucchini and pole slicing beans). During my free time, I also had the pleasure of going to adventures, killing dragons, riding (and curving!) mine carts, talking to woodpeckers (Woody!) and, of course, buying kickass weapons! Thanks **Noraly** ('our beloved GM, that would never dare killing us'), **Henri**, **Lana**, **Pulkit** and **Tiffany** for these great moments! Finally, thanks **Maria** for the beautiful walks, the macarons and the exciting discussions. Your support during my last year has been really important for me.

De nombreuse fois pendant mon doctorat, j'ai repensé à tous les moments de mon parcours en France qui ont contribué à me passionner pour la recherche sur la biomécanique du vol des insectes. Parmi ces moments, il y a sans aucun doute les années que j'ai passé à l'UAOVLCM, le club d'aéromodélisme d'Orléans. Merci énormément, **Paul**, **Dédé**, **Jacques Delcroix** et **Jacques Blanchard**, pour m'avoir appris comment fabriquer et faire voler un avion, pour m'avoir donné le virus du modélisme et le gout de résoudre des problèmes en bricolant. J'ai eu avec vous certains de mes meilleurs souvenirs d'enfance. Au collège j'ai rencontré deux de mes meilleurs amis, **Clément** et **Guillaume**. Merci beaucoup à vous deux de m'avoir donné la passion de la chasse aux insectes. J'ai eu ma première expérience de recherche scientifique au Lycée avec **Thomas** et **Aventin**, et grâce aux conseils avisés de **Marie-Christine Baurrier** (j'ai appris tant grâce à vous!). Merci infiniment pour cette super aventure! Je n'aurais sans doute pas fait ce doctorat sans avoir eu la chance d'étudier la chute des graines ailées d'érable avant. **Ramiro** et **Jérôme**, je vous remercie beaucoup d'avoir parlé de moi lorsque j'étais à la recherche d'un doctorat. Je n'aurais sans doute jamais été aux Pays-Bas sans cela. **Lucille**, quand je suis arrivé à Wageningen, je ne connaissais

personne d'autre. Ta générosité me fut très précieuse dans ces premiers mois. Merci aussi de m'avoir fait faire mes premières découvertes aux Pays-Bas, comme l'arboretum à Amsterdam et les huttes de castors à Wageningen. Enfin et surtout, je voudrais remercier ma famille et plus particulièrement **Manon**, **Jehan**, **Maman** et **Papa**. Vous avez toujours cru en moi, et sans cela je n'aurais surement pas osé quitter la France. Il est parfois compliqué de vivre si loin de sa famille et votre soutien me fut très précieux durant toutes ces années. **Mamie** et **Grand-père**, à mon adolescence, vous m'avez offert la musette du naturaliste de la hulotte, avec à l'intérieur un très pratique filet à papillons. Depuis, je n'ai jamais reçu un cadeau d'anniversaire qui ai autant changé ma vie. **Maman** et **Papa**, vous avez été les premiers à me faire découvrir la beauté de la nature et à me montrer ce que faire de la recherche signifiait. Merci pour ces inestimables présents.

It is well known that only acknowledgments are read. Thus, in an attempt to trigger your curiosity and to make you check some of my figures, here are a few questions I tried to answer in this thesis[1].

How do mosquitoes achieve flight?   answer in Fig. 1.2, page 14

How do mosquitoes find you?   answer in Fig. 1.4, page 21

How do odour-baited traps work?   answer in Fig. 2.1, page 44

How mosquitoes behave near traps?   answer in Fig. 2.9, page 62

How did we develop a new trap?   answer in Fig. 6.3, page 255

Is our new trap more efficient?   answer in Fig. 3.1, page 99

How do mosquitoes escape from an attack?   answer in Fig. 5.3, page 196

---

[1]Original idea from Cees Voesenek.

About the author

Antoine Cribellier was born in 1992 in Orléans, France. At a young age, he was already passionate about flying things. His passion started with birds and quickly spreads to flying machines. At the age of nine, he joined the local aeromodelling club where he learned how to build and fly model aeroplanes made of balsa wood and powered by rubber bands. Already then, he enjoyed the meticulous process necessary to get these aeroplanes (sometimes as light as a bee) to fly as long as possible. In middle school, his passion extends to insects, and especially to dragonflies that he likes to pursue and photograph.

The seed of Antoine's interest for scientific research was planted when, with two high-school friends and under the supervision of his physics teacher, he started a one-year project to study the fall of the winged maple-tree seed. In 2010, this project was extended for a second year and was awarded two first prizes at two national scientific competitions (Olympiades de Physique and C. Génial, France). In the meantime, a team of researchers in the Netherlands published their study on the aerodynamic of maple-tree seed in the scientific journal Science. After discovering this fascinating paper, he and his friends designed their own vertical wind tunnel in order to visualize the vortex above the rotating seeds. In September 2010, they presented this wind tunnel and their results in the international scientific competition EUCYS (European Union Contest for Young Scientists) in Lisbon (Portugal).

After this first experience, Antoine decides to follow studies which would lead him to do scientific research. During his BSc in physics and engineering (University of Orléans), in 2013, he went on Erasmus mobility at the University of Cork (Ireland). Then, he obtained his Master's degree in mechanics at the University of Versailles (UVSQ). Having first considered studying astrophysics, Antoine did an internship on pulsars in the CNRS (National Centre of Scientist Research) of Orléans, and another one on the deorbiting of satellites at the CNES (National Centre of Space Study) of Toulouse. Finally, he decided to return to his original interest: biomechanics. Thus he carried out his MSc thesis at the ONERA (the French Aerospace Lab) of Lille on the characterization of the flapping wings of a micro-drone similar to insect wings.

A

In 2016, Antoine obtained his second MSc degree of fluid mechanics at the University of Lille 1, after completing his MSc thesis at the Research Institute on Insects Biology (IRBI) in Tours. During this project, he studied the hydrodynamics of the movement of water striders and mechanically simulated a leg at the air/water interface. At the same time, and with the help of Florian Muijres, he obtained a personal PhD grant from the Wageningen Institute of Animal Science (WIAS), to study 'How to catch a mosquito?' in Wageningen University (The Netherlands). This is only after starting his PhD in Wageningen that he realized that his promoter, Johan L. van Leeuwen, was in the team of researchers published the scientific article on the fall of maple seeds that had interested him so much years before.

In July 2021, he started a postdoctoral research project at the University of Wageningen to better understand how malaria mosquitoes swarm and mate. This project was funded by a Human Frontier Science Program research grant and will be carried out by an interdisciplinary collaboration of four teams around the world (The Netherlands, Belgium, Burkina Faso and USA).

List of publications

Pulkit Goyal, <u>Antoine Cribellier</u>, Guido C. H. E. de Croon, Martin J. Lankheet, Johan L. van Leeuwen, Remco P.M. Pieters, Florian T. Muijres (2021). Bumblebees land rapidly and robustly using a sophisticated modular flight control strategy. *iScience* **24, issue 5**, 102407.

Thomas Steinmann, <u>Antoine Cribellier</u>, Jérôme Casas (2021). Singularity of the water strider propulsion mechanisms. *Journal of Fluid Mechanics* **915**, A118.

<u>Antoine Cribellier</u>, Jeroen Spitzen, Henry Fairbairn, Cedric Van De Geer, Johan L. Van Leeuwen, Florian T. Muijres (2020). Lure, retain, and catch malaria mosquitoes. How heat and humidity improve odour-baited trap performance. *Malaria journal* **19, issue 1**, 1-16.

<u>Antoine Cribellier</u>, Jens A. van Erp, Alexandra Hiscox, Martin J. Lankheet, Johan L. van Leeuwen, Jeroen Spitzen, Florian T. Muijres (2018). Flight behaviour of malaria mosquitoes around odour-baited traps: capture and escape dynamics. *Royal Society open science* **5, issue 8**, 180246.

P

Educational activities

Course	Year	ECTS
The basic package		**1.8**
WIAS Introduction Course	2016	0.3
Scientific Integrity and Ethics	2019	1.5
Disciplinary Competences		**12.2**
Grant Proposal	2017	6.0
Statistics for the Life Sciences – WIAS	2017	2.0
Python Data Science (IBM online course on edX)	2021	4.2
Professional Competences		**5.9**
Survival Guide to Peer Review – WIAS	2017	0.3
High Impact Writing - WIAS	2017	1.3
Supervising BCs and MSc thesis students	2017	0.6
Efficient Writing Strategies	2018	1.3
Brain Training	2018	0.3
Stress Identification & Management	2018	0.0
Project and Time Management	2018	1.5
The Final Touch: Writing the General Introduction and Discussion - WIAS	2020	0.6
Societal Relevance		**1.2**
Ansering the question of Everyday Health - Article on Mosquito host-seeking behaviour	2019	0.2
Participation to the PreMal Supervisory Board + Advising activity	2019 -	1.0
Presentation Skills		**4.0**
SEB Conference, oral presentation (5th) of July), Sweden	2017	1.0
Burgers Symposium, oral presentation (31st of May)	2017	1.0
Insect bio-inspired microtechnology, poster presentation (21st of November)	2019	1.0
WIAS Annual conference, oral presentation (13th of february)	2020	1.0
SICB Online Conference, oral presentation (1st January)	2021	/
Teaching competences		**6.0**
Supervising a BSc student (Ton Kaarsgaren)	2017	1.0
Supervising one MSc thesis students (Henry Fairbairn)	2018	2.0
Supervising one MSc thesis students (Cedric van de Geer)	2019	2.0
Supervising one MSc thesis students (Antigoni Bougatsia)	2020	/
Teaching-assistant for Functional Zoology ($\approx$ 20 hours)	2017	1.0

Teaching-assistant for Functional Zoology (≈ 35 hours)   2018   /
Teaching-assistant for Functional Zoology (≈ 35 hours)   2019   /
Teaching-assistant for Functional Zoology (≈ 15 hours)   2020   /

Total   **31**

Completion of the training activities is in fulfilment of the requirements for the education certificate of the Graduate School Wageningen Institute of Animal Sciences (WIAS). One ECTS equals a study load of 28 hours.

Caption of the covers
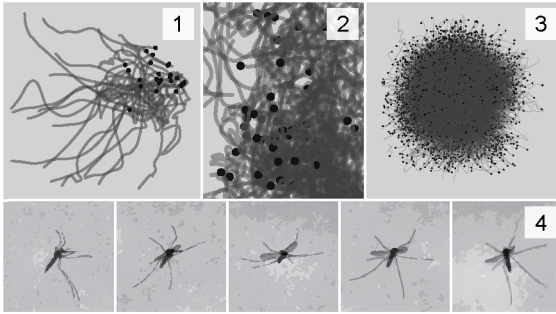
1. All the mosquito tracks that lead to a capture by the hanging Suna trap.

2. Details of tracks that lead to capture near the M-Tego.

3. All the mosquito tracks showing successful escapes from the looming swatter.
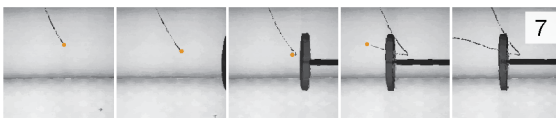
4. Images showing a successful escape from the swatter.
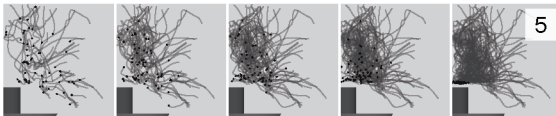
5. All the tracks that lead to a capture by the standing Suna trap (each panel show a different step up until capture).
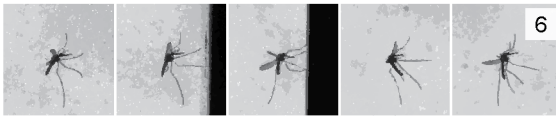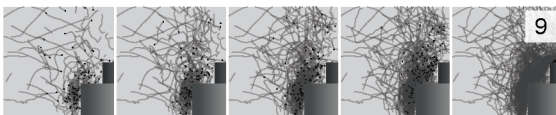
6. Images showing a collision between a flying mosquito and the swatter.

7. Images showing a successful escape from the swatter

8. Images showing a successful escape from the swatter.

9. All the tracks that lead to a capture by the M-Tego (each panel show a different step up until capture).

E

287